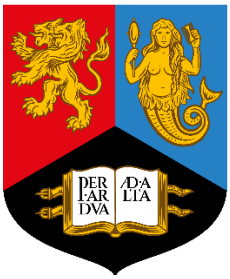
NUCLEOPHILIC “X”-YNE POLYMERISATION FOR MATERIAL SYNTHESIS

by

Daniele Giannantonio



UNIVERSITY OF BIRMINGHAM

A thesis submitted to the University of Birmingham for the degree of

DOCTOR OF PHILOSOPHY

School of Chemistry

College of Engineering and Physical Sciences

University of Birmingham

August 2024

UNIVERSITY OF
BIRMINGHAM

University of Birmingham Research Archive

e-theses repository

This unpublished thesis/dissertation is copyright of the author and/or third parties. The intellectual property rights of the author or third parties in respect of this work are as defined by The Copyright Designs and Patents Act 1988 or as modified by any successor legislation.

Any use made of information contained in this thesis/dissertation must be in accordance with that legislation and must be properly acknowledged. Further distribution or reproduction in any format is prohibited without the permission of the copyright holder.

Abstract

Polymeric materials shape the world we live in, and imagining our reality without them seems an impossible task. However, concerns about their sustainability are rapidly arising since most of them are synthesised from crude oil derivatives and accumulate in the environment with little known consequences.

The inclusion of bio-based renewable monomers into polymer structures represents a significant and valuable effort in building more sustainable materials. However, attention must be placed on the polymerisation method too, to adhere to green chemistry principles. Current step-growth polymerisation techniques succeed in including heteroatoms into polymer backbones aiming to introduce new reactivity handles, but they often require harsh reaction conditions such as high temperature. On the other hand, polymerisations proceeding *via* chain-growth mechanism occur at lower temperatures but produce mostly carbon-carbon based backbones.

The goal of this thesis was to leverage the nucleophilic addition of heteroatoms to activated alkynes, *i.e.*the thiol- and hydroxyl-yne click reactions, to synthesize a new range of polymers. In light of its simplicity and selectivity, this reaction has been successfully employed to yield designer polyesters, both linear and crosslinked, with tuneable thermomechanical properties and controlled degradability. Moreover, the same approach could be expanded into the production of polyester amides from bio-sourced monomers to access a novel class of amino acids-based polymers.

Acknowledgments

The first thanks go to Prof. Andrew Dove, who gave me the chance to pursue a PhD in his laboratories. Since the beginning, Andrew has been a tough but fair supervisor, who trusted me and helped me develop into a more mature scientist.

These last four years have been really intense. Adapting to a new country along with the pressure of pursuing a PhD was not an easy task. However, if I have learned something during this period, is that I am not alone. There are many people whom I am grateful to have met, and without them, all of this would not have been possible. Of all these people, some deserve a special acknowledgment. First, I must thank David “Daviçito” Londoño, who approached me in first year and taught me many things since then. From coffee club to night out in Manchester, te quiero mucho mi amigo! Another person I am grateful to have met is Dr. Benjamin Allott, a personal reminder to never be “too caught up”. The two years we lived together have been the most memorable and I am really thankful for all the adventures, with more to come! Lastly, I would like to thank Dr. Alexis Perrot. You are an incredible scientist, but mostly a true friend. You believed in me when I could not, and our chats have always been incredibly insightful and inspiring. You have been a great mentor to me, and if I now know something about chemistry and thinking you are the culprit.

The rest of the O’Doveillys people deserve my gratitude too. The academic reality is a tough environment, and each of you was always available to chat, vent, or just sit in silence, always helping each other. Of all the people, Dr. Natalia Reis, and Dr. Ana Alvarez deserve special praise. I have been very lucky to start at the same time

as Natalia, as she has always been very kind and helpful, both in the lab and in improving the introduction of this thesis. Sharing the office desk with Ana has also been one of the blessings of this PhD, your work ethic was really motivating, but what was even more wonderful was your ability to always lend an ear to listen. Dr. Thiago Ouriques Machado must be thanked for all the coffee shared and for proofreading this thesis, along with Dr. Arianna Brandolese, who really helped me improve my writing with her sharp and keen eye. Lastly, I would like to Ms. Rachel Stracey for all the playful distractions during my writing and Mr. Lukmanul Hakim Samada for always sharing his love and passion for Indonesian culture, makasih!

Good things don't only happen in the lab; a year ago I met a wonderphul person, with whom I have laughed and cried a lot, and learned about myselph and the world around me, thanks to your original perspective and precious soul. Thank you Ej for being there for me, for your endless kind gestures, and phor pushing me towards the end. I am the most gratephul, and while I hope I can give you back at least a phragment of what you give to me, I cheer for more of this!

Questi ringraziamenti non potrebbero essere completi senza un pensiero alla mia parte italiana. Grazie ai Fellas, amici sinceri e unici, sempre presenti da ormai più di 10 anni. Grazie a Paul, Alle, Bolla e Catta per le ore passate a giocare, ma soprattutto ad ascoltarci. Grazie a Viso, Vitto, Cito e Albi, per esserci sempre ogni volta che l'opportunità si presenta. Grazie agli amici di Monte Orsaro, Claudio, la Gio, Pier, e il drago Dario, per le vacanzine di questi anni e l'offrirmi sempre un posto in cui tornare. Grazie alla Sere, in questi anni ci siamo conosciuti meglio, e l'unica

cosa che mi dispiace e non averlo fatto prima! Grazie a Mazza, insostituibile punto di riferimento, per il confronto sincero e l'amicizia vera. Un pensiero va a tutti voi, vi voglio bene.

Infine, non posso che terminare ringraziando la mia famiglia. Senza di loro nulla di quello che ho fatto sarebbe stato possibile. Grazie alla Mamma e al Babbo, per il supporto incondizionato e l'esempio che mi hanno sempre dato. Grazie a Giac, con cui sono molto fratello. Grazie alla Noni e al Nonno, che mi hanno insegnato l'amore quello vero, privo di ogni interesse.

Grazie a te, che stai leggendo queste parole, per il tempo che mi stai dedicando, spero tu possa imparare qualcosa da questa tesi, che tu la legga dall'inizio o stia solo cercando uno spettro NMR, come ho fatto io.// Thanks to you reader, for the time you are giving to me, I hope you can learn something from this thesis, whether you are reading it from the start or just looking for an NMR spectrum, just as I did.

Table of Contents

List of Figures III

List of Equations VI

List of Symbols, Abbreviations and Acronyms VII

Author declaration XIII

Chapter 1 – Introduction 1

1.1 Polymers 2

1.1.1 Polymer composition and architecture 4

1.1.2 Molar mass and degree of polymerisation 7

1.2 Bulk properties of polymers 9

1.2.1 The amorphous state 9

1.2.2 The crystalline state 12

1.2.3 Measurement of thermal properties 15

1.2.4 Measurement of mechanical properties 17

1.3 Polymerisation techniques: step growth polymerisation 19

1.3.1 Step-growth synthesis of linear polymers and networks 20

1.4 Click polymerisation: nucleophilic X-Yne addition 23

1.4.1 Thiol-yne polymerisation 25

1.4.2 Phenol-yne polymerisation 30

1.5 Stereochemistry in polymers 32

1.6 Conclusions 39

1.7 References 41

Chapter 2 – Synthesis of disulfide containing thermoplastics *via* nucleophilic thiol-yne polymerisation. 44

Manuscript and overview..... 45

Supporting information 65

Chapter 3 – Access to degradable and reprocessable thermosets with tuneable thermomechanical properties *via* nucleophilic thiol-yne polymerisation. 132

Manuscript and overview..... 133

Supporting information 156

Chapter 4 – Accessing diketopiperazines-based polymers through phenol-yne polymerisation 182

Manuscript and overview..... 183

Supplementary information..... 200

Chapter 5 – Enantiopure and racemic BINOL-based polymers by hydroxyl-yne polymerisation 227

Manuscript and overview..... 228

Supporting information 252

Chapter 6 – Conclusions and outlook 281

List of Figures

Figure 1. Amount of plastic (expressed in millions of tonnes) produced from the 1950 to 2019. Data plotted by the author obtained from Sci. Adv.3,e1700782(2017).[9] 4

Figure 2. Different skeletal structures of polymeric materials. 5

Figure 3. Polymers can be classified according to the number of monomer species..... 6

Figure 4. Factors controlling the T_g such as main chain flexibility (left) and side groups bulkiness (right). 10

Figure 5. Stacked DSC thermograms (left) and stacked powder X-ray diffraction patterns (right) of atactic, syndiotactic, and isotactic PHAs all showing formation of crystalline domains. Reprinted (adapted) with permission from J. Am. Chem. Soc. 2023, 145, 48, 25983–25988. Copyright 2023 American Chemical Society. 14

Figure 6. Typical DSC run of a semi-crystalline polymer. Heating run (solid line), cooling run (dashed line), glass transition temperature (T_g), crystallisation events (T_c & T_{cc}), melting temperature (T_m). 16

Figure 7. Exemplary stress vs. strain curve with the deducible properties (left). Stress vs. strain curves of different polymers (right). 18

Figure 8. Schematic representing typical DMA thermograms with storage modulus and tan δ plotted against temperature. T_g highlighted..... 19

Figure 9. Cartoon exemplifying the mechanistic difference between step-growth and chain-growth polymerisation (left) and typical plot of degree of polymerisation vs. functional group conversion of the two types of polymerisations (right). 20

Figure 10. 1,4-Michael addition to an activated alkyne (top box), structures of commonly used Michael acceptors (box bottom left) and Michale donors (box bottom right) 25

Figure 11. The dynamic nature of the second addition enables the synthesis of dynamic materials with tuneable exchange rates according to the electronic of the activated alkyne. 30

Figure 12. Chemical structure of gutta percha (left) and natural rubber (right). 33

Figure 13. Chemical structure of polypropylene molecules of different tacticity associated with decreasing level of crystallinity (from left to right). 34

Figure 14. Chemical structure of lactide diasteroisomers and tacticity of diads and triads of PLA molecules. 34

Figure 15. A) Polymers degradation rates dependent on cis content and composition. Adapted from ref. 66 reproduced under a Creative Commons Attribution 4.0 International License. B) Stress vs. strain curves of polymers having different backbone cis/trans isomerism showing that the trans polymer (T_{100}) is stronger than the cis polymer (C_{100}). Reprinted (adapted) with permission from Macromolecules 2020, 53, 1, 174–181. Copyright 2020 American Chemical Society. C) Young's modulus and T_g values found for different cis content in polyamides. Adapted from ref. 35 reproduced under a Creative Commons Attribution 4.0 International License. 36

Figure 16. Different isoidide/isomannide ratios dictate polymers mechanical properties and degradation rate. Adapted from ref. 114 under license CC-BY-NC-ND 4.0. 38

Figure 17. A) Increasing cis content was found to decrease compressive strength in hydrogels developed via thiol-yne polymerisation. Adapted from ref. 39 under the terms of Creative Commons CC BY license. B) DSC thermograms showing the difference in crystallinity due to different cis/trans ratio in different 3D printable resins of different molecular weight. Adapted from ref. 72 under CC-BY-NC-ND 4.0. 38

List of Equations

Equation 1. Molar mass of a homopolymer obtained multiplying the molar mass of the repeating unit with the degree of copolymerisation. 8

Equation 2. Molar mass of a copolymer obtained multiplying the molar mass of the repeating unit considering the monomers constituting it with the degree of copolymerisation. 8

Equation 3. Number average molecular weight equation (M_n) equation, where the molecular mass of all polymer chains is divided by the number of polymer chains. 8

Equation 4. Weight average molecular weight equation (M_w) equation, where the molecular mass of all polymer chains is divided by the total mass of all the molecules. 9

Equation 5. Evaluation of the degree of crystallinity by comparison of the enthalpies of melting and crystallisation. 14

Equation 6. Formula describing the calculation of Young's modulus. 17

Equation 7. Extended Carothers' equation. 21

List of Symbols, Abbreviations and Acronyms

1,6-HDT = 1,6-Hexanedithiol

1-HT = Hexanethiol

3-AT = Three-arms thiol

Å = Angstroms

ADMET = Acyclic diene metathesis

ATRP = Atom transfer radical polymerisation

BINAM = [1,1'-Binaphthalene]-2,2'-diamine

BINOL = 1,1'-Bi-2-naphthol

CANs = Covalent adaptable networks

$CDCl_3$ = Deuterated chloroform

$CHCl_3$ = Chloroform

DABCO = 1,4-diazabicyclo[2.2. 2]octane

DBU = 1,8-Diazabicyclo[5.4.0]undec-7-ene

DEG = Diethyleneglycol dipropiolate

DKP = Diketopiperazine

DMA = Dynamic mechanical analysis

DMAP = 4-dimethylamino pyridine

DMF = Dimethylformamide

DMSO = Dimethylsulfoxide

DSC = Differential scanning calorimetry

DTT = Dithiothreitol

E = Young's modulus

EPDM = Ethylene propylene diene monomer

Et_2O = Diethyl ether

Et_3N = Triethylamine

EtOAc = Ethyl acetate

EWG = Electron withdrawing group

FT-IR = Fourier-transform infrared spectroscopy

G = Complex modulus

G = Gibbs free energy

g = grams

G' = Storage modulus

G'' = Loss modulus

GERD = Gastroesophageal reflux disease

GPC = Gel permeation chromatography

H = Enthalpy

H_c = Enthalpy of crystallisation

HDP = Hexane dipropiolate

HDPE = High-density polyethylene

H_m = Enthalpy of melting

HR-MS = High resolution mass spectroscopy

HSQC = heteronuclear single quantum coherence

J = Joule

K = Kelvin

Kg = kilograms

L = Litre

LDPE = Low-density polyethylene

L-Ser = L-Serine

L -Tyr = L-Tyrosine

LVE = Limit of the viscoelastic region

M = Molar mass

M^0 = Molar mass of repeating unit

M^0_{cop} = Mean molar mass of repeating unit in a copolymer

M_c = Molecular weight between crosslinks

min = Minute

mL = millilitre

mm = Millimiter

mmol = Millimole

M_n = Number-average molar mass

mol = Mole

MPa = Megapascals

M_w = Weight-average molar mass

N = Newton

η = Viscosity

NaHCO3 = Sodium bicarbonate

NMR = Nuclear magenic resonance

Pa = Pascals

PDLA = Poly-d-lactic acid

PE = Polyethylene

PEG = Poly(ethylene glycol)

PET = Polyethylene terephthalate

PHA = Polyhydroxyalkanoate

PHB = Polyhydroxybutirate

p*K*a = Acid dissociation constant

PLA = Poly(lactic acid)

PLAs = Poly-lactides

PLLA = Poly-l-lactic acid

PMMA = Poly(methylmethacrylate)

PMMA = Poly(methylmethacrylate)

PP = Polypropilene

PS = Polystyrene

RAFT = Reversible addition-fragmentation chain transfer

ROP = Ring opening polymerisation

S = Entropy

s = Seconds

SBR = Styrene butadiene rubber

SEC = Size exclusion chromatography

T = Temperature

Tan δ = Dampening factor

TBD = 1,5,7-triazabicyclo[4.4.0]dec-5-ene

$T_{d,5\%}$ = Temperature at 5% weight loss

TEGDP = tetraethyleneglycol dipropiolate

TFA = Trifluoroacetic acid

T_g = Glass transition temperature

TGA = Thermal gravimetric analysis

THF = Tetrahydrofuran

TLC = Thin layer chromatography

T_m = Melting temperature

UTS = Ultimate tensile strength

WAXS = Wide angle X-ray scattering

X = Degree of polymerisation

Xc = Degree of crystallinity

δ = Chemical shift

ε = Strain

µL = Microliter

σ = Stress

Author declaration

This thesis is submitted to the University of Birmingham in support of my application for a Doctor of Philosophy award. This work has not been submitted for any degree or award previously.

Parts of this thesis have been published as open access articles in peer-reviewed journal or are displayed in a format suitable for publication in peer-reviewed journal, as outlined in the University of Birmingham alternative thesis format guidelines. The work presented in this thesis (including data generated and data analysis, materials characterisation, writing and figure design) was performed by myself, except for co-author contributions which are outlined below and before each chapter.

Chapter 2 – Manuscript prepared: Daniele Giannantonio, Alexis G. Perrot, Arianna Brandolese, Andrew P. Dove, Synthesis of disulfide containing thermoplastics via nucleophilic thiol-yne polymerisation.

Alexis G. Perrot provided synthetic, technical, and analytical guidance along with editing of the manuscript. Arianna Brandolese provided editing of the manuscript and guidance. Prof. Andrew P. Dove supervised in addition to providing guidance and funding acquisition.

Chapter 3 – Manuscript prepared: Daniele Giannantonio, Arianna Brandolese, Andrew P. Dove, Degradable and reprocessable thermosets with tuneable thermomechanical properties developed via nucleophilic thiol-yne polymerisation.

Arianna Brandolese provided editing of the manuscript and guidance. Prof. Andrew P. Dove supervised in addition to providing guidance and funding acquisition.

Chapter 4 – Manuscript prepared: Daniele Giannantonio, Arianna Brandolese, Andrew P. Dove, Accessing diketopiperazines-based polymers through phenol-yne polymerisation.

Arianna Brandolese provided editing of the manuscript and guidance. Prof. Andrew P. Dove supervised in addition to providing guidance and funding acquisition.

Chapter 5 – Manuscript prepared: Daniele Giannantonio, Alexis G. Perrot, Arianna Brandolese, Andrew P. Dove, Enantiopure and racemic BINOL-based polymers by hydroxyl-yne polymerisation.

Alexis G. Perrot provided synthetic, technical, and analytical guidance along with editing of the manuscript. Arianna Brandolese provided editing of the manuscript and guidance. Prof. Andrew P. Dove supervised in addition to providing guidance and funding acquisition.

Chapter 1 – Introduction

1.1 Polymers

Since 1820, when Thomas Hancock reported the change in mechanical properties of natural rubber upon mastication[1] (*i.e.* subjected to high shear forces several times), the understanding of the behaviour of polymeric materials has increased greatly. Following on from Hancock's findings, in 1839, Nathaniel Hayward assigned his patent US 1090 to Charles Goodyear for his discoveries regarding the vulcanisation of natural rubber.[2] However, albeit several reports regarding the various properties associated with this class of compounds, polymers were thought to be the physical association of small molecules. A significant shift has happened since the Nobel Prize Herman Staudinger laid down the foundation of polymer science proposing the term "macromolecules", defining polymers as composed of large molecules made of shorter repeating units linked by chemical bonds.[3] Thanks to his pioneering work among others, such as crystallographic studies by Herman Mark and Kurt Meyer on natural polymers and Carothers's work on the preparation of polyamide and polyesters[4], polymer science is now a branch of chemistry with a direct influence on society. This is highlighted by the significant increase in polymeric product production since their introduction in the 1950s (Figure 1). Given the current trend, it is predicted that plastic production will account for almost half of the increase in oil consumption, it takes up 15% of our carbon budget, and has resulted in serious environmental concerns.[5] For these reasons, it is imperative to investigate new polymerisation routes to improve the sustainability of polymer synthesis. In addition to leveraging bioderived monomers

from renewable feedstock coupled with considerations about recycling and performances, adherence to green chemistry principles (atom economy, hazard reduction, lower energy requirements)[6] must be maximised. Typical polymer synthesis occurring through a step-growth mechanism enables the introduction of heteroatoms into the polymer backbone, which is crucial for recycling and polymer performance. However, this requires very high temperature (>200 °C), thus making it a highly energy intensive process. On the other hand, polymers produced *via* chain-growth polymerisation requires lower temperatures, but incorporation of heteroatoms without compromising the mechanical performances or the polymerisation efficiency remain elusive. It is worth noting that recent efforts into the depolymerisation of fully carbon-carbon based polymers produced *via* radical mediated polymerisation have constituted inspiring and valuable novel approaches.[7, 8] For these reasons, it is proposed that replacing condensation reactions with click reactions performed at lower temperature may be a viable methods to build functional polymers under milder conditions.

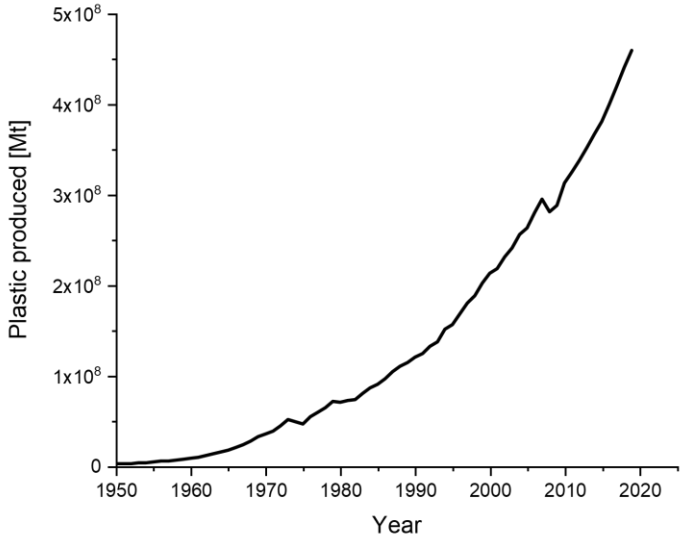


Figure 1. Amount of plastic (expressed in millions of tonnes) produced from the 1950 to 2019. Data plotted by the author obtained from Sci. Adv.3,e1700782(2017).[9]

1.1.1 Polymer composition and architecture

Nowadays, the term polymer refers to a substance composed of large macromolecules, which are formed by linking together monomer molecules in a process called polymerisation and can display different architectures and, therefore, physical properties. These polymers can be divided into linear, where the macromolecules present two chain ends, and non-linear which have no chain ends (cyclic or ring polymers). An example of different properties in ultrahigh-molar mass (UHMM) polymers was reported recently by Chen and co-workers.[10] The authors found out that the thermal degradation temperature of linear poly(2,2-dimethyl-3-thiopropiolactone) (*l*-P3T(Me)$_2$P) was 14 °C lower than the that of a cyclic analogue, and differences in mechanical properties were observed too. The skeletal structure of polymers can also present side chains, called branches, with different lengths

and frequencies, which are bonded to the main chain at branching points. Branched polymers are classified as dendrimers or hyperbranched according to the definition of the molecular mass and structure. These differences are also known to impact the physical properties of polymers. For example, it is known that the intrinsic viscosity of a linear polymer increases with its molecular weight, and the maximum is associated with the formation of dendrimers.[11] Branches can also act as crosslinkers between different macromolecules, creating a polymer network that can be characterised by their number of junction points per unit volume, which is known as crosslinking density (Figure 2).

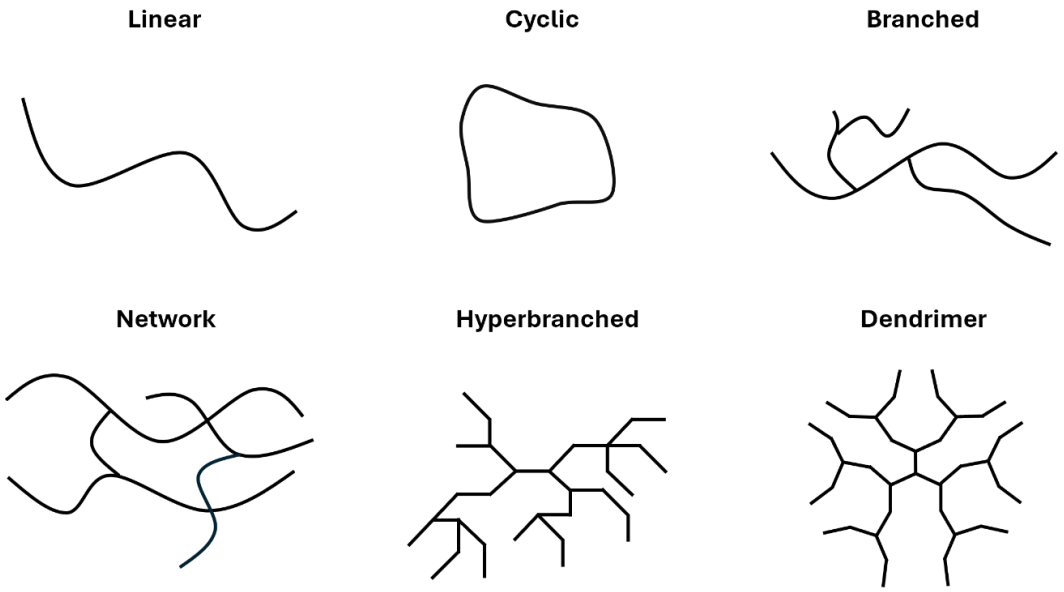


Figure 2. Different skeletal structures of polymeric materials.

Another important factor is the nature of the monomers that constitute the polymers. Polymers constituted only from one kind of monomer are called homopolymer,[12] whilst if two or more different repeating units are present, they are called copolymers.[13] Copolymers are further classified according to the way the different monomers are distributed along the chain. Statistical copolymers are

polymers in which the monomer distribution obeys statistical laws[14], but if the monomer distribution cannot be predicted they are defined as random copolymers,[15] whereas alternating copolymers are polymers where the monomers are perfectly alternated.[16] Another type of polymer are block copolymers. In this case, the polymer is made of alternating blocks composed of repetition of one single monomeric unit.[17] Subtle variation in the monomer sequence can lead to huge differences in terms of thermomechanical properties. For example, melt viscosity of random butadiene and styrene copolymers was found to be different when compared to block copolymers made of the same monomers, which exhibited a two-phase domain structure.[18] Copolymers can have branches composed of monomers differing from the monomers of the main chain, in this case, they are called comb copolymers (Figure 3).[19]

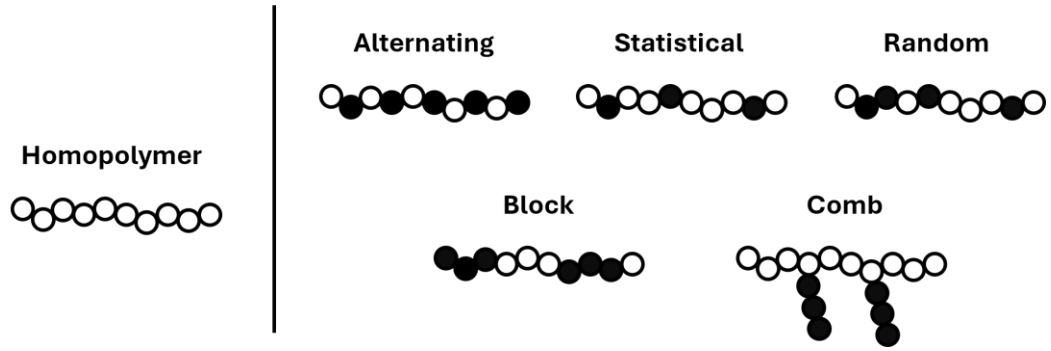


Figure 3. Polymers can be classified according to the number of monomer species.

Polymers are also classified based on their thermomechanical behaviour. *Thermoplastics* are linear, branched or cyclic polymers, which can flow when the temperature is sufficiently high, and can be further differentiated according to their ability to crystallise, *i.e.* their chains align to form highly ordered structures.[20, 21] In most cases, it is impossible to obtain a fully crystalline polymer, and generally

crystalline domains are dispersed into a non-crystalline phase (semi-crystalline). The crystalline phase is characterised by a melting temperature (T_m) In turn, polymers that are not able to form crystalline domains are defined as amorphous. These polymers, together with the amorphous phase of semi-crystalline polymers, are characterised by their glass transition temperature (T_g). Transitioning above the T_g means shifting from the glassy state (hard) to the rubbery state (soft).[22] Crosslinked polymers can be further divided into *elastomers* and *thermosets*. Elastomers are rubbery networks, generally characterised by a *low crosslinking density,* that can repeatedly be stretched and recover their initial shape when the deforming stimulus is removed.[23] On the other hand, thermosets are characterised by *higher crosslinking density* which confers higher rigidity and solvent resistance, as the materials swell rather than solubilise, and the inability to flow even at higher temperatures, making these materials hard to degrade.[24] For example, the onset temperature of the rubbery plateau of silicon polymer networks increases with increased crosslink density.[25]

1.1.2 Molar mass and degree of polymerisation

Since polymers properties show dependency on the size of the chains, it is important to characterise their dimensions. This is done by measuring the *molar mass* (M) of a polymer, which represent the mass of 1 mol of polymer and it is expressed in g × mol^{-1}. This value depends on the *degree of polymerisation* (x), which is the number of repeating units in the polymer chain, multiplied by the molar mass of the repeating unit (M_0), through equation 1.

Equation 1. Molar mass of a homopolymer obtained multiplying the molar mass of the repeating unit with the degree of copolymerisation.

$$M = xM_0$$

Equation 1 can be used for copolymers if M_0 is replaced by M_0^{cop}, which is the mean molar mass of the repeating units considering the different monomers constituting it (Equation 2).

Equation 2. Molar mass of a copolymer obtained multiplying the molar mass of the repeating unit considering the monomers constituting it with the degree of copolymerisation.

$$M_0^{cop} = \Sigma x_k M_0^k$$

Where x_k represents the mol fraction and M_0^k the molar mass of the monomer "k" in the copolymer. Since a polymer is composed of chains of different sizes, their distribution is characterised in terms of average molar mass. Macromolecules forming the polymer will be grouped in discrete fractions "j" containing N_j molecules of molar mass M_j. The *number-average molar mass* (M_n) is calculated as the sum of the products of the molar mass of each fraction multiplied by its mole fraction, which is given by the ratio of N_j to the total number of molecules (Equation 3).

Equation 3. Number average molecular weight equation (M_n) equation, where the molecular mass of all polymer chains is divided by the number of polymer chains.

$$M_n = \frac{\Sigma N_j M_j}{\Sigma N_j}$$

Molecular weight can also be expressed using the *weight-average molar mass* (M_w), which considers the weight fractions instead of the number of molecules. The weight fraction is calculated as the ratio between the mass of molecules of molar mass M_j divided by the total mass of all the molecules (Equation 4).

Equation 4. Weight average molecular weight equation (M_w) equation, where the molecular mass of all polymer chains is divided by the total mass of all the molecules.

$$M_n = \frac{\Sigma N_j M_j^2}{\Sigma N_j M_j}$$

The ratio between M_w and M_n gives the *dispersity* ($Đ_M$) value, which indicates how uniform the size of the macromolecules forming the polymer is. A perfectly uniform polymer would have a $Đ_M$ of 1 but most polymers display higher values, according to the method of polymerisation. Evaluation of M_w and M_w is usually performed via size exclusion chromatography (SEC), also referred to as gel permeation chromatography (GPC). The retention time of polymers eluting through a column packed with a resin having pores of known size is evaluated against standards of known M value and narrow $Đ_M$, such as polystyrene (PS) or poly(methylmethacrylate) (PMMA).

1.2 Bulk properties of polymers

1.2.1 The amorphous state

As previously discussed, polymers that do not display any crystalline domain are denoted as amorphous and are characterised by a lack of precise molecular order. When these materials are cooled, and do not present any crystallisation, their viscosity increases, and the material flows less. When the temperature is lower than the T_g, the polymers are frozen and transition from a rubbery to a glass state, where chain mobility is significantly hindered. This transition is linked to a drastic change in the thermomechanical properties, where the material becomes more

brittle and a significant change in heat capacity is recorded.[26] Semi-crystalline materials will display a T_g relative to their amorphous region. Importantly, the recorded T_g value will depend on the heating rate, meaning that the value will depend on the experimental conditions. The glass transition is often described using the concept of free volume: at higher temperatures, materials undergo volumetric expansion, increasing the separation between the polymer chains, and therefore, the rates of molecular motion and availability of different conformational states. When the temperature is reduced, less energy will be available for molecular motion, limiting the number of conformations the chains can assume. When the temperature decreases below T_g, chain mobility is eventually hindered to the point that the polymer can be considered frozen. The T_g of polymers can be affected by different factors such as the chain flexibility, associated with the easiness of rotation along main chain bonds, as poly(ethylene oxide) displays a much lower T_g when compared to the more rigid poly(*p*-xylene).[27, 28] Another factor that affects the T_g is the presence of side chains, as bulkier side chains tend to restrict bonds rotation increasing the T_g, (Figure 4).

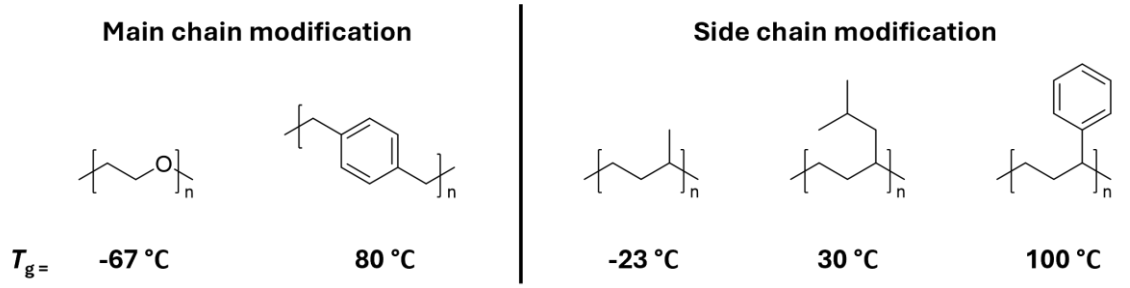


Figure 4. Factors controlling the T_g such as main chain flexibility (left) and side groups bulkiness (right).

The T_g can also be affected by molar mass, branching, and crosslinking. Increasing molar mass leads to an increase in T_g as the chain ends, which are associated with more free volume when compared with the central segments of the chains, will see a reduction in their contribution to the total free volume of the polymer. This has been observed by Singh *et al*. on polystyrene thin films *via* spectroscopic ellipsometry.[29] As branches act as chain ends, they can modulate the T_g too. Generally, an increase in branches will reduce the T_g but, when the number of branches increases significantly, the restriction imposed on the degree of freedom of the chain will significantly outweigh the contribution to the free volume, leading to an overall increase in T_g.[30, 31] A similar restriction on molecular motion is exerted by crosslinking, which leads to an increase in T_g. Another aspect influencing the T_g is the thickness of the polymer film as it has been demonstrated that the onset of molecular mobility, *i.e*. transitioning to the rubbery state, happens at a lower temperature on the surface of a polymeric film than in its bulk.[32] This is explained by the fewer constraints associated with the surface layer of the polymer, and it has been measured on various polymers such as poly(α-methylstyrene)[33], PMMA[34], and polystyrene.[29, 32] The onset of molecular motion at the T_g is studied by macromolecular dynamics, and it is stated that a long polymeric chain can move according to two different processes. The chain can change its conformation without moving its centre of mass, or it can move its centre of mass relatively to the position of neighbouring chains. Both these motions occur through thermal activated Brownian motion, and they are limited by the physical constrained imposed by the mesh.[35] The two main theories associated with the motion of

polymer chains are the Rouse-Beuche theory and the De Gennes reptation theory.[36] One of the main differences associated with these theories is the different degree of dependency of the viscosity of the polymer (η) on the molar mass. In fact, the Rouse-Bueche theory underestimates this dependency when the molar mass of the polymer is above a certain threshold (high molecular weight polymers) and was found to agree with experimental values only in highly diluted polymeric solution or with polymer of low M_w. The change in behaviour happening at higher molecular weight can be explained by the concept of chain entanglement, as the chains grow longer, they will entangle as a consequence of their uncrossability given their covalently bonded backbones. The entanglement can act as a physical cross-linker, thus, higher energy is necessary for its unravelling, enhancing the stress of the material.[35]

1.2.2 The crystalline state

Depending on the chemical structure and physical factors such as molecular weight and branching, polymers can form crystalline, *i.e.* ordered, domains when they are cooled below their T_m. Crystallisation happens if the entropy penalty associated with an increase of order in the system is offset by the reduction in enthalpy (H), leading to a negative Gibbs free energy (G) value.[35] The degree of crystallinity and the size of the crystals have a profound effect on the thermomechanical properties of the material, hence controlling this phase is paramount in modulating the thermomechanical properties of polymers. Since crystallisation is a thermodynamic process, it is possible to control it by changing

the rate at which the polymers are being cooled. Upon rapid cooling, the crystallisation process is controlled by kinetics, and in certain cases, it is possible to prevent the polymers from crystallising altogether. On the other hand, crystallisation can be induced by annealing, where the polymer is heated at a temperature between its T_g and T_m.[37, 38] Different factors play a role in polymer crystallisation behaviour. For example, symmetric polymers, such as homopolymers, tend to crystallise easier than co-polymers, as the sequence of crystallisable units can be interrupted by co-monomer units unable to crystallise.[39] Another factor influencing the formation of crystalline domain is the tacticity of the polymer, meaning the orientation of side groups along the main chain. Generally, isotactic and syndiotactic polymers will crystallise, while atactic polymers will not.[35] However, this is not always true: Coates and co-workers reported a series of synthetic polyhydroxyalkanoates (PHAs) of tacticity-independent crystallinity.[40] In fact, the syndiotactic, isotactic, and atactic polymers all displayed high melting points and similar crystal structures (Figure 5). Since covalent bonds control the spatial arrangement of a chain in space, while secondary interactions (*e.g.* hydrogen bonding, van der Walls forces…) control the orientation of different segments towards each other, drawing structure-properties relationships encompassing all different kinds of polymer structures represent a very challenging task.

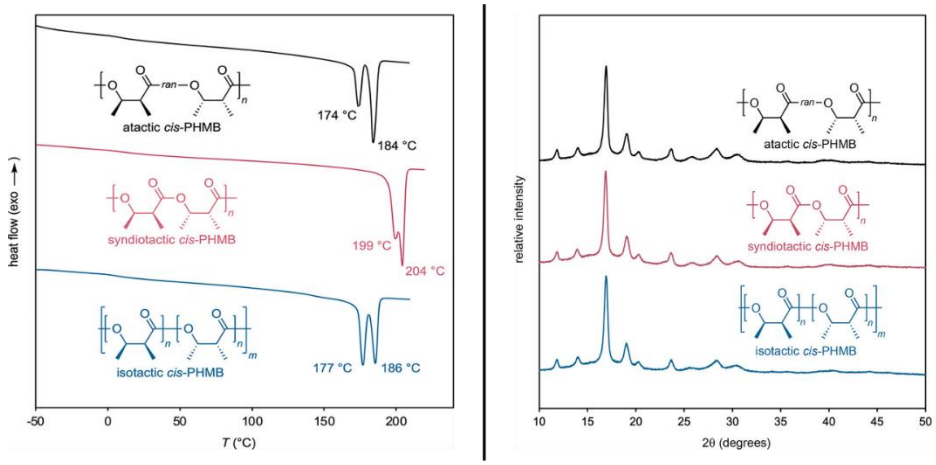


Figure 5. Stacked DSC thermograms (left) and stacked powder X-ray diffraction patterns (right) of atactic, syndiotactic, and isotactic PHAs all showing formation of crystalline domains. Reprinted (adapted) with permission from *J. Am. Chem. Soc*. 2023, 145, 48, 25983–25988. Copyright 2023 American Chemical Society.

The morphology of the crystals obtained depends on the conditions under which the polymer was crystallised. Common morphologies are bidimensional lamellae that can extend into spherulites when growing in the third dimension.[41] Notably, because of their size, numerous conformations available, and chain entanglement, polymers almost never form a perfect crystal, they instead display crystalline regions presenting defects, the amorphous phase. Nonetheless, it is possible to estimate a degree of crystallinity (x_c) for each polymer by comparing them with a completely crystalline analogous, when present. This is calculated by comparing their respective enthalpy of melting (ΔH_m), accordingly to equation 5, where ΔH_m is the value obtained experimentally, ΔH_c is the experimental enthalpy of crystallisation, and ΔH_m^0 is the value associated with a perfectly crystalline polymer.[42]

Equation 5. Evaluation of the degree of crystallinity by comparison of the enthalpies of melting and crystallisation.

$$x_c = \frac{\Delta H_m - \Delta H_c}{\Delta H_c^0}$$

This value is of technological importance as it dictates numerous properties such as melting temperature and mechanical behaviour.[43, 44] A common example would be polyethylene (PE), where linear high-density polyethylene (HDPE) and branched low-density polyethylene (LDPE) display different degrees of crystallinity, $x_c \geq 90\%$ and $x_c = 50/60\%$, respectively.[45] The melting temperature of the crystals limits the practical use of polymeric materials, as they do not retain mechanical stability at temperatures above T_m. Generally, factors controlling the T_g affect the T_m in the same way, as both are primarily influenced by main-chain stiffness and branching. T_m can be further controlled by the presence of polar groups such as the amide group, as exemplified by the different T_m of nylon 6.6 (T_m = 265-280 °C) and nylon 7.7 (T_m = 196-214 °C). While in homopolymers it is virtually impossible to control these two variables independently, co-polymers emerge as a possibility to better control these parameters.[46, 47]

1.2.3 Measurement of thermal properties

The most common technique used to characterise crystallinity and thermal properties (T_g & T_m) of polymers is *differential scanning calorimetry* (DSC). Going above T_g means changing the heat capacity of the polymer. During this pseudo-second order transition, measured in a heat -flux DSC, the enthalpy does not change and can be detected by an endothermic shift of the baseline. This is because the heat capacity of the polymer increases as it changes from the glassy to the rubbery state.[26] The value of T_g is usually taken as the onset temperature of this event. Crystallinity is observed by detection of a first-order transition (melting)

displayed as an endothermic peak during the heating cycle and as an exotherm (crystallisation) upon cooling. Crystallisation can also happen upon heating, usually at temperatures between T_g and T_m. The change of enthalpy (ΔH) associated with the phase transition is given by the ratio between the area of the peak (usually expressed in W K [J K s^{-1}]) and the heating/cooling rate (Figure 5).

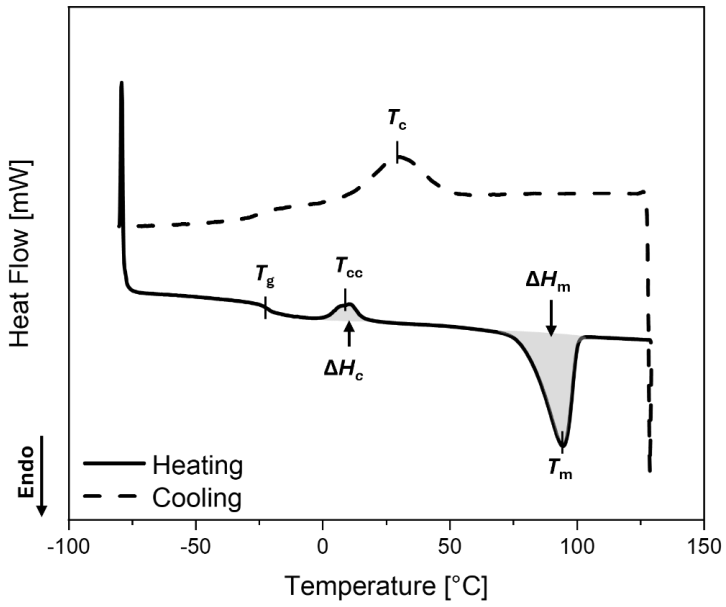


Figure 6. Typical DSC run of a semi-crystalline polymer. Heating run (solid line), cooling run (dashed line), glass transition temperature (T_g), crystallisation events (T_c & T_{cc}), melting temperature (T_m).

Another important parameter is the thermal stability of polymers and can be obtained by thermal gravimetric analysis (TGA) *i.e.* at what temperature the mass of the polymer starts decreasing indicating thermal degradation.

1.2.4 Measurement of mechanical properties

The mechanical properties of polymers are assessed by their response to a variety of mechanical stresses (σ) such as shear, compression, elongation, and bending. In response to an applied force, atoms change their position known as strain (ε), and at low values, ε is proportional to stress, expressed by Hooke's law. Hooke's law allows the measurement of the material resistance against uniaxial extension or compression, known as Young's modulus (E). This value is obtained by the ratio between stress and strain (Equation 6). However, polymeric materials obey Hooke's law only at low strain because of a phenomenon named yielding. The yield point of a material corresponds to the onset of permanent plastic deformation, and the material is not able to return to its original shape after the stress is removed.

Equation 6. Formula describing the calculation of Young's modulus.

$$E = \frac{\varepsilon}{\sigma}$$

Generally, mechanical performances are studied by tensile testing. This allows evaluation of properties such as stiffness, strength, elasticity, and toughness (Figure 6A). Different polymers will display different stress *vs.* strain curves when tested by uniaxial tensile testing. Usually, amorphous polymers tend to have low Young's moduli and show flexibility (high stretchability) but low strength when compared to their semi-crystalline counterparts. Semi-crystalline polymers can be considered similar to composite materials where the mechanical properties depend on the combined modulus of the amorphous and crystalline region. When the crystalline domain becomes predominant, polymers gain in strength but

generally, their flexibility decreases leading to brittle materials (Figure 6B).[48, 49] The temperature at which the polymer is tested, *i.e.* above or below T_g, and the presence of non-covalent interactions can also play a role in determining the stress *vs*. strain profile.

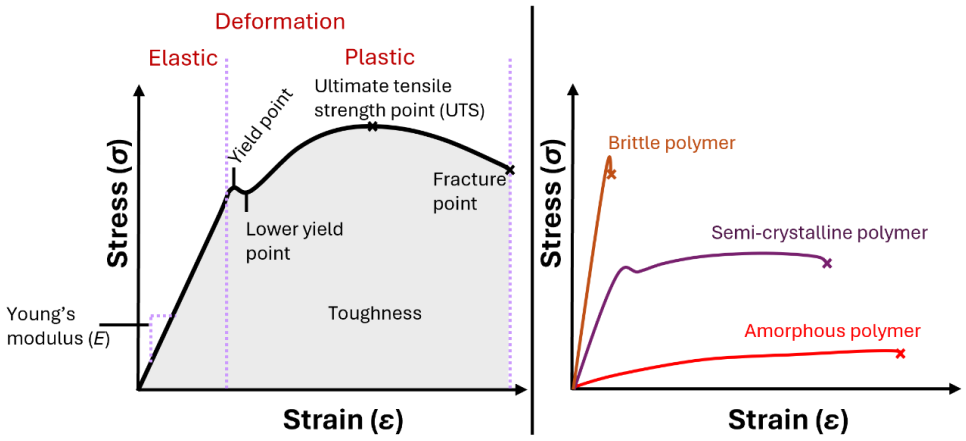


Figure 7. Exemplary stress vs. strain curve with the deducible properties (left). Stress vs. strain curves of different polymers (right).

Another way to assess mechanical properties is through Dynamic Mechanical Analysis (DMA), where a polymer is subjected to an oscillating force at constant temperature (isothermal) or across a certain range (dynamic). Most materials will display a viscoelastic response (Complex modulus, *G*) that is separated into the elastic component (Storage modulus, *G'*) and viscous component (Loss modulus, *G''*). The ratio between G'' and G' is the dampening factor (tan δ) and it represents the tangent of the phase angle between the application of the stress and the response of the material and can also be used to identify the T_g (Figure 7). The closer this angle is to 90 degrees the greater the viscous behaviour of the material. Generally, linear polymers will begin to flow at certain temperatures, which is highlighted by a great drop in the storage modulus after a plateau region. Common

thermosets do not display this behaviour in light of their crosslinked nature. However, certain crosslinked polymers referred to as covalent adaptable networks (CANs) can flow because of the presence of dynamic bonds.[50]

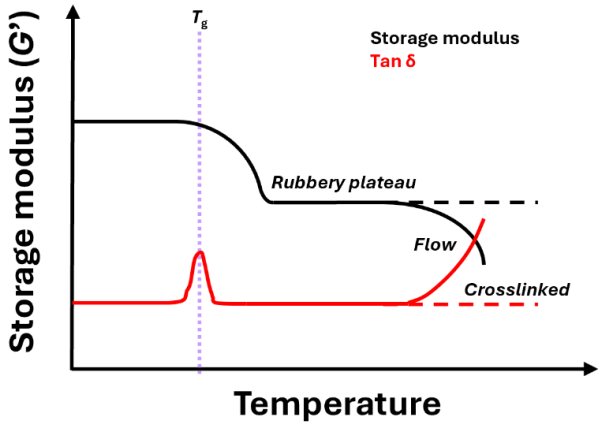


Figure 8. Schematic representing typical DMA thermograms with storage modulus and tan δ plotted against temperature. T_g highlighted.

1.3 Polymerisation techniques: step growth polymerisation

According to how monomers are linked during the polymerisation process, two main classes of polymerisation reaction can be found, step-growth polymerisation; if the polymer grows from the stepwise reaction of any two species in the reaction mixture, and chain growth polymerisation; when the polymer chain forms after the reaction of the monomer with a reactive end-group.[51] This mechanistic difference is evident when the degree of polymerisation is plotted against functional group conversion (Figure 8). In step-growth polymerisation, a high degree of polymerisation can be reached only at very high conversion, even if monomers are

consumed at a very early stage. Inversely, in chain-growth polymerisation a high degree of polymerisation can be reached at low monomer conversion, as a great number of monomers rapidly react on the reactive-end of a growing chain until termination. Thus, as polymerisation proceeds, the number of polymer chains increases.

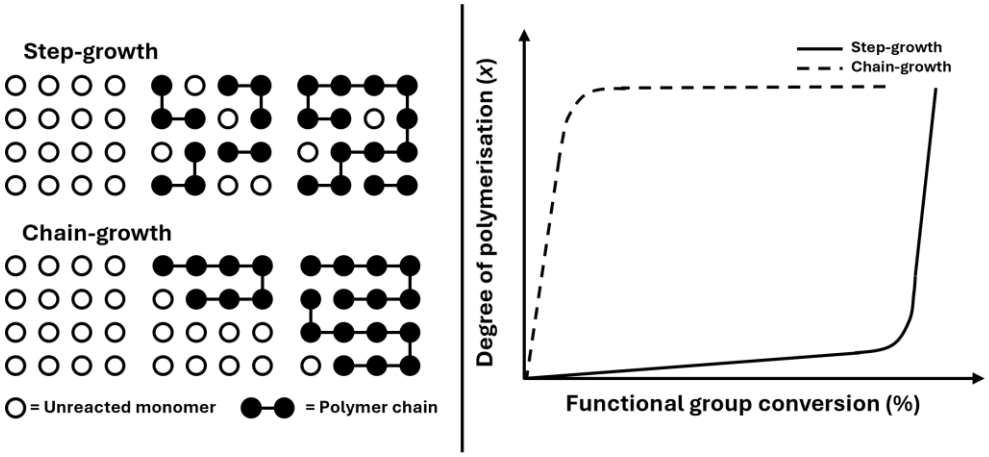


Figure 9. Cartoon exemplifying the mechanistic difference between step-growth and chain-growth polymerisation (left) and typical plot of degree of polymerisation *vs*. functional group conversion of the two types of polymerisations (right).

1.3.1 Step-growth synthesis of linear polymers and networks

Polymerisation reactions producing polymers in a step-growth fashion can be broadly classified into polycondensation, where the formation of a link is associated with the elimination of a small molecule (*e.g.* water, methanol…), or polyaddition, where two monomers react together without the elimination of other molecules. A typical example of polycondensation would be the production of polyesters *via* condensation reaction between diols and difunctional carboxylic acids, with one molecule of water being eliminated for each ester bond being

formed, while the synthesis of polyurethanes reacting diols with diisocyanates is an example of polyaddition reaction. Step-growth polymerisations, both polycondensation and polyaddition, are described according to the Carothers theory or the statistical theory. In both cases, the principle of equal reactivity of functional groups is assumed. This principle, first proposed and demonstrated by Flory[52], states that the reactivity of the active chain-end(s) of a growing chain is equivalent to the one of the monomer, making it independent from the degree of polymerisation. Considering a polymerisation of two generic monomers A and B containing 2 functionalities each, according to the Carothers theory, the number-average degree of polymerisation (x_n) can be calculated using the extended Carothers equation (Equation 7), where *r* represents the reactant ratio, *i.e.* the ratio of the numbers of the two different types of functional groups present initially, and *p* is the extent of reaction at time *t*, which is obtained dividing number of functional groups that have reacted with the number of functional groups present initially.

Equation 7. Extended Carothers' equation.

$$x_n = \frac{1 + r}{1 + r - 2rp}$$

From this equation, it is possible to observe that a drastic reduction in x_n happens whenever *r* is less than a unity. Hence, monomers used for step-growth should have high purity to access polymerisation reactions with high selectivity. However, if high conversion can be reached, slight stoichiometric imbalances can be used to place an upper limit on the attainable x_n thus controlling the molecular weight of the resulting polymer. On the other hand, the statistical theory, or Flory-Schulz

distribution, allows prediction of the degree of polymerisation distributions, either by weight- or mole-fraction distribution, at different *p* values.[53] A complication of step-growth polymerisation processes is represented by ring formation from the intramolecular reaction between two extremities of a growing chain, leading to high dispersity and low molecular weight.[35] The probability of these structures forming is highly dependent on ring size; the formation of small rings (≤ 4-membered rings) is energetically unfavoured as a consequence of the high strain, while larger rings (≥ 12-membered rings) may not form because the probability of two chain-ends to meet decrease as their distance increase. Since cyclisation is a unimolecular process, while polymerisation is a bimolecular process, the latter can be favoured by increasing monomer concentrations. In fact, many step-growth polymerisations are conducted in bulk.[54] When the step-growth is conducted with at least one monomer with more than 2 functionalities, a network can be obtained with different properties than its linear counterpart. While the synthesis of linear polymer is linked to the formation of viscous solutions, the formation of polymer networks is recognised by a gelation event. The gel point is the point at which the first network molecule is formed, and the solution goes from viscous to solid gel with no tendency to flow. Commonly used polymer networks produced in a step-growth manner are epoxy resins that find application as coatings or in composites, or polyurethanes often in the form of foams. As for the linear polymers, Carothers theory and statistical theory can be used to predict the gel points, but only if the principle of equal reactivity is perfectly respected. Generally, these theories yield lower gelation points values when compared to the experimental ones, as the

formation of loops or other structural defects can affect and the reaction should proceed to higher conversion to compensate for the loss of functional groups.[35]

1.4 Click polymerisation: nucleophilic X-Yne addition

The introduction of the concept of click chemistry by Sharpless and co-workers[55] revolutionised the way chemistry is conducted in many fields, from drug discovery to material science. Ultimately, this has been acknowledged with the attribution of the 2022 Nobel Prize in chemistry to Sharpless, Bertozzi, and Meldal for their efforts in the development of this field, and biorthogonal chemistry. The key feature of click chemistry is the focus on building new properties rather than structures, coupled with efforts to leverage reactions that do not require hard-to-obtain skills or equipment. To be classified as "click" process, a chemical reaction must be modular, stereospecific, possess a wide scope, high yielding, and in case byproducts are generated they should be harmless and able to be removed by non-chromatographic methods. Thus far, many reactions falling under the "click" umbrella have been reported, such as nucleophilic ring opening processes (epoxides, aziridines, episulfonium ions...), "non-aldol" carbonyl chemistry (production of ureas, thioureas, amides...), cycloaddition reactions of unsaturated species (1,3-dipolar cycloaddition, Diels-Alder reaction, azide-alkyne cycloaddition...), and additions to carbon-carbon multiple bonds (epoxidation, sulfenyl halide addition, Michael additions...).[56]

The use of highly efficient click reactions in polymer synthesis plays an important role in achieving more sustainable polymeric materials, as it maximises atom economy, reduces chemical hazards, and lowers energy consumption.[57] Whereas traditional step-growth processes succeed in inserting heteroatoms in the polymer backbone, which is desired as they can increase the degradability of the materials, they generally require harsh conditions, such as high temperature or vacuum, for prolonged periods of time. As such, many efforts have been devoted into exploring alternatives that would enable obtaining high molar mass polymers in high yield under milder conditions.[58]

Among the plethora of reactions reported, nucleophilic Michael addition to activated alkynes represents an interesting platform for polymer synthesis. These reactions, belonging to the class of heteronucleophilic 1,4-conjugated addition, combine the efficiency of typical click reaction with the possibility of introducing heteroatoms into the polymer backbone.[59] While thiols are the most used considering their enhanced nucleophilicity, they are usually expensive and not abundant in natural products but can be accessed through chemical transformations. On the other hand, amines and alcohols are generally cheaper and more abundant and can also be found in natural compounds. The drawback associated with the use of hydroxyl groups is the diminished nucleophilic character that leads to reduced efficiency. Propiolates represent the most used Michael acceptor because of their simple accessibility and highly tuneable structures together with ynones, propiolamides, propiolnitrile and ethynylsulfones.

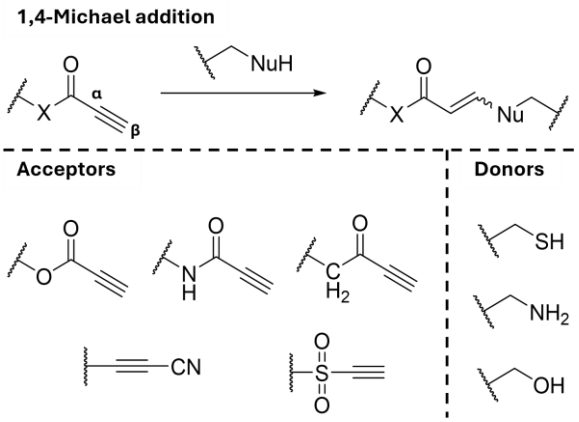
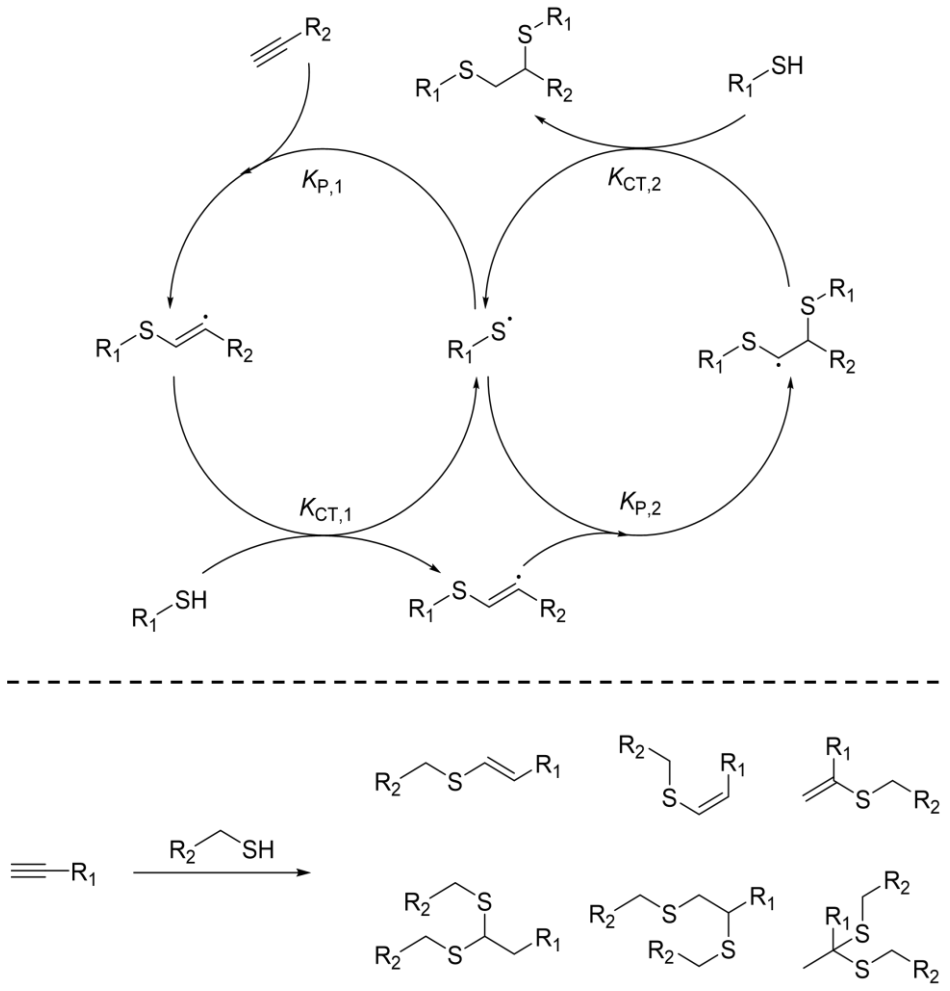


Figure 10. 1,4-Michael addition to an activated alkyne (top box), structures of commonly used Michael acceptors (box bottom left) and Michale donors (box bottom right)

1.4.1 Thiol-yne polymerisation

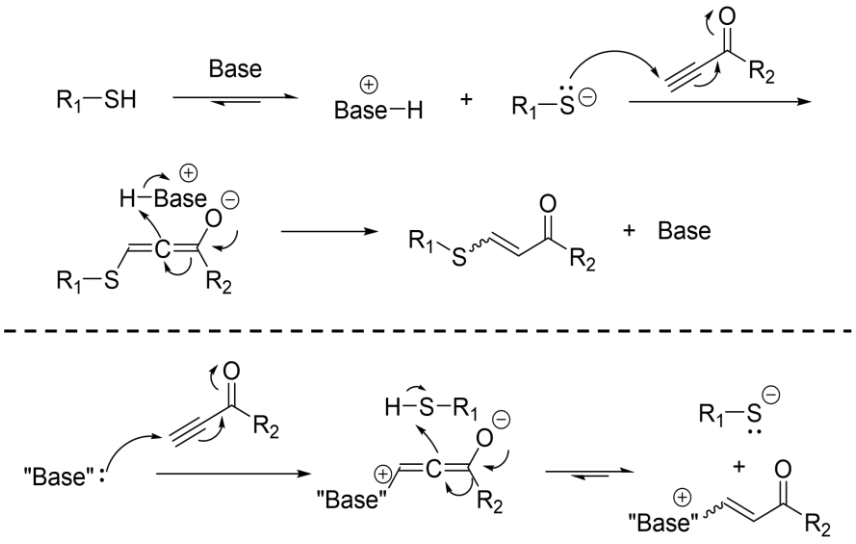
Similarly to the thiol-ene addition, the addition of a sulfur atom to an alkyne can happen following a radical or a nucleophilic mechanism. The radical-mediated thiol-yne reaction has been pioneered by Bowman and co-workers for the production of polymeric networks.[60] The reaction mechanism was analogous to the radical thiol-ene reaction, where the propagation of a thiyl radical with an alkyne or a vinyl group is followed by chain transfer of the radical to another thiol (Scheme 1).[61] Despite this method being optimal to obtain high crosslinking density materials, this process lacks in control over the attainable product. In fact, the secondary addition to the vinyl moiety possesses a higher rate than the initial one,[62] hence it cannot be used to produce linear polymers. Moreover, as a consequence of the possible migration of the formed radical, up to six possible products can form, thus disqualifying this reaction from meeting the click criteria (Scheme 1).[63]



Scheme 1. Sequential addition and hydrogen abstraction steps of a primary alkyne and vinyl sulfide during a radical thiol-yne polymerisation (top). Different products are formed from radical thiol-yne addition (bottom).

The nucleophilic thiol-Michael reaction, on the other hand, offers greater control over the double addition product because of the preferential attack of the nucleophile to the alkyne, even in the presence of a vinyl sulfide and excess of thiols.[64] However, electron-deficient alkynes must be employed for this reaction to be high-yield and effective; in fact, the increased electron-withdrawing character of the functional group leads to higher yields.[65] Several catalysts have been probed to promote this reaction; these include stoichiometric sodium,[66] inorganic-based reagents such as BF_3[67] or NaH,[68] and neutral alumina.[69] However, these did not

prove as effective as organo-catalysts such as amines and phosphines.[70-73] The reaction seems to proceed *via* two main pathways, depending on the nucleophilicity of the catalyst. Sufficiently strong bases, without notorious nucleophilic character, can deprotonate the thiol to form a nucleophilic thiolate, but the catalyst can also attack the electron deficient alkyne to form an allene enolate that is responsible for the deprotonation of the thiol (Scheme 2).



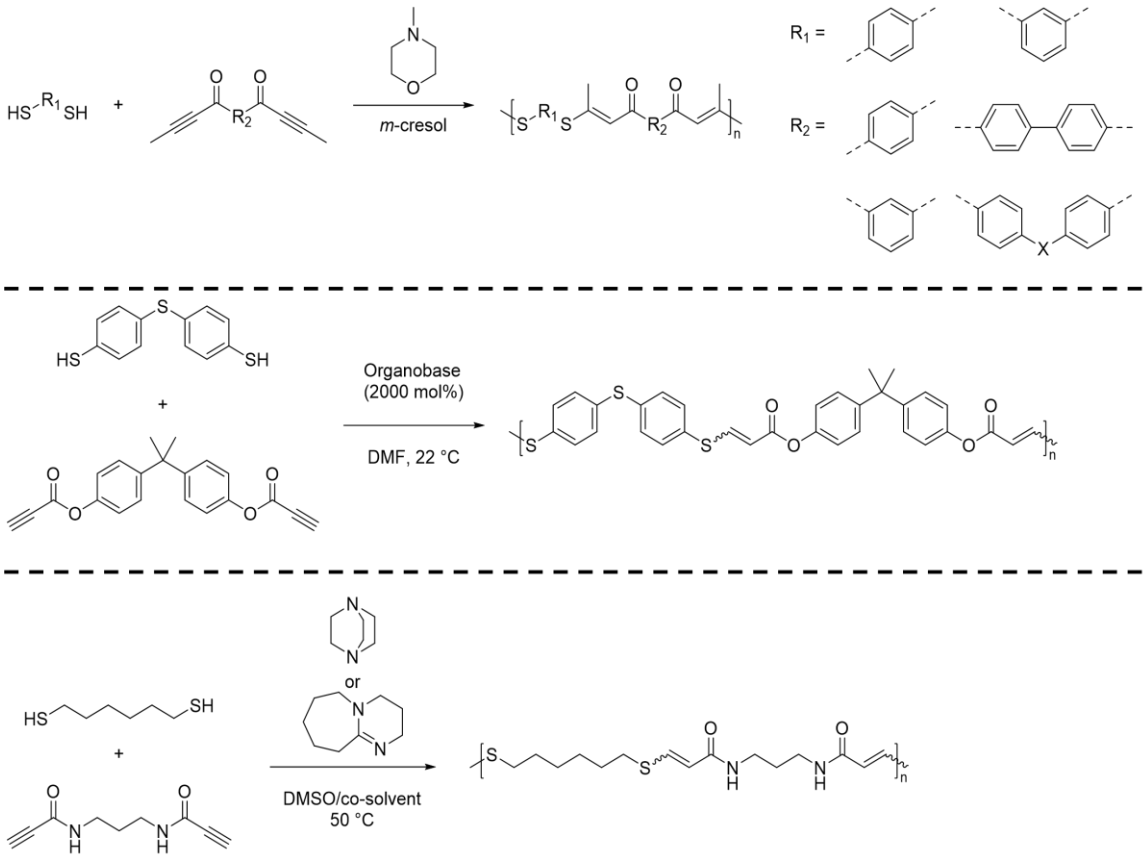
Scheme 2. Base catalysed thiol-yne Michael addition where the base deprotonate the thiol to form a reactive thiolate (top) or where the base attacks the alkyne to form an allene enolate responsible for the deprotonation of the thiol (bottom).

As can be seen in the mechanism, *cis* or the *trans* isomers can be formed during the reaction, after isomerisation of the allene intermediate. Interestingly, it was found that the catalyst and solvent choice can induce the formation of one of them. As an example, the reaction between dodecane-1-thiol and ethyl propiolate catalysed by triethylamine (Et_3N) yielded almost quantitatively the *trans* product (97%), however, switching the catalyst to stronger bases, such as 1,8-diazabicyclo(5.4.0)undec-7-ene (DBU) or 1,5,7-triazabicyclo 4.4.0 dec-5-ene (TBD),

the *cis* isomer was obtained as the major product in both reactions (80% and 90%, respectively). When the reaction was performed in non-polar or moderately polar solvents such as benzene or chloroform, the *E*-adduct was isolated predominantly (*trans*>97%), while the *Z*-isomer was the major product (*cis*>66%) when the reaction was performed in more polar solvents such as acetonitrile and DMSO.[70] The electron density of the Michael acceptor is also responsible for the preferential formation of a stereoisomer. Shiu *et al*. reacted a protected cysteine with several activated alkynes and observed that the *E*/*Z* stereoselectivity was correlated to the electron density of the acceptor: propiolamide gave the highest *Z* content, followed by propiolate and then aryl ynone.[65]

In light of these findings, the nucleophilic thiol-yne reaction has been used in polymer synthesis to produce a broad range of materials such as conjugated polymers synthesised from aromatic thiols and ynones[74], linear polyesters obtained from aromatic dithiol and aromatic dipropiolates[75] and linear polyamides (Scheme 3).[76] Moreover, the possibility of controlling the alkene isomerism was used to modulate the crystallinity of the polymer, implying that it is possible to obtain a material with different thermomechanical properties without changing the composition of the polymer.[77] Finally, the resulting double bond of the single addition can be used as a handle for post-synthetic functionalisation, for example through vulcanisation. Durmaz and co-workers reported an interesting approach where different dithiols were reacted with an activated internal alkyne to produce polythioethers, the polymer obtained could be effectively depolymerised after the addition of monofunctional thiol and TBD.[78] This reaction can also be used to

functionalise polymeric materials as a consequence of its high efficiency, as demonstrated by Patton and co-workers to attach groups of different polarity to bottlebrush polymers generated *via* surface-initiated photopolymerisation.[79]



Scheme 3. Polymers synthesised *via* organobase catalysed nucleophilic thiol-yne addition. Conjugated polyketone[74] (top), aromatic polyester[75] (middle), aliphatic polyamide[80] (bottom).

Alongside linear polymers, the nucleophilic thia-Michael addition to activated alkyne has also been used to produce crosslinked materials. Given the tolerance of this reaction to moisture, mechanically strong hydrogels with tuneable pore size based on multiarms PEG-thiols or PEG-propiolates have been reported.[81-83] Likewise, backbone stereoisomerism resulting from the addition reaction was demonstrated to modulate the mechanical performances of the gels.[83] Lastly, thiol-functionalised alginates were introduced in gels showing the potential of this

reaction to create value-added product from naturally available starting materials.[84] More recently, the dynamic nature of the second thiol-addition has been exploited in hydrogels[85] and thermosets[64] to produce dynamic materials (Figure 10). These materials were able to flow under stress (shear-tinning behaviour) or at high temperatures. These works showed that the exchange reactions could be tuned by varying the electronic profile of the alkyne, thus allowing the synthesis of materials with different stress-relaxation profiles.

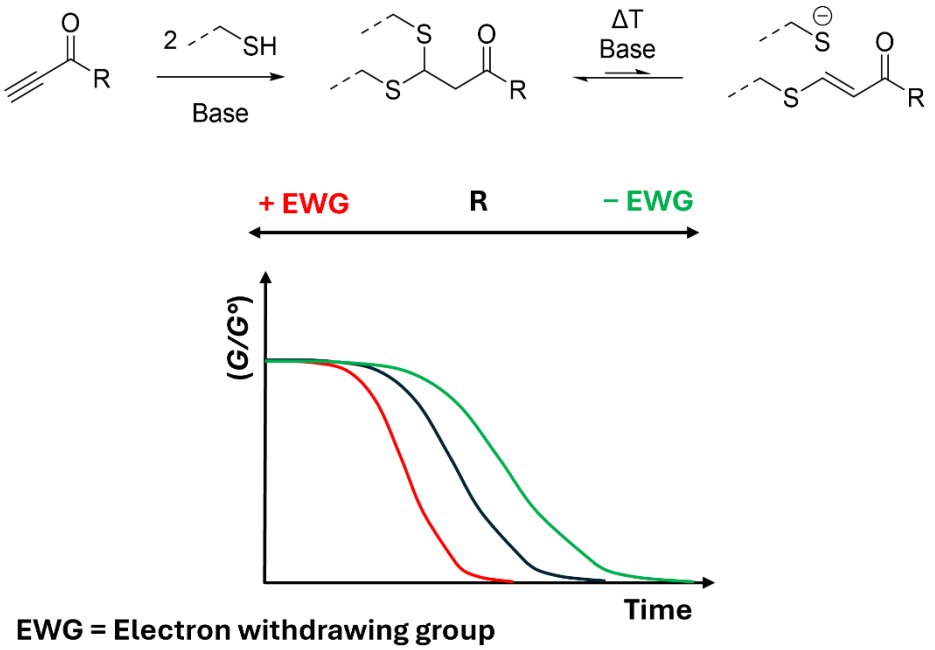


Figure 11. The dynamic nature of the second addition enables the synthesis of dynamic materials with tuneable exchange rates according to the electronic of the activated alkyne.

1.4.2 Phenol-yne polymerisation

Despite being one of the most used functional groups in organic chemistry, the diminished acidity and nucleophilicity of the hydroxyl group when compared to thiols make this moiety less prone to react in Michael additions, and consequently, less explored. Nevertheless, with the appropriate catalyst and suitable conditions,

hydroxyl- or phenol-yne reactions can undergo click reactions. As expected, primary alcohols were the most reactive, whereas when secondary or tertiary alcohols are used the reaction rarely goes to completion.[86] Like the thiol-yne reaction, the hydroxyl-yne addition largely favours the formation of *E* adducts, and the influence of solvent polarity seems reduced, as observed by Inanaga *et al*. when benzyl alcohol and methyl propiolate were used in the reaction.[87] The authors found that when the reaction was catalysed by triphenylphosphine, the quantity of *E*-product recovered was between 75 and 83%, despite great differences in solvent polarity. Moreover, when the reaction was catalysed by tributylphosphine, absolute stereoselectivity for the *E* isomer was observed, but 70% of *Z* isomers could be isolated when the reaction was performed using propiolamide as a substrate.[88] Notably, the authors observed that the hydroxyl-yne addition was dynamic when conducted with phenols, in highly polar solvents.

In regards to its application in polymer chemistry, this conjugate addition has been pioneered by Endo and co-workers, who explored phosphine-catalysed reactions to produce a wide range of ynones from bifunctional acetylenes, obtaining a library of polymers of modest molecular weight (up to 20 kDa) with almost exclusively *E* content.[89, 90] Recently, Tang and co-workers reported organic bases such as 4-dimethylamino pyridine (DMAP) and 1,4-diazabicyclo[2.2.2]octane (DABCO) can be used to catalyse the hydroxyl-yne reaction to produce stereoregular (*E*) polyesters and polyketones with high molecular weight (up to 35 kDa) and thermal stability (>259 °C).[91, 92] In light of their modularity and selectivity, thiol- and hydroxyl-yne polymerisation have been used to produce sequence-

defined macromolecules for information storage by Song *et al.*[93] Lastly, the same group expanded their work into the development of cross-linked polymer networks possessing shape-memory properties by reacting bifunctional propiolates (aliphatic and aromatic) with hydroxyl-terminated four-arms macromers.[94]

1.5 Stereochemistry in polymers

Natural sources offer a great diversity of functionalities and stereochemistry such as amino acids, known to possess divergent physico-chemical properties, that are already used in polymer synthesis and can be obtained through sustainable pathways.[95-97] The influence of stereochemistry over the effect of small molecules – such as drugs – or larger and more complex biological systems is well-known. For example, L-β-blockers showed greater potency in blocking β-adrenoceptors than their dextrorotary-isomer,[98] and the enantiopure S-omeprazole provided greater therapeutic benefit for gastroesophageal reflux disease (GERD) treatment as compared to the racemic mixture.[99] Another example is DNA, for the double helix to be formed correctly the stereochemistry of the deoxyribose moieties in the backbone should be respected. In natural polymeric materials, differences in stereochemistry lead to differences in the mechanical properties as shown in natural rubber (*cis*-polyisoprene) and gutta-percha (*trans*-polyisoprene) (Figure 12). Gutta-percha is hard and brittle while natural rubber is amorphous, soft, and flexible with a T_m almost three times greater than gutta-percha. This difference in thermal properties can be explained as *cis* configuration allows for better packing

of the polymer chains when the material is stretched, thus imparting greater elasticity.[100]



***trans*-1,4-polyisoprene** ***cis*-1,4-polyisoprene**

Figure 12. Chemical structure of gutta percha (left) and natural rubber (right).

Despite the promising findings on the influence of stereochemistry on material properties, this topic is still not fully explored. Moreover, as increased efforts are devoted into building polymers out of renewably sourced monomers, which are often rich in stereocenters, it is likely that modulation of polymers' properties *via* stereochemistry will become more attractive in the future. Currently, new material properties are obtained by leveraging different chemical groups or substituents in the polymer chains, however, the control over the spatial arrangement of atoms can also be crucial to tune the material's performance. In fact, by controlling the stereochemistry of polymer chains, how polymer chains are packed and ordered can be modulated, leading to polymers with different degrees of crystallinity, and thus different thermomechanical properties. Accessing different thermomechanical properties without significant changes in composition could prove useful in simplifying waste treatment once a material is discarded. Nowadays, different stereocontrolled polymers are already being used such as polypropylene (PP), where its physical properties are deeply dependent on the orientation (tacticity) of the pendant methyl groups along the main polymer chain, allowing the crystallinity to be adjusted. Therefore, isotactic PP is a hard

thermoplastic, possessing a T_m of 160 °C, while atactic PP is rubbery and amorphous with poor mechanical properties.[101] By synthesising PP containing both amorphous and crystalline segments in different ratios it is possible to tune its properties.[102]

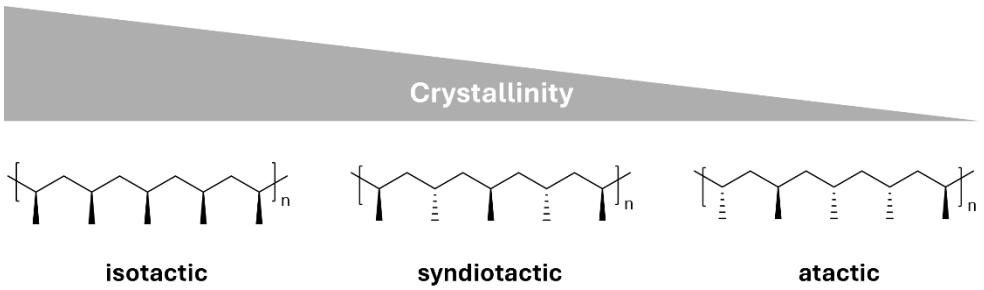


Figure 13. Chemical structure of polypropylene molecules of different tacticity associated with decreasing level of crystallinity (from left to right).

Among all bio-sourced molecules, lactic acid is arguably the most widely used in polymer chemistry, and it serves as a hallmark example of a bio-sourced low-cost monomer feedstock.[103-105] Lactic acid possesses a chiral carbon atom, hence lactide, the cyclic diester of lactic acid, possesses two stereocenters and three diastereomers: *meso*-lactide, L-lactide, and D-lactide (Figure 14).

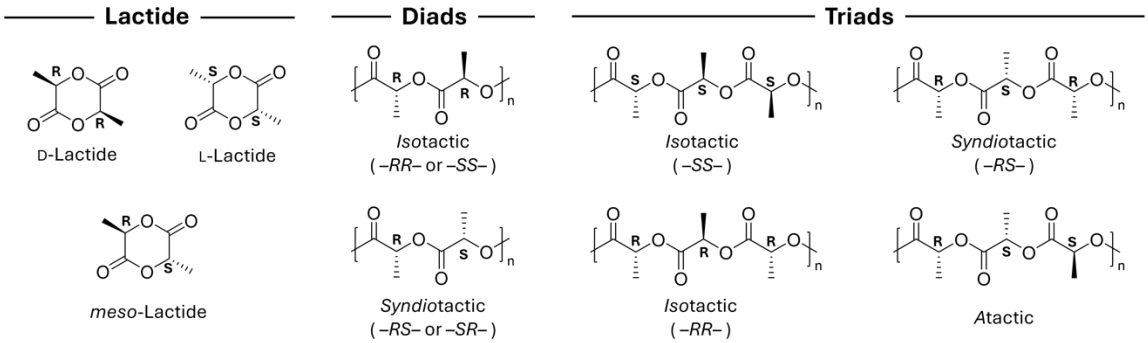


Figure 14. Chemical structure of lactide diasteroisomers and tacticity of diads and triads of PLA molecules.

When the isomers are polymerised, several macromolecules, with different microstructures can be obtained depending on how the stereocenters are

distributed in the polymer backbone (e.g. isotactic and heterotactic PLAs). Thereby, polymers with different physicochemical and thermomechanical properties can be obtained. Examples are heterotactic PLA which is usually amorphous with a T_g of ≃30 °C,[106] semi-crystalline enantiopure isotactic PLA (PLLA) with a T_g of ≃55 °C and a T_m of ≃175 °C.[107] Notably, a mixture of equivalent quantities of PLLA and PDLA possess a similar T_g when compared to PLLA only, but a much greater T_m of ≃230 °C.[108] Similarly to PLAs, polyhydroxybutyrate (PHB) can also present different thermal properties according to its microstructure with a decrease in the T_m value when the isotactic fraction in polymers was diminished.[109]

The influence of *cis*-*trans* stereoisomerism on polymer properties can be translated from natural polymers to synthetic ones. Alkene-containing polymers with tuneable *cis*/*trans* ratios – hence different mechanical properties - were obtained from the thiol-yne step-growth polymerization of propane-1,3-diyl dipropriolate with bis(3-mercaptopropyl) succinate and/or with 1,6-hexane dithiol.[110] The authors found that increased *cis*-alkene led to content higher Young's modulis, decreased strain at break, and slower degradation rates (Figure 14A). Furthermore, this concept has been used to modulate properties of different polymers' classes. For example, stress and strain at break of poly(ester-urethane)s[111] was found to diminish with increased *cis*-content (Figure 14B), while the Young's modulus was found to increase with increasing *cis*-content in polyamides (Figure 14C).[80] As the variation in properties does not follow a unique trend with varying *cis*/*trans* content, *e.g.* materials get always stronger with

increased *trans* content, it means that functionality of the polymers also play a major role in the influence of stereoisomerism on thermomechanical properties.

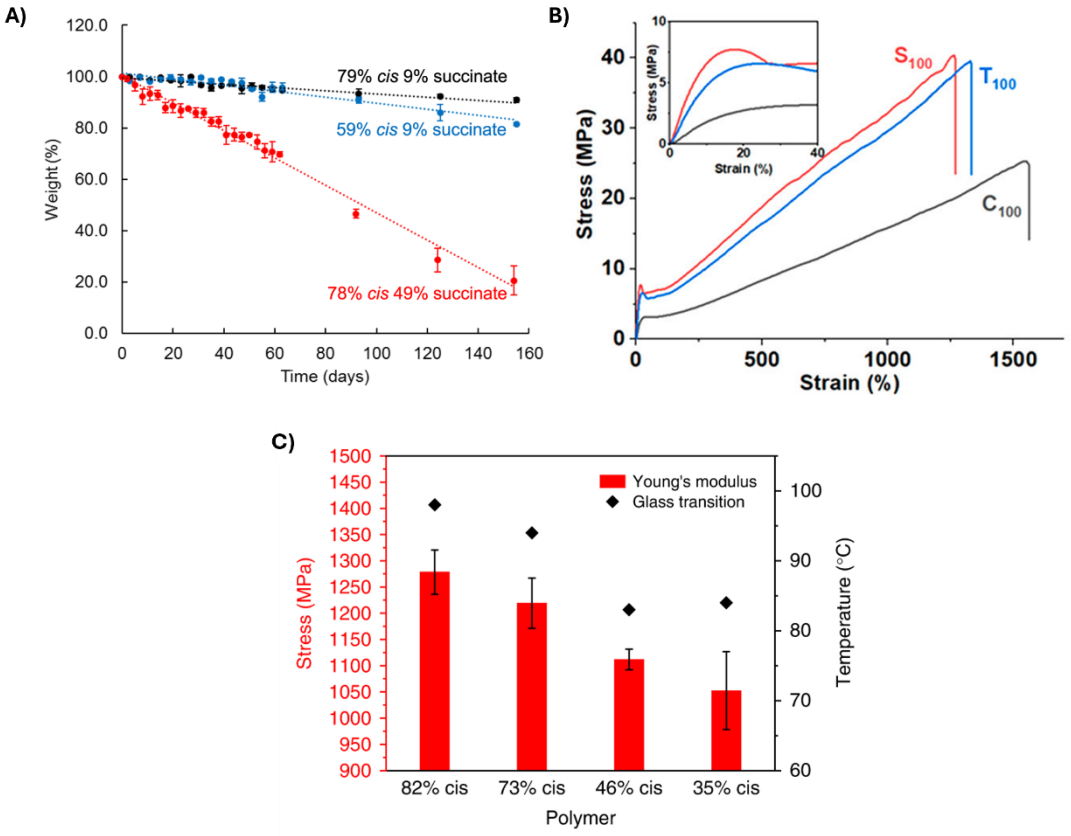


Figure 15. A) Polymers degradation rates dependent on *cis* content and composition. Adapted from ref. 66 reproduced under a Creative Commons Attribution 4.0 International License. B) Stress *vs*. strain curves of polymers having different backbone *cis*/*trans* isomerism showing that the *trans* polymer (T_{100}) is stronger than the *cis* polymer (C_{100}). Reprinted (adapted) with permission from *Macromolecules* 2020, 53, 1, 174–181. Copyright 2020 American Chemical Society. C) Young's modulus and T_g values found for different *cis* content in polyamides. Adapted from ref. 35 reproduced under a Creative Commons Attribution 4.0 International License.

Polymers containing ring-based moieties also feature *cis/trans* isomerism as a consequence of the relative orientation of substituents to the plane of the ring. It has been reported that by varying the content of *trans*-cyclohexanedimethylene units in poly(ethylene-co-1,4-cyclohexanedimethylene 2,5-furandicarboxylate) from 25 to 98%, polyesters with higher crystallinity could be produced.[112] Wang *et al*. also investigated cyclohexane moieties in polymer backbones, where the

relative content of *cis*-1,4-cyclohexylene in poly(butylene 1,4-cyclohexanedicarboxylate) significantly altered the thermomechanical properties with higher *cis* content polymers being less crystalline and weaker, yet more ductile.[113] In 2017, Kieber and co-workers reported the synthesis of a new class of polyurethanes obtained by reacting 2,5-bishydroxymethylfuran with two diisocyanate functionalised stereoisomers, isosorbide bis(3-isocyanatopropanoate) and isomannide bis(3-isocyanatopropanoate).[114] Polymers with different content of isomannide against isosorbide presented different chain entanglements molecular weight and, consequently, differences in mechanical properties such as density and viscosity. In particular, the authors pointed out that isomannide-containing polyurethanes presented a higher degree of entanglement when compared to isosorbide-based polyurethanes of similar molecular weight. Similar work has been reported by Stubbs *et al*.[115] The authors reported sugar-based polyurethanes developed through nucleophilic thiol-ene addition with thermomechanical properties and degradation rates highly dependent on the crystallinity, which was dictated by the different isoidide:isomannide ratio in the polymer's backbones (Figure 16).

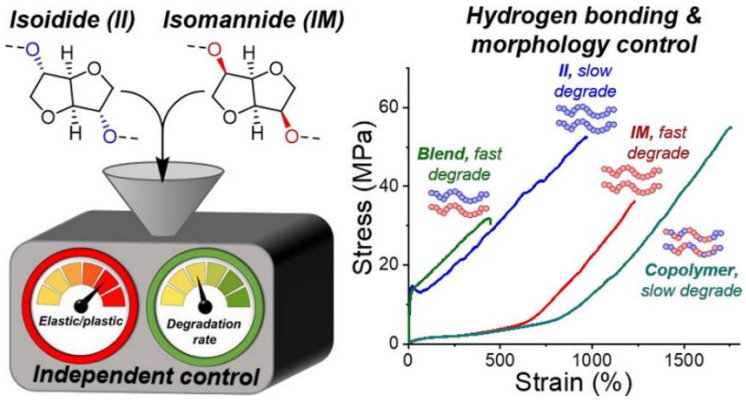


Figure 16. Different isoidide/isomannide ratios dictate polymers mechanical properties and degradation rate. Adapted from ref. 114 under license CC-BY-NC-ND 4.0.

While stereochemical enhancement of linear polymer properties is being widely investigated, this phenomenon has been less exploited in crosslinked materials. Macdougall *et al*. demonstrated that hydrogels' properties developed *via* thiol-yne polymerisation could be modulated in light of the controllable *cis*/*trans* ratio,[83] while Khalfa *et al*. showed that *cis*/*trans* isomerism can be used to modulate thermomechanical properties and degradation rates in photocurable networks for additive manufacturing, showing that *trans*-rich oligomers used to produce the resin display molecular weight-independent crystallinity, while the *cis*-rich prepolymers were crystalline only above a certain threshold (Figure 16).[116]

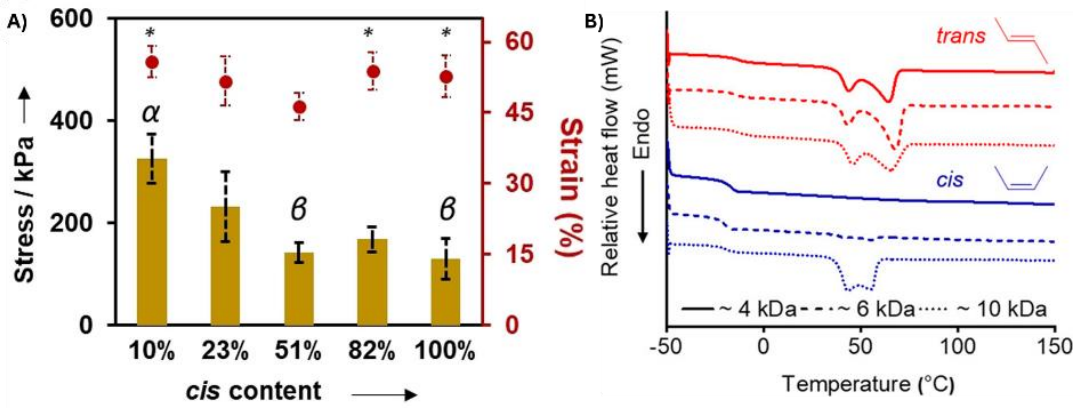


Figure 17. A) Increasing *cis* content was found to decrease compressive strength in hydrogels developed *via* thiol-yne polymerisation. Adapted from ref. 39 under the terms of Creative Commons CC BY license. B) DSC

thermograms showing the difference in crystallinity due to different *cis*/*trans* ratio in different 3D printable resins of different molecular weight. Adapted from ref. 72 under CC-BY-NC-ND 4.0.

1.6 Conclusions

In summary, nucleophilic Michael addition to activated alkyne is suggested to be a valuable tool to build sustainable and functional materials for the following reasons:

1. Nucleophilic heteroatoms such as sulfur, nitrogen, and oxygen (among others) are widely abundant in natural and synthetic compounds, meaning that many different scaffolds can be introduced into polymers. Moreover, activated alkynes can also be easily installed through a variety of methods - acid-catalysed esterification,[117] Steglich esterification,[118] Weinreb-Nahm amide pathway[119] to name a few- further adding to the scope of this reaction.
2. The selectivity of this reaction makes it compatible with several functional groups. Moreover, the high efficiency and yields, paired with simple operation conditions, make it a widely applicable tool in developing materials without the need to control different parameters such as oxygen or moisture.
3. Focusing on inserting heteroatoms instead of building exclusively carbon-carbon bonds will help to synthesise polymeric materials with better reactive handles, that can be used for post-synthetic reactions such as functionalisation or end-of-life treatment, like chemical recycling.[120, 121]
4. The tuneable stereochemistry of the single-addition product is a powerful tool to modulate the thermomechanical properties of polymers. The

> synthesis of materials with different properties containing the same microstructure can be useful to prevent the overcrowding of the waste stream with polymers of different chemical natures hindering their separation and treatment.[122]

Inspired by the conceptual framework of the use of nucleophilic "X"-yne polymerisation (X = S, O), this work explored this reaction to build functional polymeric materials. The nucleophilic thiol-yne reaction was used to create linear (Chapter 2) and network (Chapter 3) polymers possessing thermomechanical properties comparable with commercially available materials. The reaction was proved to be compatible with the presence of dynamic disulfide bonds, thus allowing degradability and reprocessability. The phenol-yne polymerisation was used to develop biobased materials out of L-tyrosine diketopiperazines (DKP) (Chapter 4). DKP-based monomers have historically been difficult to polymerise resulting in low molecular weight polymers, therefore, their potential as functional materials were never explored. By employing this "click" approach, different materials with tuneable properties could be synthesised and their thermomechanical behaviour evaluated, revealing the potential of this class of compounds to yield a novel generation of biobased building blocks. Lastly, as the influence of stereochemistry on polymers' properties has been established, the phenol-yne reaction was used to harness axial chirality to modulate these properties. While this investigation did not yield the desired outcome, it provides insight into the facile inclusion of 1,1'-bi-2-naphthol (BINOL) into polymers drawing some essential structure-property

relationships that can be further explored for properties manipulation *via* axial chirality.

1.7 References

1. CH Chan, J Joy, HJ Maria and S Thomas, *Natural Rubber-Based Composites and Nanocomposites: State of the Art, New Challenges and Opportunities*, The Royal Society of Chemistry, 2013.
2. *United States of America Pat.,* Improvement in the mode of preparing caoutchouc with sulphur for the manufacture of various articles 1839.
3. H Staudinger, presented in part at the Nobel Lecture, 1953.
4. WH Carothers, *Chem. Rev.*, 1931, **8**, 353-426.
5. *Nature Reviews Materials*, 2022, **7**, 67-67.
6. PT Anastas and JC Warner, *Green chemistry : theory and practice*, Oxford University Press, Oxford [England], 1998.
7. Z Wang and J Wang, *Polym. Chem.*, 2023, **14**, 4927-4932.
8. RW Hughes, ME Lott, IS Zastrow, JB Young, T Maity and BS Sumerlin, *J. Am. Chem. Soc.*, 2024, **146**, 6217-6224.
9. R Geyer, JR Jambeck and KL Law, *Sci. Adv.*, 2017, **3**, e1700782.
10. L Zhou, LT Reilly, C Shi, EC Quinn and EYX Chen, *Nat Chem*, 2024, **16**, 1357-1365.
11. TH Mourey, S Turner, M Rubinstein, J Fréchet, C Hawker and K Wooley, *Macromolecules*, 1992, **25**, 2401-2406.
12. International Union of Pure and Applied Chemistry (IUPAC), 3.0.1 edn., 2019, DOI: doi:10.1351/goldbook.H02854.
13. International Union of Pure and Applied Chemistry (IUPAC), 3.0.1 edn., 2019, DOI: doi:10.1351/goldbook.C01335.
14. International Union of Pure and Applied Chemistry (IUPAC), 3.0.1 edn., 2019, DOI: doi:10.1351/goldbook.S05955.
15. International Union of Pure and Applied Chemistry (IUPAC), 3.0.1 edn., 2019, DOI: doi:10.1351/goldbook.R05126.
16. International Union of Pure and Applied Chemistry (IUPAC), 3.0.1 edn., 2019, DOI: doi:10.1351/goldbook.A00250.
17. International Union of Pure and Applied Chemistry (IUPAC), 3.0.1 edn., 2019, DOI: doi:10.1351/goldbook.B00683.
18. G Kraus and KW Rollmann, *Angew Makromol Chem*, 1971, **16**, 271-296.
19. International Union of Pure and Applied Chemistry (IUPAC), 3.0.1 edn., 2019, DOI: doi:10.1351/goldbook.G02675.
20. International Union of Pure and Applied Chemistry (IUPAC), 3.0.1 edn., 2019, DOI: doi:10.1351/goldbook.TT07268.
21. International Union of Pure and Applied Chemistry (IUPAC), 3.0.1 edn., 2019, DOI: doi:10.1351/goldbook.C01432.
22. International Union of Pure and Applied Chemistry (IUPAC), 3.0.1 edn., 2019, DOI: doi:10.1351/goldbook.G02640.
23. International Union of Pure and Applied Chemistry (IUPAC), 3.0.1 edn., 2019, DOI: doi:10.1351/goldbook.ET07547.
24. International Union of Pure and Applied Chemistry (IUPAC), 3.0.1 edn., 2019, DOI: doi:10.1351/goldbook.TT07168.
25. C Robert, A Crespy, S Bastide, J-M Lopez-Cuesta, S Kerboeuf, C Artigue and E Grard, *J. Appl. Polym. Sci.*, 2003, **87**, 1152-1160.
26. AS Keys, JP Garrahan and D Chandler, *Proc Natl Acad Sci*, 2013, **110**, 4482-4487.
27. T Moss and A Greiner, *Adv Mater Interfaces*, 2020, **7**, 1901858.
28. M Polaskova, P Peer, R Cermak and P Ponizil, *Polymers*, 2019, **11**, 1384.
29. L Singh, PJ Ludovice and CL Henderson, *Thin Solid Films*, 2004, **449**, 231-241.
30. K Wooley, C Hawker, J Pochan and J Fréchet, *Macromolecules*, 1993, **26**, 1514-1519.
31. Q Zhu, J Wu, C Tu, Y Shi, L He, R Wang, X Zhu and D Yan, *J. Phys. Chem. B*, 2009, **113**, 5777-5780.

32. Y Chai, T Salez, JD McGraw, M Benzaquen, K Dalnoki-Veress, E Raphaël and JA Forrest, *Science*, 2014, **343**, 994-999.
33. JH Kim, J Jang and W-C Zin, *Langmuir*, 2001, **17**, 2703-2710.
34. DS Fryer, RD Peters, EJ Kim, JE Tomaszewski, JJ de Pablo, PF Nealey, CC White and W-l Wu, *Macromolecules*, 2001, **34**, 5627-5634.
35. RJ Young and PA Lovell, *Introduction to Polymers (3rd ed.). CRC Press.*, 2011.
36. SF Edwards and TA Vilgis, *Rep. Prog. Phys.*, 1988, **51**, 243.
37. EW Fischer, *Pure Appl. Chem.*, 1972, **31**, 113-132.
38. AT Lorenzo, ML Arnal, JJ Sánchez and AJ Müller, *J. Polym. Sci., Part B: Polym. Phys.*, 2006, **44**, 1738-1750.
39. PJ Flory, *Trans Faraday Soc*, 1955, **51**, 848-857.
40. Z Zhou, AM LaPointe and GW Coates, *J. Am. Chem. Soc.*, 2023, **145**, 25983-25988.
41. F Jin, S Yuan, S Wang, Y Zhang, Y Zheng, Y-l Hong and T Miyoshi, *ACS Macro Lett.*, 2022, **11**, 284-288.
42. Y Kong and JN Hay, *Polymer*, 2002, **43**, 3873-3878.
43. A El-Hadi, R Schnabel, E Straube, G Müller and S Henning, *Polym. Test.*, 2002, **21**, 665-674.
44. M Gopalan and L Mandelkern, *J Phys Chem*, 1967, **71**, 3833-3841.
45. M Munaro and L Akcelrud, *J Polym Res*, 2008, **15**, 83-88.
46. CF Horn, BT Freure, H Vineyard and HJ Decker, *J. Appl. Polym. Sci.*, 1963, **7**, 887-896.
47. M Nagata and T Kiyotsukuri, *Eur. Polym. J.*, 1992, **28**, 1069-1072.
48. M Leitner, *Trans Faraday Soc*, 1955, **51**, 1015-1021.
49. TT Wang, *J. Appl. Phys.*, 1973, **44**, 4052-4057.
50. CWH Rajawasam, OJ Dodo, MASN Weerasinghe, IO Raji, SV Wanasinghe, D Konkolewicz and N De Alwis Watuthanthrige, *Polym. Chem.*, 2024, **15**, 219-247.
51. CH Chan, J-T Chen, WS Farrell, CM Fellows, DJ Keddie, CK Luscombe, JB Matson, J Merna, G Moad, GT Russell, P Théato, PD Topham and L Sosa Vargas, *Polym. Chem.*, 2022.
52. PJ Flory, *Principles of polymer chemistry*, Cornell university press, 1953.
53. PJ Flory, *J. Am. Chem. Soc.*, 1936, **58**, 1877-1885.
54. HR Kricheldorf, *Macromol. Rapid Commun.*, 2008, **29**, 1695-1704.
55. HC Kolb, MG Finn and KB Sharpless, *Angew. Chem. Int. Ed.*, 2001, **40**, 2004-2021.
56. S Chandrasekaran, *Click reactions in organic synthesis*, John Wiley & Sons, 2016.
57. JB Zimmerman, PT Anastas, HC Erythropel and W Leitner, *Science*, 2020, **367**, 397-400.
58. Z Geng, JJ Shin, Y Xi and CJ Hawker, *J Polym Sci*, 2021, **59**, 963-1042.
59. Y Li, J Yu, Y Bi, G Yan and D Huang, *Adv. Synth. Catal.*, 2019, **361**, 4839-4881.
60. BD Fairbanks, TF Scott, CJ Kloxin, KS Anseth and CN Bowman, *Macromolecules*, 2009, **42**, 211-217.
61. BD Fairbanks, EA Sims, KS Anseth and CN Bowman, *Macromolecules*, 2010, **43**, 4113-4119.
62. AT Blomquist and J Wolinsky, *J. Org. Chem.*, 1958, **23**, 551-554.
63. AB Lowe, *Polymer*, 2014, **55**, 5517-5549.
64. N Van Herck, D Maes, K Unal, M Guerre, JM Winne and FE Du Prez, *Angew. Chem. Int. Ed.*, 2020, **59**, 3609-3617.
65. H-Y Shiu, T-C Chan, C-M Ho, Y Liu, M-K Wong and C-M Che, *Chem Eur J*, 2009, **15**, 3839-3850.
66. WE Truce and DL Goldhamer, *J. Am. Chem. Soc.*, 1959, **81**, 5795-5798.
67. QF Zhou, XP Chu, S Zhao, T Lu and WF Tang, *Chin. Chem. Lett.*, 2012, **23**, 639-642.
68. R Medel, MI Monterde, J Plumet and JK Rojas, *J. Org. Chem.*, 2005, **70**, 735-738.
69. M Kodomari, G Saitoh and S Yoshitomi, *Bull. Chem. Soc. Jpn.*, 2006, **64**, 3485-3487.
70. VX Truong and AP Dove, *Angew. Chem. Int. Ed.*, 2013, **52**, 4132-4136.
71. S Zhao, QF Zhou, JZ Liu, WF Tang and T Lu, *Chin. Chem. Lett.*, 2011, **22**, 397-400.
72. DA White and MM Baizer, *Tetrahedron Lett.*, 1973, **14**, 3597-3600.
73. S Ruhemann, *J. Chem. Soc.*, 1905, **87**, 461-468.
74. RG Bass, E Cooper, PM Hergenrother and JW Connell, *J. Polym. Sci., Part A: Polym. Chem.*, 1987, **25**, 2395-2407.
75. CKW Jim, A Qin, JWY Lam, F Mahtab, Y Yu and BZ Tang, *Adv. Funct. Mater.*, 2010, **20**, 1319-1328.
76. JC Worch, AC Weems, J Yu, MC Arno, TR Wilks, RTR Huckstepp, RK O'Reilly, ML Becker and AP Dove, *Nat. Commun.*, 2020, **11**, 3250.
77. CA Bell, J Yu, IA Barker, VX Truong, Z Cao, AV Dobrinyin, ML Becker and AP Dove, *Angew. Chem. Int. Ed.*, 2016, **55**, 13076-13080.
78. O Daglar, US Gunay, G Hizal, U Tunca and H Durmaz, *Macromolecules*, 2019, **52**, 3558-3572.
79. RM Hensarling, VA Doughty, JW Chan and DL Patton, *J. Am. Chem. Soc.*, 2009, **131**, 14673-14675.
80. JC Worch, AC Weems, J Yu, MC Arno, TR Wilks, RTR Huckstepp, RK O'Reilly, ML Becker and AP Dove, *Nat. Commun.*, 2020, **11**.
81. LJ Macdougall, MM Pérez-Madrigal, MC Arno and AP Dove, *Biomacromolecules*, 2018, **19**, 1378-1388.

82. LJ Macdougall, MM Pérez-Madrigal, JE Shaw, M Inam, JA Hoyland, R O'Reilly, SM Richardson and AP Dove, *Biomater Sci*, 2018, **6**, 2932-2937.
83. LJ Macdougall, MM Pérez-Madrigal, JE Shaw, JC Worch, C Sammon, SM Richardson and AP Dove, *Angew. Chem. Int. Ed.*, 2021, **60**, 25856-25864.
84. MM Pérez-Madrigal, JE Shaw, MC Arno, JA Hoyland, SM Richardson and AP Dove, *Biomater Sci*, 2020, **8**, 405-412.
85. B Fan, K Zhang, Q Liu and R Eelkema, *ACS Macro Lett.*, 2020, **9**, 776-780.
86. D Tejedor, SJ Álvarez-Méndez, JM López-Soria, VS Martín and F García-Tellado, *Eur. J. Org. Chem.*, 2014, **2014**, 198-205.
87. J Inanaga, Y Baba and T Hanamoto, *Chem. Lett.*, 2006, **22**, 241-244.
88. T Santos, Y Pérez-Pérez, DS Rivero, R Diana-Rivero, F García-Tellado, D Tejedor and R Carrillo, *Org. Lett.*, 2022.
89. H Kuroda, I Tomita and T Endo, *Macromolecules*, 1995, **28**, 433-436.
90. H Kuroda, I Tomita and T Endo, *Polymer*, 1997, **38**, 3655-3662.
91. Y Shi, T Bai, W Bai, Z Wang, M Chen, B Yao, JZ Sun, A Qin, J Ling and BZ Tang, *Chem. Eur. J.*, 2017, **23**, 10725-10731.
92. H Si, K Wang, B Song, A Qin and BZ Tang, *Polym. Chem.*, 2020, **11**, 2568-2575.
93. B Song, D Lu, A Qin and BZ Tang, *J. Am. Chem. Soc.*, 2022, **144**, 1672-1680.
94. K Wang, H Si, Q Wan, Z Wang, A Qin and BZ Tang, *J. Mater. Chem. C*, 2020, **8**, 16121-16128.
95. K Bauri, M Nandi and P De, *Polym. Chem.*, 2018, **9**, 1257-1287.
96. S Mallakpour and M Dinari, *J. Macromol. Sci. Chem.,A.*, 2011, **48**, 644-679.
97. Y Usuda, Y Hara and H Kojima, *Toward Sustainable Amino Acid Production*, Springer Japan, Tokyo, 2017.
98. AM Barrett and VA Cullum, *Br. J. Pharmacol.*, 1968, **34**, 43-55.
99. W Kromer, *Scand. J. Gastroenterol.*, 2001, **36**, 3-9.
100. CW Bunn, *Proc. R. soc. Lond. Ser. A-Contain. Pap. Math. Phys. Character*, 1942, **180**, 40-66.
101. G Natta, P Pino, P Corradini, F Danusso, E Mantica, G Mazzanti and G Moraglio, *J. Am. Chem. Soc.*, 1955, **77**, 1708-1710.
102. N Ahmad, R Di Girolamo, F Auriemma, C De Rosa and N Grizzuti, *Macromolecules*, 2013, **46**, 7940-7946.
103. E Castro-Aguirre, F Iñiguez-Franco, H Samsudin, X Fang and R Auras, *Adv. Drug Deliv. Rev.*, 2016, **107**, 333-366.
104. MA Abdel-Rahman, Y Tashiro and K Sonomoto, *Biotechnol. Adv.*, 2013, **31**, 877-902.
105. MA Abdel-Rahman, Y Tashiro and K Sonomoto, *J. Biotechnol.*, 2011, **156**, 286-301.
106. L-E Chile, P Mehrkhodavandi and SG Hatzikiriakos, *Macromolecules*, 2016, **49**, 909-919.
107. D Garlotta, *J. Polym. Environ.*, 2001, **9**, 63-84.
108. MJ Stanford and AP Dove, *Chem. Soc. Rev.*, 2010, **39**, 486-494.
109. H Abe, I Matsubara, Y Doi, Y Hori and A Yamaguchi, *Macromolecules*, 1994, **27**, 6018-6025.
110. MB Wandel, CA Bell, J Yu, MC Arno, NZ Dreger, Y-H Hsu, A Pitto-Barry, JC Worch, AP Dove and ML Becker, *Nat. Commun.*, 2021, **12**, 446.
111. CJ Stubbs, JC Worch, H Prydderch, ML Becker and AP Dove, *Macromolecules*, 2020, **53**, 174-181.
112. J Wang, X Liu, Y Zhang, F Liu and J Zhu, *Polymer*, 2016, **103**, 1-8.
113. J Wang, X Liu, Z Jia, L Sun, Y Zhang and J Zhu, *Polymer*, 2018, **137**, 173-185.
114. RJ Kieber, SA Silver and JG Kennemur, *Polym. Chem.*, 2017, **8**, 4822-4829.
115. CJ Stubbs, JC Worch, H Prydderch, Z Wang, RT Mathers, AV Dobrynin, ML Becker and AP Dove, *J. Am. Chem. Soc.*, 2022, **144**, 1243-1250.
116. AL Khalfa, ML Becker and AP Dove, *J. Am. Chem. Soc.*, 2021, **143**, 17510-17516.
117. HS Rhinesmith, *J. Org. Chem.*, 1975, **40**, 1773-1776.
118. B Neises and W Steglich, *Angew. Chem. Int. Ed.*, 1978, **17**, 522-524.
119. S Nahm and SM Weinreb, *Tetrahedron Lett.*, 1981, **22**, 3815-3818.
120. JM Garcia and ML Robertson, *Science*, 2017, **358**, 870-872.
121. JC Worch and AP Dove, *ACS Macro Lett.*, 2020, **9**, 1494-1506.
122. BD Vogt, KK Stokes and SK Kumar, *ACS Appl. Polym. Mater.*, 2021, **3**, 4325-4346.

Chapter 2 – Synthesis of disulfide containing thermoplastics *via* nucleophilic thiol-yne polymerisation.

Manuscript and overview

Title: Synthesis of disulfide containing thermoplastics *via* nucleophilic thiol-yne polymerisation

Authors: Daniele Giannantonio[a], Alexis Perrot[a,b], Arianna Brandolese[a], Andrew P. Dove[a]

Affiliations: [a]School of Chemistry, University of Birmingham, Edgbaston, Birmingham, B15 2TT (UK)

[b]LCMT, ENSICAEN, 6 bd Maréchal Juin, 14050 Caen, France.

Manuscript prepared

Co-authors contribution: Alexis G. Perrot provided synthetic, technical, and analytical guidance along with editing of the manuscript. Arianna Brandolese provided editing of the manuscript and guidance. Prof. Andrew P. Dove supervised in addition to providing guidance and funding acquisition.

Overview:

The aim of this chapter was to explore the use of the nucleophilic thiol-yne addition reaction to build thermoplastic polymeric materials that could compete with commonly used olefines. Moreover, the compatibility of this reaction with dynamic disulfide bonds was investigated, establishing it as suitable for installing this kind of bond into polymers. Thanks to this, these polymers showed enhanced degradability, the extent of which could be regulated according to the monomer feeding ratio. This parameter was also found to modify the thermomechanical

properties of the polymers, allowing for precise structure-properties relationships evaluation.

Synthesis of disulfide containing thermoplastics *via* nucleophilic thiol-yne polymerisation

Daniele Giannantonio[a], Alexis Perrot[a,b], Arianna Brandolese[a], Andrew P. Dove[a]

[a]School of Chemistry, University of Birmingham, Edgbaston, Birmingham, B15 2TT (UK)

[b]LCMT, ENSICAEN, 6 bd Maréchal Juin, 14050 Caen, France.

Abstract: *The introduction of dynamic covalent bonds in polymeric material endows them with novel properties, including self-healing and enhanced degradability. Despite the wide range of polymerisation protocols available to introduce dynamic disulfide bonds in linear polymers, these techniques do not provide a sufficiently versatile method to modulate the mechanical properties of the materials. In this study, nucleophilic thiol-yne polymerisation was employed to synthesise polymers with a controllable amount of disulfide bonds in the backbone. The crystallinity, and therefore the thermomechanical properties of these polymers, can be tuned through the variation of different parameters such as disulfide bond content, polymer backbone conformational features (i.e. E/Z isomerism), and monomer combinations. Lastly, polymer degradability was confirmed by leveraging on the reversible disulfide bonds in the presence of chemical stimuli.*

Introduction

The introduction of dynamic bonds into polymeric materials has emerged as a viable strategy to impart novel properties such as self-healing or triggered degradability.[1, 2] Still, the trade-off between the inclusion of dynamic bonds and polymer thermomechanical properties has been scarcely investigated. Among the different dynamic bonds available, disulfide bonds have received significant attention because of their widespread presence in biological systems and known dynamic behaviour.[3, 4] With a dissociation energy of around 60 kcal mol^{-1}, lower than that of the aliphatic C–C bond of 80-90 kcal mol^{-1}, disulfide bonds provide a good balance between dynamicity and robustness.[5, 6] Different strategies have been used to introduce this reversible bond into polymers, spanning from radical polymerisations, *e.g.* atom transfer radical polymerisation (ATRP) and reversible addition–fragmentation chain transfer (RAFT)[7-9], to non-radical processes, including ring-opening polymerisation (ROP), oxidation polymerisation, and polycondensation or polyaddition to produce polyesters and polyurethanes, respectively.[10-24]

Having precise knowledge of structure-property relationships is crucial when it comes to the rational design of polymeric materials. While many reported methods succeed in yielding materials covering a wide range of thermomechanical properties, their application often requires strict monomer design that would hinder larger-scale applicability. Moreover, these systems often lack the modularity necessary to precisely evaluate the impact of varying the disulfide bonds content

on the thermomechanical properties of the polymers. Step growth polymerisation reactions, widely used for the synthesis of industrially relevant polymers, represent an exception to this, as a result of the easy accessibility to structurally diverse bifunctional monomers. Despite their versatility, the high conversion needed to yield high molecular weight polymers through polycondensation is generally achieved only with prolonged reaction times, vacuum distillation of side products, and high temperatures that can ultimately lead to reagents decomposition and loss of volatile compounds which translate into stoichiometric imbalance. Polyaddition approaches can be conducted under milder conditions but are generally confined to the synthesis of polyurethanes meaning that they require toxic and moisture-sensitive isocyanates.[25-27]

Recently, we demonstrated that organobase-catalysed nucleophilic-thiol-yne "click" reaction serves as a straightforward tool to obtain materials with tuneable properties under mild conditions.[28] Leveraging on the control over the crystalline phase of the polymers achieved by the controllable stereochemistry of the addition product, material features such as toughness and degradability can be modulated.[29-31] Herein, thanks to the wide monomer scope compatible with this reaction, polyesters with adjustable amounts of disulfide bonds in the backbone were prepared. Moreover, because of the controllable crystalline phase, a broad range of thermomechanical properties could be accessed from a limited pool of monomers. Notably, some of these materials display mechanical properties comparable to common polyolefins such as high-density (HDPE) and low-density polyethylene (LDPE).

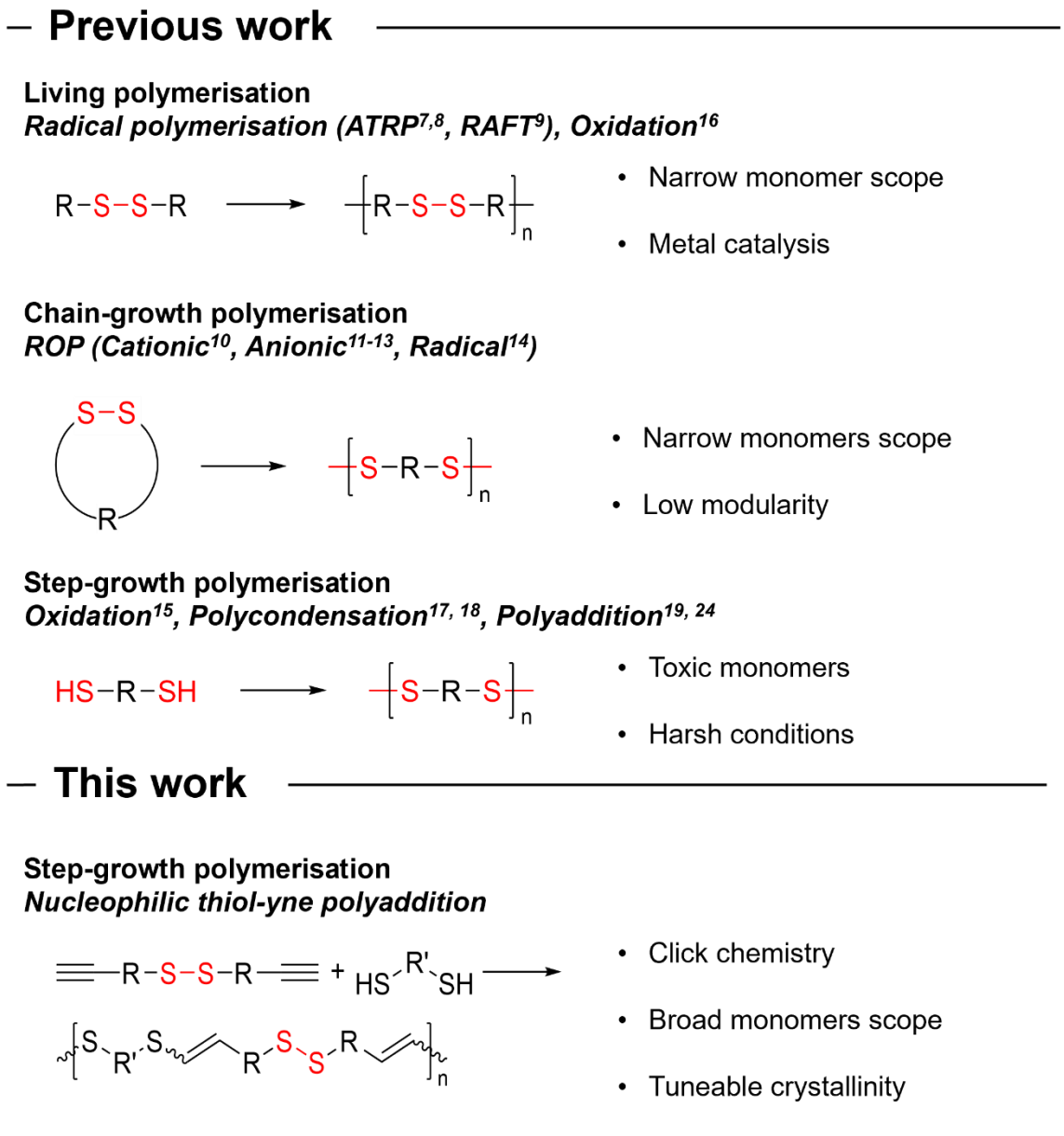


Figure 1. Previously reported polymerisation methods used to develop polymers possessing internal disulfide bonds *vs.* approach explored in this work.

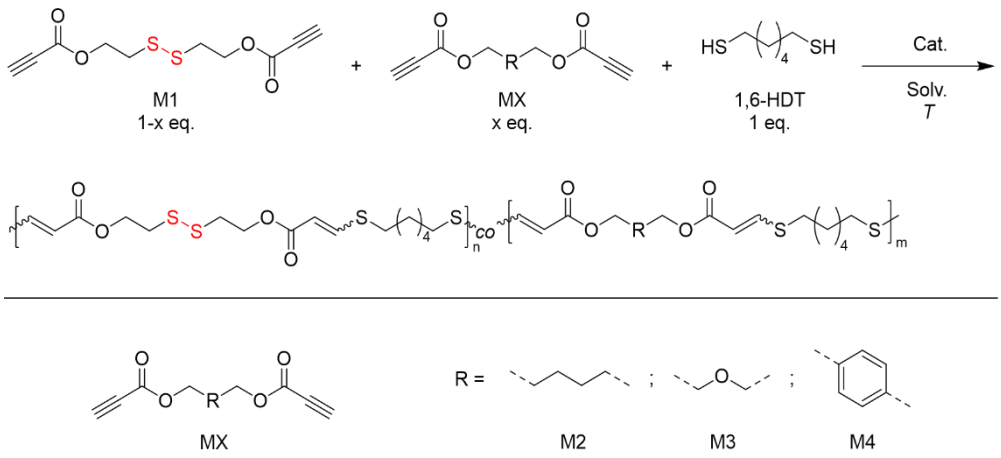
Results and discussion

Synthesis of disulfide bond containing polymers

In order to access different polymers with controlled architecture and disulfide bond content, different dipropiolate monomers were synthesised and polymerised

with 1,6-hexanedithiol *via* nucleophilic thiol-yne step growth polymerisation (Scheme 1).

All these monomers could be easily obtained *via* Fisher esterification adapting precedent reported procedures using commercially available diols as starting materials. The structures were confirmed *via* proton (^{1}H) and carbon (^{13}C) nuclear magnetic resonance (NMR) spectroscopy and mass spectroscopy (HR-MS) (See experimental data, Figure S1-S8).



Scheme 1. General nucleophilic thiol-yne polymerisation between monomer M1, 1,6-HDT and MX (top). Structures of non-disulfide monomers MX used in this study (bottom).

Since nucleophilic thiol-yne polymerisation requires the formation of thiolates anions, which are known to exchange in the presence of disulfide bonds leading to possible defects in the polymer structure, it was crucial to find a solvent/catalyst combination that would minimise this scrambling process. Given the solubility of the monomers, polymerisation between M1 and 1,6-hexanedithiol (1,6-HDT) was investigated in chloroform ($CHCl_3$) and dimethylformamide (DMF), using either triethylamine (Et_3N) and 1,8-diazabicyclo[5.4.0]undec-7-ene (DBU) as bases. Previous work done in the group identified solvent polarity and strength of the base

as crucial in controlling the stereochemistry of the addition product of the nucleophilic thiol-yne reaction.[30-32] Notably, these factors also greatly affect thiol-disulfide exchange. $CHCl_3$ and Et_3N were selected as the suitable solvent/base combination given the monodisperse GPC trace and ^1H NMR spectrum, showing fewer and better-resolved signals. The latter suggests that side reactions are less favourable with a weaker base in the least polar environment (Figure S9-S10). To further confirm these results, a small molecule study reacting 2 equivalents of 1-hexanethiol (1-HT) with 1 equivalent of M1 (Figure 2A) was performed. Successful thiol-yne reaction was confirmed by ^1H NMR spectroscopy that showed disappearance of the signals relative to the thiol proton (triplet, δ = 1.33 ppm) and the terminal alkyne proton (singlet, δ = 2.92 ppm), combined with the appearance of doublets at 5.74 ppm and 7.73 ppm assigned to the formation of the vinyl moiety (Figure 2B and Figure S12). The characteristic vinyl proton signals were used to confirm the preferential formation of *trans* linkages (85%). Heteronuclear Single Quantum Coherence (HSQC) NMR spectroscopy was also used to confirm the structure of the addition product (Figure S13). Furthermore, FT-IR spectroscopic analysis on the crude revealed the absence of S-H stretching frequencies in the typical region between 2584–2598 cm^{-1}, confirming the absence of unreacted thiols (Figure S11).[33] Finally, mass spectroscopy (MS) analysis proved the presence of the addition product, thus indicating that the exchange reaction does not hinder the polymerisation reaction.

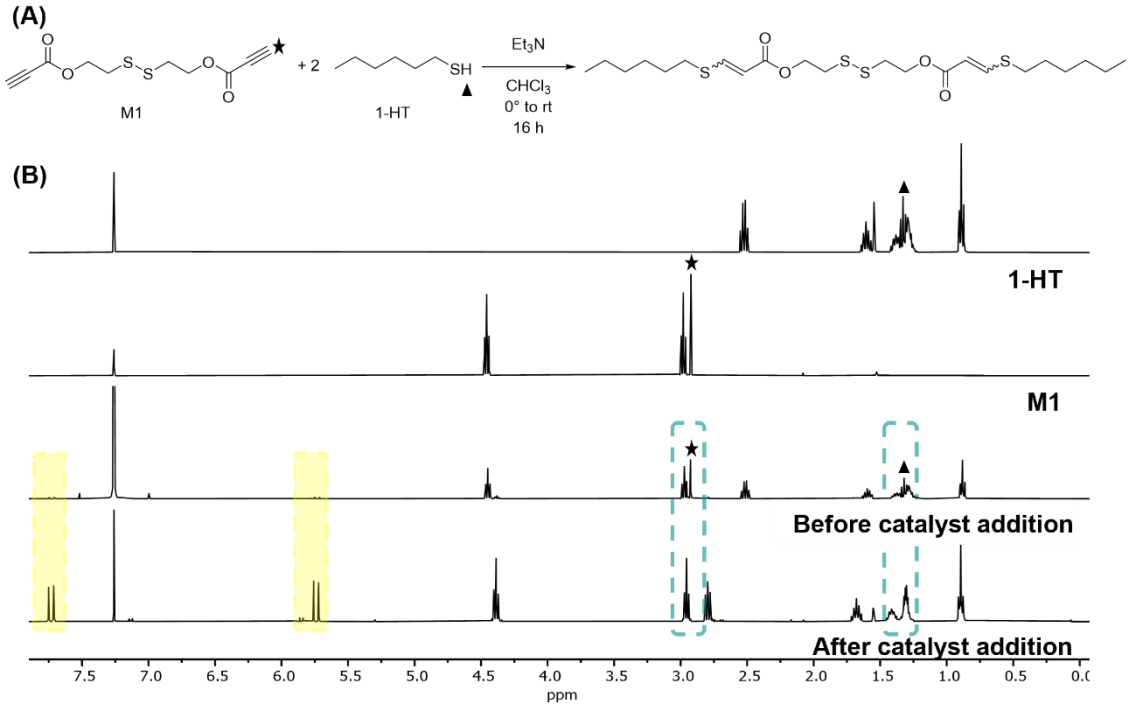


Figure 2. (A) Thiol-yne addition reaction between 2 equivalents of 1-HT and 1 equivalent of M1. (B) ^{1}H NMR spectra (400 MHz, 300 K, $CDCl_3$) of reactants (1-HT, M1) and reaction mixture before and after catalyst addition. Yellow boxes and light blue dashed line added to help visualise the change.

After having identified Et_3N and $CHCl_3$ as suitable base and solvent combination, a series of polymers having different disulfide bond content was synthesised. Differentiated polymer structures were obtained by varying the feeding ratio of monomer M1 and 1,6-hexanedipropiolate (M2) keeping a 1:1 equivalent ratio between thiols and alkynes (Figure 3A). Polymers with an M1 content ranging from 100% ($PolyM1_{100}$), in terms of total dipropiolate monomer fed into the reaction, to 0% ($PolyM2_{100}$) were recovered in moderate to high yield (Table 1). Analysis *via* ^{1}H and ^{13}C NMR spectroscopy (Figure S14-S27) revealed all the polymers to have high *trans* linkage content (>80%), as determined by the characteristic vinyl proton resonances indicative of thiol-yne addition detected in the ^{1}H NMR spectra. The different disulfide bond content was confirmed to vary with the feed ratio of M1, as

supported by the increased intensity of the disulfide methylene proton signal (2.9 ppm) in the ^{1}H NMR spectrum (Figure 3B). Furthermore, ^{13}C NMR spectroscopy shows the characteristic disulfide bond ^{13}C signal at δ > 35 ppm only in polymers containing M1, thus confirming the presence of the disulfide bond in the backbone of the polymers (Figure S28).[34] GPC analysis was used to characterise M_n and $Đ_M$, revealing high molecular weight and relatively narrow dispersity, especially for step growth polymerisation (Figure 3C, Table 1).

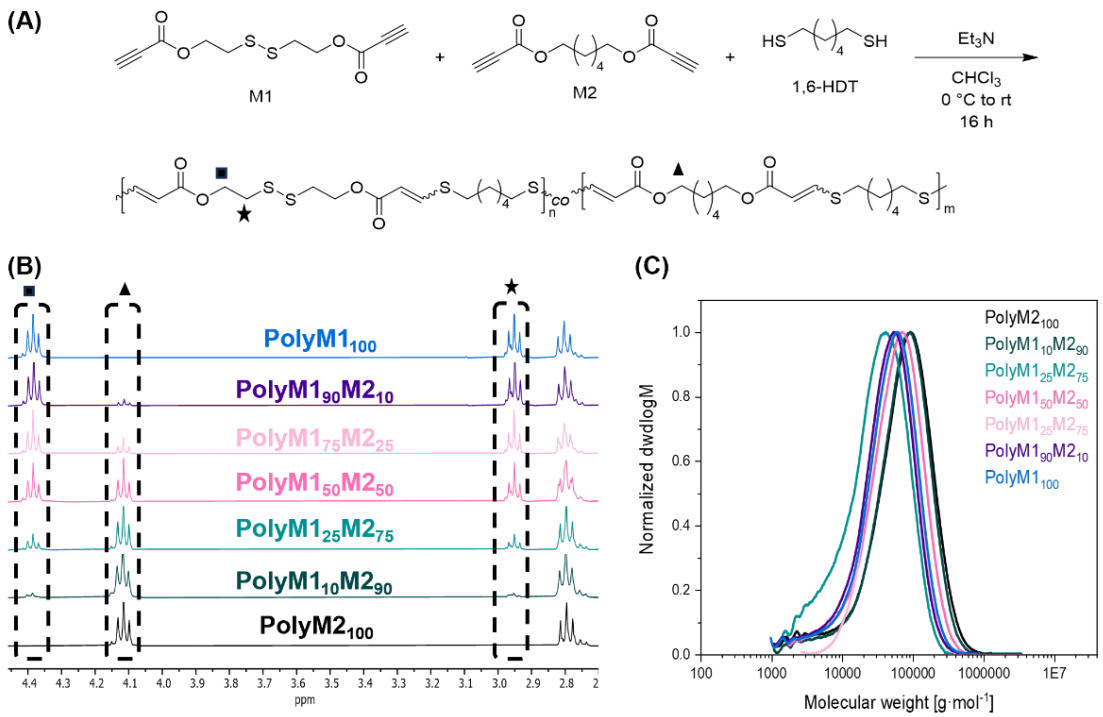


Figure 3. (A) Synthesis of polymers having different disulfide bond content *via* nucleophilic thiol-yne polymerisation. (B) ^{1}H NMR (400 MHz, 300 K, $CDCl_3$) spectroscopy of polymers synthesised varying the M1/M2 ratio going from 0 equivalents (bottom) of M1 to 1 equivalent (top) expressed to the equivalent of thiol. The intensity of the signal at 4.4 ppm, 4.1 ppm and 2.95 ppm follows the monomers feeding ratio. (C) GPC ($CHCl_3$, 0.5 % Et_3N, against polystyrene standards) traces of polymers having different degrees of M1 in the backbone.

Table 1. Table summarising yield, M_n, and $Đ_M$ for polymers obtained by changing the M1/M2 ratio.

Name	Yield (%)[a]	M_W (kg·mol^{-1})[b]	$Đ_M$[b]
PolyM2$_{100}$	85	102.9	3.6
PolyM1$_{10}$M2$_{90}$	84	95.9	2.9
PolyM1$_{25}$M2$_{75}$	82	43.8	2.8
PolyM1$_{50}$M2$_{50}$	84	76	2.5
PolyM1$_{75}$M2$_{25}$	67	60.2	1.7
PolyM1$_{90}$M2$_{10}$	73	56.9	2.7
PolyM1$_{100}$	76	64.1	2.8

[a]Isolated yield after drying. [b]Value obtained *via* GPC in chloroform (0.5% Et_3N), comparison with polystyrene standard (M_p = 162–3,187,000 g·mol^{-1}).

Influence of disulfide bond content on thermomechanical properties

The thermal properties of polymers were assessed *via* thermogravimetric analysis (TGA) and differential scanning calorimetry (DSC). The degradation temperature was taken as the temperature associated with a mass loss of 5% ($T_{d,5\%}$), and all polymers displayed thermal stability under N_2 with degradation temperature above 300 °C (Table 2, Figure S29). Increasing the amount of disulfide bonds led to a decrease of the $T_{d,5\%}$ of the polymers, from 346 to 300 °C, coherently with the weaker energy associated with it when compared to C – C bonds.[5] DSC analysis showed that the crystallinity of these polymers decreases with increasing equivalents of M1 (Figure S30-S36). Polymers having an M1 content of 25% or below displayed melting transitions, associated with an endothermic peak on the DSC trace, happening between 88 and 99 °C. Enthalpy of melting (ΔH_m^0) values calculated for polyM2$_{100}$, polyM1$_{10}$M2$_{90}$, and polyM1$_{25}$M2$_{75}$ were respectively −37.9 J·g^{-1}, −41.7 J·g^{-1}, and −38.4 J·g^{-1}. Exothermic peaks indicating cold crystallisation upon heating are present at temperatures increasing from 4 °C to 18 °C with increasing content of M1.[35] These data suggest that M2 is responsible for the crystallisation of the polymer and its ordering is hindered by increasing the amount

of M1. Given the structural similarity between M1 and M2, it is understood that the presence of bulkier sulfur atoms suffices to disrupt the alignment of polymer chains.[36] Polymers having an M1 content of 50% or above did not display any melting peak and resulted in being amorphous (Figure 4A). Glass transition temperature (T_g) increased slightly with increasing M1 content (from −20 to −16 °C).

These changes in crystallinity are reflected in the mechanical properties, tested *via* uniaxial tensile testing after heating compression moulding of the polymers into free-standing films. ^{1}H NMR spectroscopy and GPC analysis were conducted on the heat-pressed polymers demonstrating little to no change after the moulding process, hinting at the stability of the internal alkene bonds (Figure S37–S40). Polymers having an M1 content of 75% or above in regards to the total alkyne content resulted to be too soft to be reliably tested by this process (Figure S45, Table 2). These materials showed tuneable mechanical properties with Young's modulus values ranging from 173 to 45 MPa when the amount of disulfide bond was increased (Figure 3A). Notably, ultimate tensile strength and strain at break values were comparable to the ones of HDPE and LDPE.[37, 38] The increase in both toughness and strain with increasing disulfide bond content could be explained by the disulfide bond acting as energy dissipators in light of their lower bond strength. The same phenomenon was also observed in polyesters synthesised by polycondensation and epoxy thermosets.[18, 39] The lower strain at break and toughness observed for poly$M1_{25}M2_{75}$ can be explained by its lower molecular weight when compared to the other polymers. Similar behaviour was also observed when lower M_w poly$M2_{100}$ and poly$M1_{10}M2_{90}$ were synthesised calculating the

stoichiometric imbalance using the extended Carothers' equation (Figure S48-S51).[40] Shorter chains lead to higher Young's modulus due to increased easiness of crystallisation but this is often accompanied by a decrease in the maximum strain as chain entanglement is reduced.[41] The lack of significant difference in terms of crystalline behaviour observed in polymers of different M_w further suggests that the varying sulfur content is responsible for the modulation of the thermomechanical properties.

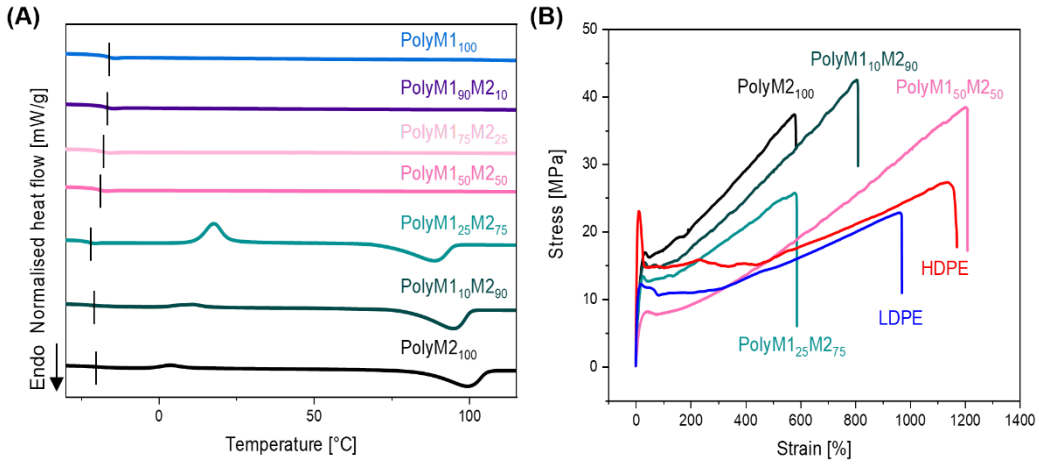


Figure 4. (A) DSC thermograms (second heating scan, -30 °C to 130 °C, 10 K/min) of polymers having different amount of disulfide bonds in the backbone. T_g marked with a vertical dash. (B) Exemplary stress *vs.* strain curves obtained by uniaxial tensile test (10 mm/min, 22 °C).

Table 2. Thermomechanical characterisation of polymers having different amounts of disulfide bonds in the backbone.

Name	T_g[a] [°C]	T_c[b] [°C]	T_m[b*] [°C]	$T_{d,5\%}$[c] [°C]	Young's modulus (E) [MPa]	Stress at break (σ) [MPa]	Strain at break (ε) [%]	Toughness (U_T) [J·m^{-3}]
PolyM2$_{100}$	−20.4	3.82	99.71	346.8	173.3 ± 6.3	35.6 ± 1.6	560.7 ± 19.1	133.5 ± 9.5
PolyM1$_{10}$M2$_{90}$	−21.0	10.7	95.05	335.1	128.7 ± 21.4	36.3 ± 5.5	733.1 ± 72.8	167.9 ± 37.8
PolyM1$_{25}$M2$_{75}$	−22.0	17.9	88.9	307.3	107.4 ± 10.7	25.2 ± 0.5	585.7 ± 3.4	100.5 ± 4.3
PolyM1$_{50}$M2$_{50}$	−18.9	n.a.	n.a.	308.9	45.5 ± 1.8	31.8 ± 8.8	1099.6 ± 157.9	199.2 ± 64.5
PolyM1$_{75}$M2$_{25}$	−17.9	n.a.	n.a.	303.8	n.a.	n.a.	n.a.	n.a.
PolyM1$_{90}$M2$_{10}$	−16.7	n.a.	n.a.	306.5	n.a.	n.a.	n.a.	n.a.
PolyM1$_{100}$	−16.0	n.a.	n.a.	300.5	n.a.	n.a.	n.a.	n.a.

[a]Value determined by the inflection point in the second heating cycle of DSC (N_2 atmosphere, −80 °C to 130 °C, 10 K/min). [b]Calculated taking the maximum of the exothermic peak in the second heating cycle of DSC. [b*]Calculated taking the minimum of the endothermic peak in the second heating cycle of DSC. [c]Taken as the temperature associated with a 5% mass loss in the thermogravimetric analysis (TGA) (25 °C to 600 °C, 10 K/min, N_2 atmosphere).

Modulation of thermomechanical properties and degradability

Further understanding of the influence of *cis*/*trans* ratio on the thermomechanical properties was investigated by synthesising a high *cis* content polyM1$_{10}$M2$_{90}$ (M_n = 11 kg mol^{-1}, $Đ_M$ = 4.9) by conducting the polymerisation in a more polar environment *i.e.,* dimethylsulfoxide (DMSO).[30, 32] The slightly lower M_n and higher $Đ_M$ obtained under with this reaction conditions, can be explained by the higher rate of disulfide metathesis happening in a more polar environment, in analogy to what was observed during reaction condition screening (Figure S9-S10) and with previously reported data.[42, 43] The *cis* content of this polymer was evaluated

by the vinyl proton resonance to be around 67% (Figure S52). TGA analysis revealed a similar degradation temperature (335 °C for the high *trans* polymer and 312 °C for the high *cis*) but differences in crystallinity were observed *via* DSC (Figure 4C). The high *cis*-content polymer was completely amorphous, as shown by the absence of a melting peak in the DSC trace. The T_g of this material was higher than the one of the corresponding high *trans* polymer, −13.9 °C against −21.01 °C. This difference in crystallinity was reflected in the high *cis* polymer displaying reduced stretchability and strength when tested *via* tensile testing (Figure 4b, Figure S53-S54). Modulation of crystallinity was also achieved by switching M2 for two other monomers, a diethylene glycol derivative (M3) and a *p*-xylylene glycol dipropiolate (M4) (Figure 4A). These monomers were designed to evaluate the impact of introducing another heteroatom (presence of oxygen in M3) while maintaining similar monomer length and flexibility, and to assess the impact of reduced monomer flexibility while introducing non-covalent interactions. The polymer structures and molecular weight distributions were elucidated *via* ^{1}H NMR spectroscopy and GPC (Figure S56-S57, Table S1). TGA revealed comparable degradation temperatures (between 327 and 335 °C), while DSC analysis confirmed the reduced crystalline phase, stressing the importance of monomer choice when designing polymeric materials. T_gs of these polymers were found to increase switching from M2 to M3 and M4 (Figure 5A). This increase can be explained by decreased free volume between polymer chains caused by increased non-covalent interactions between chains and decreased flexibility, as the same trend is observed for polyethyelene, poly(ethylene oxide), and poly(*p*-xylylene).[44-46] Both

poly$M1_{10}M3_{90}$ and poly$M1_{10}M4_{90}$ were considerably softer when compared to polymers having the same amount of M1 in the backbone but synthesised using M2, highlighting the importance of the crystalline phase in obtaining strong materials (Figure 5B). Notably, polymers synthesised using M4 showed enhanced elongation at break and toughness, possibly in light of the additional π-π stacking (Figure S61-S62).[47]

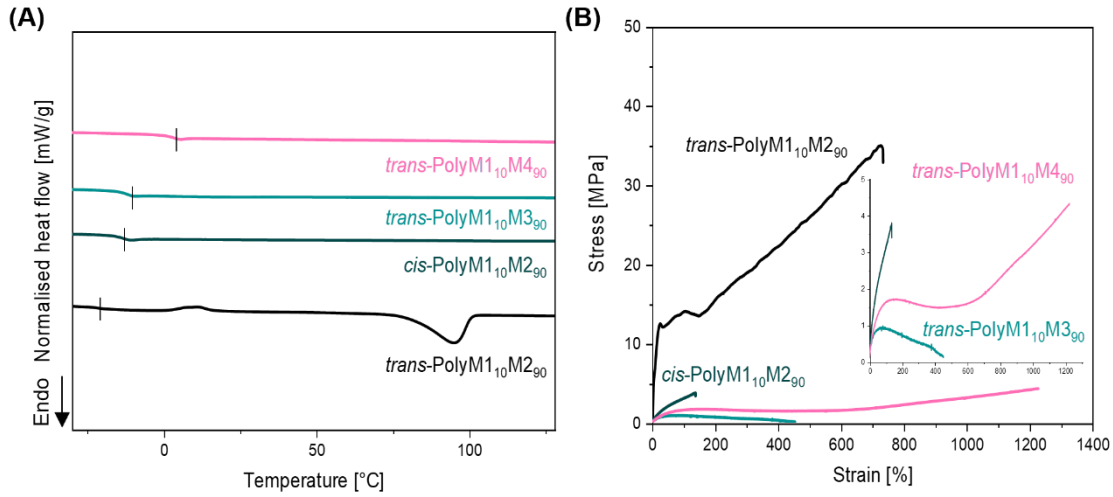


Figure 5. (A) DSC thermograms (second heating scan, −30 °C to 130 °C, 10 K/min) of different polymers synthesised keeping M1 content at 0.1 equivalent to the equivalent of thiol used. (B) Exemplary stress *vs.* strain curves obtained by uniaxial tensile test (10 mm/min, 22 °C).

Table 3. Thermomechanical characterisation of different polymers synthesised keeping M1 content at 0.1 equivalent to equivalent of thiol used.

Name	T_g[a] [°C]	T_c[b] [°C]	T_m[b*] [°C]	$T_{d,5\%}$[c] [°C]	Young's modulus (E) [MPa]	Stress at break (σ) [MPa]	Strain at break (ε) [%]	Toughness (U_T) [J·m^{-3}]
PolyM1$_{10}$ M2$_{90}$_high trans	−21.0	10.7	95.1	335.1	124.6 ± 16.5	36.3 ± 5.5	733.1 ± 72.8	167.9 ± 37.8
PolyM1$_{10}$ M2$_{90}$_high cis	−13.2	n.a.	n.a.	312.0	n.a.	3.7 ± 0.2	123.1 ± 16.1	2.8 ± 0.5
PolyM1$_{10}$ M3$_{90}$	−10.4	n.a.	n.a.	333.7	n.a.	n.a.	n.a.	n.a.
PolyM1$_{10}$ M4$_{90}$	3.8	n.a.	n.a.	327.9	3.6 ± 0.8	3.6 ± 0.8	1145.4 ± 139.7	20.4 ±7.1

[a] Value determined by the inflection point in the second heating cycle of DSC (N_2 atmosphere, −80 °C to 130 °C, 10 K/min). [b] Calculated taking the maximum of the exothermic peak in the second heating cycle of DSC. [b*] Calculated taking the minimum of the endothermic peak in the second heating cycle of DSC. [c] Taken as the temperature associated with a 5% mass loss in the thermogravimetric analysis (TGA) (25 °C to 600 °C, 10 K/min, N_2 atmosphere).

Lastly, to show that degradation can be achieved under mild conditions in a controlled manner, reduction mediated by dithiothreitol (DTT), a common disulfide bond-reducing agent, was performed.[48] Degradation of polyM1$_{25}$M2$_{75}$ and polyM1$_{75}$M2$_{25}$ was followed *via* GPC, and the reaction stopped after 24 hours. This analysis revealed fragments obtained from the degradation of polyM1$_{25}$M2$_{75}$ to have a M_w around 9 kg/mol, roughly a quarter of the initial M_w, suggesting that the inclusion of the different monomers happens statistically according to the feed ratio, and not in a random fashion. Degradation of polyM1$_{75}$M2$_{25}$ yielded smaller fragments of M_w around 2 kg/mol, which is coherent with the presence of shorter non-degradable moieties in the main chain due to the higher amount of degradable monomer in the backbone. Notably, since the amount of disulfide bonds in the

backbone depends on the monomer feed ratio, which also influences the mechanical properties, there is a trade-off between material strength and the extent of degradability.

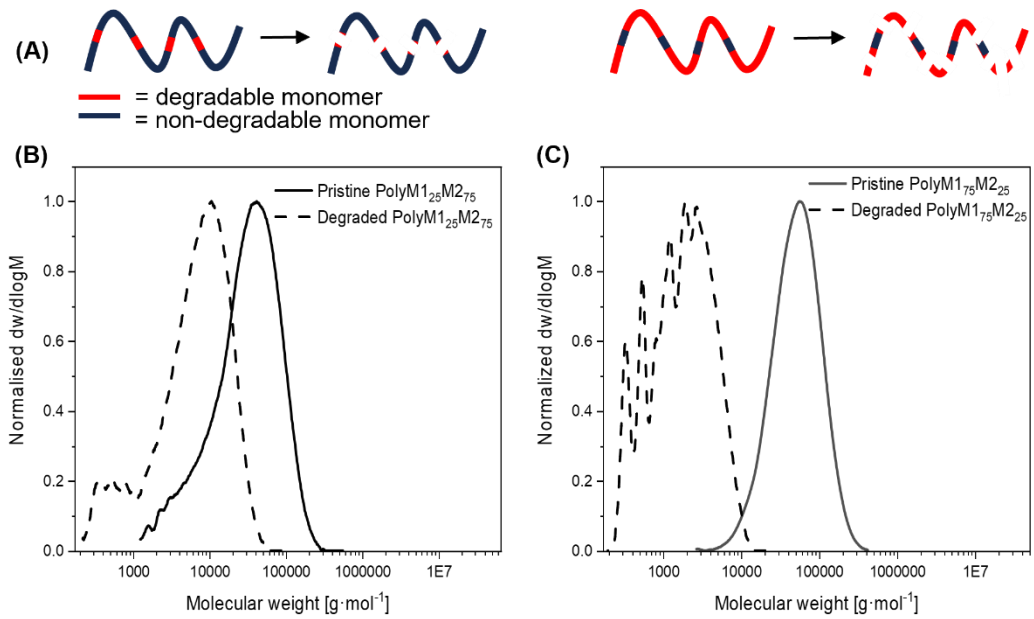


Figure 6. (A) Cartoon exemplifying the influence of increasing degradable monomer content in the polymer backbone on the degradation process: fewer degradable units (left) lead to longer and less disperse polymer chains after degradation when compared to more degradable units (right). GPC ($CHCl_3$, against polystyrene standard) traces of PolySS$_{25}$ (B) and PolySS$_{75}$ (C) before and after degradation *via* DTT mediated reduction (reaction time = 24 h).

Conclusions

The compatibility of nucleophilic thiol-yne step growth polymerisation with aliphatic disulfide bonds was demonstrated by synthesising a library of degradable polymers under mild conditions. When compared to previously reported methods, this reaction allows for greater control over the crystalline phase of the resulting polymers, meaning that a wide range of thermomechanical properties can be accessed from a small pool of monomers and intelligent design. Notably, some of these polymers displayed thermomechanical properties comparable to HDPE and

LDPE. Future studies will focus around the modulation of the dynamic behaviour of the disulfide bond by variation of the surrounding environment (*i.e.* aromatic *vs.* aliphatic disulfides, variation in the length of the aliphatic chains, the introduction of side groups) and establishment of a circular life cycle for these materials. Furthermore, it is envisioned that this reaction to be compatible with a wider range of dynamic units, meaning it can be a powerful tool in designing responsive polymers.

References

1. N. Zheng, Y. Xu, Q. Zhao and T. Xie, *Chem. Rev.*, 2021, **121**, 1716-1745.
2. S. V. Wanasinghe, O. J. Dodo and D. Konkolewicz, *Angew. Chem. Int. Ed.*, 2022, **61**, e202206938.
3. N. Darby and T. E. Creighton, *Mol. Biotechnol.*, 1997, **7**, 57-77.
4. S. P. Black, J. K. M. Sanders and A. R. Stefankiewicz, *Chem. Soc. Rev.*, 2014, **43**, 1861-1872.
5. Y.-M. Yang, H.-Z. Yu, X.-H. Sun and Z.-M. Dang, *J. Phys. Org. Chem.*, 2016, **29**, 6-13.
6. A. A. Zavitsas, *J. Phys. Chem. A*, 2003, **107**, 897-898.
7. N. V. Tsarevsky and K. Matyjaszewski, *Macromolecules*, 2002, **35**, 9009-9014.
8. J. Kamada, K. Koynov, C. Corten, A. Juhari, J. A. Yoon, M. W. Urban, A. C. Balazs and K. Matyjaszewski, *Macromolecules*, 2010, **43**, 4133-4139.
9. K. R. Albanese, P. T. Morris, J. Read De Alaniz, C. M. Bates and C. J. Hawker, *J. Am. Chem. Soc.*, 2023, **145**, 22728-22734.
10. B.-S. Wang, Q. Zhang, Z.-Q. Wang, C.-Y. Shi, X.-Q. Gong, H. Tian and D.-H. Qu, *Angew. Chem. Int. Ed.*, 2023, **62**, e202215329.
11. Y. Deng, Q. Zhang, D.-H. Qu, H. Tian and B. L. Feringa, *Angew. Chem. Int. Ed.*, 2022, **61**, e202209100.
12. K. Endo, T. Shiroi, N. Murata, G. Kojima and T. Yamanaka, *Macromolecules*, 2004, **37**, 3143-3150.
13. Y. Liu, Y. Jia, Q. Wu and J. S. Moore, *J. Am. Chem. Soc.*, 2019, **141**, 17075-17080.
14. C. Choi, J. L. Self, Y. Okayama, A. E. Levi, M. Gerst, J. C. Speros, C. J. Hawker, J. Read De Alaniz and C. M. Bates, *J. Am. Chem. Soc.*, 2021, **143**, 9866-9871.
15. T. Lee, P. T. Dirlam, J. T. Njardarson, R. S. Glass and J. Pyun, *J. Am. Chem. Soc.*, 2022, **144**, 5-22.
16. E. Q. Rosenthal, J. E. Puskas and C. Wesdemiotis, *Biomacromolecules*, 2012, **13**, 154-164.
17. H. Otsuka, S. Nagano, Y. Kobashi, T. Maeda and A. Takahara, *Chem. Commun.*, 2010, **46**, 1150-1152.
18. H. Hu, Q. Luan, J. Li, C. Lin, X. Ouyang, D.-Q. Wei, J. Wang and J. Zhu, *Biomacromolecules*, 2023, **24**, 5722-5736.
19. Y. Xu and D. Chen, *Macromol. Chem. Phys.*, 2016, **217**, 1191-1196.
20. W. Ge, B. Zhao, W. Liu, K. Nie and S. Zheng, *Macromol. Rapid Commun.*, 2021, **42**, 2000718.
21. A. Rekondo, R. Martin, A. Ruiz de Luzuriaga, G. Cabañero, H. J. Grande and I. Odriozola, *Mater. Horiz.*, 2014, **1**, 237-240.
22. M. Liu, J. Zhong, Z. Li, J. Rong, K. Yang, J. Zhou, L. Shen, F. Gao, X. Huang and H. He, *Eur. Polym. J.*, 2020, **124**, 109475.
23. F. Dong, X. Yang, L. Guo, Y. Wang, H. Shaghaleh, Z. Huang, X. Xu, S. Wang and H. Liu, *J. Mater. Chem. A*, 2022, **10**, 10139-10149.
24. Y. Huang, J. Wang, Z. Shi, H. Wang and Z. Xue, *Polym. Chem.*, 2022, **13**, 6002-6009.
25. D. R. Varma and I. Guest, *J. Toxicol. Environ. Health*, 1993, **40**, 513-529.
26. H. Henneken, M. Vogel and U. Karst, *Anal. Bioanal. Chem.*, 2007, **387**, 219-236.
27. A. J. Singer, J. V. Quinn and J. E. Hollander, *Am. J. Emerg. Med.*, 2008, **26**, 490-496.
28. J. C. Worch and A. P. Dove, *Acc. Chem. Res.*, 2022, **55**, 2355–2369.
29. M. B. Wandel, C. A. Bell, J. Yu, M. C. Arno, N. Z. Dreger, Y.-H. Hsu, A. Pitto-Barry, J. C. Worch, A. P. Dove and M. L. Becker, *Nat. Commun.*, 2021, **12**, 466.

30. J. C. Worch, A. C. Weems, J. Yu, M. C. Arno, T. R. Wilks, R. T. R. Huckstepp, R. K. O'Reilly, M. L. Becker and A. P. Dove, *Nat. Commun.*, 2020, **11**, 3250.
31. C. A. Bell, J. Yu, I. A. Barker, V. X. Truong, Z. Cao, A. V. Dobrinyin, M. L. Becker and A. P. Dove, *Angew. Chem. Int. Ed.*, 2016, **55**, 13076-13080.
32. V. X. Truong and A. P. Dove, *Angew. Chem. Int. Ed.*, 2013, **52**, 4132-4136.
33. R. A. Nyquist, in *Interpreting Infrared, Raman, and Nuclear Magnetic Resonance Spectra*, Academic Press, San Diego, 2001, ch. Thiols, Sulfides and Disulfides, Alkanethiols, and Alkanedithiols (S-H stretching), pp. 65-83.
34. D. Sharma and K. Rajarathnam, *J. Biomol. NMR*, 2000, **18**, 165-171.
35. Y. Furushima, C. Schick and A. Toda, *Polym. Cryst.*, 2018, **1**, e10005.
36. J. C. Slater, *J. Chem. Phys.*, 1964, **41**, 3199-3204.
37. O. Szlachetka, J. Witkowska-Dobrev, A. Baryła and M. Dohojda, *J. Build. Eng.*, 2021, **44**, 103386.
38. G. Sarkhel, A. Banerjee and P. Bhattacharya, *Polym.-Plast. Technol. Mater.*, 2006, **45**, 713-718.
39. B. Lewis, J. M. Dennis and K. R. Shull, *ACS Appl. Polym. Mater.*, 2023, **5**, 2583-2595.
40. W. H. Carothers, *Trans. Faraday Soc.*, 1936, **32**, 39.
41. J.-M. Chenal, L. Chazeau, L. Guy, Y. Bomal and C. Gauthier, *Polymer*, 2007, **48**, 1042-1046.
42. S. Nevejans, N. Ballard, J. I. Miranda, B. Reck and J. M. Asua, *Phys. Chem. Chem. Phys.*, 2016, **18**, 27577-27583.
43. F. N. Behrendt and H. Schlaad, *Macromol. Rapid Commun.*, 2018, **39**, 1700735.
44. D. E. Kirkpatrick and B. Wunderlich, *Makromol.*, 1985, **186**, 2595-2607.
45. M. Polaskova, P. Peer, R. Cermak and P. Ponizil, *Polymers*, 2019, **11**, 1384.
46. Q. Yang, X. Chen, Z. He, F. Lan and H. Liu, *RSC Adv.*, 2016, **6**, 12053-12060.
47. R. J. Wojtecki and A. Nelson, *J. Polym. Sci., Part A: Polym. Chem.*, 2016, **54**, 457-472.
48. S. N. Mthembu, A. Sharma, F. Albericio and B. G. Torre, *ChemBioChem*, 2020, **21**, 1947-1954.

Supporting information

Synthesis of disulfide containing thermoplastics *via* nucleophilic thiol-yne polymerisation

Daniele Giannantonio[a], Alexis Perrot[a,b], Arianna Brandolese[a], Andrew P. Dove[a]

[a]School of Chemistry, University of Birmingham, Edgbaston, Birmingham, B15 2TT (UK)

[b]LCMT, ENSICAEN, 6 bd Maréchal Juin, 14050 Caen, France.

Experimental methods

All compounds, unless otherwise indicated were purchased from commercial sources and used as received. The following chemicals were vacuum distilled prior to use and stored in Young's tapped ampoules under N_2: 1,6-hexanedithiol (Sigma-Aldrich, ≥ 97%), propiolic acid (Sigma-Aldrich ≥ 97%). Heating was applied through a stirring plate equipped with an oil bath.

NMR Spectroscopic Analysis. All NMR spectroscopy experiments were performed at 300 K on a Bruker DPX-400 NMR instrument equipped with a BBFO smart probe operating at 400 MHz for H (100.57 MHz for ^{13}C). ^{1}H NMR spectra are referenced to solvent residual proton (δ = 7.26 for $CDCl_3$) and ^{13}C NMR spectra are referenced to the solvent signal (δ = 77.16 for $CDCl_3$). The resonance multiplicities are described as s (singlet), d (doublet), t (triplet), q (quartet) or m (multiplet).

Mass Spectrometry. High Resolution Electrospray Ionization Mass Spectrometry was performed in the School of Chemistry at the University of Birmingham on a Waters Xevo G2-XS QTof Quadrupole Time-of-Flight mass spectrometer.

Fourier-transform Infrared Spectroscopy (FTIR): All FTIR spectroscopic analyses were performed on an Agilent Technologies Cary 630 FTIR spectrometer at a resolution of 4 cm^{-1}. 16 Scans from 600 to 4000 cm^{-1} were performed and the spectra were corrected for background absorbance.

Size Exclusion Chromatography (SEC). SEC measurements were performed in $CHCl_3$ on an Agilent 1260 Infinity II Multi-Detector SEC System fitted with RI,

ultraviolet (UV, λ = 309 nm), and viscometer detectors. The polymers were eluted through an Agilent guard column (PLGel 5 µM, 50 × 7.5 mm) and two Agilent mixed-C columns (PLGel 5 µM, 300 × 7.5 mm) using $CHCl_3$ (buffered with 0.5% Et_3N) as the mobile phase (flow rate = 1 mL·min^{-1}, 40 °C). Number average molecular weights (M_n), weight average molecular weights (M_w) and dispersities ($Đ_M = M_w/M_n$) were determined using Agilent GPC software (vA.02.01) against a 10-point calibration curve (Mp = 162–3,187,000 g·mol^{-1}) based on poly(styrene) standards (Easivial PSM/H, Agilent).

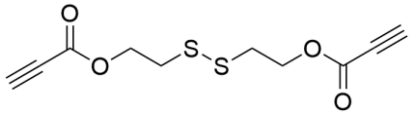
Differential Scanning Calorimetry (DSC). The thermal characteristics of the polymers were determined using differential scanning calorimetry (STARe system DSC3, Mettler Toledo) from −80 to 120 °C at a heating rate of 10 °C·min^{-1} for three heating/cooling cycles unless otherwise specified. The glass transition temperature (T_g) was determined from the inflection point in the second heating cycle of DSC. Total enthalpy of melting (ΔH_m) was calculated from the integration and normalization of all endothermic peaks present using the STARe software. The melting temperature was determined from the minimum value of the endothermic peak using the STARe software.

Thermogravimetric Analysis (TGA). TGA thermograms were obtained using a Q550 Thermogravimetric Analyzer (TA instruments). Thermograms were recorded under an N_2 atmosphere at a heating rate of 10 °C·min^{-1}, from 10 to 600 °C, with an average sample weight of *ca*. 5 mg. Aluminium pans were used for all samples.

Decomposition temperatures were reported as the 5% weight loss temperature ($T_{d,5\%}$).

Tensile testing. Samples were prepared into thin polymer films using 3 Specac Atlas™ Manual Hydraulic Press 15T fitted with Specac heated plates. The polymer was added into a 40 × 50 × 0.50 mm stainless steel mold and placed into pre-heated press at 120 °C. The sample was heated for 10 min (with no pressure) before degassing 5 × (500 kg pressure/release). Next, 2000 kg pressure was applied, and the sample was held at 120 °C for 5 min before cooling to ~ 25 °C under the same pressure. Film samples were visually inspected for deformation and bubbles. Finally, dumbbell shaped samples were cut using custom ASTM Die D-638 Type 5. Uniaxial tensile testing was performed using a Testometric M350-5CT universal mechanical testing instrument fitted with a load cell of 10 kN. Each specimen was clamped into the tensile holders and subjected to an elongation rate of 10 mm·min^{-1} until failure with an applied pretension of 0.1 N. All tensile tests were repeated 3 times (unless otherwise stated), and an average of the data was taken to find the ultimate tensile stress and strain. Data was analysed using winTest™ Analysis software (v.5.0.34) and OriginPro® software. Young modulus was calculated by taking the slope of the tensile curve at 1% strain. Toughness was calculated as the area under the curve up to break.

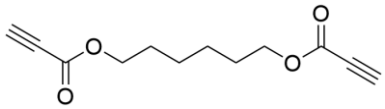
Synthetic procedures

Disulfide dipropiolate (M1): Monomer **M1** was prepared by adapting a  procedure reported by Hüppe *et al.*[1] Bis(2-hydroxyethyl) disulfide (5.3 g, 34.5 mmol), propiolic acid (9.7 g, 137.8 mmol) and *para*-toluenesulfonic acid monohydrated (*p*-TsOH) (0.66 g, 3.45 mmol) were solubilised in toluene (150 mL) under stirring in a two-neck round bottom flask (250 mL) equipped with a Dean-Stark apparatus and degassed with N_2 gas for 10 minutes. The temperature of the mixture was increased until reflux occurred (*ca*. 130 °C) and the reaction was left running overnight (*ca*. 16 h). The reaction mixture was then allowed to cool down at room temperature and excess of propiolic acid was neutralised via the addition of $NaHCO_{3(aq.)}$ sat. solution under vigorous stirring. The mixture was then transferred to a separatory funnel and washed with $NaHCO_{3(aq.)}$ sat. solution (3×30 mL). The organic layer was dried over $MgSO_4$, filtered, and concentrated under reduced pressure to obtain a dark viscous fluid. The product was purified *via* column chromatography performed following the procedure described by Still *et al.*[2] using a mixture of ethyl acetate and hexane (1:3 v/v) as the mobile phase. The product was isolated as a slightly yellow liquid that solidified upon standing. The solid product was recrystallised from ethyl acetate/hexane to obtain colourless crystals (4.11 g, 46% yield) with characterisation data in agreement with previously reported results.[1]

^{1}H NMR (400 MHz, Chloroform-*d*) δ 4.46 (t, J = 6.6 Hz, 4H), 2.98 (t, J = 6.6 Hz, 4H), 2.92 (s, 2H). ^{13}C NMR (101 MHz, Chloroform-*d*) δ 152.48, 75.54, 74.45, 64.04, 36.86.

HRMS (TOF-MS-EI$^+$) (m/z): $[M]^+$ calculated for $C_{10}H_{10}O_4S_2$, 259.0049; found, 259.0047.

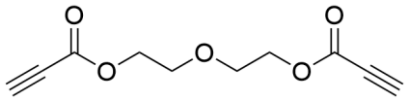
Hexane dipropiolate (M2): 1,6-Hexanediol (5.0 g, 42.31 mmol), propiolic acid



(7.81 mL, 126.93 mmol) and *p*-toluenesulfonic acid monohydrate (4.02 g, 21.15 mmol) were stirred in toluene (90 mL) in a 250 mL RBF equipped with a Dean-Stark apparatus. The temperature of the mixture was raised until reflux occurred and the reaction was left running for 17 h. The solvent was removed *via* a rotary evaporator and column chromatography (Hex:EtOAc 2:1) was performed on the crude reaction mixture. The product was further purified *via* recrystallisation (hexane) to yield white crystals (7.5 g, 80%) with spectroscopic data in agreement with previously published results.[3]

^{1}H NMR (400 MHz, Chloroform-*d*) δ 4.20 (t, J = 6.6 Hz, 4H), 2.87 (s, 2H), 1.69 (q, J = 6.5 Hz, 4H), 1.47 – 1.38 (m, 4H). ^{13}C NMR (101 MHz, Chloroform-*d*) δ 152.9, 74.9, 74.8, 66.3, 28.3, 25.6. HRMS (TOF-MS-EI$^+$) (m/z): $[M+Na]^+$ calculated for $C_{12}H_{14}O_4Na$, 245.0790: found, 245.0788.

Diethylene glycol dipropiolate (M3): Propiolic acid (8.26 g, 117.9 mmol),

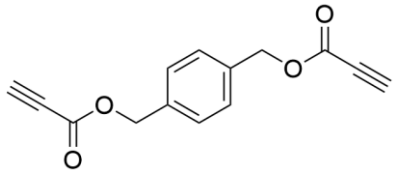


diethylene glycol (5 g, 47.1 mmol), and *p*-TsOH (0.45 g, 2,4 mmol) were solubilised in toluene (200 mL) in a 500 mL round bottom flask equipped with a Dean-Stark apparatus under constant stirring. The temperature of the mixture was increased until reflux occured, and the reaction was left overnight (*ca.* 16 h). The reaction mixture was allowed to cool down to room temperature and concentrate under reduced

pressure to obtain an orange oil that was distilled using a Kugelrohr set up to obtain a slightly yellow liquid that solidifies upon standing. Solid was recrystallised from hexane to obtain product **3** as white crystals (4.13 g, 42% yield) with spectroscopic data in agreement with previously published results.[4]

^{1}H NMR (400 MHz, Chloroform-*d*) δ 4.45 – 4.25 (m, 4H), 3.79 – 3.70 (m, 4H), 2.90 (s, 2H). ^{13}C NMR (101 MHz, Chloroform-*d*) δ 152.9, 74.7, 66.3, 28.3, 25.5. HRMS (TOF-MS-EI^{+}) (m/z): $[M+Na]^{+}$ calculated for $C_{10}H_{10}O_5Na$, 233.0426; found, 233.0429.

1,4-benzyl dipropiolate (M4): Propiolic acid (1.27 g, 18.1 mmol), 1,4 – benzene dimethanol (1.0 g, 7.24 mmol), and *p*-TsOH (0.138 g, 0.72 mmol) were solubilised in toluene (200 mL) in a 500 mL round bottom flask equipped with a Dean-Stark apparatus under constant stirring. The temperature of the mixture was increased until reflux occured and the reaction is left going overnight (*ca*. 16 h). The reaction mixture was concentrated under reduced pressure and the product was purified *via* column chromatography (Hex:EtOAc 3:1) and obtained as a white solid (0.411 g, 23%) with spectroscopic data in agreement with previously published results.[5]



^{1}H NMR (400 MHz, Chloroform-*d*) δ 7.40 (s, 4H), 5.22 (s, 4H), 2.90 (s, 2H). ^{13}C NMR (101 MHz, Chloroform-*d*) δ 152.6, 135.3, 128.9, 75.4, 74.6, 67.5. HRMS (TOF-MS-EI^{+}) (m/z): $[M+Na]^{+}$ calculated for $C_{14}H_{10}O_4Na$, 265.0447; found, 265.0482.

General procedure for polymer synthesis of high *trans* polymer

1,6-hexanedithiol (1 equivalent) was weighted in a 20 mL scintillation vial. Monomer M1 (x equivalent) and the desired non-disulfide containing monomer (M2

or M3 or M4) (1-x equivalent) were weighed in different vials according to the desired degree of monomer M1 in the final polymer. Monomers were then transferred to the vial containing the dithiol. The final concentration of the thiol was kept at 0.5 M. Reaction mixture was cooled down in an ice bath for 10 minutes before the addition of 1% mol of catalyst. The reaction was allowed to warm up to room temperature and left stirring for 14–16 h. Polymers were isolated *via* precipitation in diethyl ether followed by filtration or decantation, then dried in a vacuum oven held at room-temperature.

PolyM1$_{100}$: Recovered as a transparent soft solid (0.75 g, 76%). GPC analysis ($CHCl_3$, 0.5% Et_3N) M_n = 22.9 kg × mol^{-1}, $Đ_M$ = 2.8.

^{1}H NMR (400 MHz, Chloroform-*d*) %*trans* = 82; *δ* 7.71 (d, *J* = 15.2 Hz, *trans* 2H), 7.12 (d, *J* = 10.2 Hz, *cis*), 5.86 (d, *J* = 10.1 Hz, *cis*), 5.74 (d, *J* = 15.1 Hz, *trans* 2H), 4.38 (t, *J* = 6.4 Hz, 4H), 2.95 (t, *J* = 6.6 Hz, 4H), 2.80 (t, *J* = 7.3 Hz, 4H), 1.84 – 1.63 (m, 4H), 1.45 (dt, *J* = 7.6, 3.7 Hz, 4H). ^{13}C NMR (101 MHz, Chloroform-*d*) δ 166.4, 165.10, 151.4, 147.9, 113.2, 112., 62.2, 62.2, 37.6, 36.1, 32.0, 30.2, 28.5, 28.4, 28.0.

PolyM1$_{90}$M2$_{10}$: Recovered as a transparent soft solid (0.65 g, 73%). GPC analysis ($CHCl_3$, 0.5% Et_3N) M_n = 21.1 kg × mol^{-1}, $Đ_M$ = 2.7.

^{1}H NMR (400 MHz, Chloroform-*d*) %*trans* = 83; δ 7.80 – 7.53 (m, overlap M1 & M2 *trans* 2H), 7.12 (d, *J* = 10.2 Hz, overlap M1 & M2 *cis*), 5.86 (d, *J* = 10.2 Hz, overlap M1 & M2 *cis*), 5.74 (d, *J* = 15.1 Hz, overlap M1 & M2 *trans* 2H), 4.38 (t, *J* = 6.5 Hz, M1 4H), 4.11 (t, *J* = 6.7 Hz, M2), 2.95 (t, *J* = 6.6 Hz, 4H), 2.80 (t, *J* = 7.3 Hz, 4H), 1.87 – 1.65 (m, 4H), 1.45 (td, *J* = 5.7, 4.1, 2.1 Hz, 4H). ^{13}C NMR (101 MHz, Chloroform-*d*) δ 166.4,

165.5, 165.1, 151.4, 147.9, 146.9, 113.9, 113.2, 112.6, 64.3, 62.2, 62.2, 37.6, 36.1, 32.0, 30.2, 28.8, 28.5, 28.5, 28.0, 25.8.

PolyM1$_{75}$M2$_{25}$: Recovered as a transparent soft solid (0.58 g, 67%). GPC analysis ($CHCl_3$, 0.5% Et_3N) M_n = 37.6 kg × mol^{-1}, $Đ_M$ = 1.7.

^{1}H NMR (400 MHz, Chloroform-*d*) %*trans* = 84; *δ* 7.92 – 7.46 (m, , overlap M1 & M2 *trans* 2H), 7.12 (d, *J* = 10.2 Hz, *cis* M2), 7.06 (d, *J* = 10.2 Hz, *cis* M1), 5.85 (dd, *J* = 10.1, 7.4 Hz, overlap M1 & M2 *cis*), 5.74 (dd, *J* = 15.1, 2.6 Hz, overlap M1 & M2 *trans* 2H), 4.39 (t, *J* = 6.5 Hz, M1 4H), 4.12 (t, *J* = 6.7 Hz, M2 1 H), 2.96 (td, *J* = 6.6, 4.4 Hz, M1 4H), 2.80 (td, *J* = 7.3, 2.2 Hz, 4H), 1.69 (q, *J* = 7.0 Hz, 8H), 1.50 – 1.33 (m, 8H). ^{13}C NMR (101 MHz, Chloroform-*d*) *δ* 165.5, 165.1, 147.9, 146.9, 113.9, 113.2, 64.4, 62.2, 37.6, 32.0, 31.9, 28.8, 28.5, 28.4, 28.1, 25.8.

PolyM1$_{50}$M2$_{50}$: Recovered as a white fibrous solid (0.83 g, 84%). GPC analysis ($CHCl_3$, 0.5% Et_3N) M_n = 30.4 kg × mol^{-1}, $Đ_M$ = 2.5.

^{1}H NMR (400 MHz, Chloroform-*d*) %trans = 84; *δ* 7.71 (d, *J* = 15.2 Hz, *trans* M1 2H), 7.67 (d, *J* = 15.2 Hz, *trans* M2 2H), 7.12 (d, *J* = 10.2 Hz, *cis* M1), 7.06 (d, *J* = 10.2 Hz, *cis* M2), 5.86 (d, *J* = 10.1 Hz, *cis* M1), 5.84 (d, *J* = 10.3 Hz, *cis* M2), 5.74 (d, *J* = 15.1 Hz, *trans* M1 2H), 5.73 (d, *J* = 15.1 Hz, *trans* M2 2H), 4.38 (t, *J* = 6.4 Hz, 4H), 4.12 (t, *J* = 6.7 Hz, 4H), 2.95 (t, *J* = 6.6 Hz, 4H), 2.80 (td, *J* = 7.3, 2.2 Hz, 8H), 1.68 (dt, *J* = 10.8, 7.2 Hz, 12H), 1.45 (p, *J* = 3.6 Hz, 8H), 1.40 (q, *J* = 3.6 Hz, 4H). ^{13}C NMR (101 MHz, Chloroform-*d*) δ 165.6, 165.1, 147.9, 146.9, 113.9, 113.2, 64.4, 62.2, 37.6, 31.9, 30.2, 28.8, 28.5, 28.4, 28.1, 25.8.

PolyM1$_{25}$M2$_{75}$: Recovered as a white fibrous solid (0.87 g, 82%). GPC analysis ($CHCl_3$, 0.5% Et_3N) M_n = 15.7 kg × mol^{-1}, $Đ_M$ = 2.8.

^{1}H NMR (400 MHz, Chloroform-*d*) %trans = 84; *δ* 7.71 (d, *J* = 15.2 Hz, *trans* M1), 7.67 (d, *J* = 15.1 Hz, *trans* M2 2H), 7.12 (d, *J* = 10.2 Hz, *cis* M1), 7.06 (d, *J* = 10.2 Hz, *cis* M2), 5.86 (d, *J* = 10.1 *cis* M1), 5.84 (d, *J* = 10.1 Hz, *cis* M2), 5.74 (d, *J* = 15.0 Hz, *trans* M1), 5.73 (d, *J* = 15. *trans* M2, 2H), 4.39 (t, *J* = 6.5 Hz, M1), 4.12 (t, *J* = 6.7 Hz, M2 4H), 2.95 (t, *J* = 6.6 Hz, M1), 2.80 (dd, *J* = 8.4, 6.3 Hz, 4H), 1.76 – 1.62 (m, 8H), 1.45 (dq, *J* = 6.6, 3.2 Hz, 8H), 1.42 – 1.34 (m, 4H). ^{13}C NMR (101 MHz, Chloroform-*d*) *δ* 165.6, 165.1, 147.9, 146.9, 113.9, 113.2, 64.4, 62.2, 37.6, 31.9, 30.2, 28.8, 28.5, 28.4, 25.8.

PolyM1$_{10}$M2$_{90}$: Recovered as a white fibrous solid (0.65 g, 84%). GPC analysis ($CHCl_3$, 0.5% Et_3N) M_n = 33.1 kg × mol^{-1}, $Đ_M$ = 2.8.

^{1}H NMR (400 MHz, Chloroform-*d*) %trans = 85; *δ* 7.71 (d, *J* = 15.2 Hz, *trans* M1), 7.67 (d, *J* = 15.2 Hz, *trans* M2 2H), 7.12 (d, *J* = 10.2 Hz, *cis* M1), 7.06 (d, *J* = 10.2 Hz, *cis* M2), 5.86 (d, *J* = 10.1 Hz, *cis* M1), 5.84 (d, *J* = 10.2 Hz, *cis* M2), 5.74 (d, *J* = 15.1 Hz, *trans* M1), 5.73 (d, *J* = 15.2 Hz, *trans* M2, 2H), 4.38 (t, *J* = 6.5 Hz, M1), 4.12 (t, *J* = 6.7 Hz, M2 4H), 2.95 (t, *J* = 6.6 Hz, M1), 2.77 (dt, *J* = 16.4, 7.3 Hz, 4H), 1.76 – 1.62 (m, 8H), 1.45 (p, *J* = 3.7 Hz, 4H), 1.40 (h, *J* = 3.6 Hz, 4H). ^{13}C NMR (101 MHz, Chloroform-*d*) *δ* 166.9, 165.6, 150.3, 146.9, 113.9, 113.3, 64.3, 36.1, 31.9, 30.2, 28.8, 28.5, 28.4, 28.1, 25.8.

PolyM2$_{100}$: Recovered as a white fibrous solid (0.88 g, 85%). GPC analysis ($CHCl_3$, 0.5% Et_3N) M_n = 28.6 kg × mol^{-1}, $Đ_M$ = 3.6.

^{1}H NMR (400 MHz, Chloroform-*d*) %*trans* = 85; *δ* 7.67 (d, *J* = 15.2 Hz, *trans* 2H), 7.06 (d, *J* = 10.2 Hz, *cis*), 5.84 (d, *J* = 10.1 Hz, *cis*), 5.73 (d, *J* = 15.1 Hz, *trans* 2H), 4.12 (t, *J* = 6.6 Hz, 4H), 2.80 (t, *J* = 7.3 Hz, 4H), 1.97 – 1.59 (m, 8H), 1.45 (ddd, *J* = 7.3, 4.7, 2.1 Hz, 4H), 1.43 – 1.33 (m, 4H). ^{13}C NMR (101 MHz, Chloroform-*d*) δ 165.6, 146.9, 113.9, 64.4, 31.9, 28.8, 28.5, 28.4, 25.8.

PolyM1$_{10}$M3$_{90}$: Recovered as a transparent, tacky, soft solid (0.96 g, 84%). SEC analysis ($CHCl_3$, 0.5% Et_3N) M_n = 73.9 kg × mol^{-1}, $Đ_M$ = 1.8.

^{1}H NMR (400 MHz, Chloroform-*d*) %*trans* = 87; δ 7.70 (d, *J* = 15.1 Hz, *trans* 2H M1+M3), 7.10 (d, *J* = 10.2 Hz, *cis* M1+M3), 5.89 (d, *J* = 10.1 Hz, *cis* M1+M3), 5.77 (d, *J* = 15.2 Hz, *trans* 2H, M1+M3), 4.38 (t, *J* = 6.5 Hz, M1), 4.47 – 4.11 (m, 4H, M3), 3.88 – 3.45 (m, 4H, M3), 2.95 (t, *J* = 6.6 Hz, M1), 2.80 (t, *J* = 7.3 Hz, 4H), 2.00 – 1.63 (m, 4H), 1.45 (s, 4H). ^{13}C NMR (101 MHz, Chloroform-*d*) δ 165.4, 147.6, 113.4, 112.8, 69.3, 63.4, 31.9, 30.2, 28.4.

PolyM1$_{10}$M4$_{90}$: Recovered as a white solid (0.55 g, 84%). SEC analysis ($CHCl_3$, 0.5% Et_3N) M_n = 18.0 kg × mol^{-1}, $Đ_M$ = 2.3.

^{1}H NMR (400 MHz, Chloroform-*d*) %*trans* = 83; δ 7.72 (d, *J* = 15.1 Hz, *trans* 2H, M1+m4), 7.36 (s, 4H), 7.10 (d, *J* = 10.3 Hz, *cis*, M1+M4), 5.88 (d, *J* = 10.2 Hz, *cis*, M1+M4), 5.81 – 5.72 (m, *trans* 2H, M1+M4), 5.17 (d, *J* = 6.7 Hz, 4H), 4.38 (t, *J* = 6.5 Hz, M1), 2.95 (t, *J* = 6.5 Hz, M1), 2.77 (q, *J* = 8.3, 7.8 Hz, 4H), 1.68 (dq, *J* = 11.0, 6.8 Hz, 4H), 1.43 (p, *J* = 3.5 Hz, 4H). ^{13}C NMR (101 MHz, Chloroform-*d*) δ 165.2, 147.7, 136.4, 128.6, 113.4, 65.9, 31.9, 28.4.

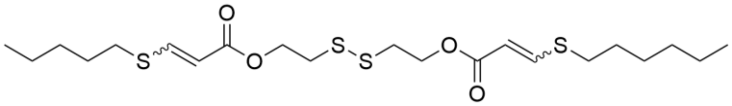
Procedure for synthesis of high cis polymer

1,6-Hexanedithiol (1 equivalent) was weighted in a 20 mL scintillation vial. Monomer M1 (x equivalent) and monomer M2 (1-x equivalent) were weighed in different vials according to the desired degree of monomer **1** in the final polymer. Monomers were then transferred to the vial containing the dithiol using DMSO. The final concentration of the thiol was kept at 0.5 M. 1% mol of catalyst was added to the reaction mixture that was left stirring for 14–16 h. The polymer was isolated *via* precipitation in diethyl ether followed by decantation and filtration, then dried in a vacuum oven held at room temperature.

***Cis*-PolyM1$_{10}$M2$_{90}$:** Recovered as a colorless, transparent, soft, tacky solid. SEC analysis ($CHCl_3$, 0.5% Et_3N) M_n = 11.5 kg × mol^{-1}, $Đ_M$ = 4.9.

^{1}H NMR (400 MHz, Chloroform-*d*) %*cis* = 64; δ 7.71 – 7.60 (m, *trans*, M1+M2), 7.06 (ddd, *J* = 10.3, 3.0, 1.6 Hz, *cis*, M1+M2), 5.84 (dd, *J* = 10.1, 1.0 Hz, M1+M2), 5.73 (dd, *J* = 15.1, 1.8 Hz, *trans*, M1+M2), 4.34 (td, *J* = 7.0, 6.2, 3.2 Hz, M1), 4.17 – 4.07 (m, 4H, M2), 3.01 (t, *J* = 7.0 Hz, M1), 2.78 (dtd, *J* = 16.4, 7.4, 2.2 Hz, 4H M1), 1.70 – 1.64 (m, 4H), 1.50 – 1.36 (m, 4H).

Small molecule study to assess the impact of disulfide bond exchange



1-Hexanethiol was weighed into a 20 mL scintillation vial. Monomer M1 was added (0.5 equivalent to thiol) and diluted with chloroform to reach a final concentration of thiol of 0.5 M. After cooling for ten minutes in an ice bath, 1% mol of catalyst (Et_3N) was added to the reaction mixture. The reaction was left warm up to room temperature and stirred overnight. Starting material consumption was evaluated by ^{1}H NMR spectroscopy.

The disappearance of the alkyne proton signal (2.9 ppm) was used to determine the end of the reaction. The solution was concentrated under reduced pressure and the crude product obtained as a colorless fluid was analysed *via* ^{1}H NMR, ^{13}C NMR, FT-IT, and MS.

^{1}H NMR (400 MHz, Chloroform-*d*) %*trans* = 85 δ 7.73 (d, J = 15.1 Hz, 2H), 7.14 (d, J = 10.2 Hz, 2H), 5.85 (d, J = 10.2 Hz, 2H), 5.74 (d, J = 15.1 Hz, 2H), 4.44 – 4.29 (m, 4H), 2.95 (t, J = 6.6 Hz, 4H), 2.84 – 2.72 (m, 4H), 1.68 (tt, J = 7.5, 6.2 Hz, 4H), 1.47 – 1.33 (m, 8H), 1.38 – 1.10 (m, 6H), 1.00 – 0.74 (m, 1H). ^{13}C NMR (101 MHz, Chloroform-*d*) δ 165.0, 148.1, 112.9, 62.1, 37.5, 32.0, 31.3, 28.5, 22.5, 13.9.

HRMS (TOF-MS-EI^{+}) (m/z): $[M+H]^{+}$ calculated for $C_{22}H_{38}O_4S_4$, 495.1731; found, 495.1736.

Degradation study

The polymer was weighed out in a 20 mL scintillation vial and solubilised with $CHCl_3$ to a final concentration of 1 mg/mL. DTT (10 eq. relative to disulfide content) was added to the solution. The reaction was left stirring at room temperature and monitored *via* SEC ($CHCl_3$ 0.5% Et_3N) until constant M_W was reached.

NMR spectroscopy of synthesised monomers

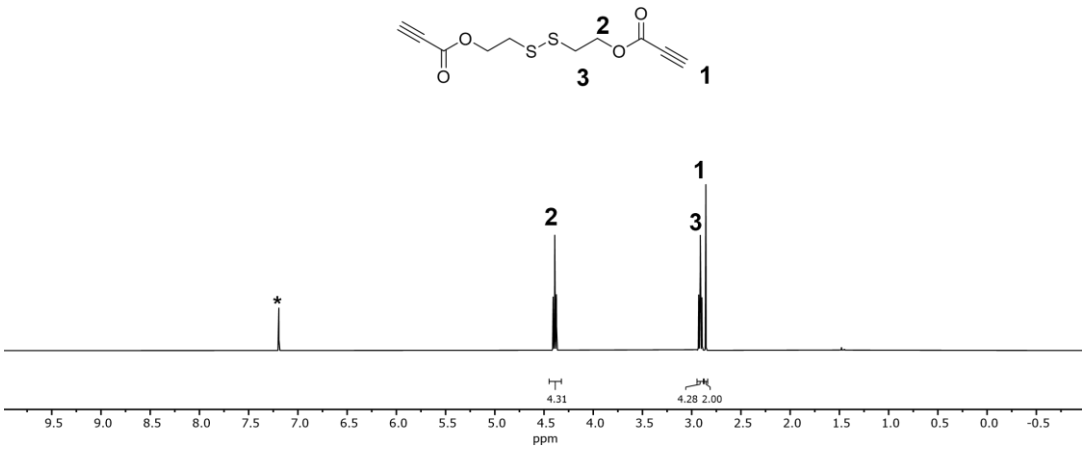


Figure S1. ^{1}H NMR (400 MHz, 300 K, $CDCl_3$) of monomer M1.

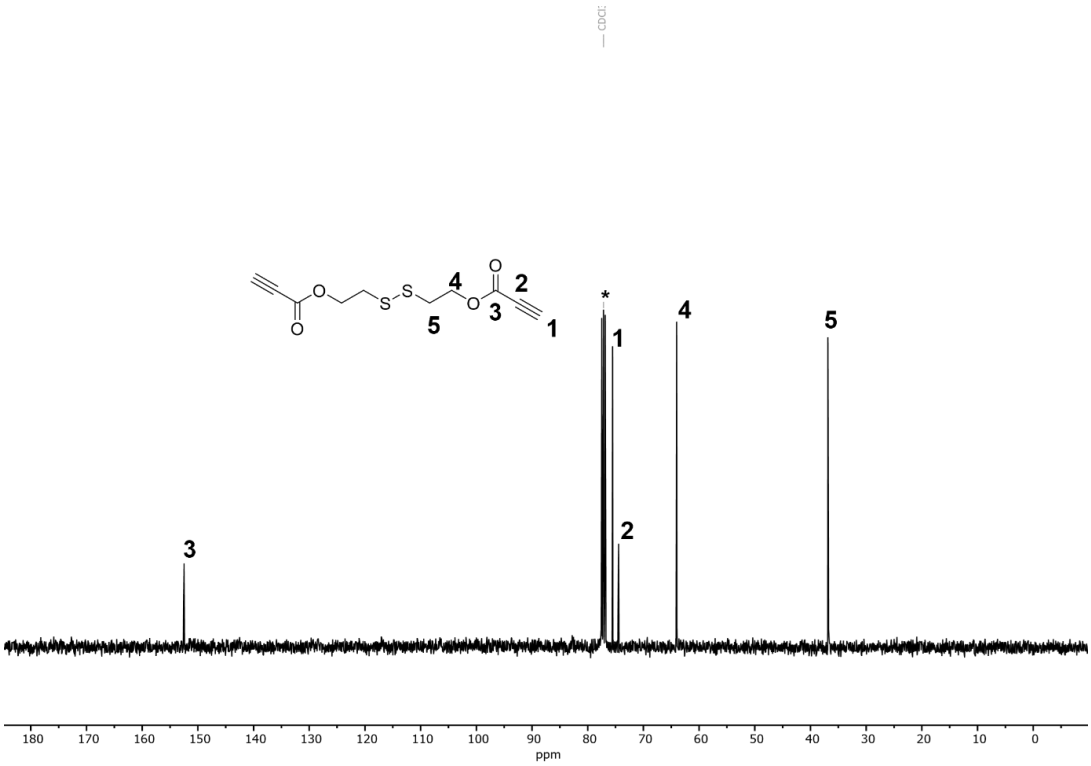


Figure S2. ^{13}C NMR (100.57 MHz, 300 K, $CDCl_3$) of monomer M1.

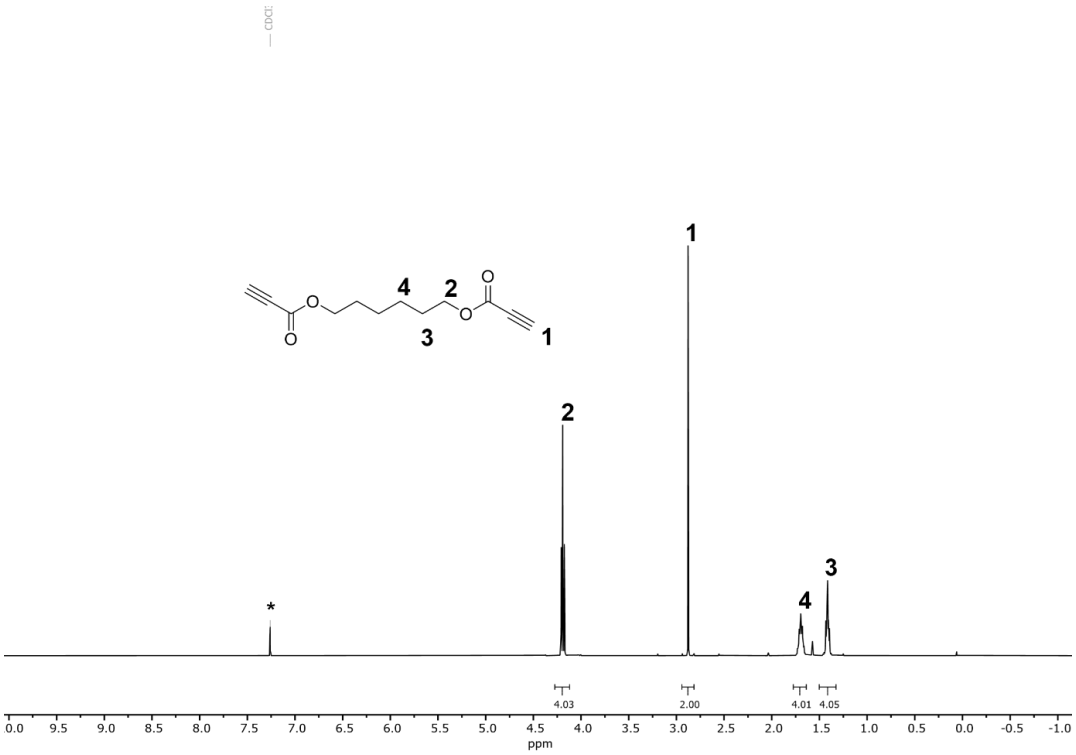


Figure S3. ^{1}H NMR (400 MHz, 300 K, $CDCl_3$) of monomer M2.

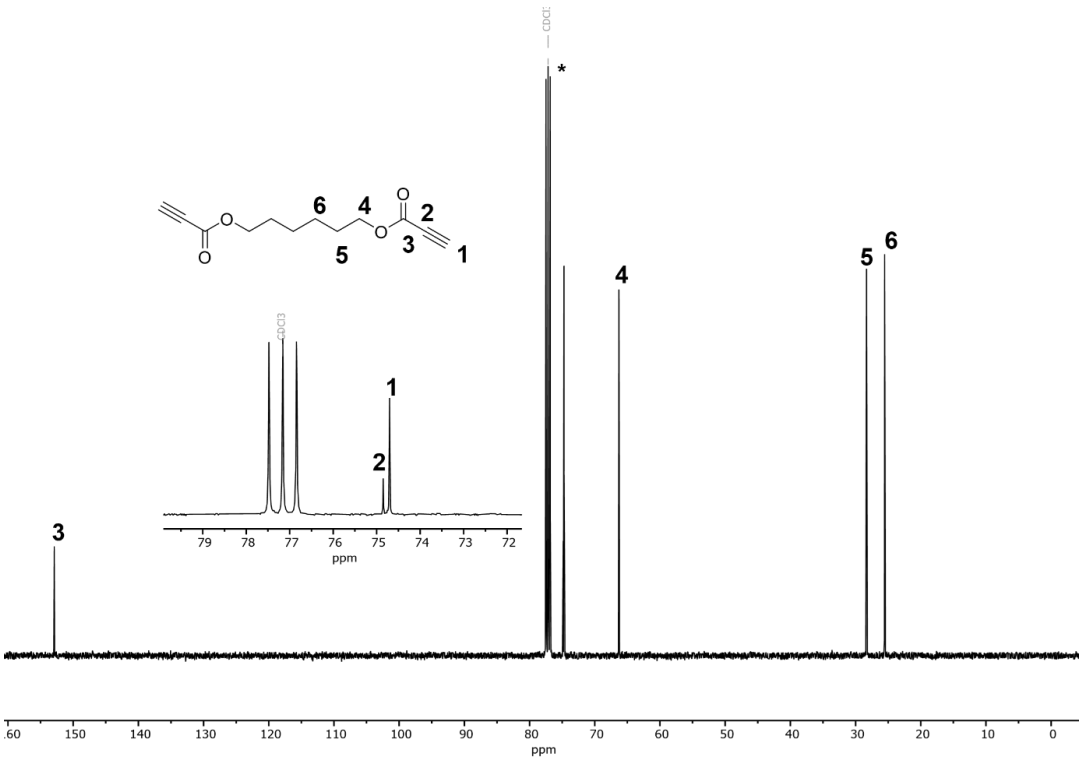


Figure S4. ^{13}C NMR (100.57 MHz, 300 K, $CDCl_3$) of monomer M2.

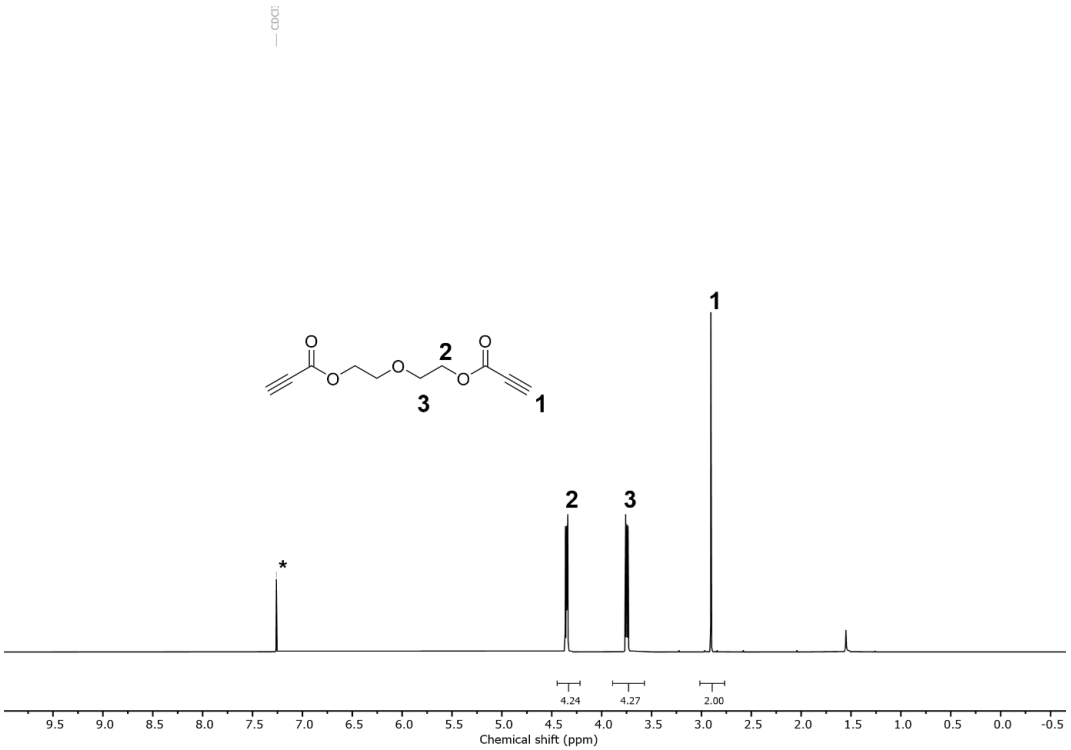


Figure S5. ^{1}H NMR (400 MHz, 300 K, $CDCl_3$) of monomer M3

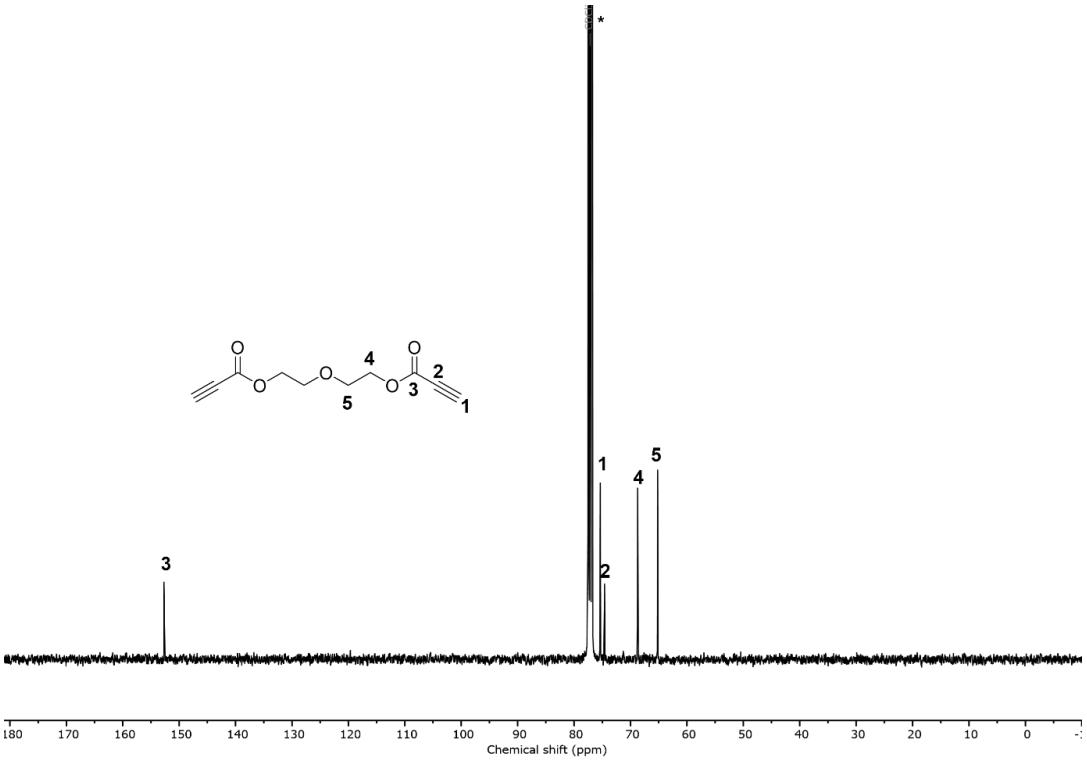


Figure S6. ^{13}C NMR (100.57 MHz, 300 K, $CDCl_3$) of monomer M3

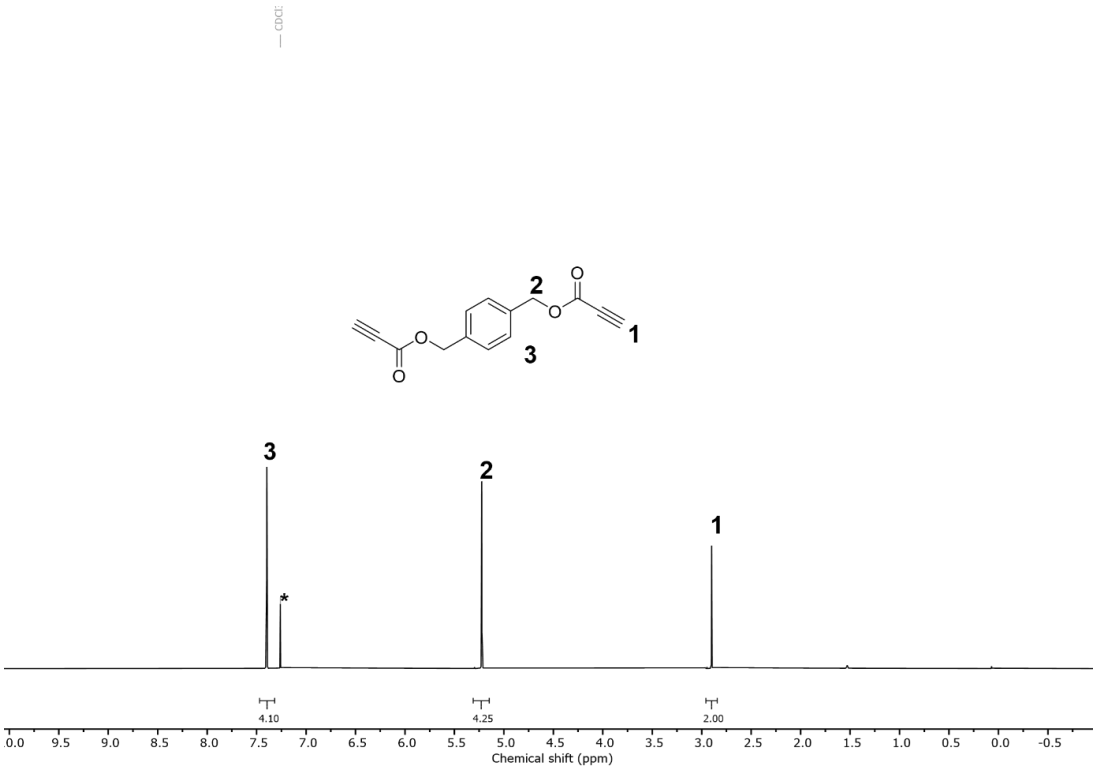


Figure S7. ^{1}H NMR (400 MHz, 300 K, $CDCl_3$) of monomer M4

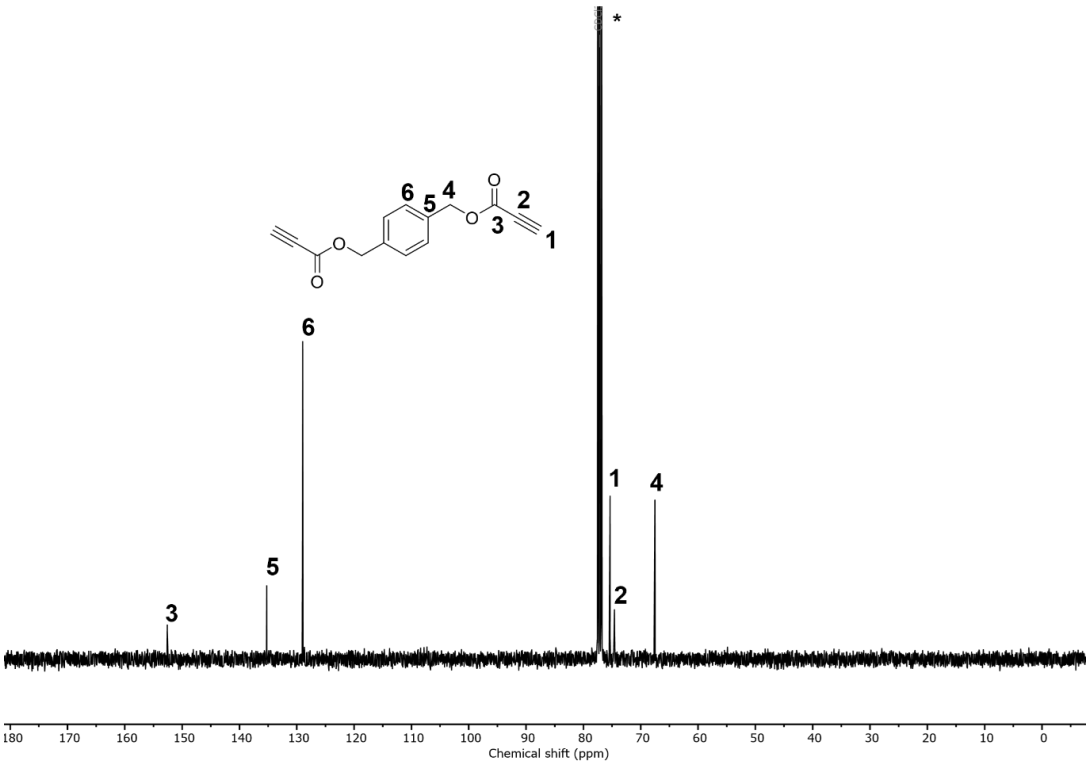


Figure S8. ^{13}C NMR (100.57 MHz, 300 K, $CDCl_3$) of monomer M4

^{1}H NMR spectra of solvent/catalyst screening

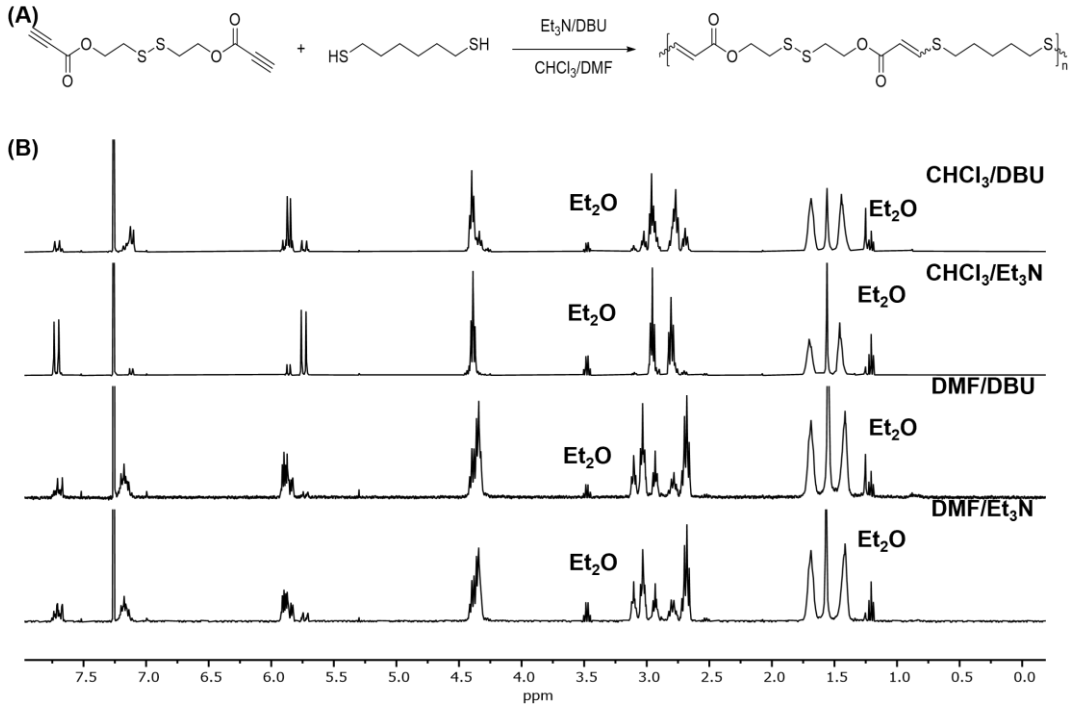


Figure S9. (A) Thiol-yne polymerization between monomer M1 and 1,6-hexanedithiol under different combinations of solvent/catalyst, with a catalyst loading of 1 mol%. (B) Stacked ^{1}H NMR (400 MHz, 300 K, $CDCl_3$) of copolymers. Residual diethyl ether (Et_2O) peaks from the precipitation solvent assigned. The $CHCl_3$/Et_3N combination was selected as it gave origin to fewer signals suggesting a more controlled reaction.

GPC traces of solvent/catalyst screening

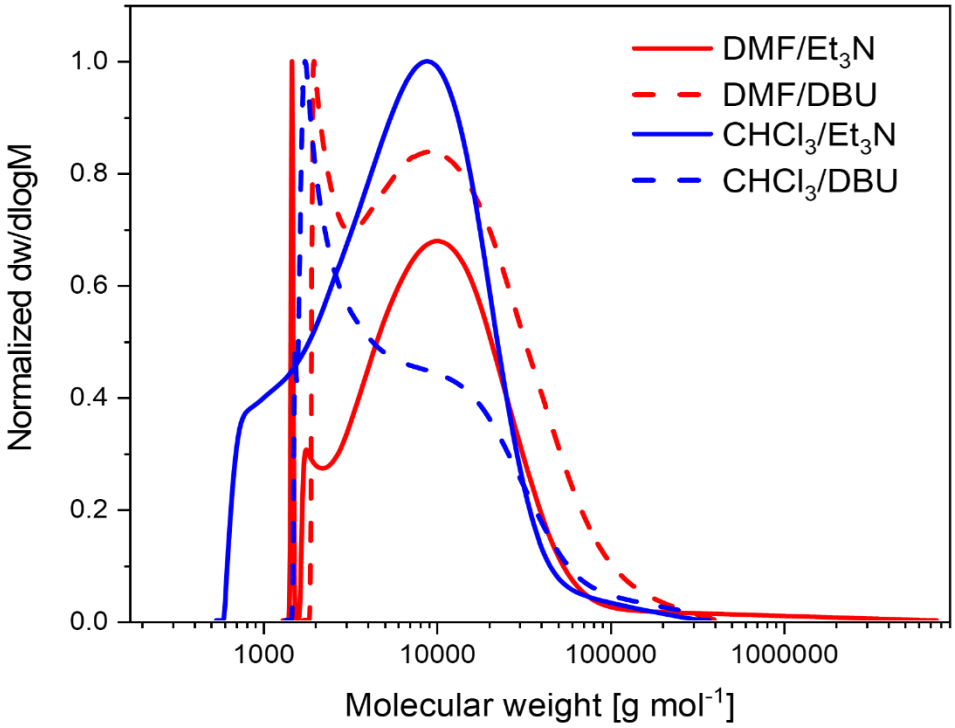


Figure S10. GPC ($CHCl_3$) traces of copolymers from different solvent/catalyst combinations.

Characterisation data of small molecules study

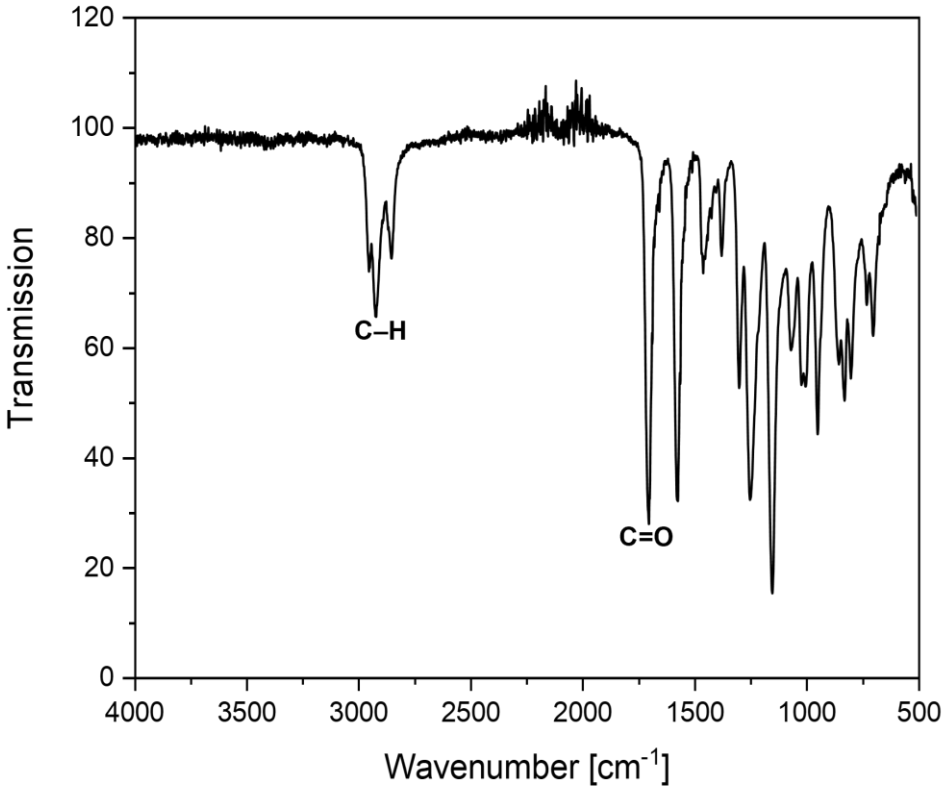


Figure S11. FT-IR spectra of crude reaction mixture after solvent removal of small molecule study.

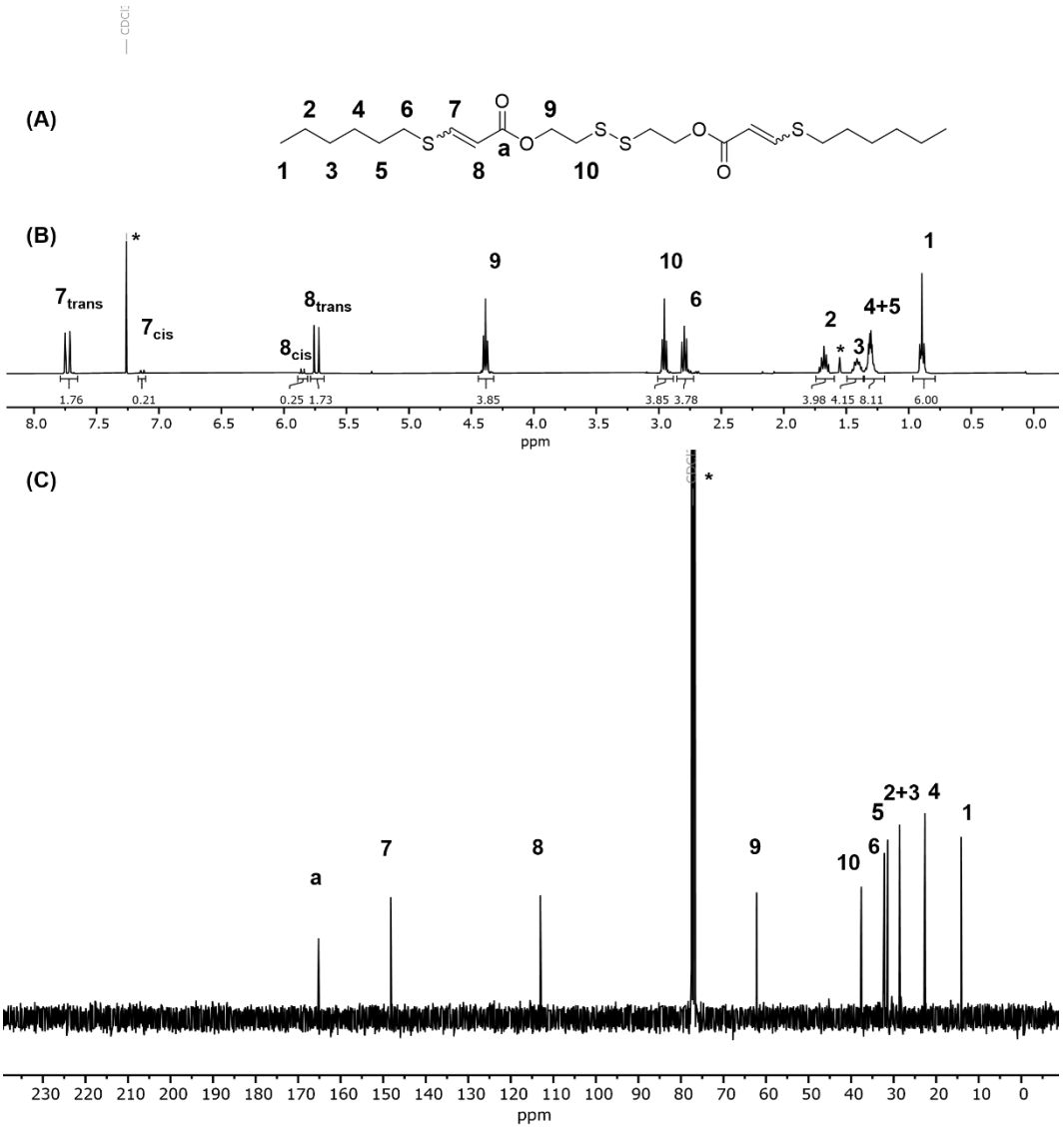


Figure S12. (A) structure of addition product (B) ^{1}H NMR (400 MHz, 300 K, $CDCl_3$), (B) ^{13}C NMR (100.57 MHz, 300 K, $CDCl_3$) of the crude reaction mixture after drying of small molecule study. Solvent and residual water peaks are marked with an asterisk.

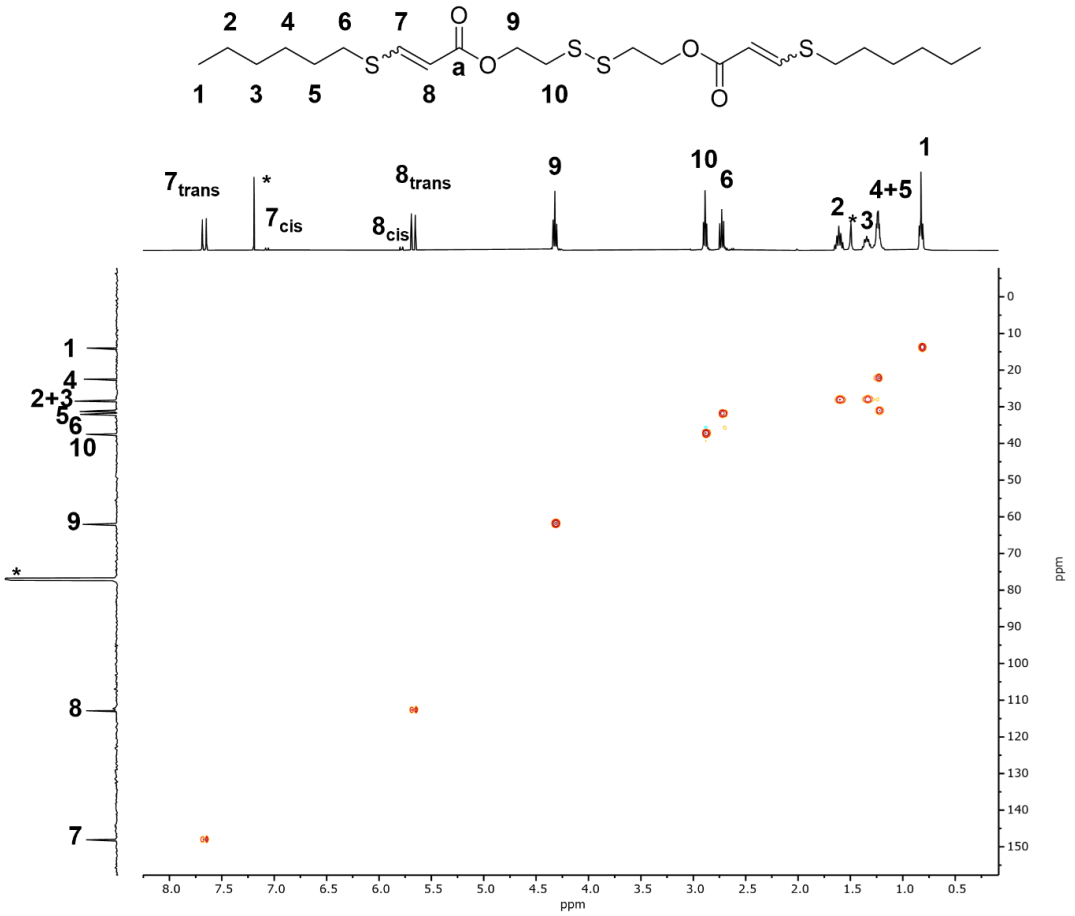


Figure S13. HSQC NMR (300 K, $CDCl_3$) of the crude reaction mixture after removal of the solvent of small molecule study. Solvent and residual water peaks are marked with an asterisk.

^{1}H NMR & ^{13}C NMR of *trans* polymers with varying amount of monomer M2

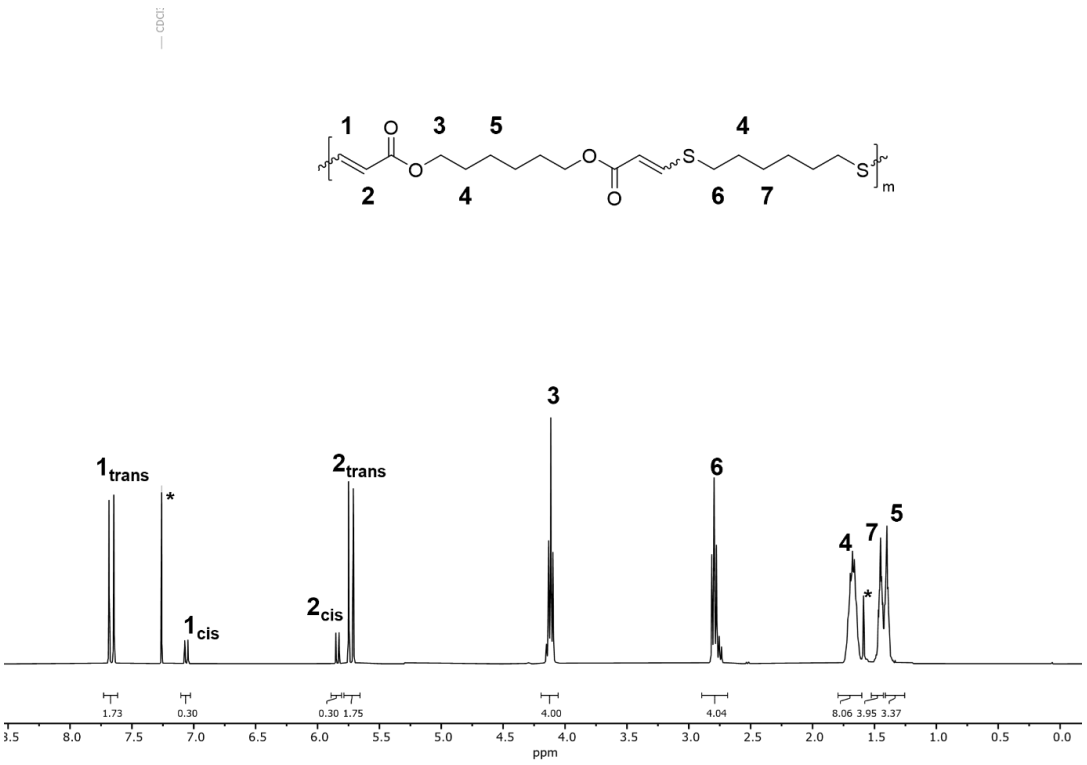


Figure S118. ^{1}H NMR (400 MHz, 300 K, $CDCl_3$) of poly$M2_{100}$. Solvent and residual water peaks are marked with an asterisk.

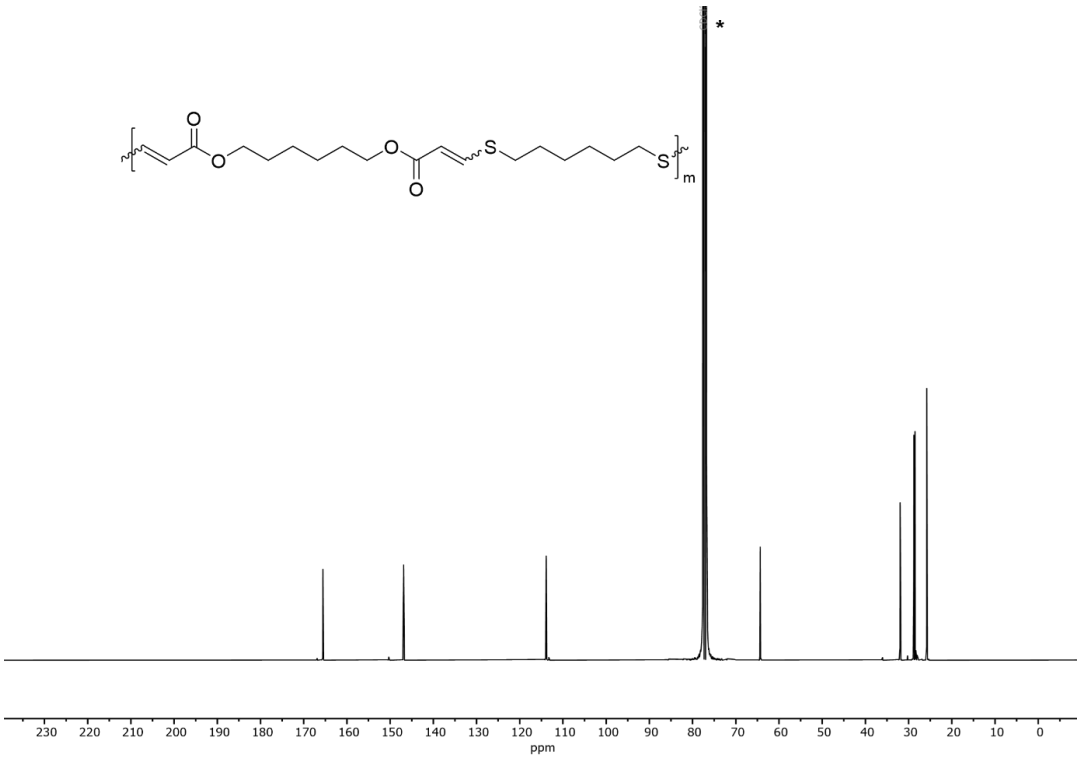


Figure S119. ^{13}C NMR (100.57 MHz, 300 K, $CDCl_3$) of poly$M2_{100}$. Solvent peak marked with an asterisk.

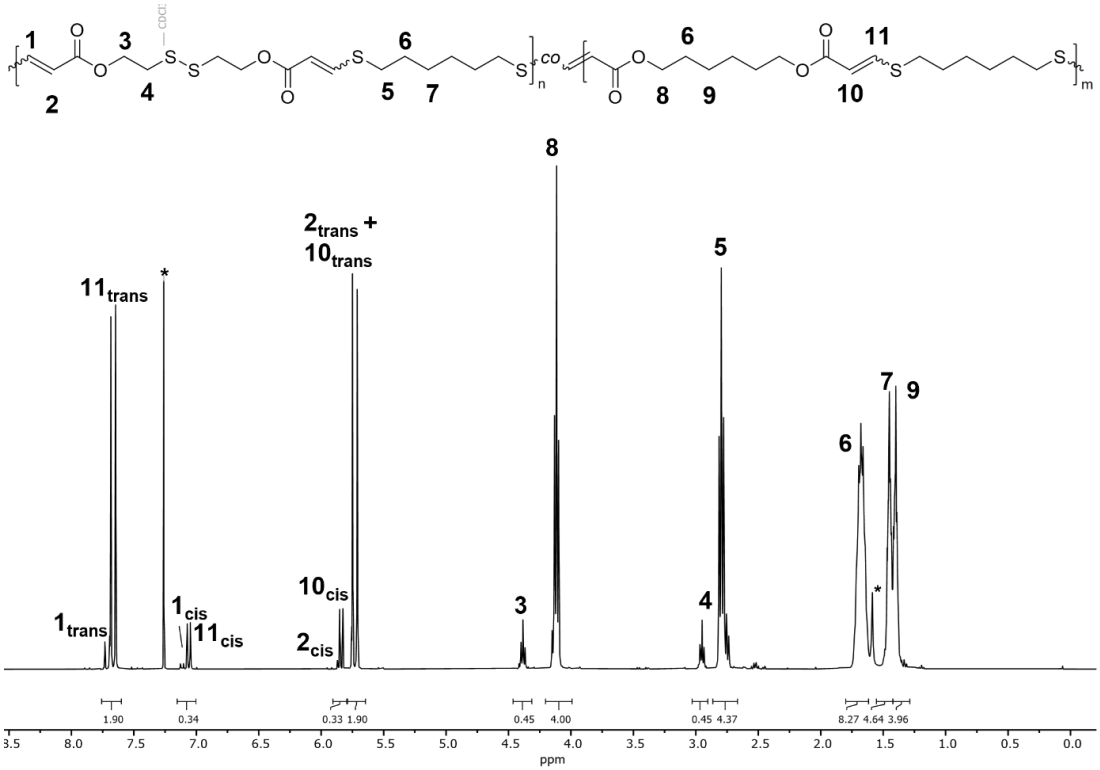


Figure S120. ^{1}H NMR (400 MHz, 300 K, $CDCl_3$) of poly$M1_{10}M2_{90}$. Solvent and residual water peak marked with an asterisk.

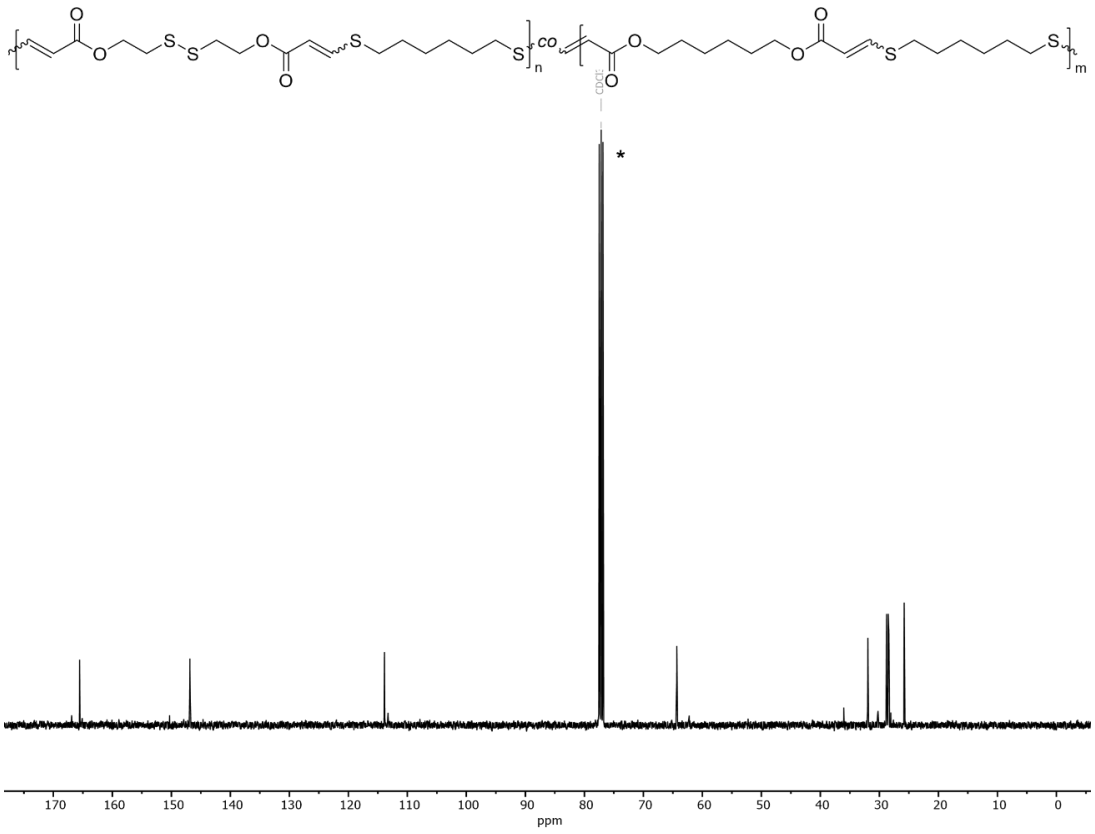


Figure S121. ^{13}C NMR (100.57 MHz, 300 K, $CDCl_3$) of poly$M1_{10}M2_{90}$. Solvent peaks marked with an asterisk.

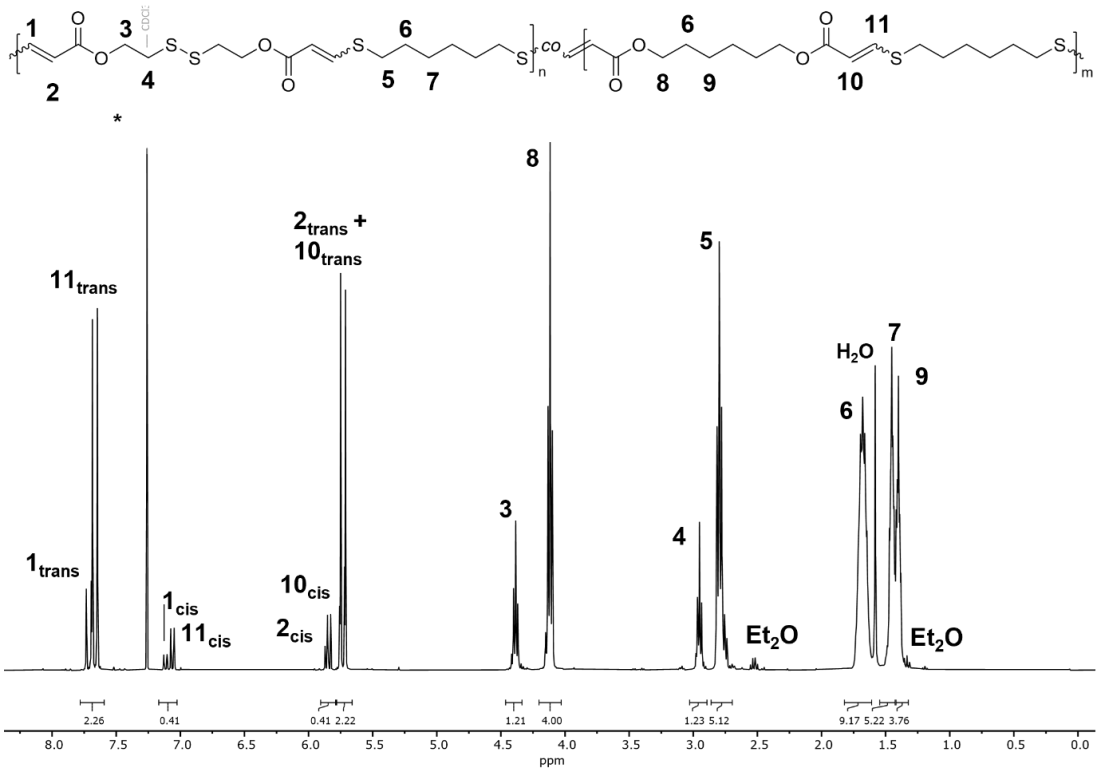


Figure S122. ^{1}H NMR (400 MHz, 300 K, $CDCl_3$) of poly$M1_{25}M2_{75}$. Residual solvent peaks assigned or marked with an asterisk.

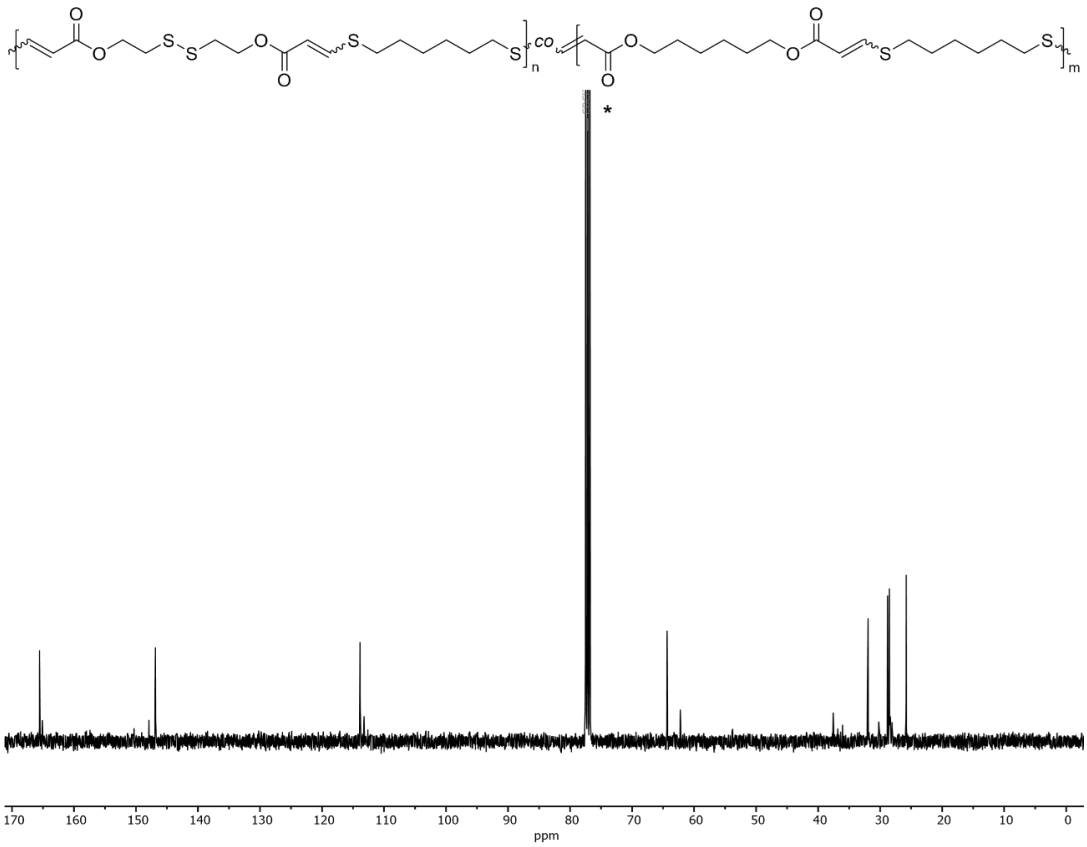


Figure S123. ^{13}C NMR (100.57 MHz, 300 K, $CDCl_3$) of poly$M1_{25}M2_{75}$. Solvent peaks marked with an asterisk.

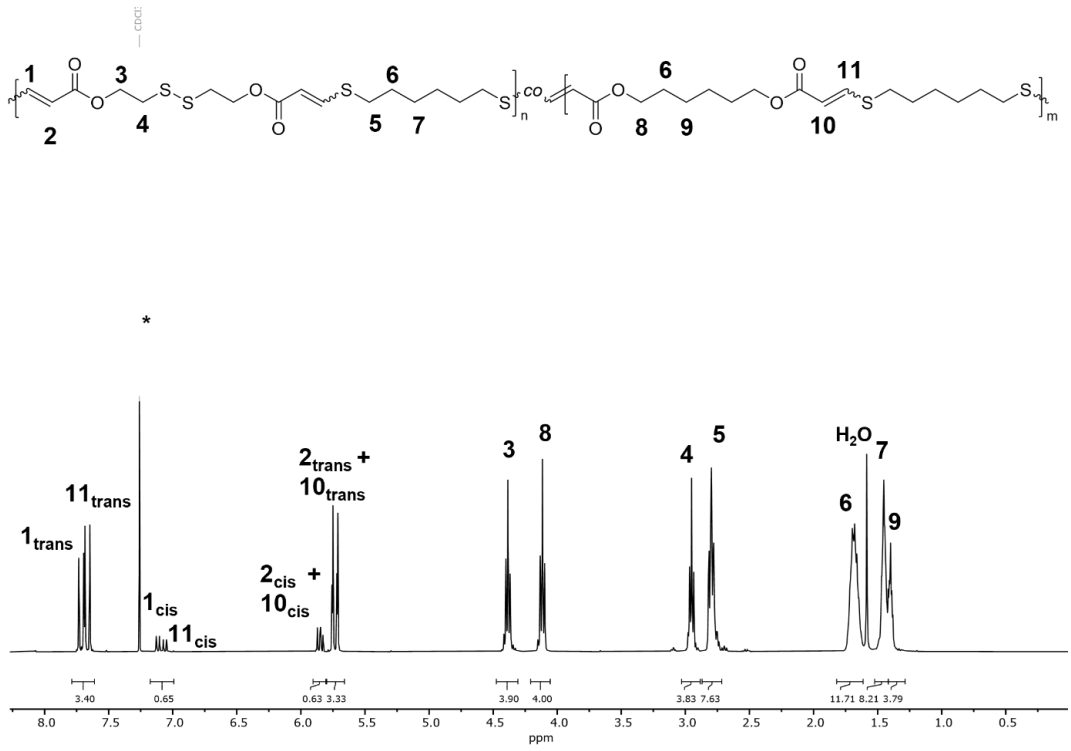


Figure S20. ^{1}H NMR (400 MHz, 300 K, $CDCl_3$) of poly$M1_{50}M2_{50}$. Residual solvent peak assigned.

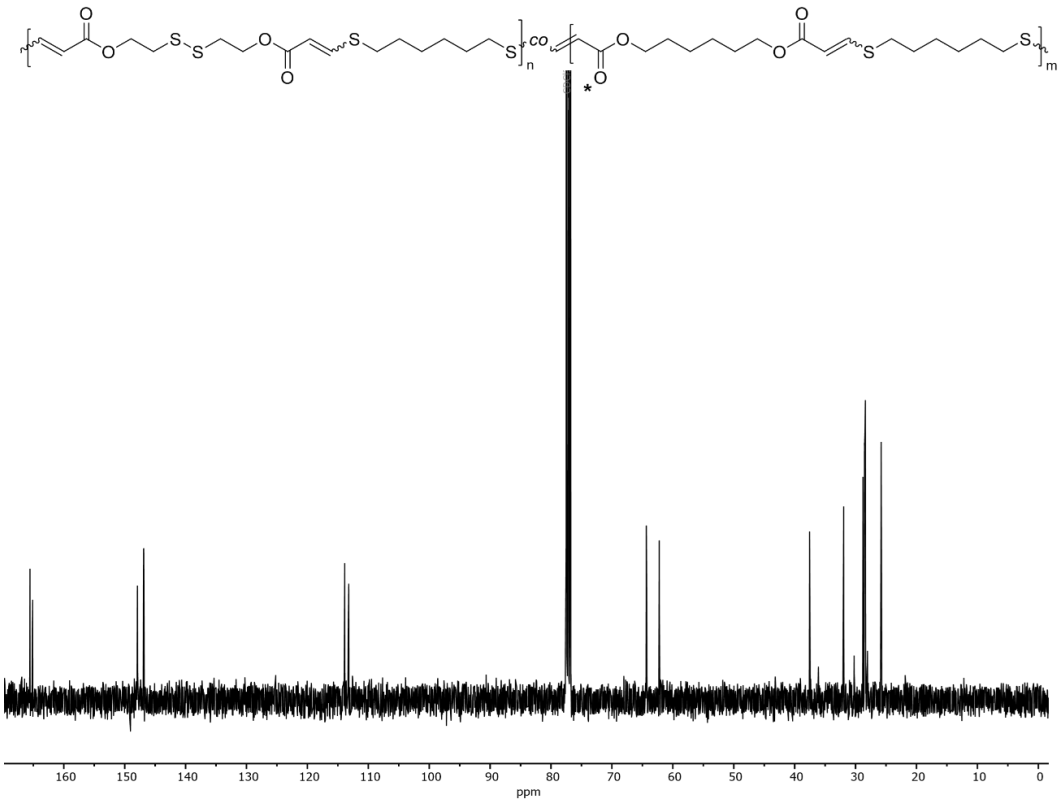


Figure S21. ^{13}C NMR (100.57 MHz, 300 K, $CDCl_3$) of poly$M1_{50}M2_{50}$. Solvent peak marked with an asterisk.

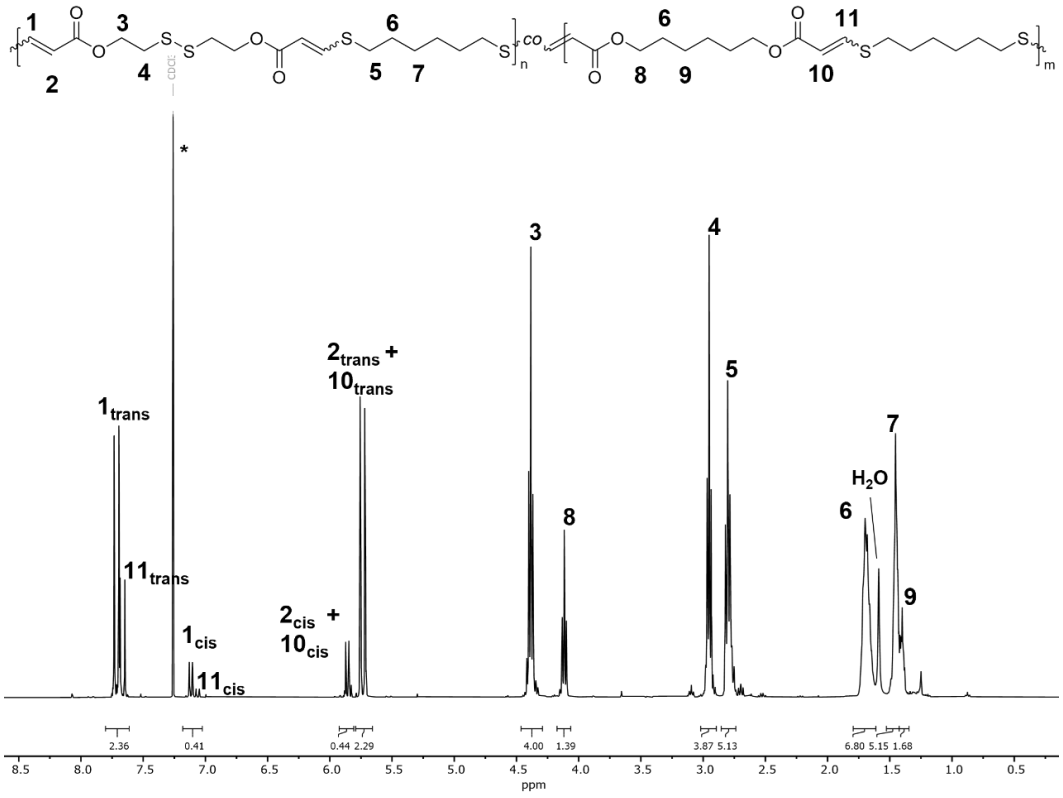


Figure S22. ^{1}H NMR (400 MHz, 300 K, $CDCl_3$) of poly$M1_{75}M2_{25}$. Residual solvent assigned.

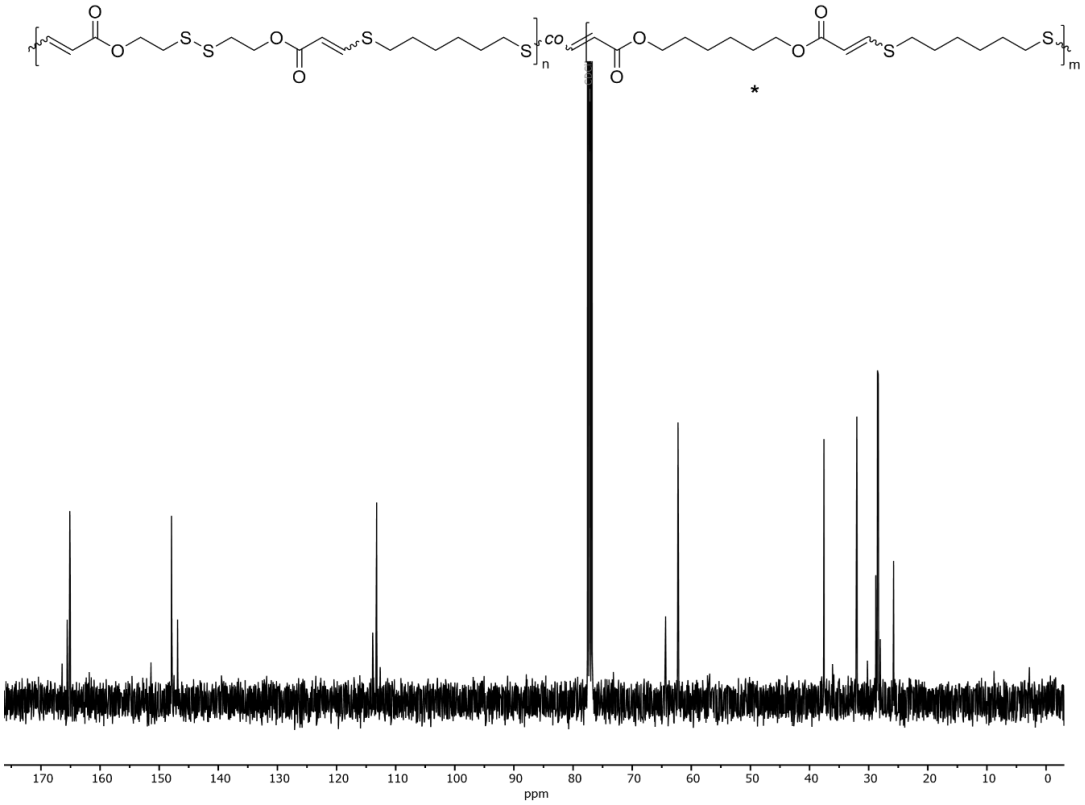


Figure S23. ^{13}C NMR (100.57 MHz, 300 K, $CDCl_3$) of poly$M1_{75}M2_{25}$. Solvent peak marked with an asterisk.

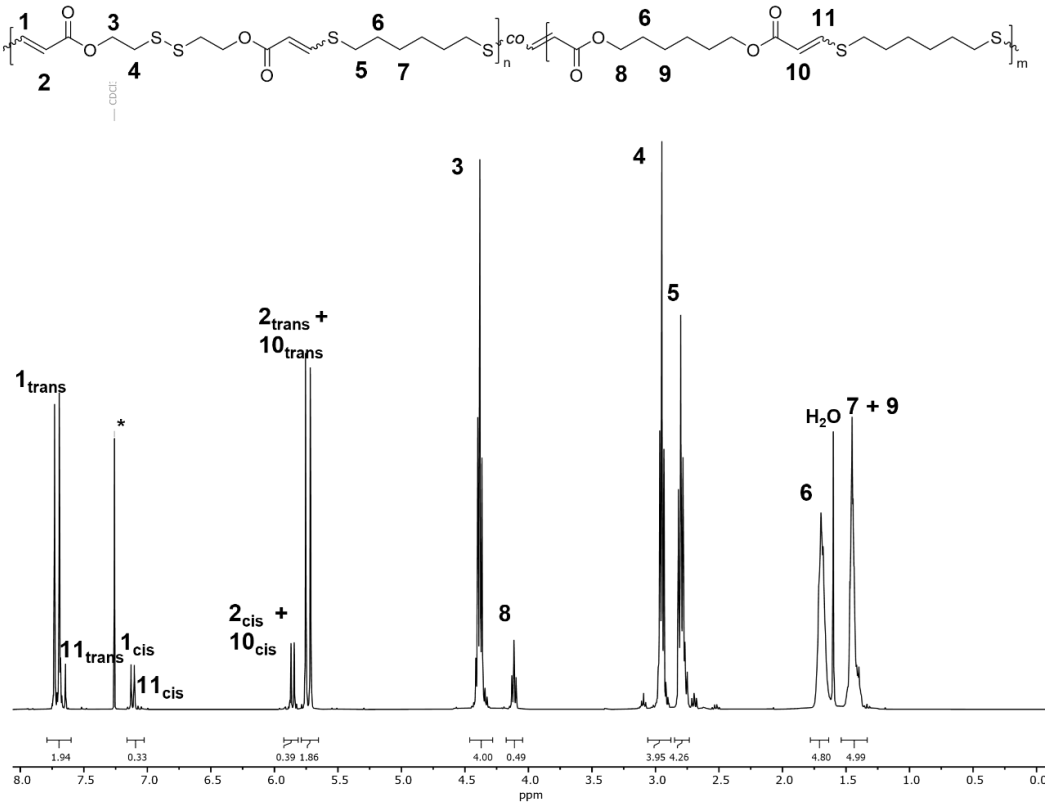


Figure S24. ^{1}H NMR (400 MHz, 300 K, $CDCl_3$) of poly$M1_{90}M2_{10}$. Residual solvent peak marked.

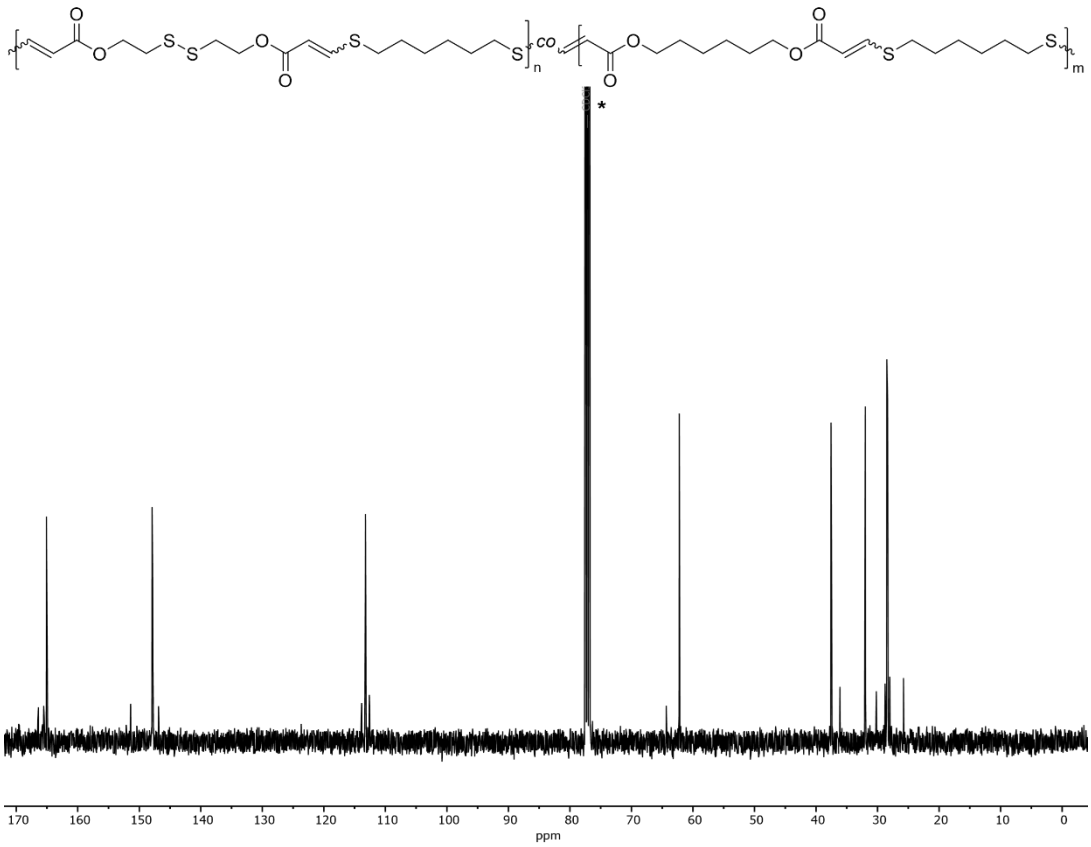


Figure S25. ^{13}C NMR (100.57 MHz, 300 K, $CDCl_3$) of poly$M1_{90}M2_{10}$. Solvent peaks are marked with an asterisk.

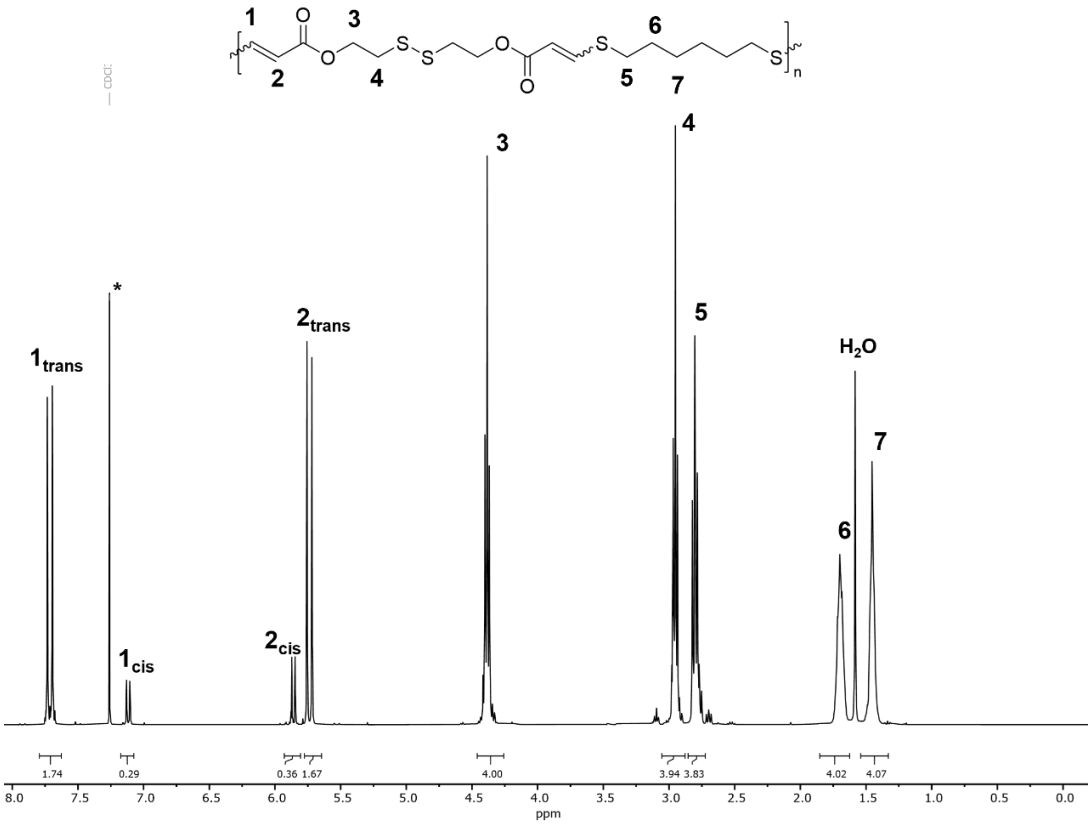


Figure S26. ^{1}H NMR (400 MHz, 300 K, $CDCl_3$) of poly$M1_{100}$. Solvent peak are marked with an asterisk.

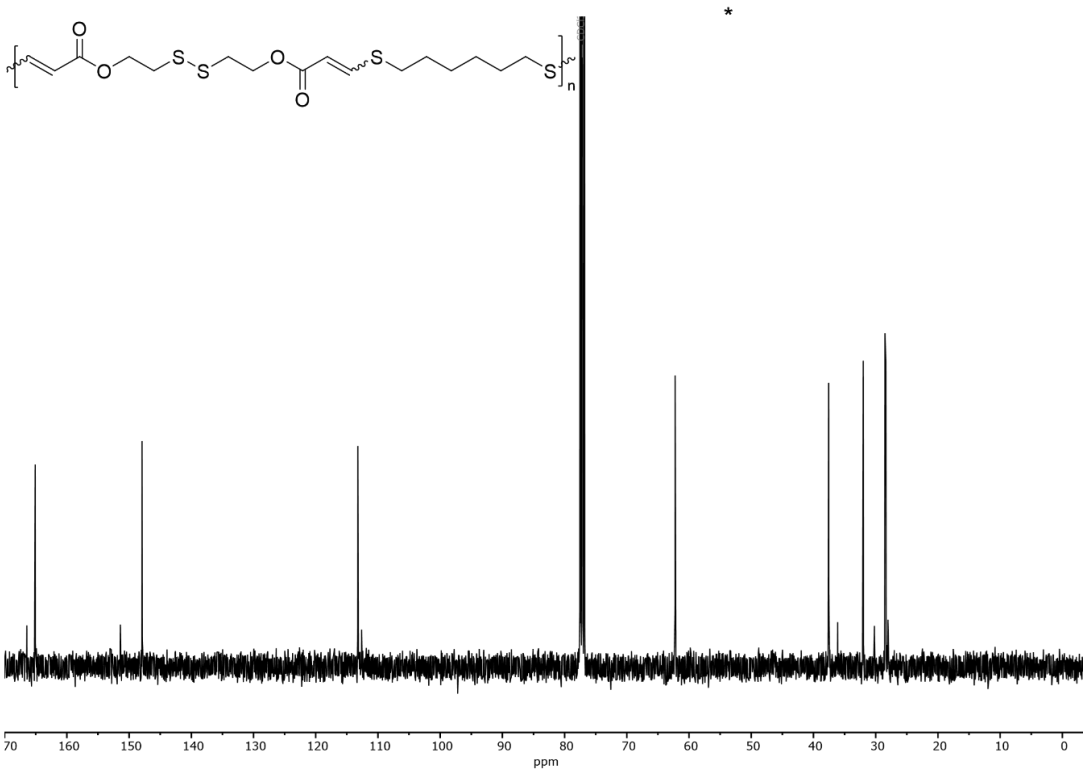


Figure S27. ^{13}C NMR (100.57 MHz, 300 K, $CDCl_3$) of polyM1$_{100}$. Solvent peaks marked with an asterisk.

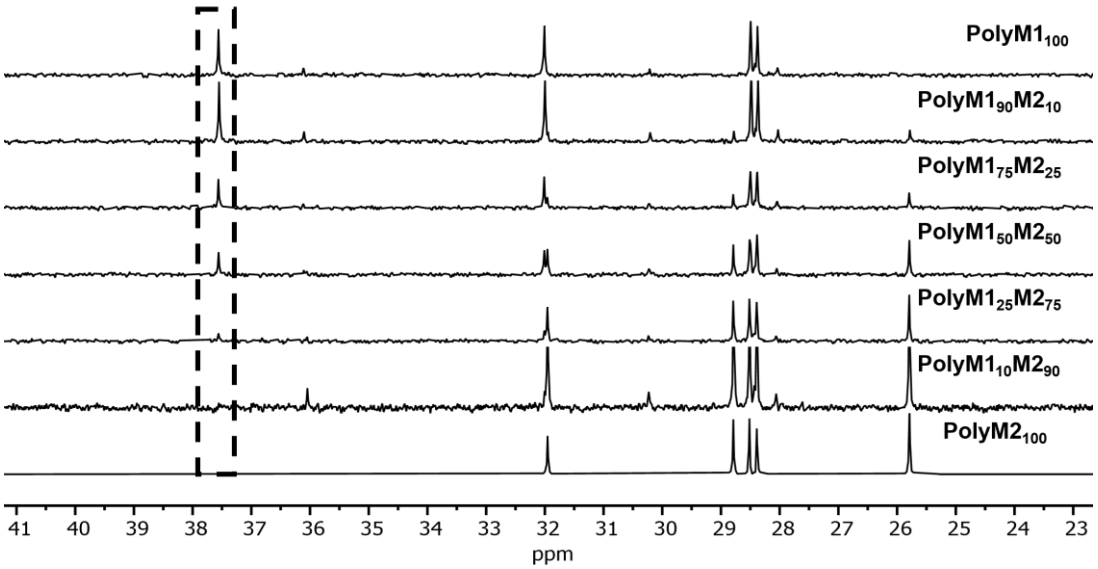


Figure S28. stacked ^{13}C NMR (400 MHz, 300 K, $CDCl_3$) of copolymer obtained reacting 1,6-hexanedithiol and different ratios of monomer 1 and 2 respectively. Characteristic S-S $^{\beta}C$ signal (ppm>35) intensity increases with increasing monomer M1 content.

Thermal characterisation of *trans* polymer of different monomer M1 content

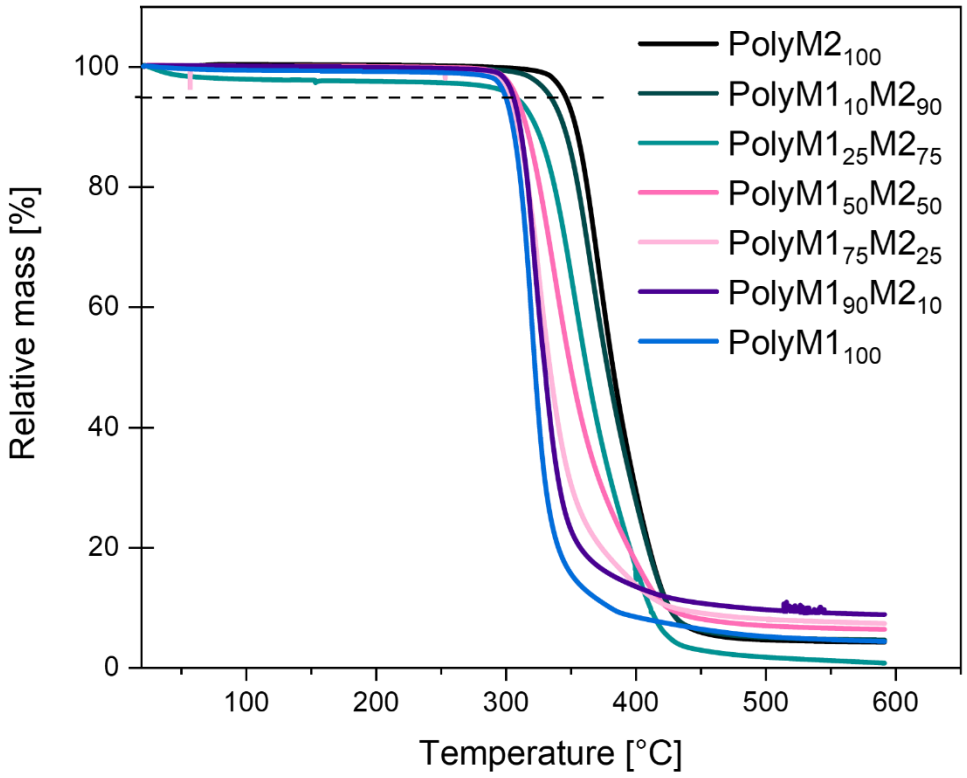


Figure S29. TGA thermograms resulted from heating at 10 °C /min up to 600 °C under a N_2 atmosphere. 5% relative mass loss is highlighted with a dashed line.

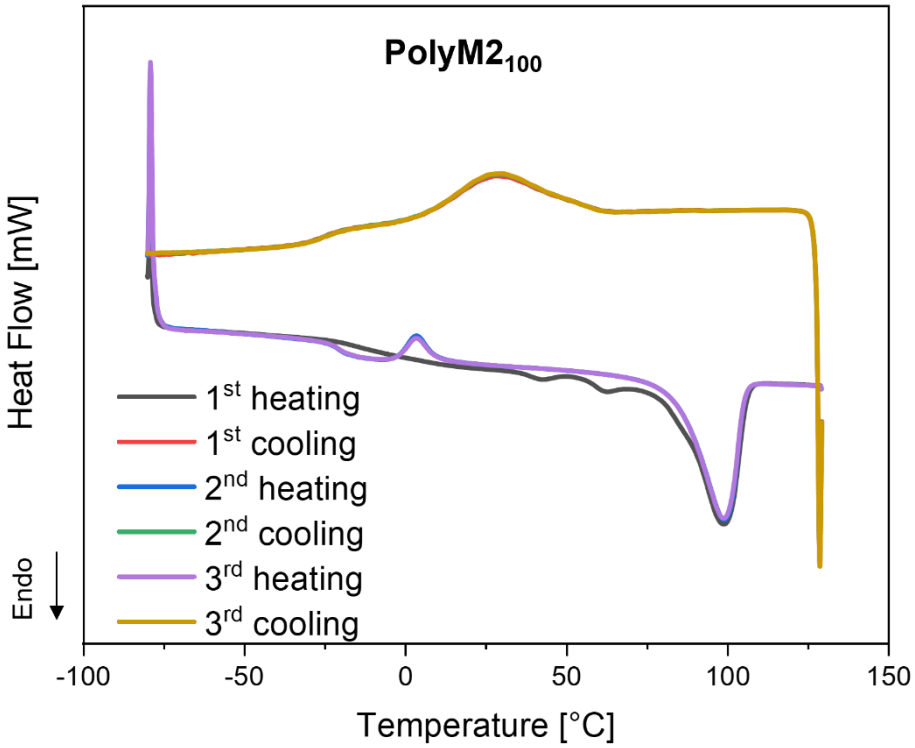


Figure S30. DSC thermograms of PolyM2$_{100}$ tested between −80 °C and 130 °C at 10 °C min^{-1}.

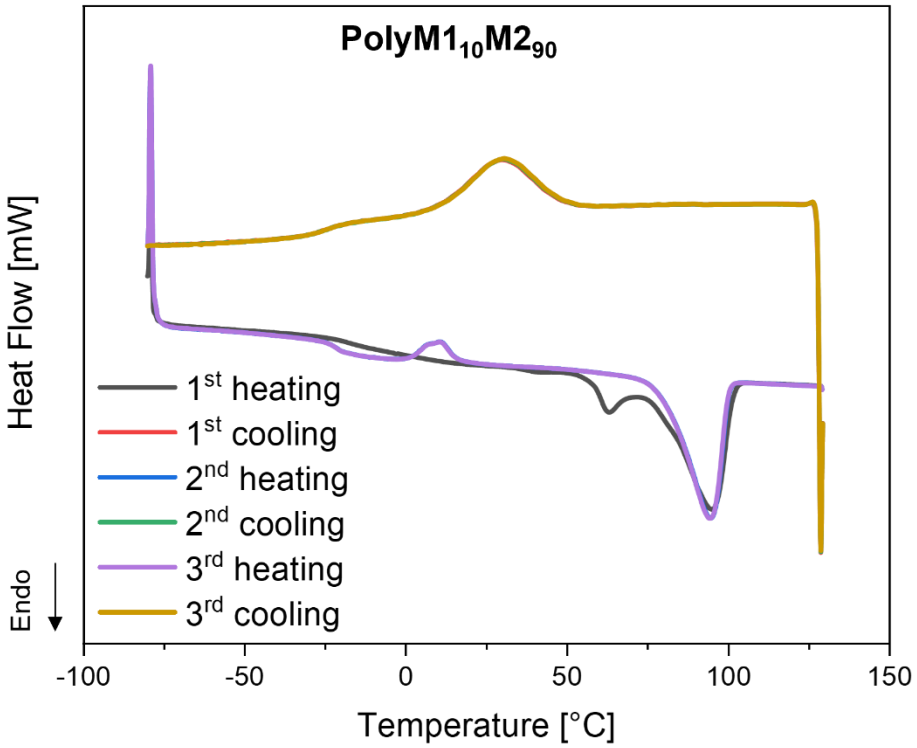


Figure S31. DSC thermograms of PolyM1$_{10}$M2$_{90}$ tested between −80 °C and 130 °C at 10 °C min^{-1}

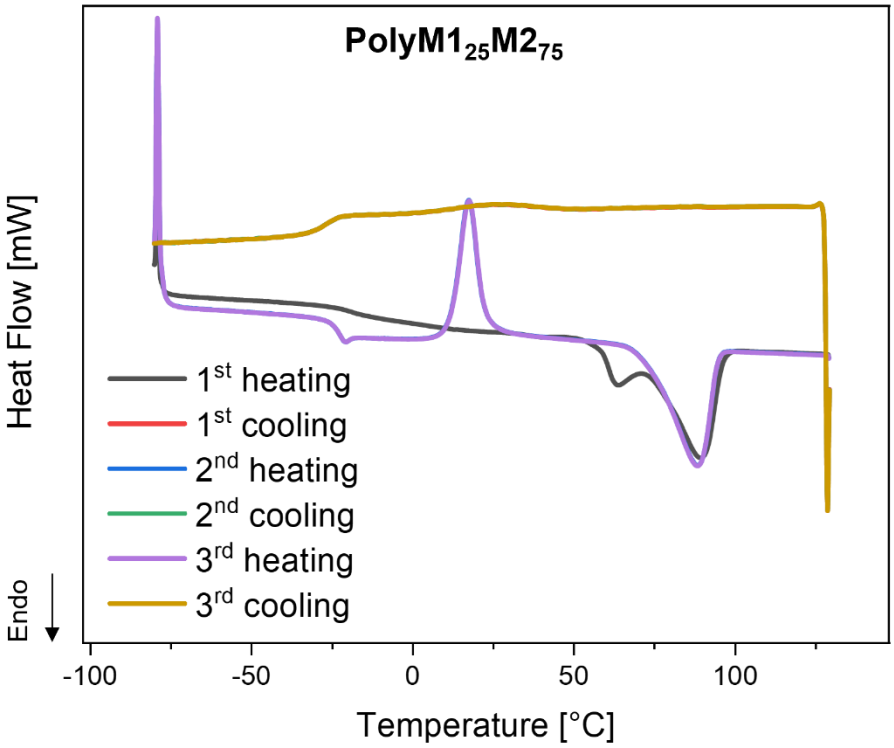


Figure S32. DSC thermograms of PolyM1$_{25}$M2$_{75}$ tested between −80 °C and 130 °C at 10 °C min^{-1}.

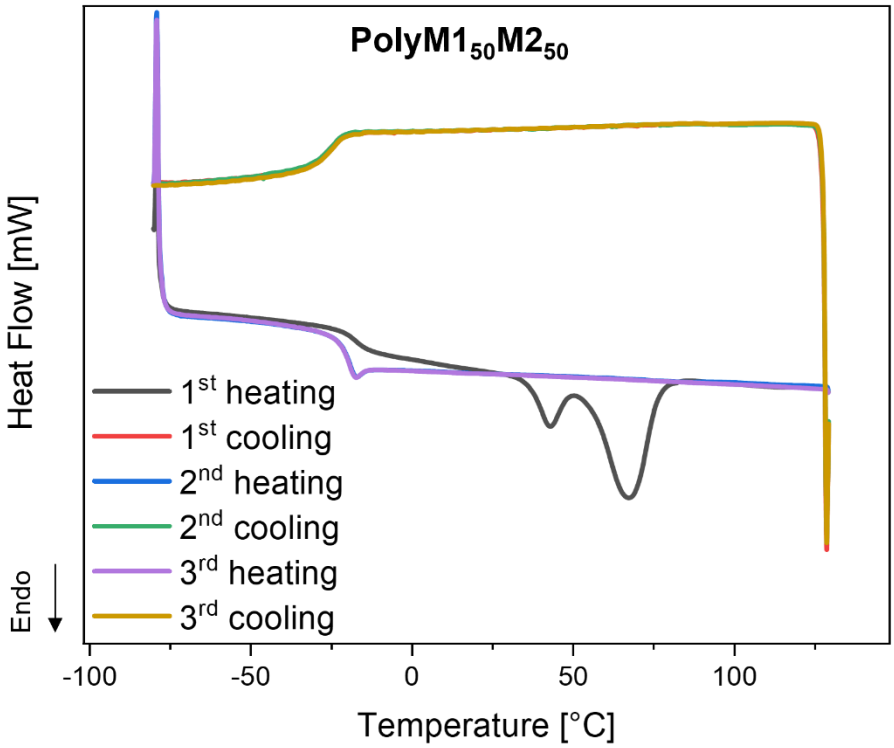


Figure S33. DSC thermograms of PolyM1$_{50}$M2$_{50}$ tested between −80 °C and 130 °C at 10 °C min^{-1}.

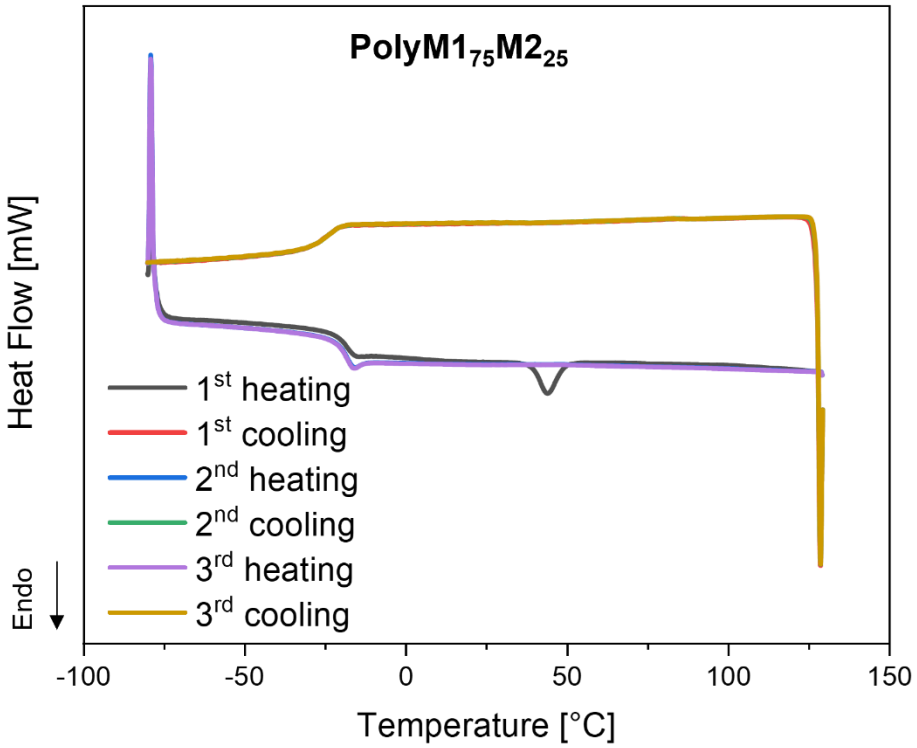


Figure S34. DSC thermograms of PolyM1$_{75}$M2$_{25}$ tested between −80 °C and 130 °C at 10 °C min^{-1}.

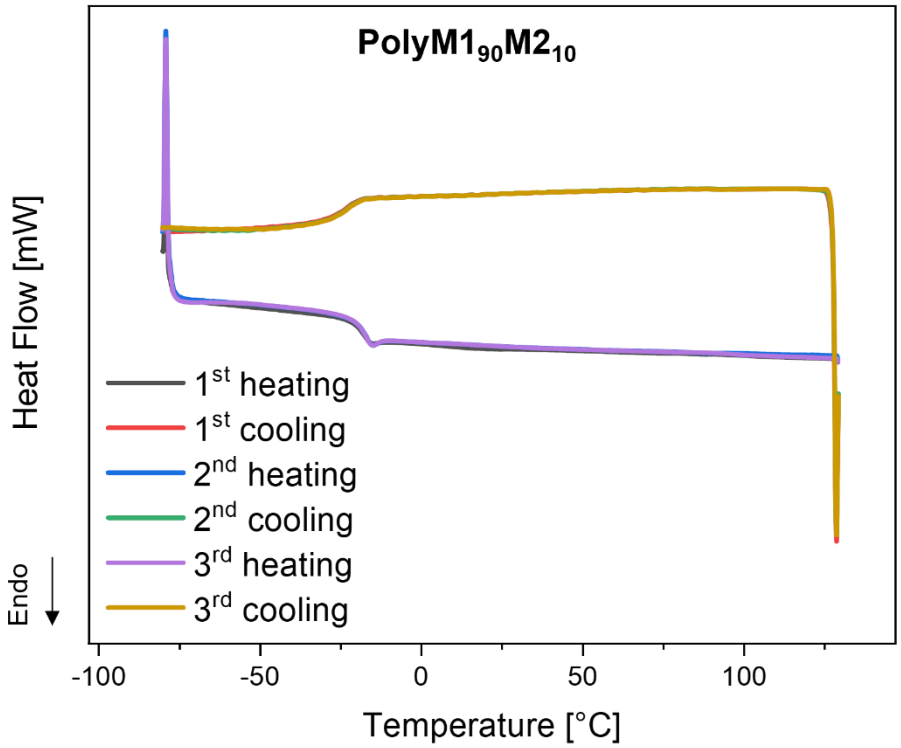


Figure S35. DSC thermograms of PolyM1$_{10}$M2$_{90}$ tested between −80 °C and 130 °C at 10 °C min^{-1}.

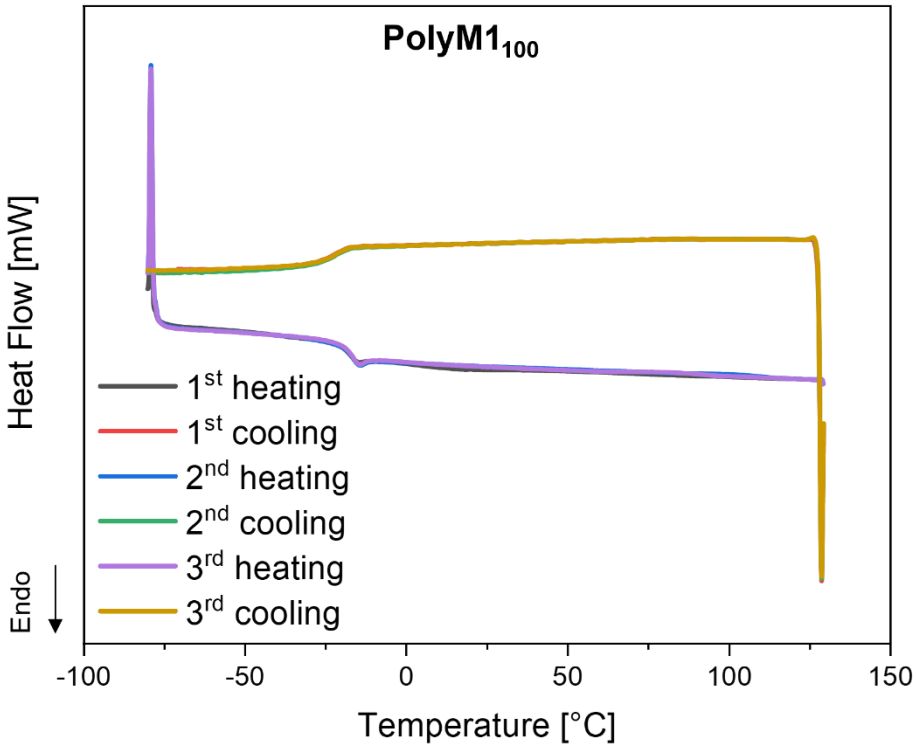


Figure S36. DSC thermograms of PolyM1$_{100}$ tested between −80 °C and 130 °C at 10 °C min^{-1}.

Influence of compression moulding on polymer structure and M_w

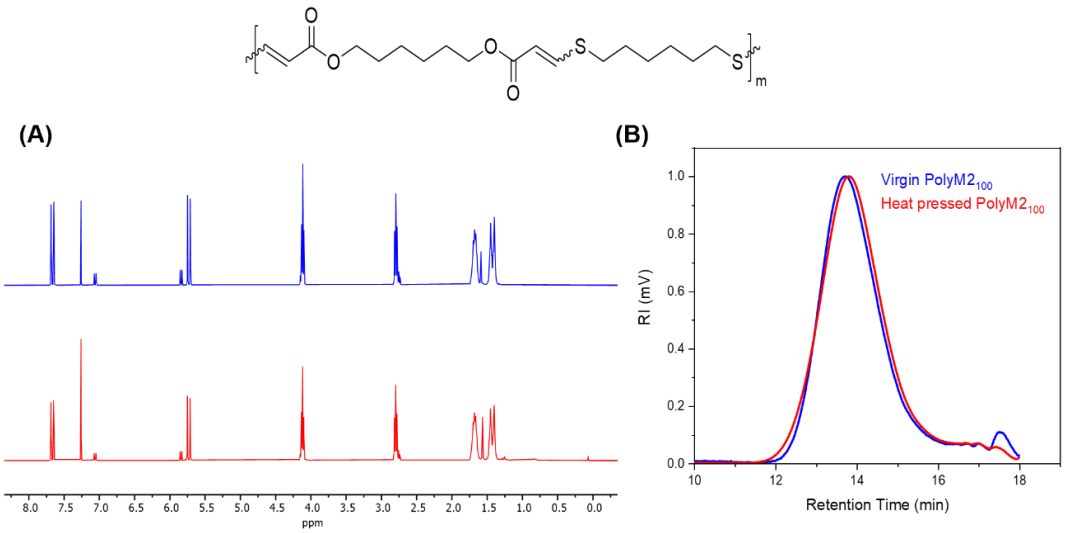


Figure S37. (A) ^{1}H NMR (400 MHz, 300 K, $CDCl_3$)and (B) GPC ($CHCl_3$, 0.5% Et_3N) of polyM2$_{100}$ before (top) and after (bottom) the moulding process.

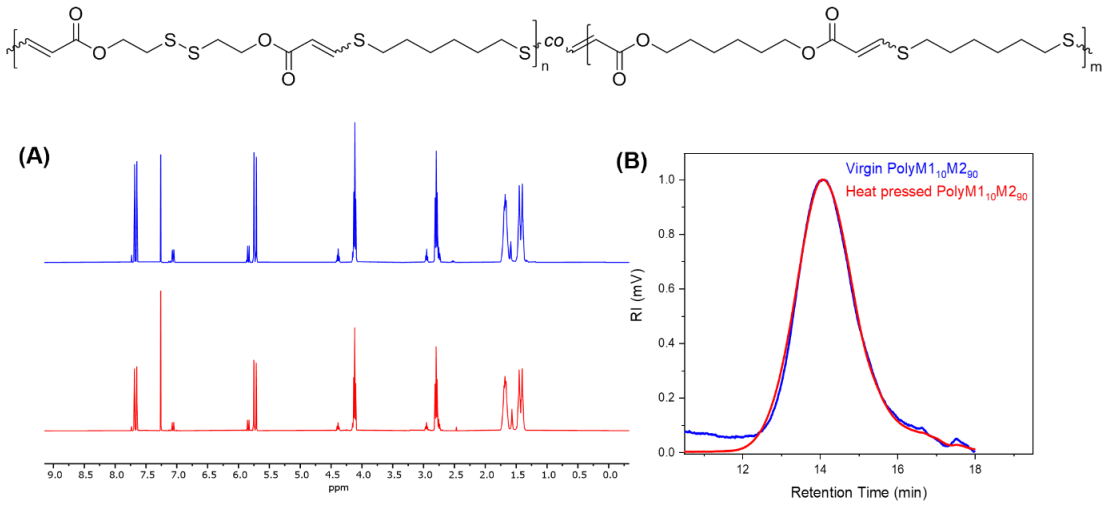


Figure S38. (A) ^{1}H NMR (400 MHz, 300 K, $CDCl_3$) and (B) GPC ($CHCl_3$, 0.5% Et_3N) of polyM1$_{10}$M2$_{90}$ before (top) and after (bottom) the moulding process.

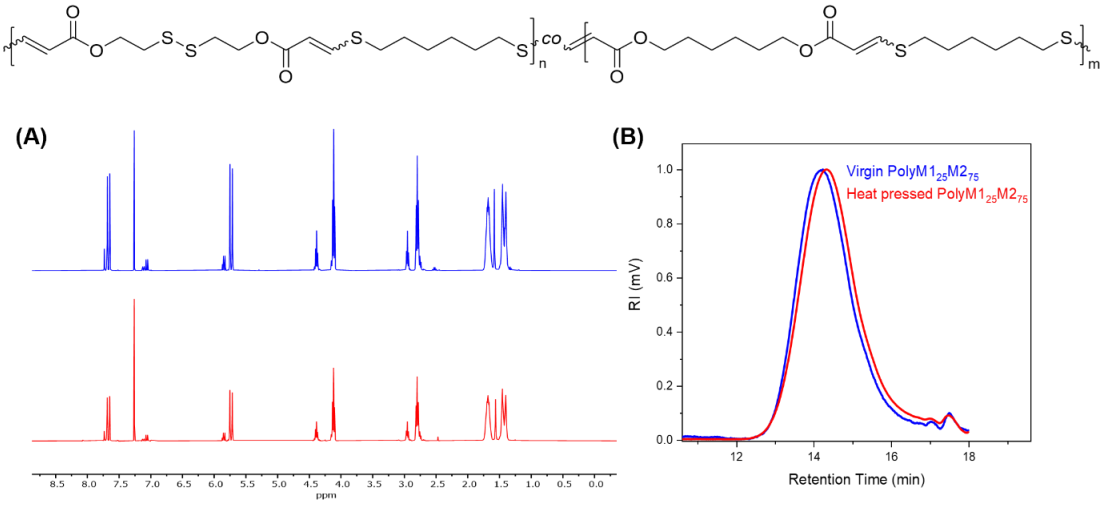


Figure S39. (A) ^{1}H NMR (400 MHz, 300 K, $CDCl_3$) and (B) GPC ($CHCl_3$, 0.5% Et_3N) of polyM1$_{25}$M2$_{75}$ before (top) and after (bottom) the moulding process.

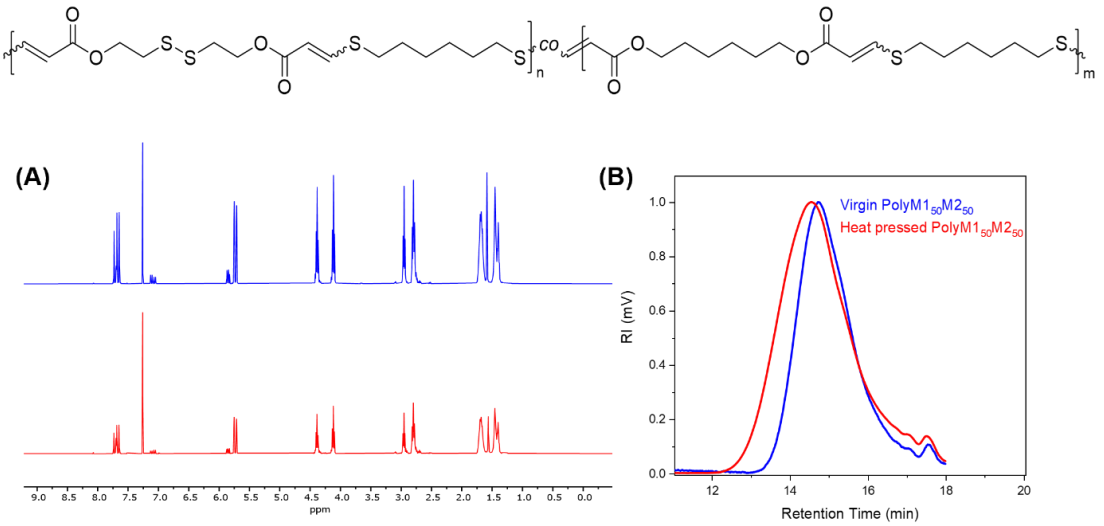


Figure S40. (A) ^{1}H NMR (400 MHz, 300 K, $CDCl_3$) and (B) GPC ($CHCl_3$, 0.5% Et_3N) of polyM1$_{50}$M2$_{50}$ before (top) and after (bottom) the moulding process.

Mechanical characterisation of *trans* polymers of different monomer M1 content

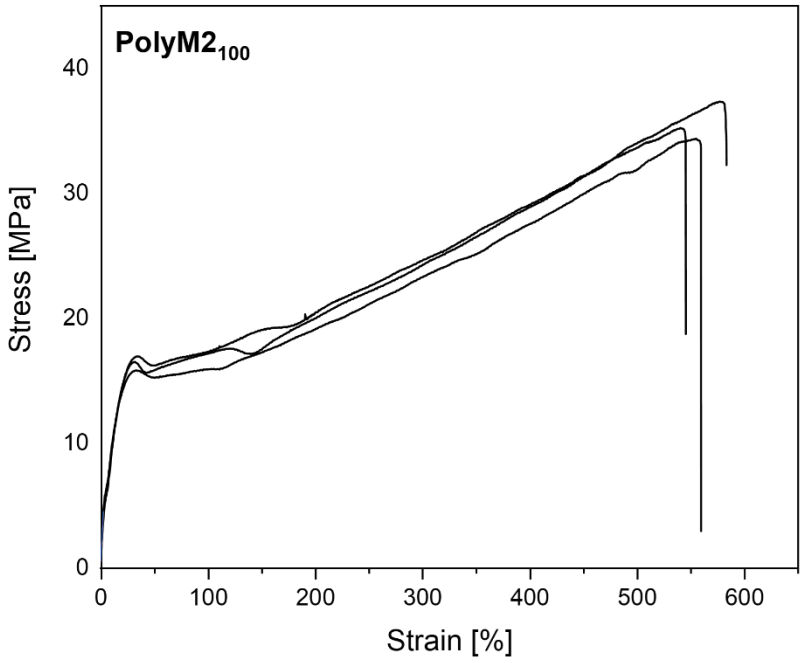


Figure S41. Stress-strain curves (10 mm/min, 22 °C) of polyM2$_{100}$.

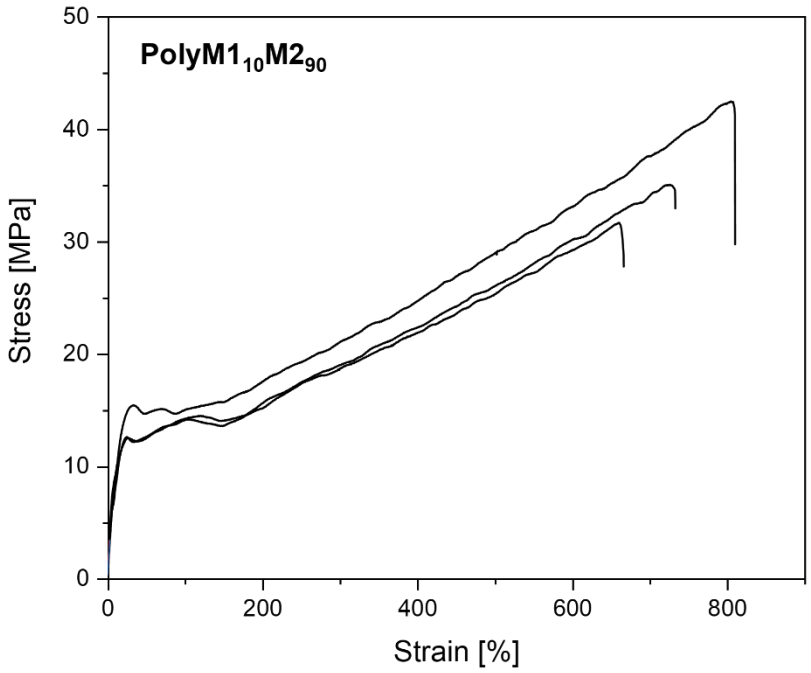


Figure S42. Stress-strain curves (10 mm/min, 22 °C) of polyM1$_{10}$M2$_{90}$.

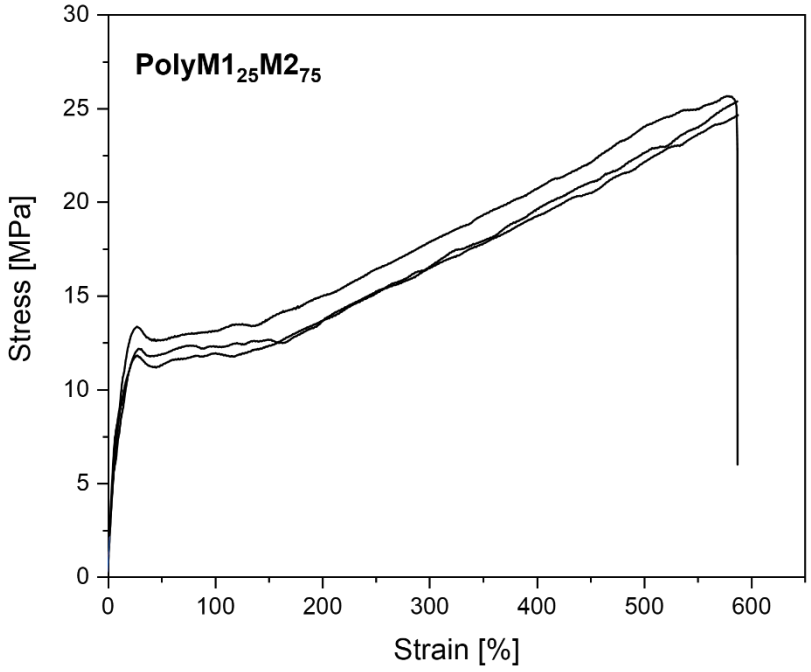


Figure S43. Stress-strain curves (10 mm/min, 22 °C) of polyM1$_{25}$M2$_{75}$.

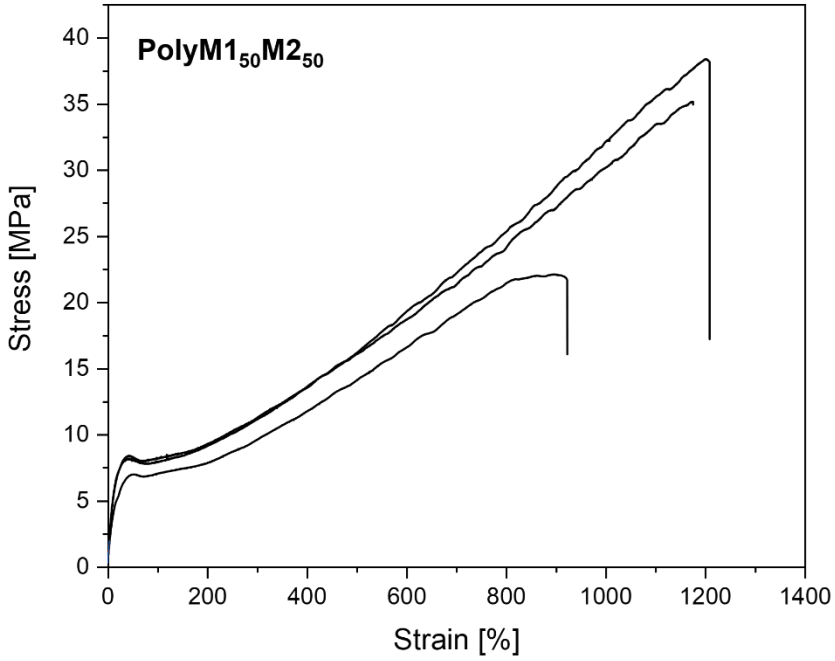


Figure S44. Stress-strain curves (10 mm/min, 22 °C) of polyM1$_{50}$M2$_{50}$.

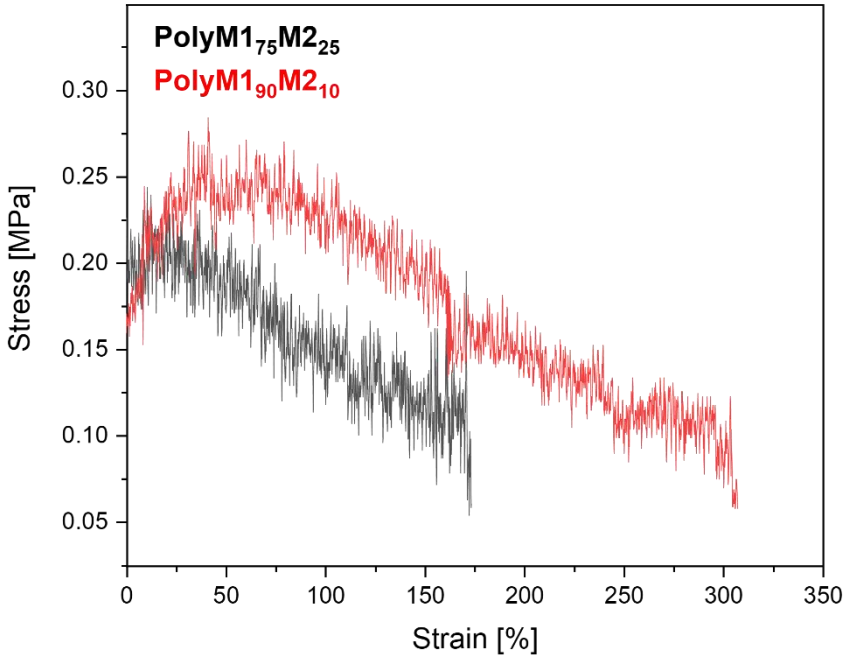


Figure S45. Stress-strain curves (10 mm/min, 22 °C) of polyM1$_{75}$M2$_{25}$ and polyM1$_{90}$M2$_{10}$. PolyM1$_{100}$ was breaking upon handling.

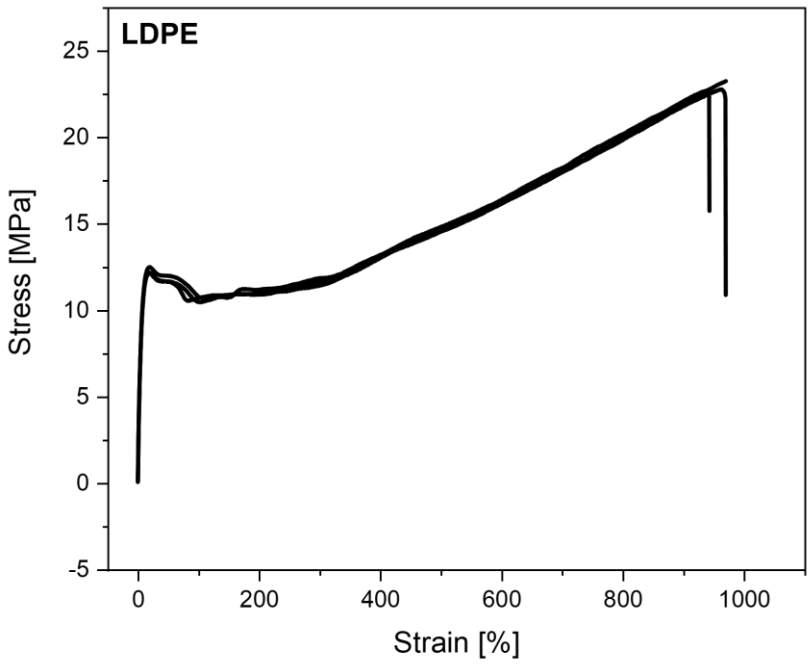


Figure S46. Stress-strain curves (10 mm/min, 22 °C) of LDPE.

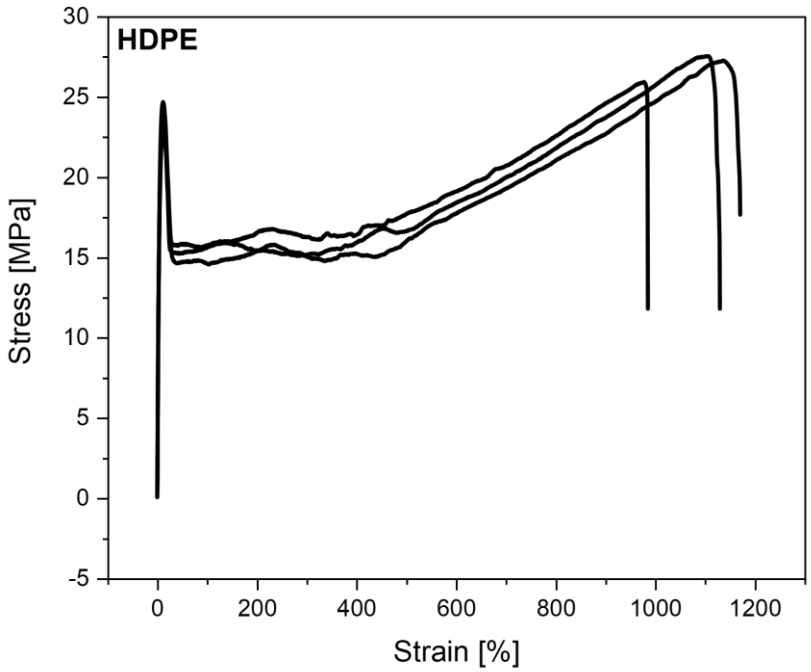
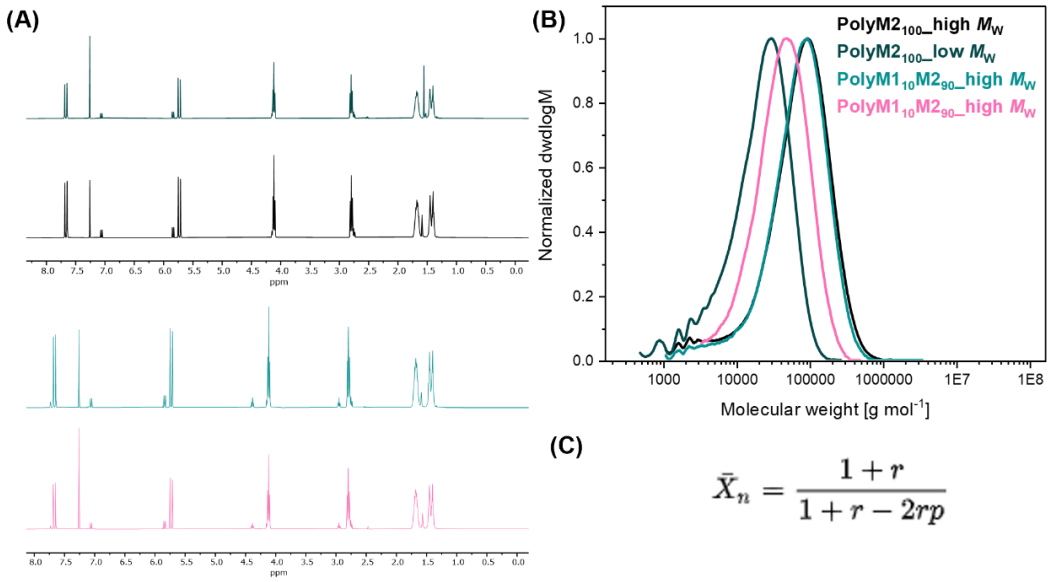


Figure S47. Stress-strain curves (10 mm/min, 22 °C) of HDPE.

Evaluation of the influence of M_W on thermomechanical properties



$$\bar{X}_n = \frac{1+r}{1+r-2rp}$$

Figure S48. (A) ^{1}H NMR (400 MHz, 300 K, $CDCl_3$) of PolyM2$_{100}$ (top) and PolyM1$_{10}$M2$_{90}$ (bottom) of different molecular weight. (B) SEC ($CHCl_3$, 0.5% Et_3N) traces of polymers. Numerical values reported. (C) Extended Carother's equation: r is the stoichiometric ratio of reagents; p is the conversion which is assumed to be 100%.

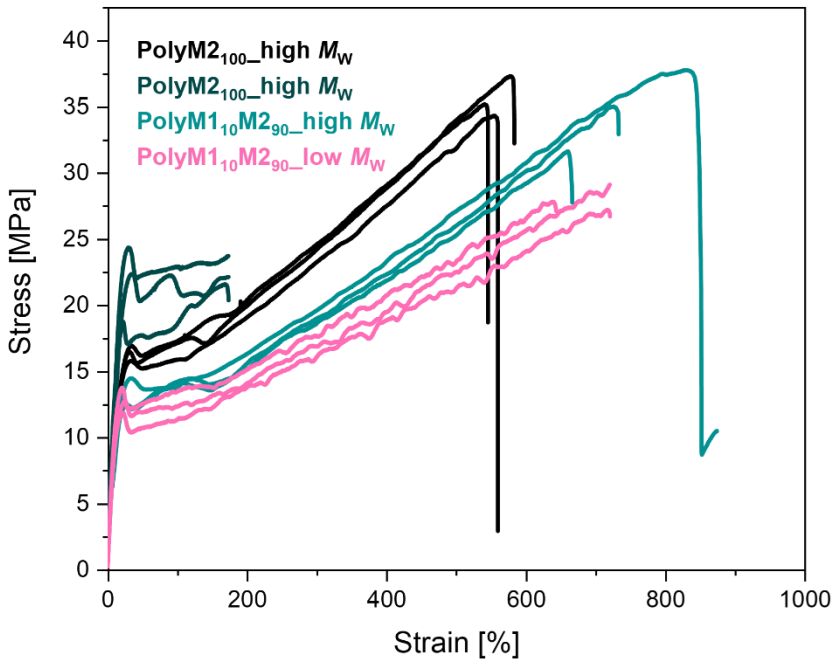


Figure S49. Stress vs strain curves tested at 10 mm min^{-1}, 22 °C of PolyM2$_{100}$ and polyM1$_{10}$M2$_{90}$ of different M_W.

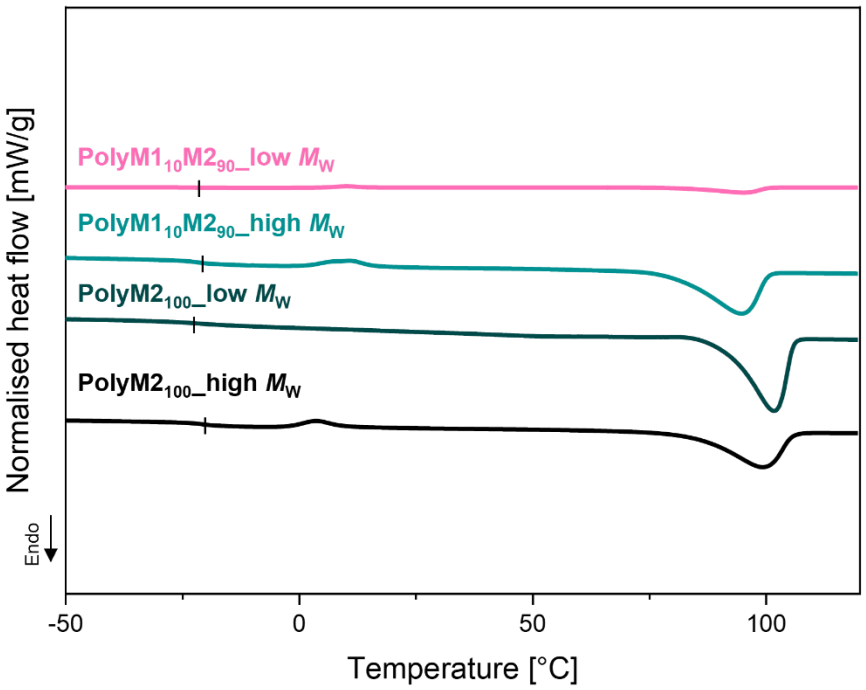


Figure S50. DSC thermograms of 2nd heating cycle tested at 10 °C min^{-1} of PolyM2$_{100}$ and polyM1$_{10}$M2$_{90}$ of different M_W. Numerical values reported in table S1.

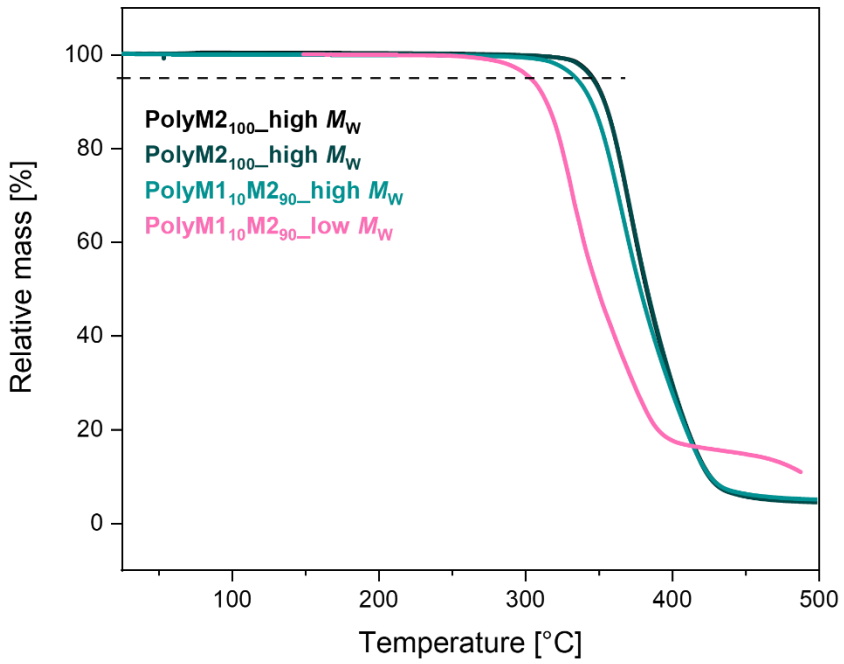


Figure S51. TGA thermograms resulted from heating at 10 °C /min up to 600 °C under a N_2 atmosphere of PolyM2$_{100}$ and polyM1$_{10}$M2$_{90}$ of different M_W.

Synthesis and characterisation of *cis*-poly$M1_{10}M2_{90}$

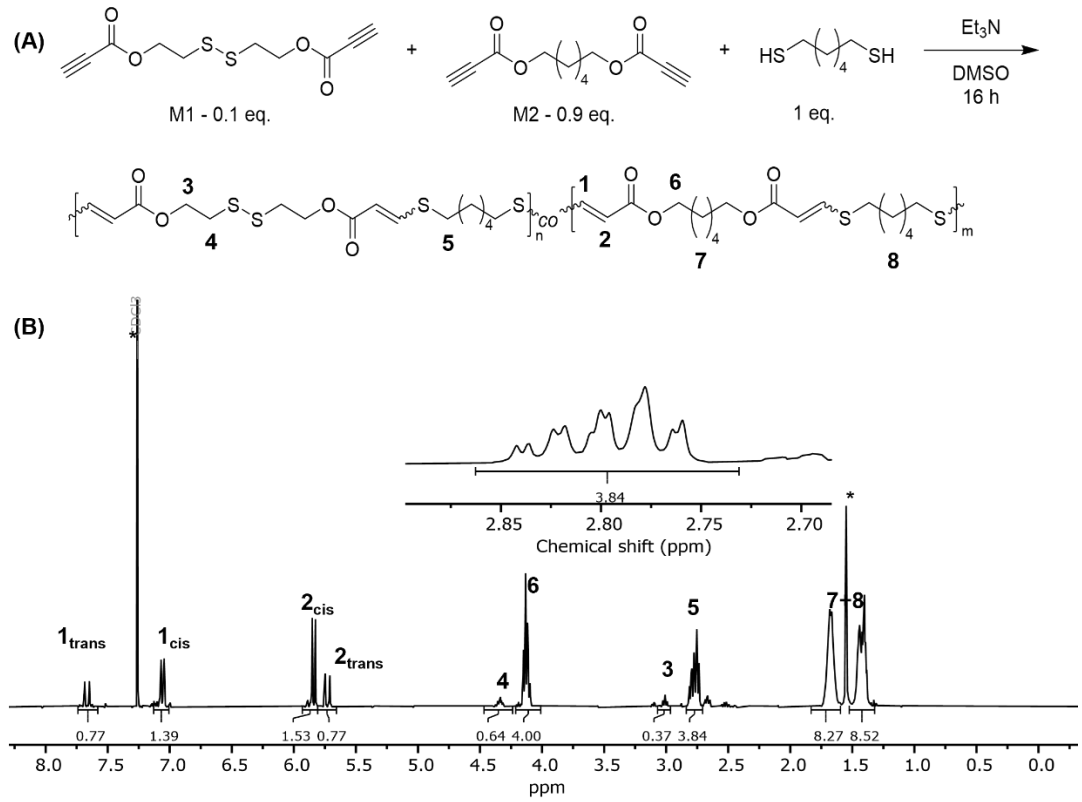


Figure S52. (A) Et_3N-catalyzed thiol-yne polyaddition between M1, M2 and 1,6-hexanedithiol in DMSO. (B) ^1H NMR (400 MHz, 300 K, $CDCl_3$) of high-*cis* content polymer. Solvent peak and residual water are marked with an asterisk.

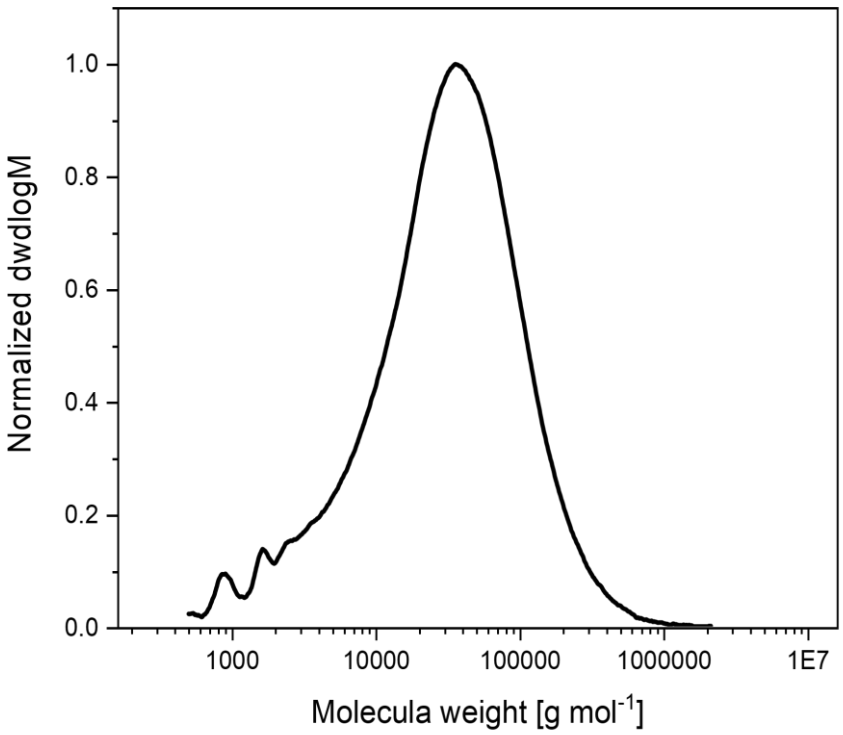


Figure S53. GPC ($CHCl_3$, 0.5% Et_3N) trace of *cis*-poly$M1_{10}M2_{90}$. Numerical value is reported in Table S1.

Thermomechanical characterisation of *cis*-PolyM1$_{10}$M2$_{90}$

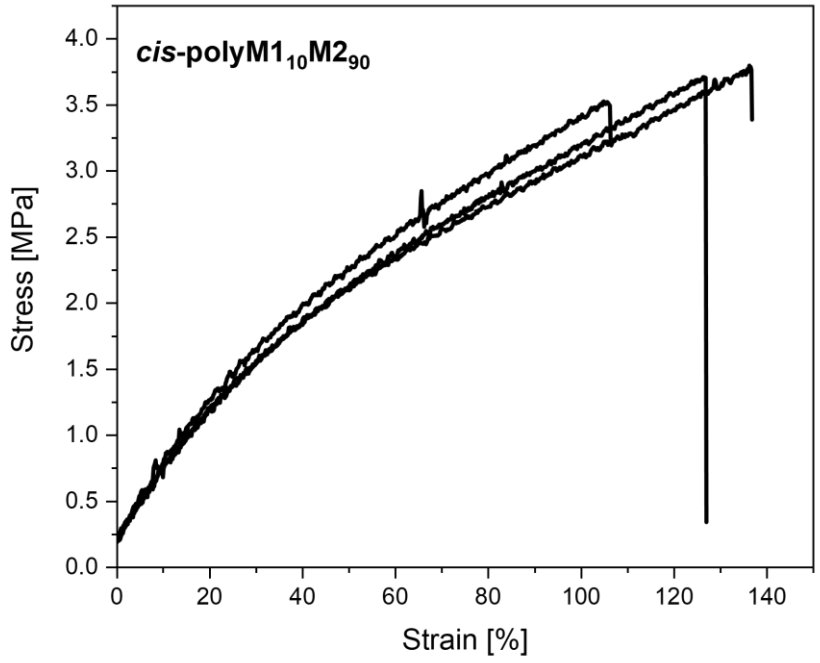


Figure S54. Stress-strain curves tested at 10 mm min^{-1}, 22 °C of *cis*-PolyM1$_{10}$M2$_{90}$.

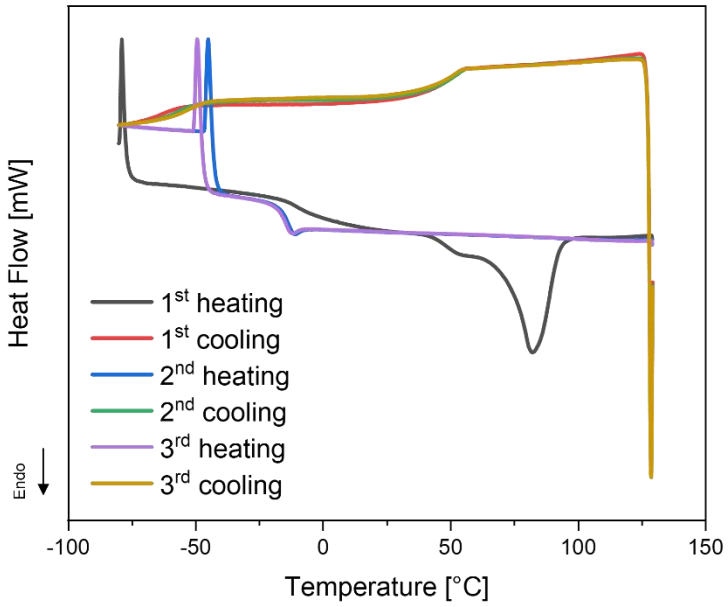


Figure S55. DSC thermograms between −80 and 130 °C at 10 °C min^{-1} of *cis*-Poly$M1_{10}M2_{90}$.

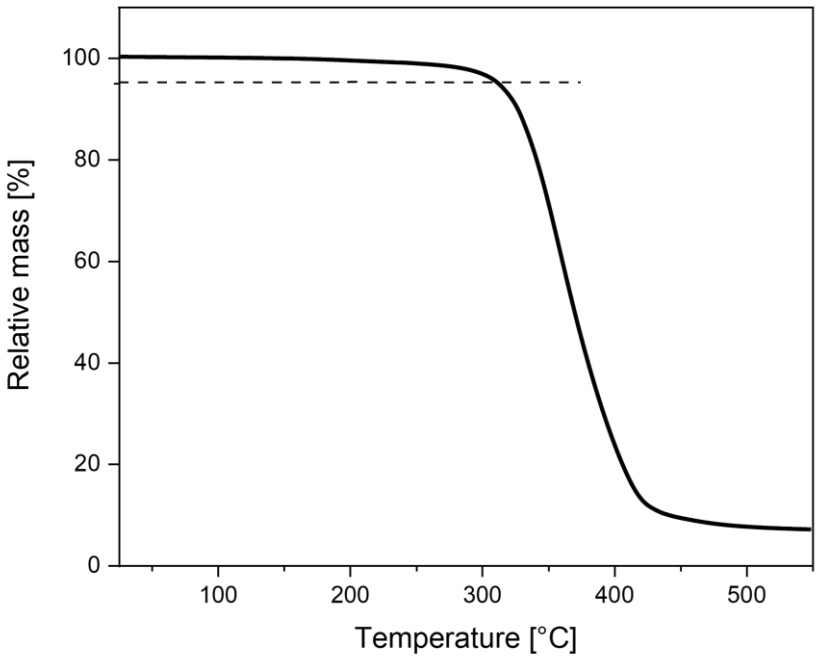


Figure S56. TGA thermograms resulted from heating at 10 °C /min up to 600 °C under a N_2 atmosphere of *cis*-Poly$M1_{10}M2_{90}$. Dashed line at 95% relative mass.

Synthesis and characterisation of polymers of different architecture with a fixed content of monomer M1

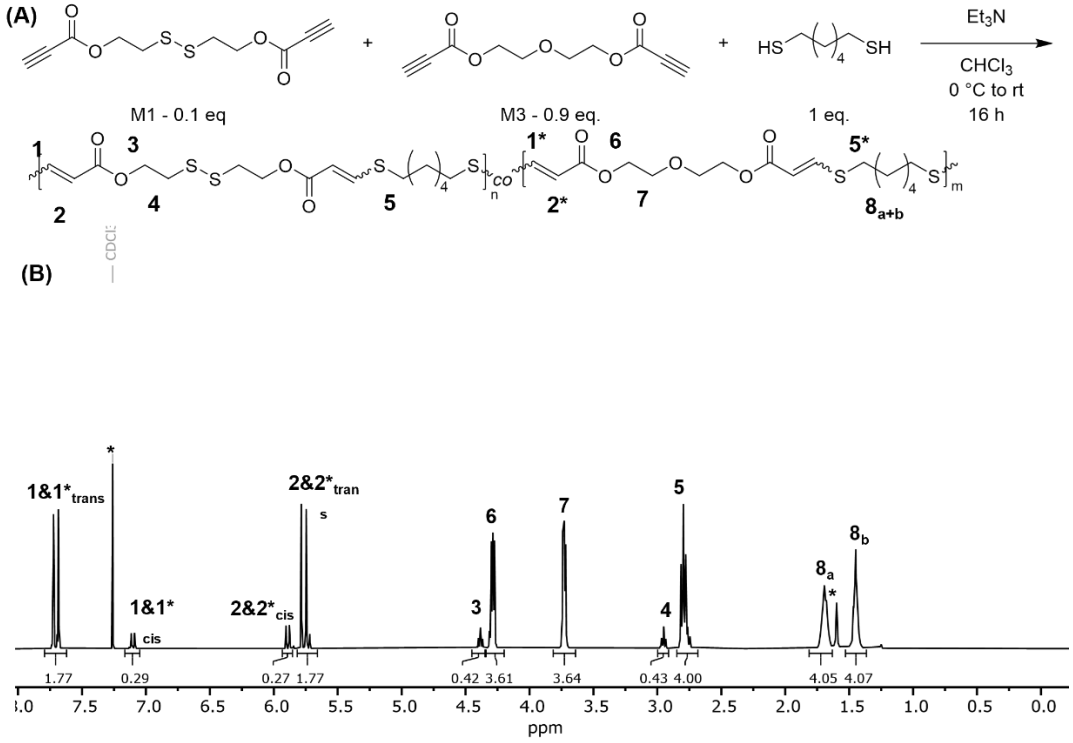


Figure S57. (A) Et_3N-catalyzed thiol-yne polyaddition between M1, M3 and 1,6-hexanedithiol. (B) ^1H NMR (400 MHz, 300 K, $CDCl_3$) of resulting polymer. Solvent and water peaks marked with an asterisk.

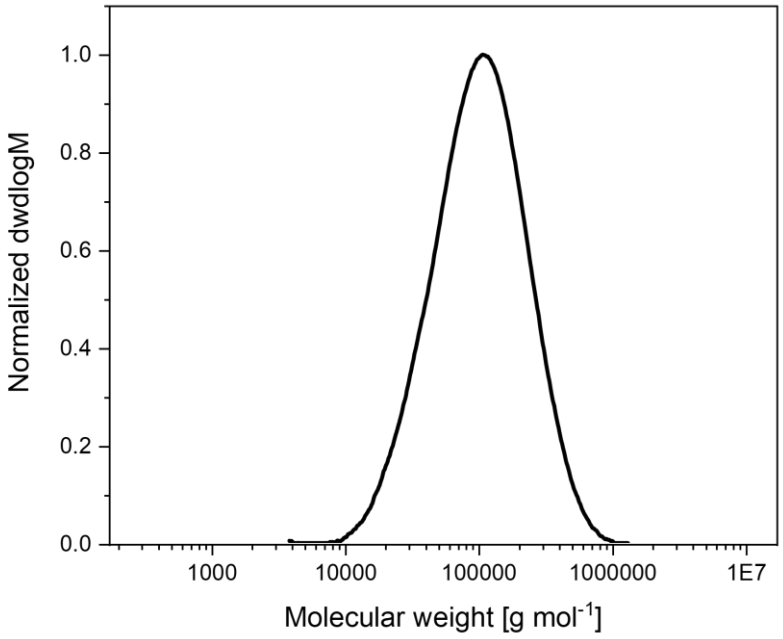


Figure S58. SEC ($CHCl_3$, 0.5% Et_3N) trace of poly$M1_{10}M3_{90}$. Numerical values reported in table S1

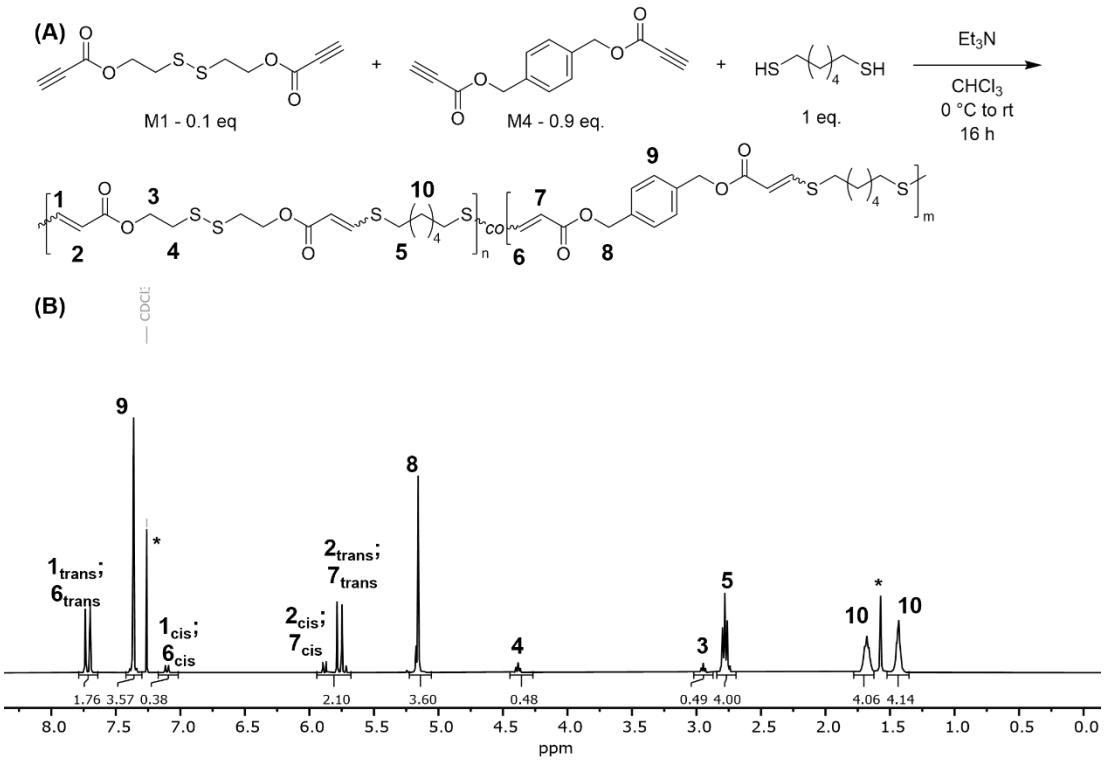


Figure S59. (A) Et_3N-catalyzed thiol-yne polyaddition between M1, M4 and 1,6-hexanedithiol. (B) ^1H NMR (400 MHz, 300 K, $CDCl_3$) of resulting polymer. Solvent and water peaks marked with an asterisk.

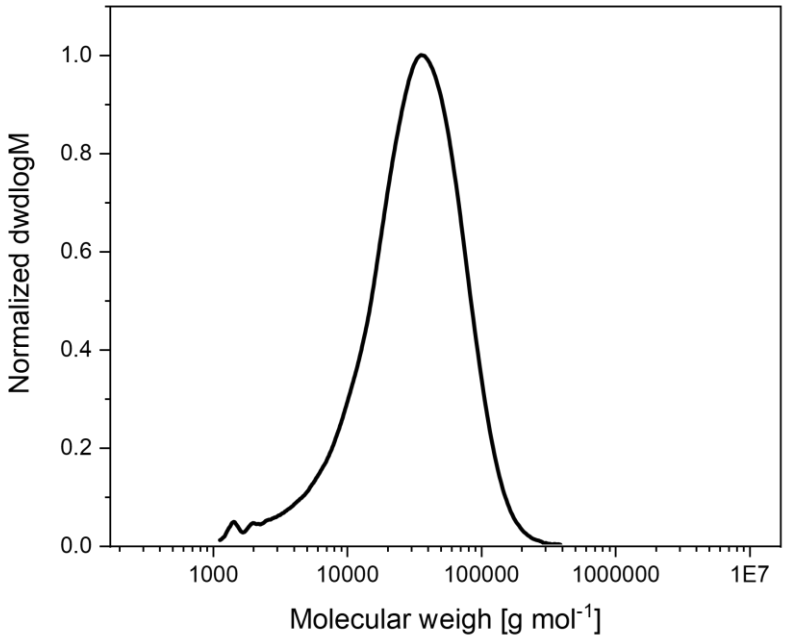


Figure S60. SEC ($CHCl_3$, 0.5% Et_3N) trace of poly$M1_{10}M4_{90}$. Numerical values reported in table S1.

Thermomechanical properties of polymers of different architectures with fixed content of monomer M1

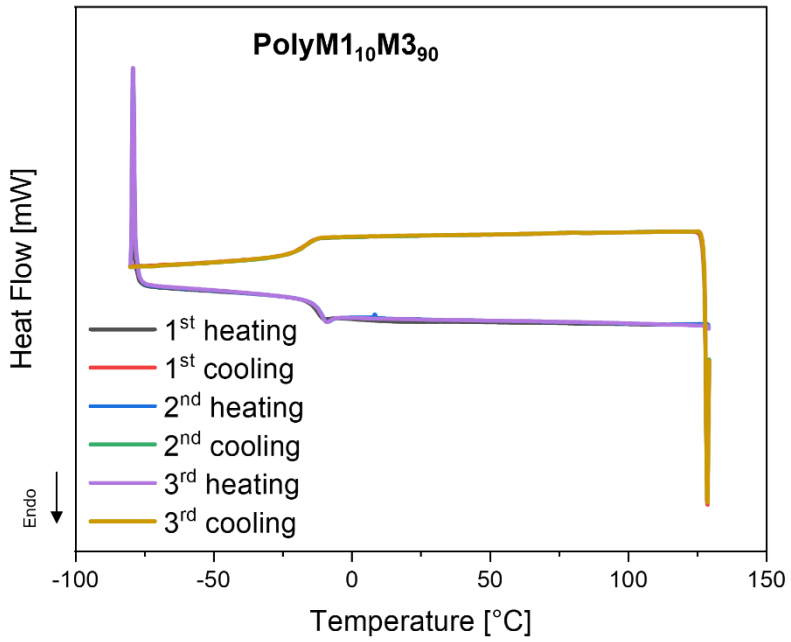


Figure S61. DSC thermograms of PolyM1$_{10}$M3$_{90}$ tested between −80 °C and 130 °C at 10 °C min^{-1}.

.

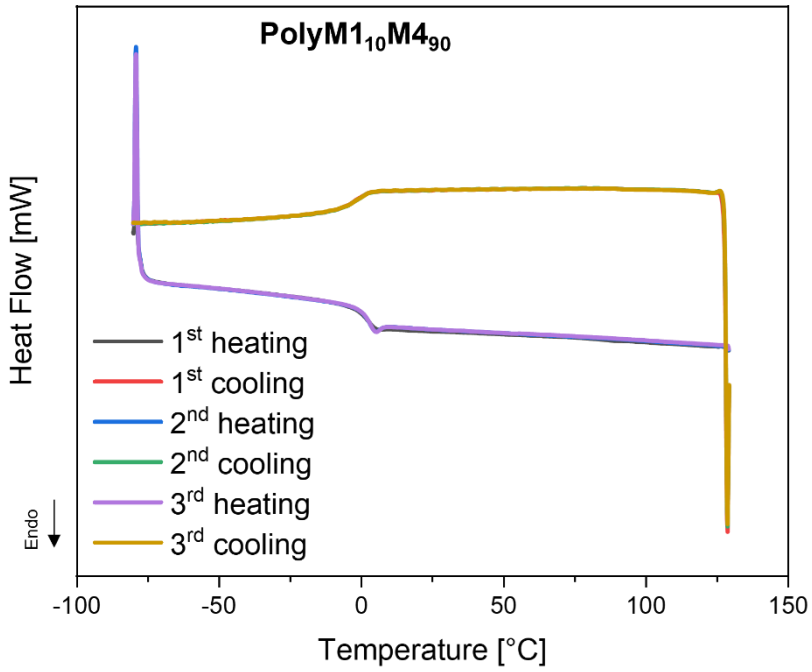


Figure S62. DSC thermograms of PolyM1$_{10}$M4$_{90}$ tested between −80 °C and 130 °C at 10 °C min^{-1}.

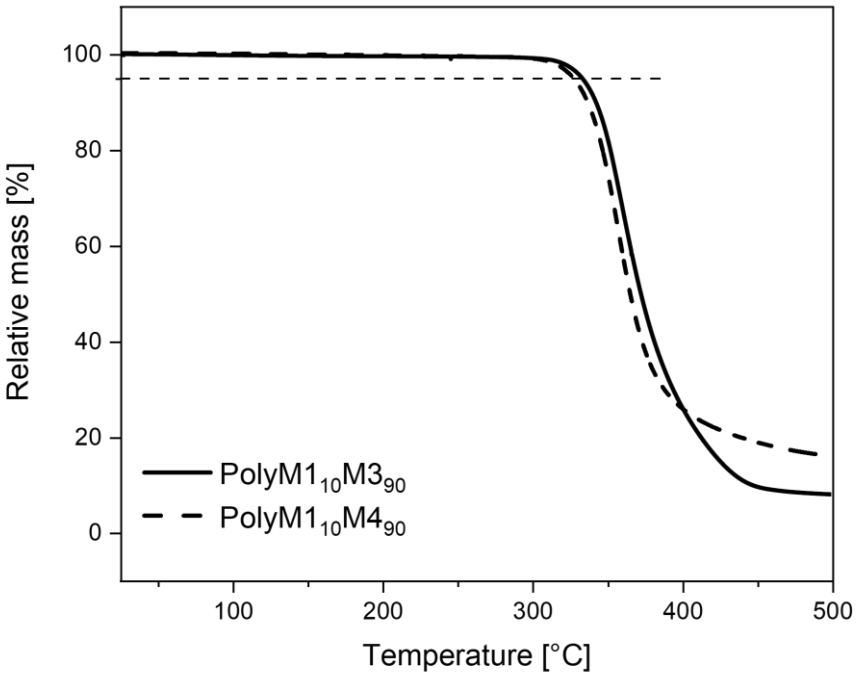


Figure S63. PolyM1$_{10}$M3$_{90}$ and PolyM1$_{0}$M4$_{90}$ TGA thermograms resulted from heating at 10 °C /min up to 600 °C under a N_2 atmosphere. Dashed line at 95% relative mass.

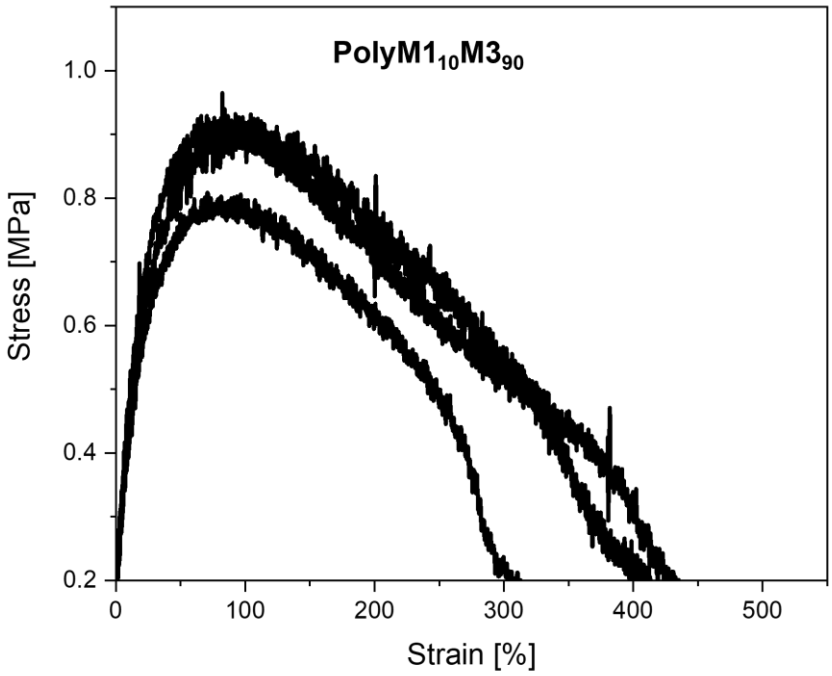


Figure S64. Stress-strain curves tested at 10 mm min^{-1}, 22 °C of PolyM1$_{10}$M3$_{90}$.

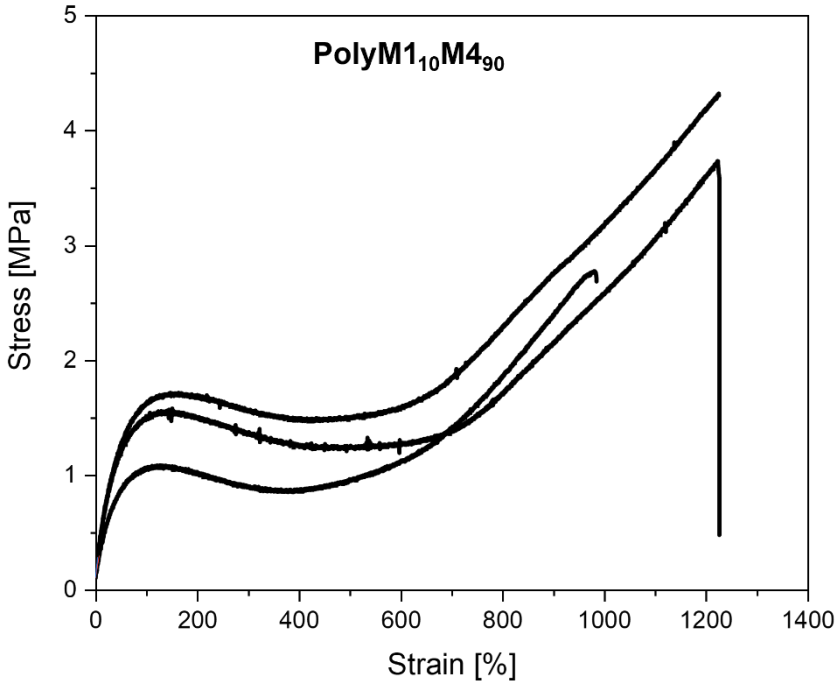


Figure S65. Stress-strain curves tested at 10 mm min^{-1}, 22 °C of PolyM1$_{10}$M4$_{90}$.

Table S1. Table summarising M_W and thermomechanical properties of polymers.

Entry	Name	M_W [kg/mol]	$Đ$	T_g [°C]	T_c [°C]	T_m [°C]	$T_{d,5\%}$ [°C]	Young Modulus (E) [MPa]	Stress at break [MPa]	Strain at break [%]	Toughness (U_T) [J·m^{-3}]
1	PolyM2$_{100}$	103	3.6	−20.35	3.82	99.71	346.8	146.3 ± 15.9	35.6 ± 1.6	560.7 ± 19.1	133.5 ± 9.5
2	PolyM2$_{100}$_low M_W	28	2.7	−22.67	n.a.	102.08	346.32	231.5 ± 29.1	22.4 ± 1.1	172.5 ± 1	34.6 ± 32
3	PolyM1$_{10}$M2$_{90}$	96	2.9	−21.01	10.65	95.05	335.08	124.6 ± 16.5	36.3 ± 5.5	733.1 ± 72.8	167.9 ± 37.8
4	PolyM1$_{10}$M2$_{90}$ _low M_W	55	1.9	−21.66	10.34	95.48	303.84	116.3 ± 8.7	27.9 ± 0.9	692.9 ± 44.5	128.6 ± 7.6
5	*Cis*_PolyM1$_{10}$M2$_{90}$	56	4.9	−13.18	n.a.	n.a.	312.01	n.a.	3.7 ± 0.2	123.1 ± 16.1	2.8 ± 0.5
6	PolyM1$_{10}$M3$_{90}$	136	1.8	−10.35	n.a.	n.a.	333.69	n.a.	n.a.	n.a.	n.a.
7	PolyM1$_{10}$M4$_{90}$	42	2.3	3.84	n.a.	n.a.	327.87	3.6 ± 0.8	3.6 ± 0.8	1145.4 ± 139.7	20.4 ± 7.1

References

1. N Hüppe, J Schunke, M Fichter, V Mailänder, FR Wurm and K Landfester, *Nanoscale Horiz.*, 2022, **7**, 908-915.
2. WC Still, M Kahn and A Mitra, *J. Org. Chem.*, 1978, **43**, 2923-2925.
3. JM Siebert, G Baier, A Musyanovych and K Landfester, *Chem. Commun.*, 2012, **48**, 5470.
4. SM June, P Bissel and TE Long, *J. Polym. Sci., Part A: Polym. Chem.*, 2012, **50**, 3797-3805.
5. Y Ren, W Dai, S Guo, L Dong, S Huang, J Shi, B Tong, N Hao, L Li, Z Cai and Y Dong, *J. Am. Chem. Soc.*, 2022, **144**, 1361-1369.

Chapter 3 – Access to degradable and reprocessable thermosets with tuneable thermomechanical properties *via* nucleophilic thiol-yne polymerisation.

Manuscript and overview

Title: Access to degradable and reprocessable thermosets with tuneable thermomechanical properties via nucleophilic thiol-yne polymerisation.

Authors: Daniele Giannantonio[a], Arianna Brandolese[a], Andrew P. Dove[a]

Affiliations: [a]School of Chemistry, University of Birmingham, Edgbaston, Birmingham, B15 2TT (UK)

Manuscript prepared

Co-authors contribution: Arianna Brandolese provided editing of the manuscript and guidance. Prof. Andrew P. Dove supervised in addition to providing guidance and funding acquisition.

Overview:

Building on the findings of chapter 2, the aim of this chapter was to apply the nucleophilic thiol-yne reaction to the synthesis of crosslinked polymers. Given the established compatibility of this reaction with aliphatic disulfide bonds, this chemistry was leveraged to impart properties such as degradability and reprocessability to conventionally non-degradable and non-reprocessable materials. Moreover, the tuneable *cis*/*trans* isomerism was used to modulate the properties of the material, along with composition and monomers ratio.

Access to degradable and reprocessable thermosets with tuneable thermomechanical properties *via* nucleophilic thiol-yne polymerisation.

Daniele Giannantonio[a], Arianna Brandolese[a], Andrew P. Dove[a]

[a]School of Chemistry, University of Birmingham, Edgbaston, Birmingham, B15 2TT (UK)

Abstract: The permanent chemical structure that makes thermosets strong and stretchable materials also hinders their reprocessability and causes their accumulation in the environment. To overcome this limitation, dynamic covalent bonds have been introduced into their backbone allowing macroscopic flow. However, when the dynamic bond is the network-forming bond, a significant trade-off between the robustness of the material and the dynamic behaviour can be encountered. In this study, nucleophilic thiol-yne click polymerisation was used to synthesise different materials possessing tuneable amounts of reversible disulfide bonds, thus accessing diverse thermomechanical properties. Furthermore, by leveraging different catalyst systems, the cis/trans conformer ratio on the backbone could be modulated suggesting an additional degree of control over the thermomechanical properties. Finally, the presence of dynamic bonds was used as a handle to promote the degradation and material reprocessing.

Introduction

Thermosets are covalently cross-linked materials that find applications in many industries, such as construction[1], transportation[2], and aerospace[3], as a result of their outstanding strength, extensibility, and solvent resistance. Their crosslinked nature, responsible for their useful properties, is also responsible for their intractability and limited reprocessability, contributing to environmental concerns.[4] Even when heated at very high temperatures these materials are not able to flow, meaning that they do not melt like thermoplastic do; hence, the development of reprocessable thermosets constitutes a major goal in polymer science.[5] Recently, the introduction of dynamic covalent bonds into thermosets established a new class of materials named covalent adaptable networks (CANs).[6] These dynamic bonds can break and reform on sufficiently short timescales, meaning that polymer chains can undergo molecular rearrangement, thus allowing macroscopic flow in a thermoplastic-like fashion. Parameters such as the nature of the dynamic bonds of choice (*i.e.* associative or dissociative) and the strategy deployed to form the network (step-growth *vs*. chain-growth polymerisation) influence the final architecture and bond distribution (Figure 1).[7, 8]

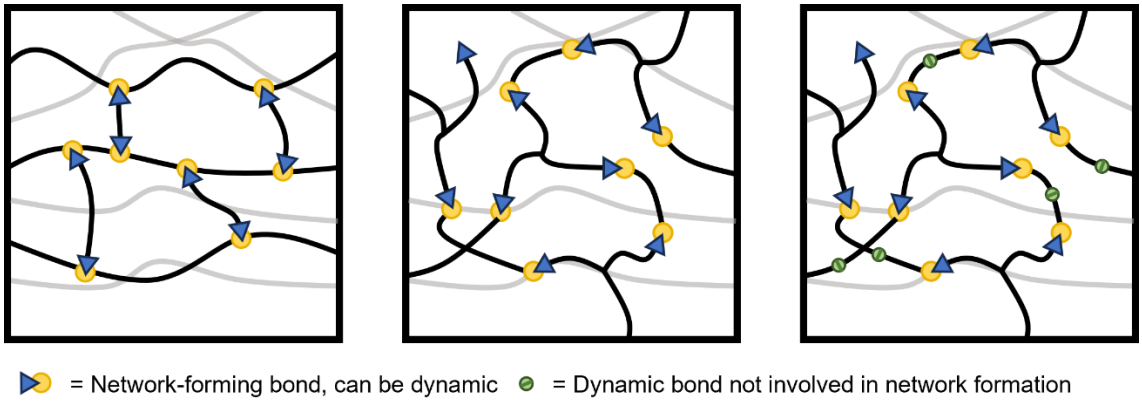


Figure 1. From left to right: CAN obtained from crosslinking of pre-polymers, CAN obtained from reversible reaction between multifunctional (>2 functionalities) monomers, CAN obtained from multifunctional monomers possessing dynamic bonds in the backbone.

In light of their efficiency and simplicity, several thiol-based reactions have been used for the synthesis or functionalisation of polymeric materials.[9] Among these, the use of thiol-ene Michael addition, radical or nucleophilic, arguably represents the most common approach given its simplicity and functional group tolerance.[10, 11] Because of the reversibility of the thia-Michael adduct, several CANs built on this reaction have been reported.[12-14] When compared to the thiol-ene addition, the thiol-yne reaction has attracted less attention in polymer chemistry. Like its -ene counterpart, this reaction can proceed through a nucleophilic- or radical-based mechanism with photo-mediated radical processes being the most explored.[15-20] Only recently Du Prez and co-workers showed that nucleophilic thiol-yne addition to activated alkynes can be used to obtain CANs with tuneable relaxation rates depending on the electronic of the alkyne of choice.[21] While this work shows that network formation can be achieved through the use of a reversible reaction, only dissociative bonds can be introduced with this approach thus limiting its scope. Moreover, since monofunctional alkynes are being used, the thiol-yne addition

reaction is responsible for the formation of pre-polymers, and only a subsequent thiol-ene addition forms the crosslinked structure.

Monomers possessing dynamic bonds in their backbones are the key to a more versatile approach to incorporating dynamic bonds in thermosets. If the presence of dynamic bond is independent from the polymerisation method, a greater range of reversible moieties can be introduced.[22] Moreover, in the case of nucleophilic thiol-yne polymerisation, by employing a bifunctional alkyne the network can be directly cast by reaction with a multifunctional thiol (wiht more than two functional groups) thus preserving the *cis*/*trans* stereochemistry resulting from the addition reaction and bypassing the prepolymer synthesis step. Backbone *cis*/*trans* isomerism has been previously used to tailor thermomechanical performances in linear polymers[23-25], hydrogels[26], and 3D printable resin[27], but this concept has not been applied to CANs yet.

Following this approach, a bifunctional propiolate possessing an internal dynamic disulfide bond (C_2SS) was successfully introduced in this study into crosslinked materials by reaction with a three-arm thiol. The thermomechanical properties of the resulting network were found to change according to the amount of disulfide bond introduced, monomer ratio, and *cis*/*trans* content. Finally, the presence of dynamic disulfide bonds rendered the thermoset materials degradable and reprocessable.

Results and discussion

Synthesis of the networks

To access networks *via* nucleophilic thiol-yne polymerisation, two different clickable monomers possessing activated terminal alkynes (C_2SS and C_6) were synthesised *via* Fisher esterification of commercially available diols with propiolic acid (Chapter 2 – Supporting Information). These monomers were then reacted with a three-arm thiol (trimethylolpropane tris(3-mercaptopropionate) – 3-AT) in different ratios in the presence of an organocatalyst (triethylamine (Et_3N) or 1,8-diazabicyclo[5.4.0]undec-7-ene (DBU)) in chloroform ($CHCl_3$). The mixtures were poured into Teflon beakers and freestanding films were recovered after slow evaporation of the solvent (Figure 2). Residual solvent was removed by heating at 50 °C under vacuum until constant weight was reached.

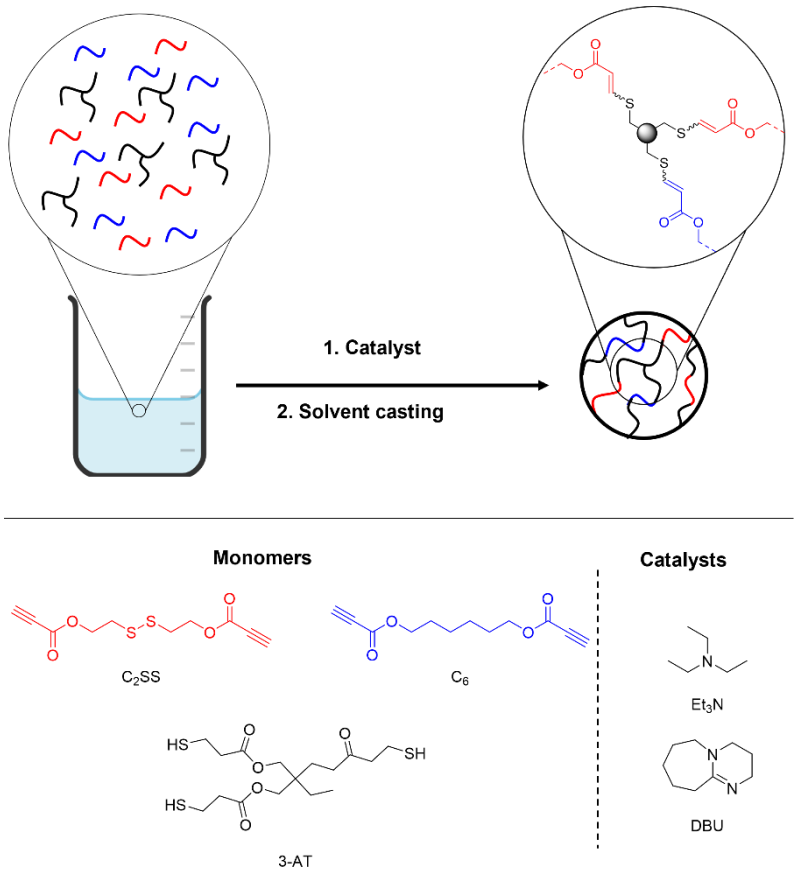


Figure 2. Schematic representing the network formation *via* solvent casting (top) and monomers and catalysts used in this work (bottom).

The versatility entailed by the nucleophilic thiol-yne reaction allows the generation of diverse networks from a limited pool of monomers by simple tuning of the reaction conditions. Networks NetC_2SS, Net(C_2SS-C_6), and NetC_6 with diverse disulfide content were synthesised by varying the ratio between monomers C_2SS and C_6 (100% C_2SS, 1:1: C_2SS:C_6, 100% C_6, respectively) while keeping the stoichiometric ratio between alkyne and thiol groups constant at 1:1. Net(3-AT)$_{1.5}$-(C_2SS)$_1$ was accessed by reacting monomer C_2SS with 3-AT in equimolar amounts, to have a thiol:alkyne ratio of 1.5:1. Lastly, *cis*-rich networks NetC_2SS and NetC_6 (100% C_2SS and 100% C_6, respectively) were accessed by employing DBU as the catalyst of the reaction.[24, 28] Consumption of the alkyne bonds following thiol-yne

addition was confirmed by Fourier-transform infrared (FTIR) spectroscopy on the free-standing films, showcasing the disappearance of the key stretching bands at 2100 cm^{-1} (Figure 3B-C). The formation of networks was further confirmed by performing swelling experiments at room temperature in $CHCl_3$. All of the networks displayed high gel content (>80%) and a swelling ratio above 250% confirming nucleophilic thiol-yne polymerisation as an excellent tool for the synthesis of crosslinked materials (Table 1).

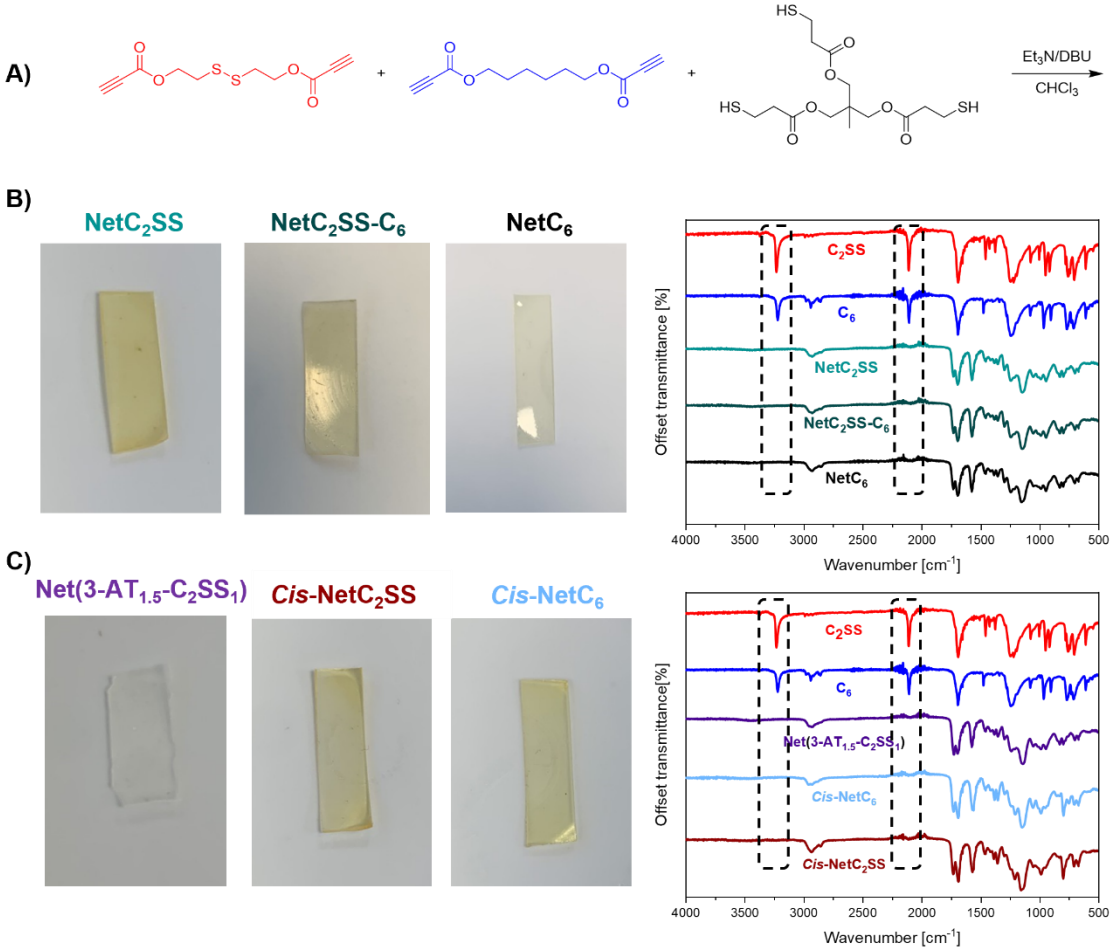


Figure 3. A) Nucleophilic thiol-yne reaction between monomers C_2SS (red), C_6 (blue), 3-AT (black) in presence of Et_3N (favoured formation of *E* adduct) or DBU (favoured formation of *Z* adduct). B) Pictures of networks $NetC_2SS$, Net(C_2SS-C_6), $NetC_6$ having different disulfide bond content. FTIR spectra showing the disappearance of the alkyne stretching bands in the networks. C) Pictures of network having different crosslinking density (Net(3-$AT_{1.5}$-C_2SS_1) and high *cis* content (*Cis*-$NetC_2SS$ and *Cis*-$NetC_6$). FTIR spectra showing the disappearance of the alkyne stretching bands in the networks.

Table 1. Summary of swelling ratio and gel content for the networks synthesised in this work

Name	Swelling ratio[a] [%]	Gel fraction [%]
***Trans*-NetC$_2$SS**	358±90	91.3±0.7
***Trans*-Net(C$_2$SS-C$_6$)**	335±49	91.6±0.6
***Trans*-NetC$_6$**	466±43	92.3±1
***Trans*-Net((3-AT$_{1.5}$-C$_2$SS$_1$)**	285±41	83.6±0.4
***Cis*-NetC$_2$SS**	247±17	91.6±0.9
***Cis*-NetC$_6$**	506±19	90.4±3.7

[a]Determined *via* gravimetry in $CHCl_3$ (Equation S1)

The influence of disulfide bonds content, crosslinking density, and *cis* content on mechanical properties

Dynamic mechanical analysis (DMA) was performed to evaluate the temperature dependences of storage modulus (*E'*) and loss factor (tan delta) of the different networks. The broad and bimodal tan *δ* curves displayed by the 1:1 thiol:alkyne ratio networks suggest a non-homogeneous structure, however, all materials showed excellent dimensional stability in the temperature range tested (−80 °C – 130 °C) as no drop in modulus was recorded (Figure 4A). Notably, *trans*-NetC$_2$SS did not display any loss in modulus even at temperatures as high as 180 °C (Figure S1). The molecular weight between crosslinks (M_C) calculated using the elastic modulus in the rubbery region obtained from the DMA curves (Equation S3) supported this conclusion, revealing higher values for networks displaying bimodal tan *δ* curves, which could hint at the presence of defects in the network structure (Table 2).[29, 30]

Notably, all materials displayed rubbery behaviour above their glass transition temperature (T_g) as the tan δ dropped to 0, as expected with these crosslinked polymers.

When compared to *trans*-NetC_2SS, *trans*-Net(3-A$T_{1.5}$-C2SS_1) displayed a monomodal and narrower tan δ curve, suggesting that a 1.5:1 ratio between thiols and alkyne leads to a more homogeneous network. This was also supported by the decreased molecular weight between crosslinking and lower swelling ratio. M_c did not seem to influence the limit of the viscoelastic region (LVE) and yield point significantly, as shown by amplitude sweeps performed on the high-*trans* networks (Figure 4C). Frequency sweeps seemed to confirm the reduced influence of different degrees of crosslinks on shear stress as *trans*-NetC_2SS and *trans*-Net(C_2SS-C_6) displayed higher storage modulus than *trans*-NetC_6 and *trans*-Net(3-A$T_{1.5}$-C_2SS_1), despite the lower M_C of the latter (Figure 4D). These contradicting results may be explained by the fact that significant differences in composition are also found between these networks and M_c evaluation was performed assuming the Poisson's ratio (v) to be 0.5 and the density of the material 1 g/mL. Moreover, as different monomer C_2SS and C_6 ratios were explored, the composition may also be responsible for the different mechanical properties, with networks having higher C_2SS content presenting lower *E'* values when analysed *via* DMA.

Cis-rich networks synthesised using DBU as catalyst showed different properties when compared to their *trans*-rich analogous. While *cis*-NetC_2SS displayed a slightly higher rubbery storage modulus ($E'_{rubbery}$) than *trans*-NetC_2SS, *cis*-NetC_6

possessed a lower $E'_{rubbery}$ value when compared to *trans*-NetC$_6$. Taken together, these results suggest that different degrees of *cis*/*trans* isomerisation can alter the modulus of thermosets, but this effect is mediated by composition as well.

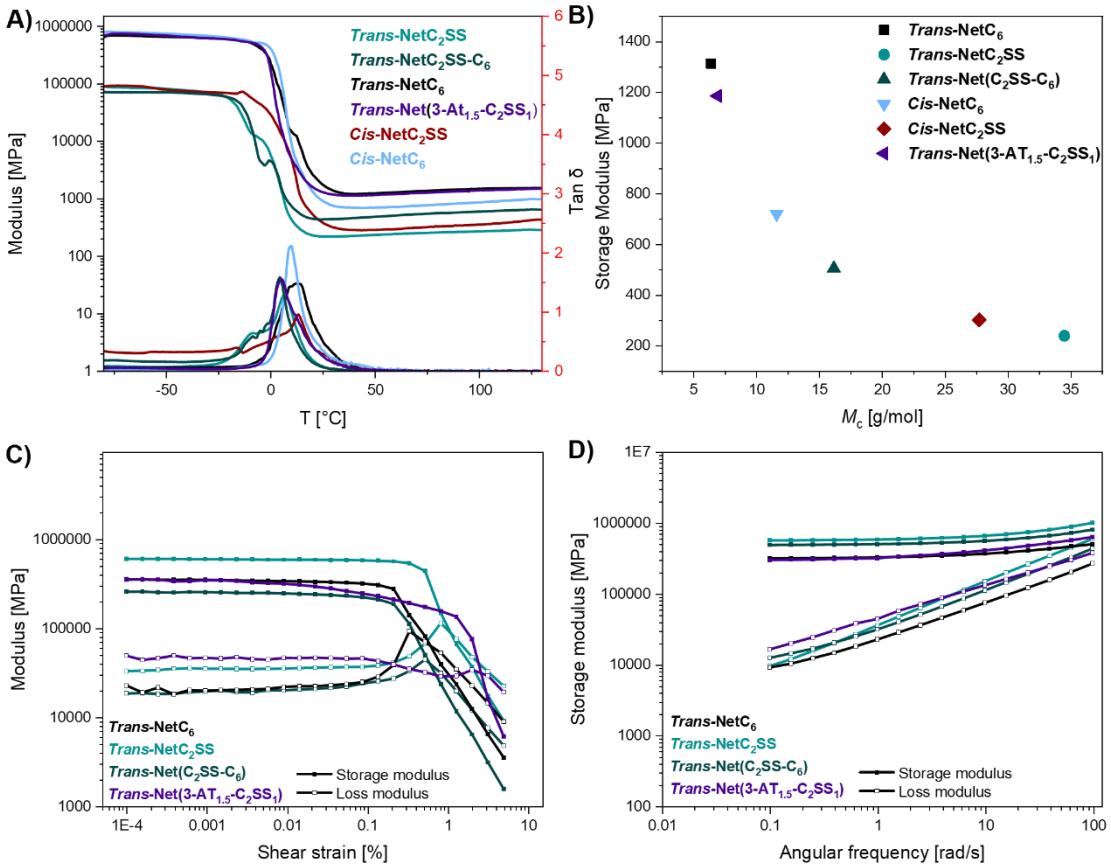


Figure 4. A) DMA (−80 – 130 °C, 5°C/min, 1 Hz, 1 µm) curves of the networks synthesised *via* nucleophilic thiol-yne polymerisation. B) Correlation between M_c and storage modulus calculated at T_g + 50 °C. C) Amplitude sweeps (25 °C, 0.1 to 500% strain, 1 rad/s). of networks. D) Frequency sweeps (25 °C, strain amplitude 5 %) of networks.

Table 2. Summary of glass transition temperatures (T_g), storage modulus at the rubbery plateau ($E'_{rubbery}$), and molecular weight between crosslinks (M_C) as determined by DMA.

Name	T_g[a] [°C]	$E'_{rubbery}$[b] [MPa]	M_c [g × mol^{-1}]
***Trans*-NetC$_2$SS**	7.25	239.7	34.5
***Trans*-NetC$_6$**	13.2	1314.2	6.39
***Trans*-Net(C$_2$SS-C$_6$)**	4.33	506.5	16.1
***Trans*-Net(3-AT$_{1.5}$-C$_2$SS$_1$)**	4.8	1186.4	6.9
***Cis*-NetC$_2$SS**	13.25	302.4	27.7
***Cis*-NetC$_6$**	10.5	720.3	11.6

[a]Determined as the peak of the *Tan δ* curve. [b]Taken as the value associated with T_g + 50 °C.

To further investigate the mechanical performances of the different networks, uniaxial tensile test was performed on dogbones cut from the cast films (Figure 5A, S2-S7). Albeit the lower M_c, *trans*-NetC$_2$SS was found to possess a similar Young's modulus (E) and elongation at break (ε) to *trans*-NetC$_6$, even though the latter was slightly stronger. This could be due to the latter being richer in stronger carbon-carbon bonds.[31, 32] Surprisingly, *trans*-Net(C$_2$SS-C$_6$) outperformed both networks under every aspect suggesting that there must be a "goldilocks" zone when this monomer ratio (1:1 C$_2$SS:C$_6$) is used, and chemical composition can significantly alter mechanical performances (Figure 5B-D). When compared to *trans*-NetC$_2$SS, *trans*-Net(3-AT$_{1.5}$-C$_2$SS$_1$) displayed higher Young's modulus (E = 3.4 ± 0.7 MPa *vs*. E = 0.73 ± 0.17 MPa) and stress at break (σ = 1.3 ± 0.6 MPa *vs*. σ = 0.63 ± 0.06 MPa), but lower elongation (ε = 51.2 ± 25.4 % *vs*. ε = 94.8 ± 22.2 %). These results are coherent with the higher crosslinking density associated with *trans*-Net(3-AT$_{1.5}$-C$_2$SS$_1$), which is also corroborated by its lower swelling ratio (Table 1) (Figure 5B-D).

Cis-rich networks were different from their high-*trans* counterparts, further suggesting that stereochemistry can alter the mechanical properties of thermosets. *Cis*-NetC_2SS displayed higher Young's modulus than *cis*-NetC_6, but no significant differences were observed in stress and strain at break. When compared to *trans*-NetC_2SS, *cis*-NetC_2SS displayed significantly higher Young's modulus and stress at break, while *cis*-NetC_6 showed higher elongation and stress at break compared to trans-NetC_6 (Figure 5B-D). These results seem to suggest that increasing *cis*-content leads to tougher thermosets (Table 3). This may be explained by mechanically induced *cis*-to-*trans* isomerisation, which was probed by Radiom and co-workers.[33] The authors found out that when *cis*-rich norborene polymers were stretched *via* atomic force microscopy (AFM), an increase in extension was measured because of the isomerisation of the shorter *cis* linkages into the longer *trans* conformation, which resulted in relaxation of the force. From a material point of view this event could lead to energy dissipation, thus allowing the material to withstand greater stress. Notably, *trans*-Net(C_2SS-C_6), *cis*-NetC_2SS, and *cis*-NetC_6, displayed ultimate tensile strength and elongation comparable to the likes of styrene butadiene rubber (SBR) and ethylene propylene diene monomer (EPDM), two commonly used elastomers.[34]

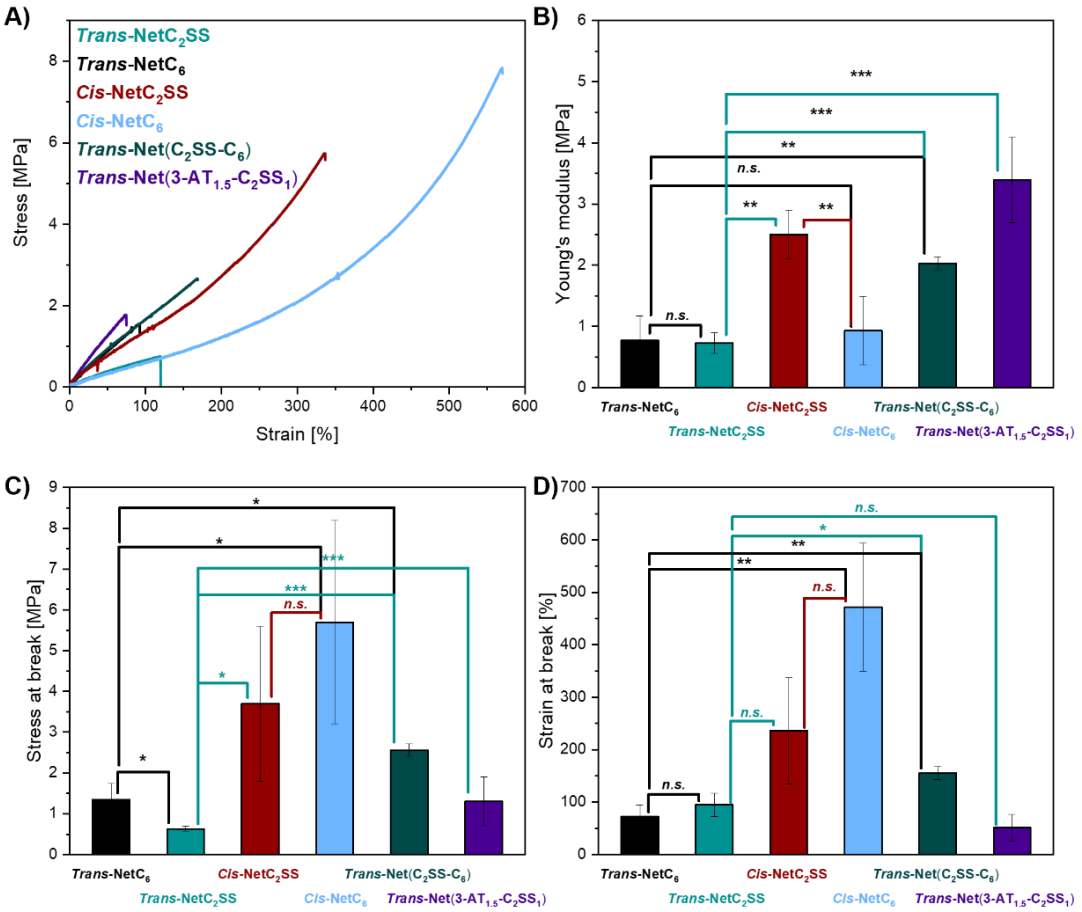


Figure 5. A) Exemplary stress *vs.* strain curves obtained from uniaxial tensile testing (10 mm/min, 22 °C) of different networks synthesised in this work. B) Averaged Young's modulus values [MPa] of different networks. C) Averaged stress at break values [MPa] of different networks. D) Averaged strain at break [%] of different networks. In boxes B-D, plot represents the mean, and the error bars represent standard deviation (n = 3, independent samples). Statistical significance and P values are determined by using the two-sided unpaired t test. *n.s.* = not significant; * = $P < 0.05$; ** = $P < 0.01$; *** = $P < 0.001$.

Table 3. Mechanical properties determined by uniaxial tensile testing (22 °C, 10 mm/min) of the networks synthesised in this work.

Entry	E^a [MPa]	σ at break [MPa]	ε at break [%]	Toughness[b] [J × m^3]
***Trans*-NetC$_2$SS**	0.73 ± 0.17	0.63 ± 0.06	94.8 ± 22.2	0.34 ± 0.12
***Trans*-NetC$_6$**	0.77 ± 0.4	1.35 ± 0.39	72.5 ± 21.9	0.59 ± 0.28
***Trans*-Net(C$_2$SS-C$_6$)**	2.03 ± 0.11	2.56 ± 0.15	155.4 ± 12.6	2.2 ± 0.3
***Trans*-Net(3-AT$_{1.5}$-C$_2$SS$_1$)**	3.4 ± 0.7	1.3 ± 0.6	51.2 ± 25.4	0.39 ±0.31
***Cis*-NetC$_2$SS**	2.5 ± 0.4	3.7 ± 1.9	235.7 ± 101.7	4.9 ± 3.7
***Cis*-NetC$_6$**	0.93 ± 0.56	5.7 ± 2.5	471.7 ± 121.9	10.7 ± 5.3

[D] Determined as the slope of the curve at 1% strain. [b] Determined as the area below the stress *vs.* strain curve.

The influence of disulfide bonds content, crosslinking density, and *cis*/*trans* ratio on thermal properties.

The thermal stability of the networks was investigated *via* thermogravimetric analysis (TGA) (Figure 6A, S8). The degradation temperature ($T_{d,5\%}$) was recorded as the temperature associated with a 5% mass loss. The difference in disulfide bond content was found to be the main source of variation among samples, as expected by the lower energy associated with it when compared to the carbon-carbon bond.[31, 32] Networks *trans*-NetC$_6$ and *cis*-NetC$_6$ displayed a $T_{d,5\%}$ of 337 °C and 315

°C, respectively, which is 151 °C and 145 °C higher than the values recorded for *trans*-NetC_2SS and *cis*-NetC_2SS. *Trans*-Net(3-A$T_{1.5}$-C_2SS_1) displayed $T_{d,5\%}$ analogous to *trans*-NetC_2SS, which is not surprising given the same chemical composition. *Trans*-Net(C_2SS-C_6) $T_{d,5\%}$ was in-between the ones of *trans*-NetC_2SS and *trans*-NetC_6 at 297 °C. Notably, high *trans*-content networks displayed better stability than their high *cis* counterparts, which agrees with the higher stability associated with *trans* linkages (Table 4).

An important parameter in material science is the glass transition temperature, as the properties of materials change drastically above or below T_g. Differential scanning calorimetry (DSC) revealed all the networks to be amorphous as no melting transitions were detected (Figure 6B, S9-S14). While the higher degree of crosslinking is generally associated with an increase in glass transition temperature (T_g), *trans*-NetC_6 underwent transition at the same temperature as *trans*-NetC_2SS (−7.4 °C). However, when both monomers were used to synthesise *trans*-Net(C_2SS-C_6) its T_g was recorded 3 °C lower at −10.4 °C. T_g of *Trans*-Net(3-A$T_{1.5}$-C_2SS_1) was determined at −14.7 °C, roughly 7 °C lower than *trans*-NetC_2SS, which is again a surprising result given its higher crosslinking density. This difference could be explained by the unreacted thiols acting as chain-ends, thus increasing the free-volume of the network. Both high-*cis* networks revealed T_gs higher than their high-*trans* counterparts, confirming that *cis*/*trans* isomerism can be used to modulate the thermal properties of thermosets (Table 4).

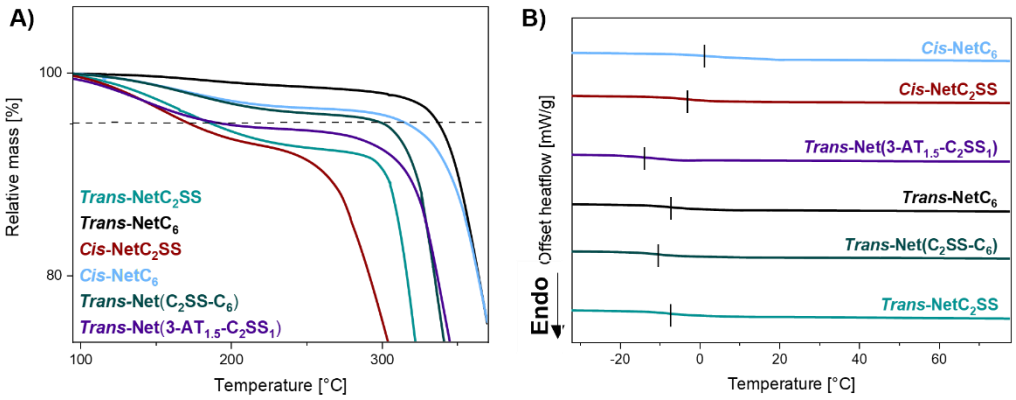


Figure 6. A) TGA thermogram (25 °C – 600 °C, N_2) of different networks synthesised in this work. $T_{d,5\%}$ decreases with increasing disulfide bond content and higher *cis* content. B) Zoomed in DSC thermograms (−30 °C – 80 °C, N_2) of second heating cycle of networks synthesised in this work. T_g highlighted by vertical dash.

Table 4. Summary of thermal properties of the networks synthesised in this work.

Entry	T_g[a] [°C]	$T_{d,5\%}$[b] [°C]
***Trans*-NetC$_2$SS**	−7.4	186.2
***Trans*-NetC$_6$**	−7.4	337.8
***Trans*-Net(C$_2$SS-C$_6$)**	−10.4	300.5
***Trans*-Net(3-AT$_{1.5}$-C$_2$SS$_1$)**	−14.4	192.2
***Cis*-NetC$_2$SS**	−3.2	171.8
***Cis*-NetC$_6$**	1.3	316.3

[a] Determined as the inflexion point of the second heating cycle of the DSC thermograms. [b] Determined as the temperature associated with a 5% mass loss.

Degradability and reprocessability

The presence of dynamic disulfide bonds was leveraged to degrade the networks in a simple reductive fashion.[35] *Trans*-NetC$_2$SS and *cis*-NetC$_2$SS were successfully degraded after treatment with an equimolar amount of DL-dithiothreitol (DTT) in regard to the disulfide bond content in 60 hours at room temperature in

dimethylformamide (DMF) (Figure 7A). The disulfide bond content was estimated based on the initial feeding of monomer C_2SS (Equation S4). Control experiments performed by treating *trans*-NetC_6 under the same conditions (DTT in DMF) and *trans*-NetC_2SS without DTT did not show any sign of degradation, confirming that degradation is induced by cleavage of the disulfide bonds (Figure S15). Gel permeation chromatography (GPC) revealed the formation of low molecular weight peaks only for the samples undergoing degradation. The reduced species could be isolated *via* solvent extraction and ^{1}H NMR spectroscopy was used to confirm the different *cis*/trans ratio of the networks by evaluation of the intensity of the resonance peaks in the vinyl region (δ = 5.79 ppm, J = 15.2 Hz, *trans* conformation; δ = 5.89 ppm, J = 10.1 Hz, *cis* conformation) (Figure 7C, S16-S17). The *cis* content was found to be 26% for *trans*-NetC2SS and 50% for *cis*-NetC2SS. However, it is worth noting that temperature promotes *cis/trans* isomerisation[36], meaning that a more accurate evaluation of the influence of annealing on *cis*-content is required, highlighting the need for further studies into the impact of *cis/trans* isomerism on thermosets' thermomechanical properties. Finally, high-resolution mass spectroscopy (TOF-HRMS-ES$^+$) revealed a molecular peak at 789 g × mol^{-1} for both samples, which matches the molecular weight of macromonomers resulting from cleavage of the disulfide bond (Figure S18-S19). Lastly, the presence of free thiols resulting from the reduction of disulfides allows the hypothesis of the possibility of establishing a closed-loop recycling life cycle for these materials.[37]

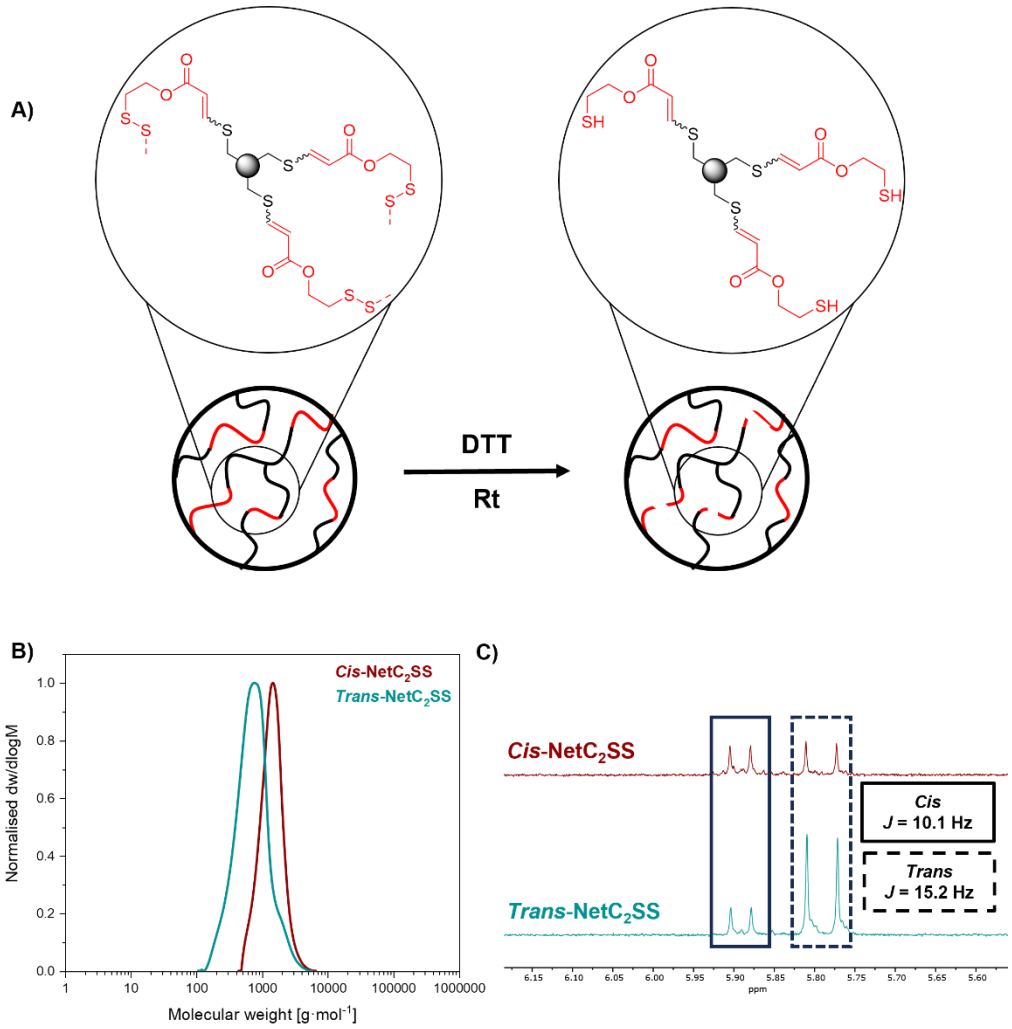


Figure 7. A) Schematic representation of DTT degradation of networks synthesised using monomer C_2SS, and formation of the fully reduced species. B) GPC (DMF, 5 mM NH_4BF_4, comparison against PMMA standard) of oligomeric species resulting from networks degradation. C) Zoomed in section of the vinyl region (between 5.60 and 6.15 ppm) of the ^1H NMR spectrum (400 MHz, 300 K, $CDCl_3$) of the products obtained from the degradation of the networks.

Finally, reprocessing of these crosslinked materials was demonstrated by heat compression moulding. Albeit no loss in modulus was detected during the thermal sweeps performed *via* DMA, a significant decrease in stress could be observed for *trans*-NetC_2SS when stress-relaxation experiments at higher strain (10 µm *vs*. 1 µm) were performed at 150 °C for 20 minutes. This loss in modulus was attributed to the dynamic dissociative nature of the disulfide bonds, as *trans*-NetC_6 modulus remained constant throughout the experiments (Figure 8A). *Trans*-NetC_2SS

fragments could be moulded into a free-standing film by heat compression moulding at 150 °C for 20 minutes at a pressure of 3000 kg. Surprisingly, the same was possible for *trans*-NetC$_6$, albeit the reprocessed films were somehow less structurally stable (Figure 8B). This result was attributed to the dynamic nature of the thiol-yne addition,[38] meaning that the presence of disulfide bonds can be used to enhance the reprocessability of an already dynamic network. Notably, both networks did not display the same homogeneity as the virgin ones, suggesting that the network structure was not perfectly reformed, possibly in light of thermal degradation of the catalysts or the network itself,[39] hence more studies into the reprocessing conditions are needed. For instance, grinding the network prior to moulding may facilitate heat transfer through the sample and lead to more homogeneous materials.

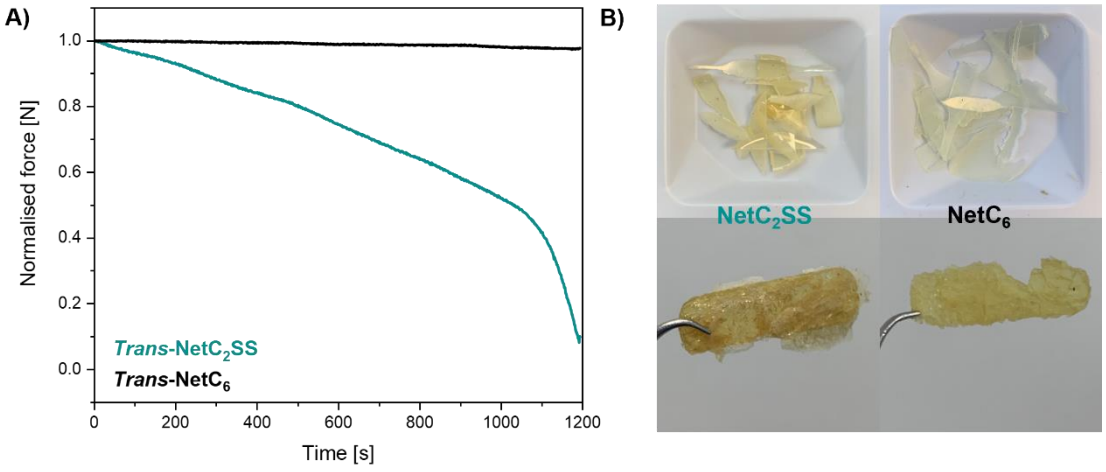


Figure 8. A) Stress relaxation experiments (150 °C, 10 µm, 20 min) performed on *trans*-NetC$_2$SS and *trans*-NetC$_6$ displaying a fast loss in modulus for *trans*-NetC$_2$SS. B) Fragments of *trans*-NetC$_2$SS and *trans*-NetC$_6$ (top) that were reprocessed into free-standing films (bottom) after heat compression moulding at 150 °C for 20 minutes, at a pressure of 3000 kg.

Conclusions

The nucleophilic thiol-yne reaction was used to synthesise a library of crosslinked materials with controllable thermomechanical properties from a limited pool of monomers composed of bifunctional propiolates and a trifunctional thiol. Notably, this method allows for the simple introduction of dynamic disulfide bonds that endowed the material with degradability without a considerable loss in performances. While the ratio between thiols and propiolates is crucial in obtaining more homogeneous networks, this method nonetheless allowed for the synthesis of robust materials. Finally, the effect *of* cis/trans isomerism on the thermomechanical properties has been evaluated revealing that *increasing* cis content can significantly improve the toughness of the network. Future work will focus on optimisation of the recycling and reprocessing conditions to achieve a circular life cycle and exploit of different alkynes and thiols monomer structures to further modulate the thermomechanical properties.

References

1. S. Agarwal and R. K. Gupta, in *Thermosets (Second Edition)*, ed. Q. Guo, Elsevier, 2018, pp. 279-302.
2. J. Fan and J. Njuguna, in *Lightweight Composite Structures in Transport*, ed. J. Njuguna, Woodhead Publishing, 2016, pp. 3-34.
3. I. Hamerton and J. Kratz, in *Thermosets (Second Edition)*, ed. Q. Guo, Elsevier, 2018, pp. 303-340.
4. R. Geyer, J. R. Jambeck and K. L. Law, *Sci Adv*, 2017, **3**, e1700782.
5. D. Rosato and D. Rosato, in *Plastics Engineered Product Design*, eds. D. Rosato and D. Rosato, Elsevier Science, Amsterdam, 2003, pp. 381-438.
6. C. J. Kloxin and C. N. Bowman, *Chem Soc Rev*, 2013, **42**, 7161-7173.
7. C. J. Kloxin, T. F. Scott, B. J. Adzima and C. N. Bowman, *Macromolecules*, 2010, **43**, 2643-2653.
8. P. Chakma and D. Konkolewicz, *Angew Chem Int Ed*, 2019, **58**, 9682-9695.
9. H. Mutlu, E. B. Ceper, X. Li, J. Yang, W. Dong, M. M. Ozmen and P. Theato, *Macromol Rapid Commun*, 2019, **40**, 1800650.
10. C. E. Hoyle and C. N. Bowman, *Angew Chem Int Ed*, 2010, **49**, 1540-1573.
11. A. B. Lowe, *Polym Chem*, 2010, **1**, 17-36.
12. B. Zhang, Z. A. Digby, J. A. Flum, P. Chakma, J. M. Saul, J. L. Sparks and D. Konkolewicz, *Macromolecules*, 2016, **49**, 6871-6878.
13. P. Chakma, L. H. Rodrigues Possarle, Z. A. Digby, B. Zhang, J. L. Sparks and D. Konkolewicz, *Polym Chem*, 2017, **8**, 6534-6543.

14. N. Kuhl, R. Geitner, R. K. Bose, S. Bode, B. Dietzek, M. Schmitt, J. Popp, S. J. Garcia, S. van der Zwaag, U. S. Schubert and M. D. Hager, *Macromol Chem Phys*, 2016, **217**, 2541-2550.
15. A. B. Lowe, C. E. Hoyle and C. N. Bowman, *J Mater Chem*, 2010, **20**, 4745.
16. R. Hoogenboom, *Angew Chem Int Ed*, 2010, **49**, 3415-3417.
17. J. W. Chan, H. Zhou, C. E. Hoyle and A. B. Lowe, *Chem Mater*, 2009, **21**, 1579-1585.
18. J. C. Worch, C. J. Stubbs, M. J. Price and A. P. Dove, *Chem Rev*, 2021, **121**, 6744-6776.
19. O. Daglar, S. Luleburgaz, E. Baysak, U. S. Gunay, G. Hizal, U. Tunca and H. Durmaz, *Eur Polym J*, 2020, **137**, 109926.
20. B. D. Fairbanks, E. A. Sims, K. S. Anseth and C. N. Bowman, *Macromolecules*, 2010, **43**, 4113-4119.
21. N. Van Herck, D. Maes, K. Unal, M. Guerre, J. M. Winne and F. E. Du Prez, *Angew Chem Int Ed*, 2020, **59**, 3609-3617.
22. V. Zhang, B. Kang, J. V. Accardo and J. A. Kalow, *J Am Chem Soc*, 2022, **144**, 22358-22377.
23. J. C. Worch, A. C. Weems, J. Yu, M. C. Arno, T. R. Wilks, R. T. R. Huckstepp, R. K. O'Reilly, M. L. Becker and A. P. Dove, *Nat Commun*, 2020, **11**, 3250.
24. C. A. Bell, J. Yu, I. A. Barker, V. X. Truong, Z. Cao, A. V. Dobrinyin, M. L. Becker and A. P. Dove, *Angew Chem Int Ed*, 2016, **55**, 13076-13080.
25. C. J. Stubbs, J. C. Worch, H. Prydderch, M. L. Becker and A. P. Dove, *Macromolecules*, 2020, **53**, 174-181.
26. L. J. Macdougall, M. M. Pérez-Madrigal, J. E. Shaw, J. C. Worch, C. Sammon, S. M. Richardson and A. P. Dove, *Angew Chem Int Ed*, 2021, **60**, 25856-25864.
27. A. L. Khalfa, M. L. Becker and A. P. Dove, *J Am Chem Soc*, 2021, **143**, 17510-17516.
28. V. X. Truong and A. P. Dove, *Angew Chem Int Ed*, 2013, **52**, 4132-4136.
29. L. R. G. Treloar, *Rep Prog Phys*, 1973, **36**, 755-826.
30. E. A. Prebihalo, M. Johnson and T. M. Reineke, *ACS Macro Letters*, 2024, **13**, 586-591.
31. Y.-M. Yang, H.-Z. Yu, X.-H. Sun and Z.-M. Dang, *J Phys Org Chem*, 2016, **29**, 6-13.
32. A. A. Zavitsas, *J Phys Chem A*, 2003, **107**, 897-898.
33. M. Radiom, P. Kong, P. Maroni, M. Schäfer, A. F. M. Kilbinger and M. Borkovec, *Phys Chem Chem Phys*, 2016, **18**, 31202-31210.
34. T. M. Nair, M. G. Kumaran and G. Unnikrishnan, *J Appl Polym Sci*, 2004, **93**, 2606-2621.
35. S. N. Mthembu, A. Sharma, F. Albericio and B. G. Torre, *ChemBioChem*, 2020, **21**, 1947-1954.
36. C. Dugave and L. Demange, *Chem Rev*, 2003, **103**, 2475-2532.
37. N. V. Tsarevsky and K. Matyjaszewski, *Macromolecules*, 2002, **35**, 9009-9014.
38. G. Joshi and E. V. Anslyn, *Org Lett*, 2012, **14**, 4714-4717.
39. M. A. Alraddadi, V. Chiaradia, C. J. Stubbs, J. C. Worch and A. P. Dove, *Polym Chem*, 2021, **12**, 5796-5802.

Supporting information

Access to degradable and reprocessable thermosets with tuneable thermomechanical properties *via* nucleophilic thiol-yne polymerisation.

Daniele Giannantonio[a], Arianna Brandolese[a], Andrew P. Dove[a]

[a]School of Chemistry, University of Birmingham, Edgbaston, Birmingham, B15 2TT (UK)

Experimental methods

All compounds, unless otherwise indicated were purchased from commercial sources and used as received. The following chemicals were vacuum distilled prior to use and stored in Young's tapped ampoules under N_2: propiolic acid (Sigma-Aldrich ≥ 97%). Heating was applied through a stirring plate equipped with an oil bath. We acknowledge the molar mass between crosslinks calculator from the Konkolewicz group and Hubbard provided by the Macromolecular Alliance for Community Resources and Outreach. NMR spectr

NMR Spectroscopic Analysis: See Chapter 2 – Supporting information, experimental methods.

Mass Spectrometry: See Chapter 2 – Supporting information, experimental methods.

Fourier-transform Infrared Spectroscopy (FTIR): See Chapter 2 – Supporting information, experimental methods.

Size Exclusion Chromatography (SEC). SEC measurements were performed on an Agilent 1260 Infinity II Multi-Detector GPC/SEC System fitted with RI and ultraviolet (UV) detectors (λ = 309 nm) and PLGel 3 μm (50 × 7.5 mm) guard column and two PLGel 5 μm (300 × 7.5 mm) mixed-C columns with DMF containing 5 mM NH_4BF_4 as the eluent (flow rate 1 mL/min, 50 °C). A 12-point calibration curve (M_p = 550–2,210,000 g×mol^{-1}) based on poly(methyl methacrylate) standards (PMMA, Easivial PM, Agilent) was applied for the determination of molecular weights.

Differential Scanning Calorimetry (DSC): See Chapter 2 – Supporting information, experimental methods.

Thermogravimetric Analysis (TGA): See Chapter 2 – Supporting information, experimental methods.

Dynamic Mechanical Analysis (DMA): Dynamic mechanical thermal analysis (DMTA) data were obtained using a Mettler Toledo DMA 1 star system and analysed using the software package STARe V13.00a Thermal sweeps were conducted using films (L x W x thickness = 15 mm x 6 mm x 0.5 mm) cooled to −80 °C and held isothermally for ca. 5 minutes. Storage and loss moduli, as well as the loss factor (ratio of E" and E', tan δ) were probed as the temperature was swept from −80 to 180 °C, 5 °C·min^{-1}, displacement of 1 μm, frequency of 1 Hz. Stress-relaxation experiment was performed with a displacement of 10 μm at 150 °C for 20 minutes.

Rheology: The flow characteristics of the polymers were studied using Anton Paar MCR302 rheometer with Peltier controlled heating. All tests were performed using parallel plates on disk-shape samples of 8 mm in diameter. For frequency sweep measurement, the frequency was varied from 100 Hz to 0.01 Hz at 25 °C, with a strain amplitude of 5%. For strain sweep measurements, strain was varied between 0.1% to 500% with a frequency of 1 rad/s.

Tensile testing. See Chapter 2 – Supporting information, experimental methods.

Reprocessing. Networks flakes were reprocessed with a 3 Specac Atlas™ Manual Hydraulic Press 15T fitted with Specac heated plates. The pieces were added into a stainless steel mold and placed into pre-heated press at 150 °C. The

sample was heated for 20 min (3000 kg pressure) before degassing 3 × (3000 kg pressure/release). The samples were then left to cool under pressure until temperature reached 25 °C.

Swell testing and gel fraction: Networks were taken and cut into disks (6.7 × 0.5 mm) and weighed before being submerged in chloroform ($CHCl_3$) and allowed to swell until equilibrium swelling was reached after 30 hours. The initial mass (W_i) and swelling mass (W_s) was used to calculate the swelling ratio (%) as shown in equation S1, where W_s is given by subtracting W_i to the sample mass measured rapidly after being removed from the solvent. The swollen networks were resubmerged in new $CHCl_3$ and finally dried after filtration to get the dry mass (W_d). This was used to calculate the gel fraction (%) as shown in equation S2.

Equation S1[1]

$$\boldsymbol{Swelling\ ratio}\ (\%) = \frac{\boldsymbol{W_s}}{\boldsymbol{W_i}} \times \mathbf{100}$$

Equation S2[1]

$$\boldsymbol{Gel\ fraction}\ (\%) = \frac{\boldsymbol{W_d}}{\boldsymbol{W_i}} \times \mathbf{100}$$

Equation S3[1, 2]

$$\boldsymbol{M_c} = \mathbf{3}\frac{\boldsymbol{\rho RT}}{\boldsymbol{E'_{rubbery}}}$$

$\boldsymbol{M_c}$ = molecular weight between crosslinks
$\boldsymbol{R}$ = universal gas constant
$\boldsymbol{\rho}$ = density of the material (assumed to be 1 g/cm^3)
$\boldsymbol{T}$ = temperature (T_g + 50 °C)

$\boldsymbol{E'_{rubbery}}$ = storage modulus

Equation S4

$$\%\boldsymbol{Wt_{SSbond}} = \frac{\left(\boldsymbol{MW_{SS}}/\boldsymbol{MW_{C_2SS}}\right) \times \boldsymbol{m_{C_2SS}}}{\boldsymbol{total\ m_{network}}} \times \mathbf{100}$$

$\boldsymbol{\%Wt_{SSbond}}$ weight percentage of sulfur atoms involved in a disulfide bond

$\boldsymbol{MW_{SS}}$ = molecular weight (g mol^{-1}) of monomer C_2SS

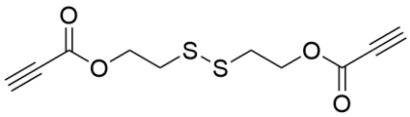
$\boldsymbol{M_{network}}$ = total mass of the resulting network

$\boldsymbol{MW_{SS}}$ = molecular weight (g mol^{-1}) of two sulfur atoms involved in the formation of a disulfide bond

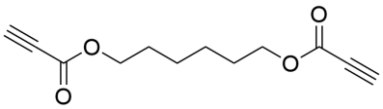
$\boldsymbol{M_{c2ss}}$ = mass of monomer C_2SS used to synthesise the network

Synthetic procedures

Disulfide dipropiolate (C_2SS): Refer to monomer M1 synthetic procedure and spectroscopic data reported in chapter 2.



Hexane dipropiolate (C_6): Refer to monomer M2 synthetic procedure and spectroscopic data reported in chapter 2.



General synthesis of network: Dipropiolate monomers in the desired ratio were solubilised in $CHCl_3$ in the presence of trimethylolpropane tris(3-mercaptopropionate) (3-AT) to achieve a final thiol:alkyne ratio of 1:1 or 1.5:1, keeping the concentration of thiol at 0.3 M. The mixture was cooled for 10 minutes in an ice bath. The catalyst (DBU or Et_3N) was then added to the mixture that was subsequently poured into a Teflon beaker covered with tin foil. The solvent was left evaporating inside a fumehood until free standing films could be recovered. Networks were then dried in a vacuum oven at 50 °C until a constant weight was reached.

Degradation experiment: Disks used to perform *gel-sol* analysis were placed in DMF with a final concentration of 20 mg/mL in a 7 mL vial. GPC analysis was performed to evaluate the presence of oligomers after addition of the solvent and after a 24 h period revealing absence of degradation. Dithiothreitol (DTT) (1 equiv. to disulfide equivalent) was added to the vials that were stirred on an orbital shaker at

250 rpm until the networks were not visible anymore (*ca*. 60 h). Aliquots (50 µL) were taken throughout the experiment to monitor the degradation *via* SEC analysis. The oligomers were isolated by diluting the reaction mixture with $LiCl_{aq.}$ 10% w/w and extracted with dichloromethane (DCM).

Thermomechanical characterisation

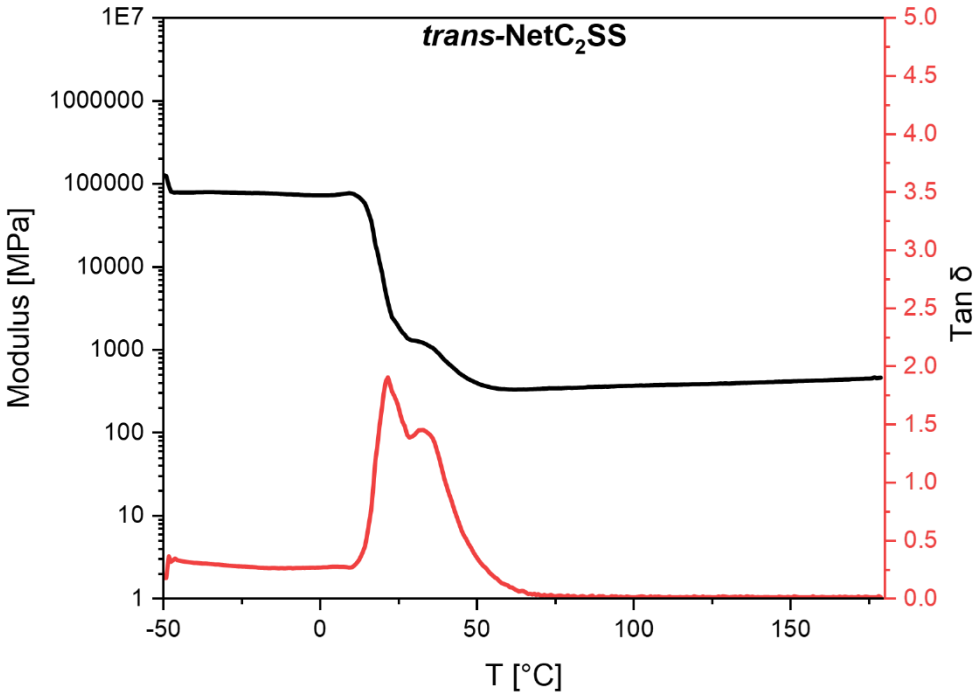


Figure S1. A) DMA thermal sweep (−50 – 180 °C, 1 Hz, 1 µm) of *trans*-NetC$_2$SS.

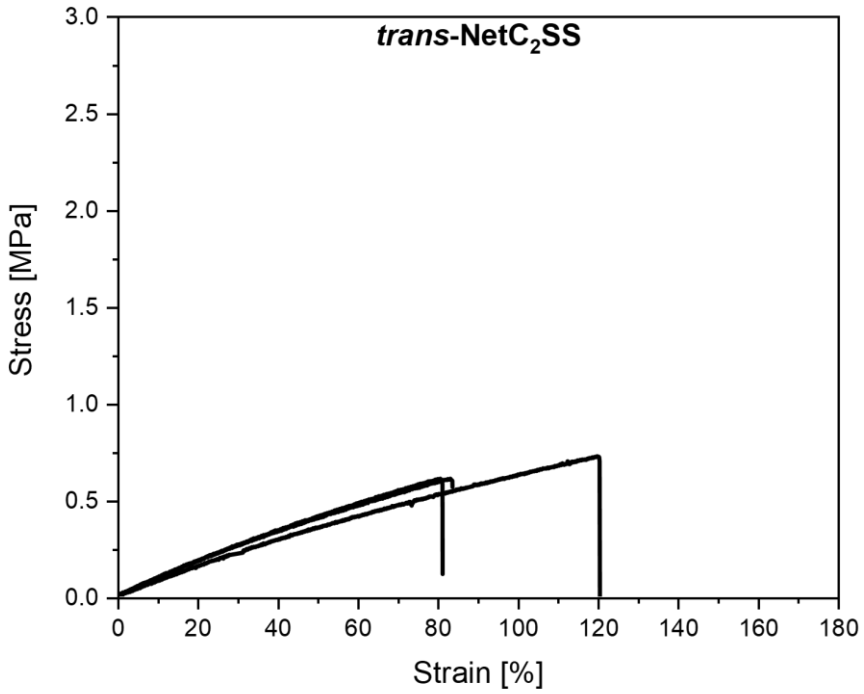


Figure S2. Stress *vs*. strain curves obtained from uniaxial tensile testing (22 °C, 10 mm/min) of *trans*-NetC$_2$SS.

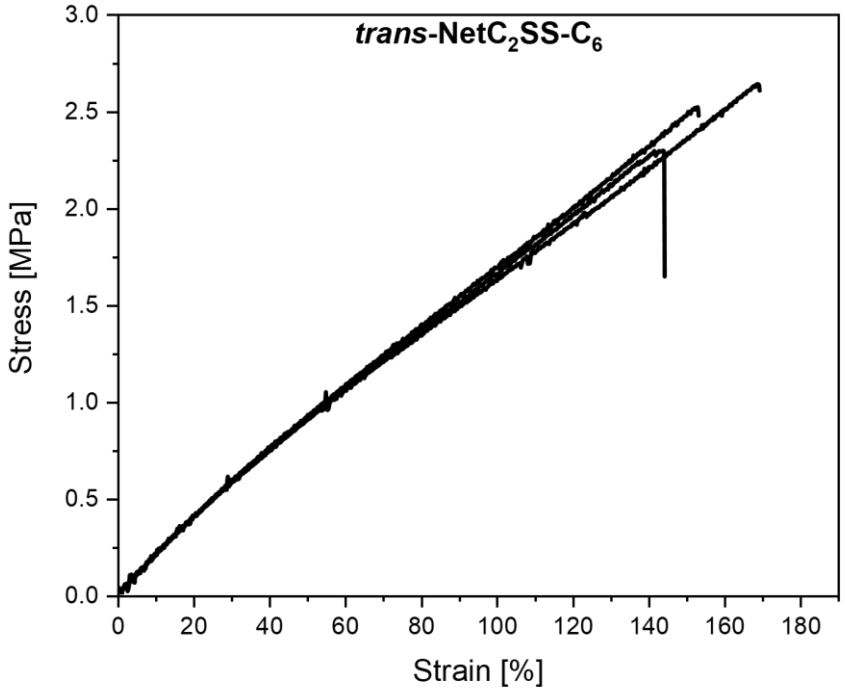


Figure S3. Stress *vs*. strain curves obtained from uniaxial tensile testing (22 °C, 10 mm/min) of *trans*-Net(C_2SS-C_6).

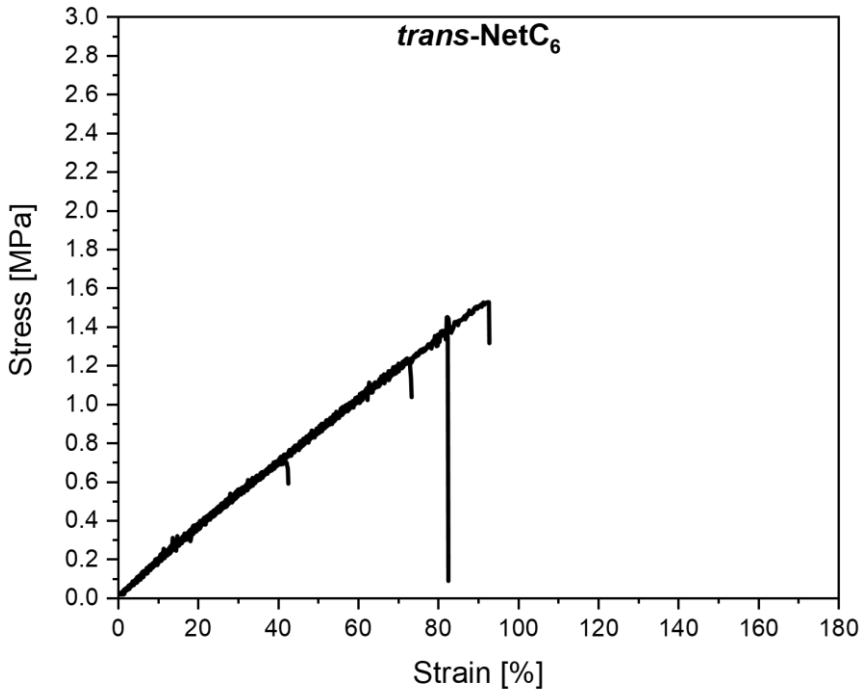


Figure S4. Stress *vs*. strain curves obtained from uniaxial tensile testing (22 °C, 10 mm/min) of *trans*-NetC$_6$.

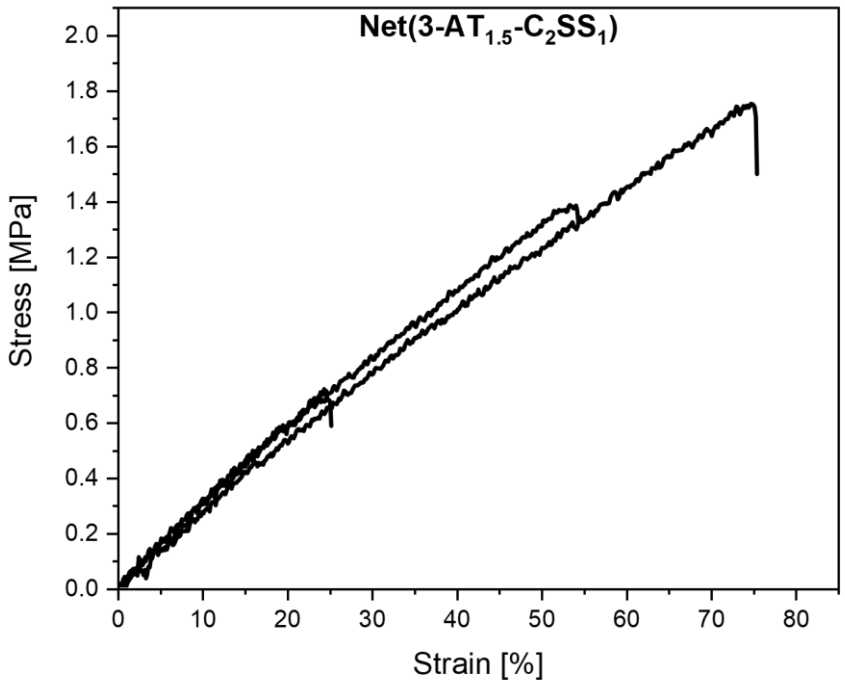


Figure S5. Stress *vs*. strain curves obtained from uniaxial tensile testing (22 °C, 10 mm/min) of *trans*-Net(3-$AT_{1.5}$-C_2SS_1).

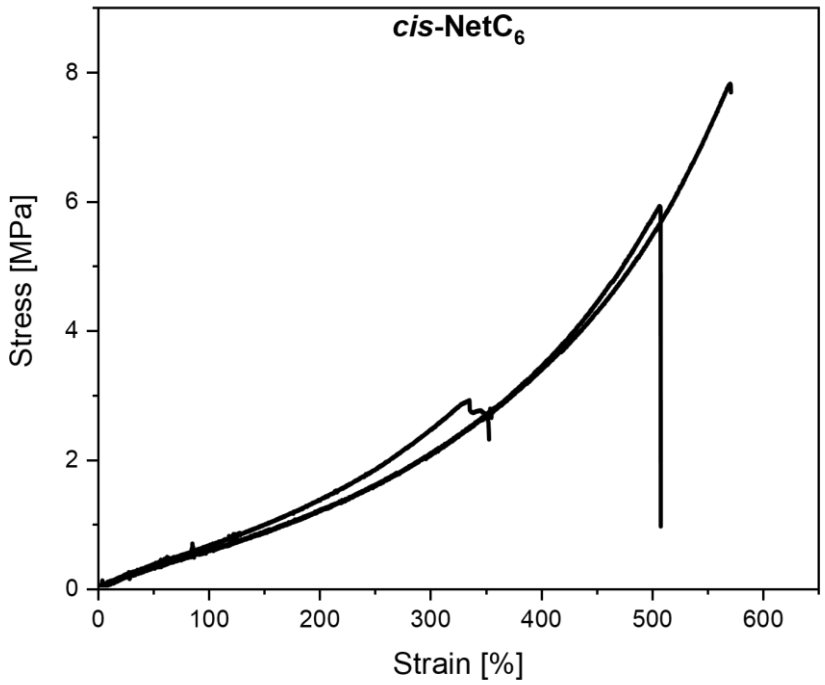


Figure S6. Stress *vs*. strain curves obtained from uniaxial tensile testing (22 °C, 10 mm/min) of *cis*-NetC$_6$.

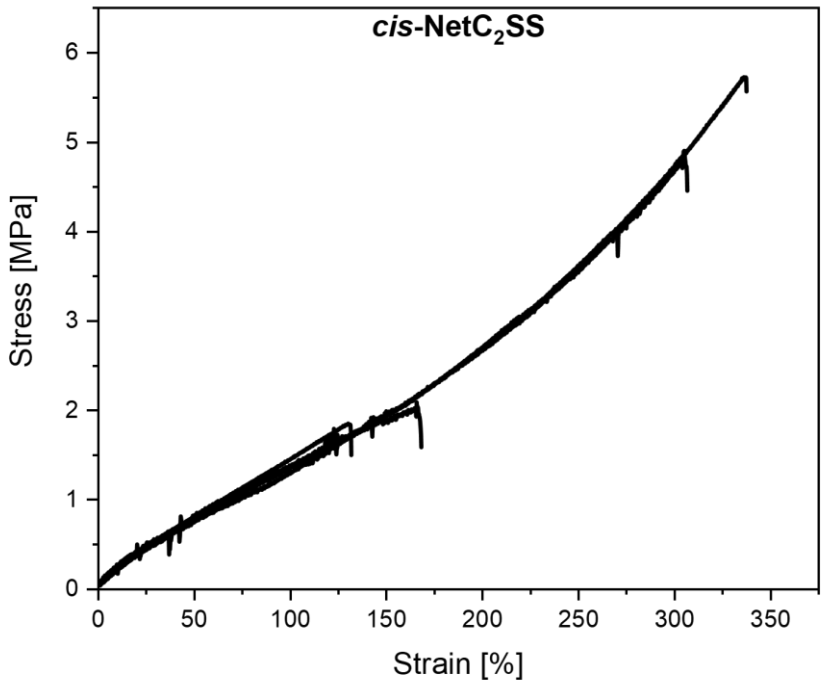


Figure S7. Stress *vs*. strain curves obtained from uniaxial tensile testing (22 °C, 10 mm/min) of *cis*-NetC$_2$SS.

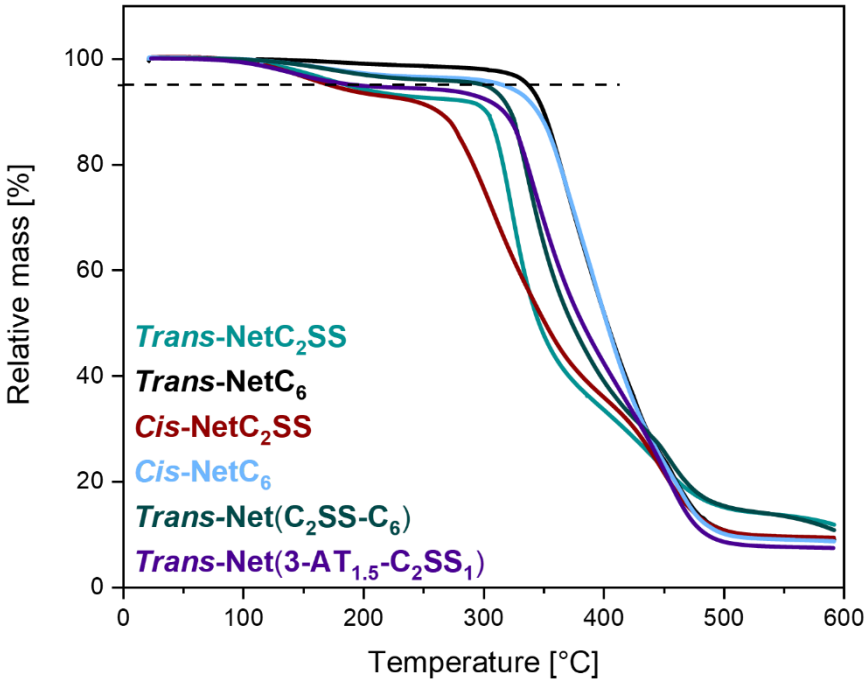


Figure S8. TGA thermogram (25 – 600 °C, N_2) of different networks synthesised in this work.

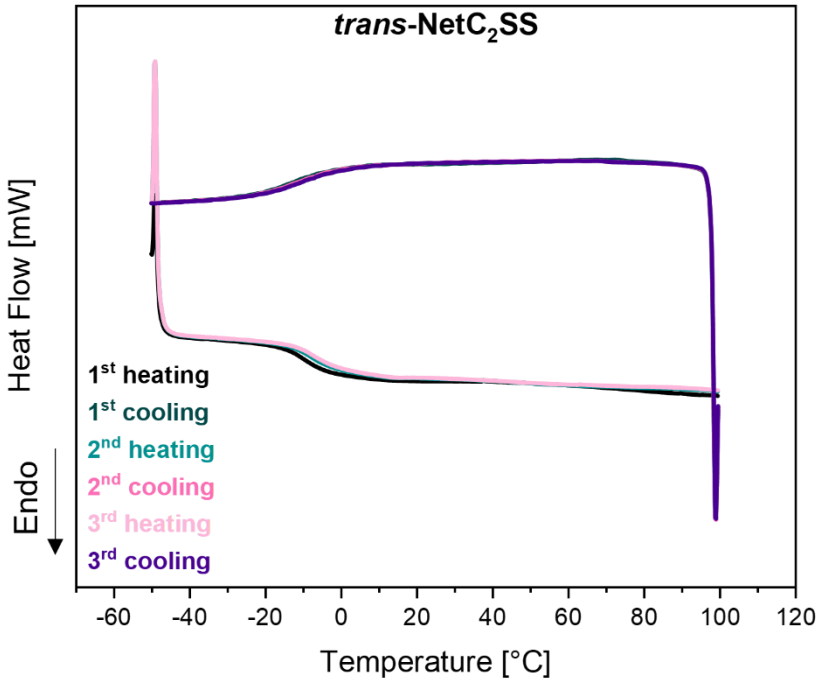


Figure S9. DSC thermogram (−50 – 100 °C, N_2) of *trans*-NetC$_2$SS.

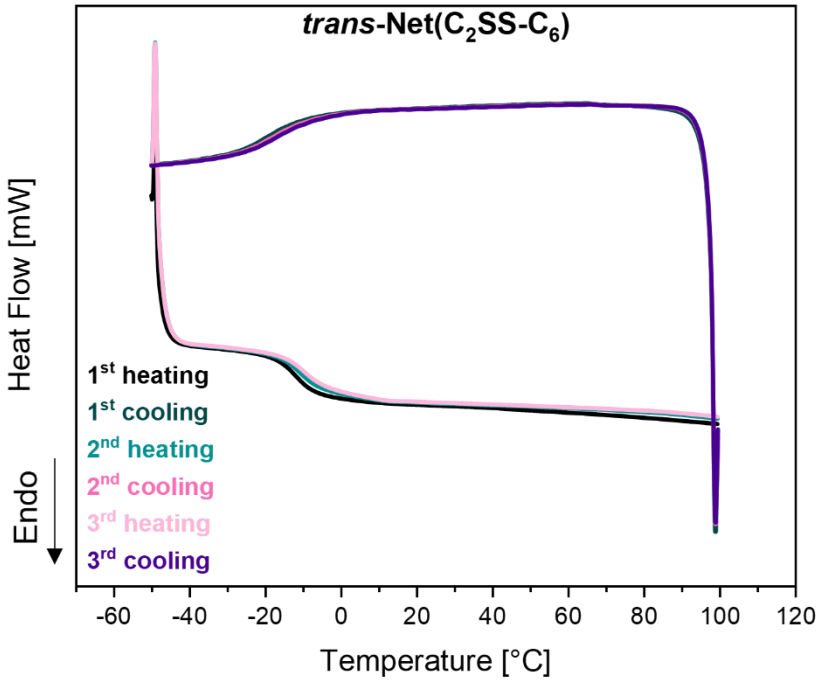


Figure S10. DSC thermogram (−50 – 100 °C, N_2) of *trans*-Net(C_2SS-C_6).

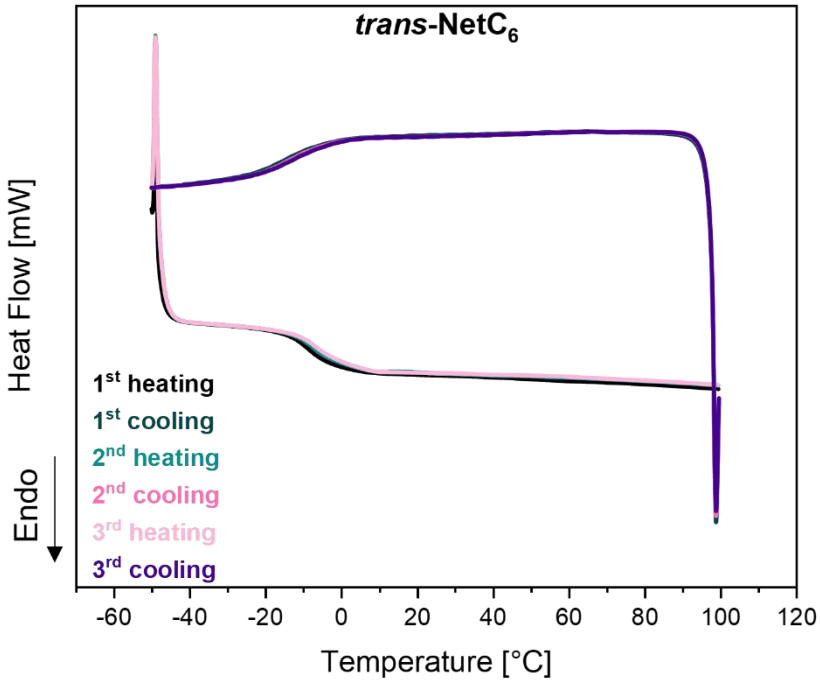


Figure S11. DSC thermogram (−50 – 100 °C, N_2) of *trans*-NetC$_6$.

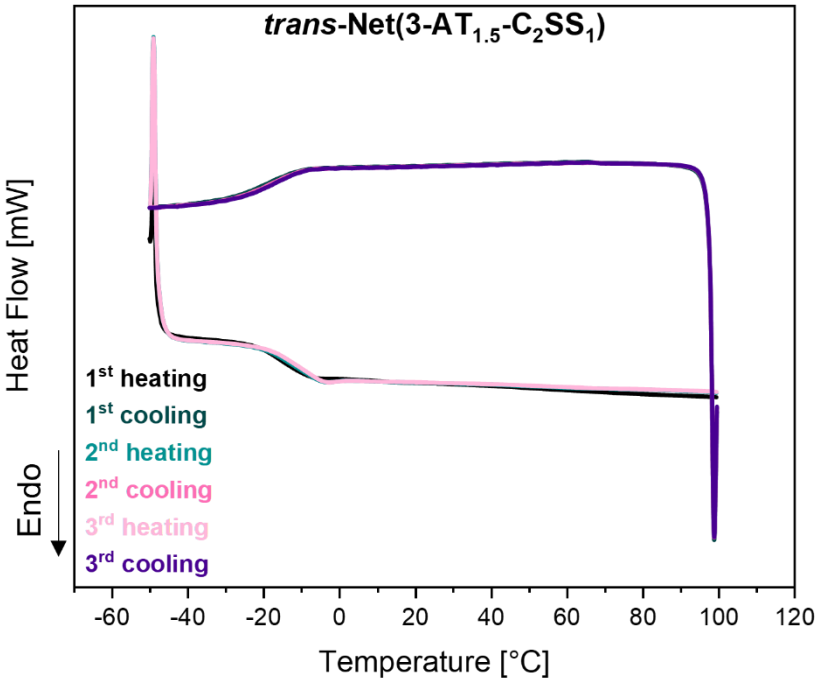


Figure S12. DSC thermogram (−50 – 100 °C, N_2) of *trans*-Net(3-AT$_{1.5}$-C$_2$SS$_1$).

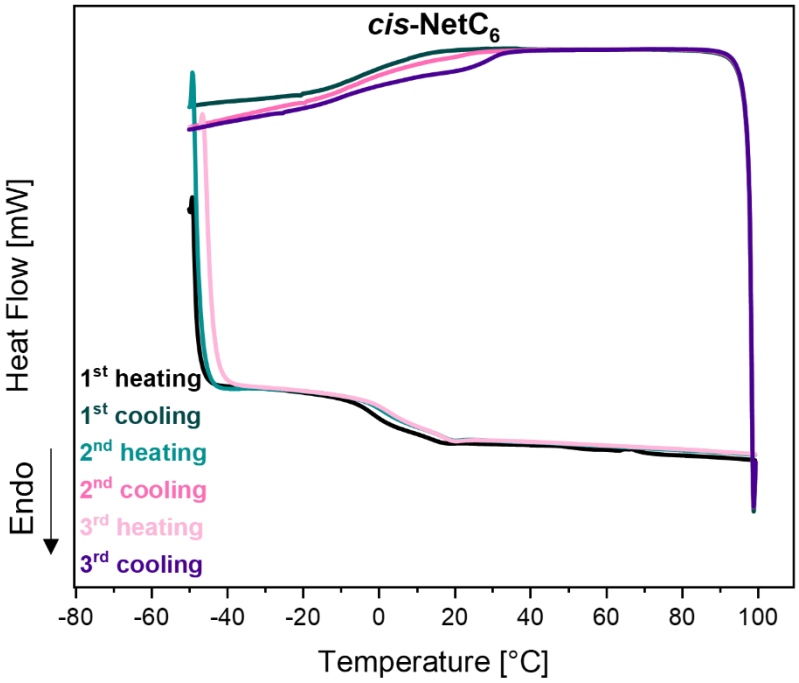


Figure S13. DSC thermogram (−50 – 100 °C, N_2) of *cis*-NetC$_6$.

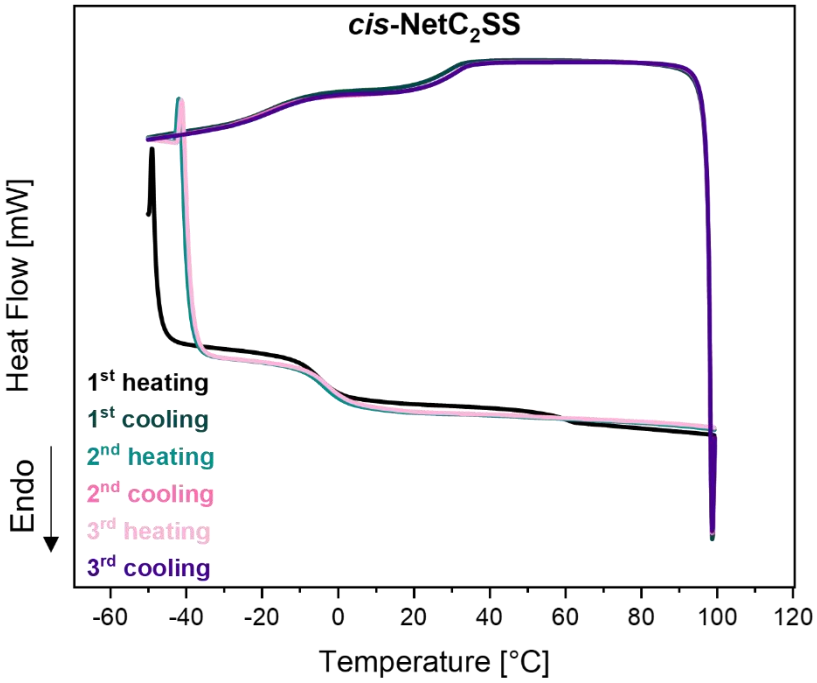


Figure S14. DSC thermogram (−50 – 100 °C, N_2) of *cis*-NetC$_2$SS.

Degradation study

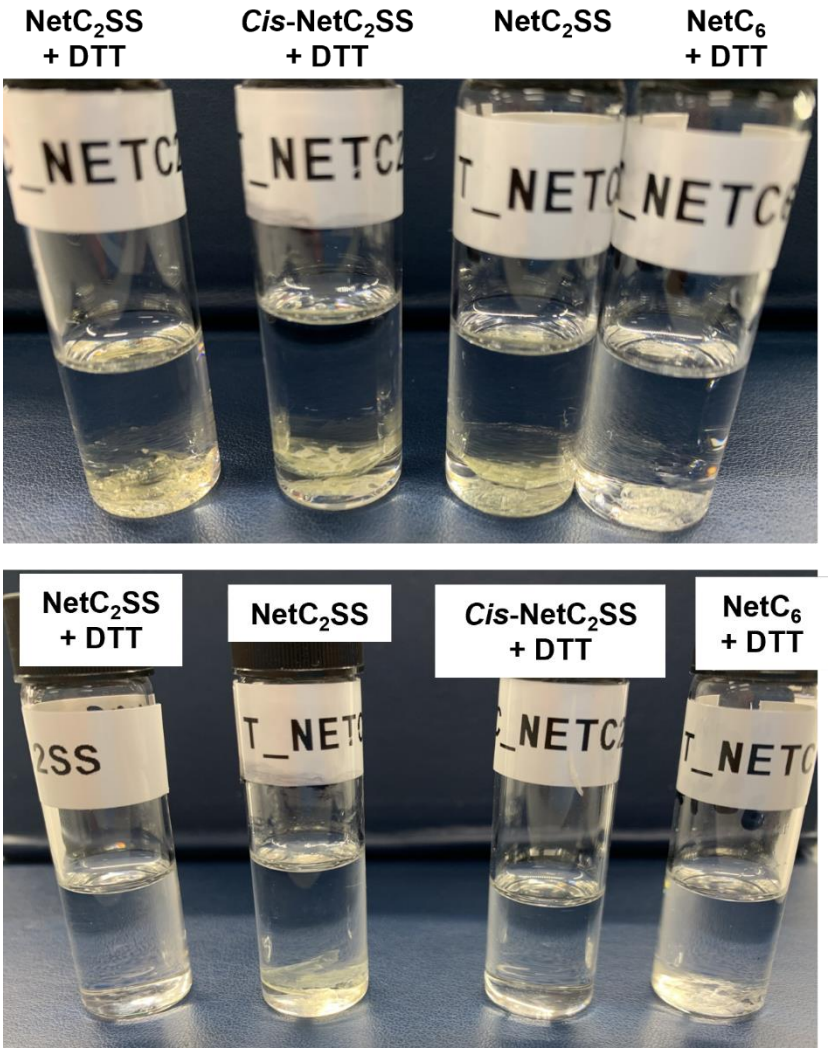


Figure S15. Networks in DMF (20 mg/mL) before (top) and after (bottom) DTT induced degradation.

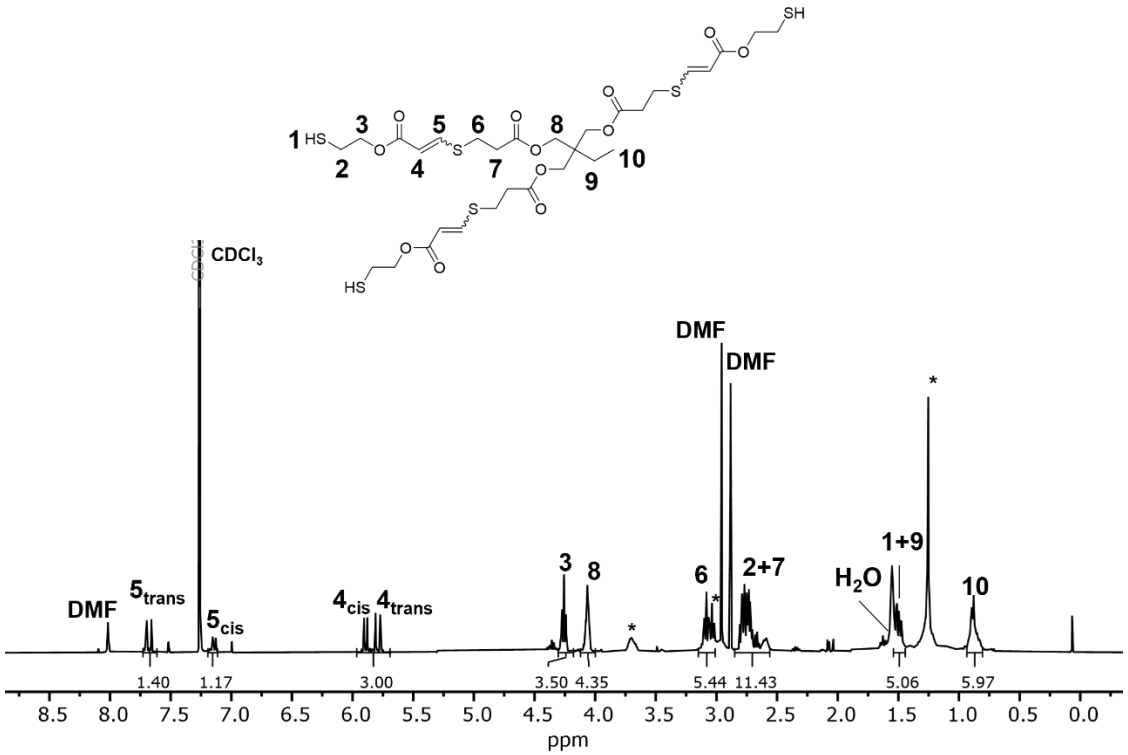


Figure S16. ^{1}H NMR spectrum (400 MHz, 300 K, $CDCl_3$) of the degradation product obtained from *cis*-NetC_2SS. Solvent peak marked with an asterisk.

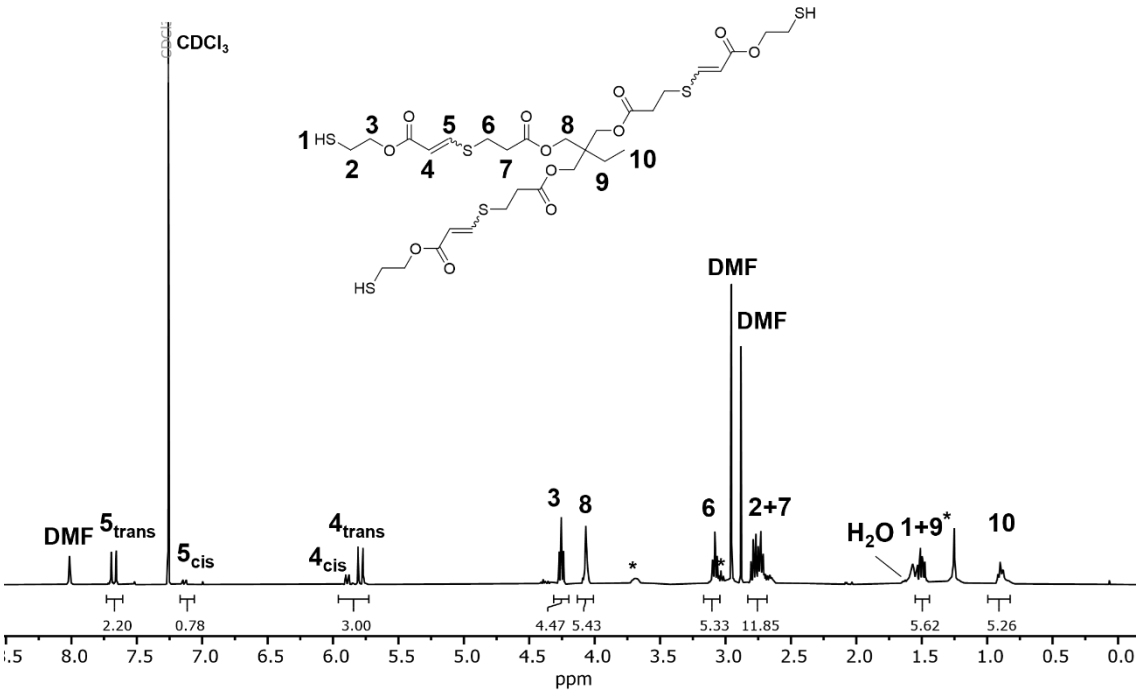


Figure S17. ^{1}H NMR spectrum (400 MHz, 300 K, $CDCl_3$) of the degradation product obtained from *trans*-NetC_2SS. Solvent peak marked with an asterisk.

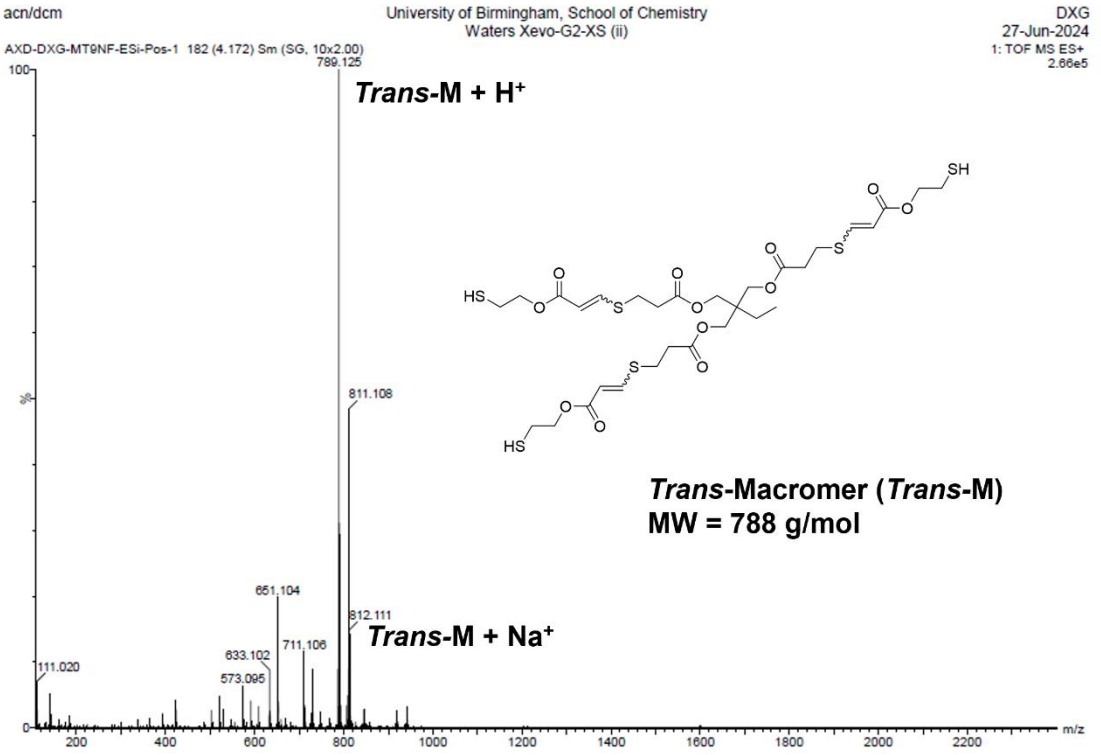


Figure S18. Mass spectrum (ES+) of degraded *trans*-NetC_2SS with plausible structure reported.

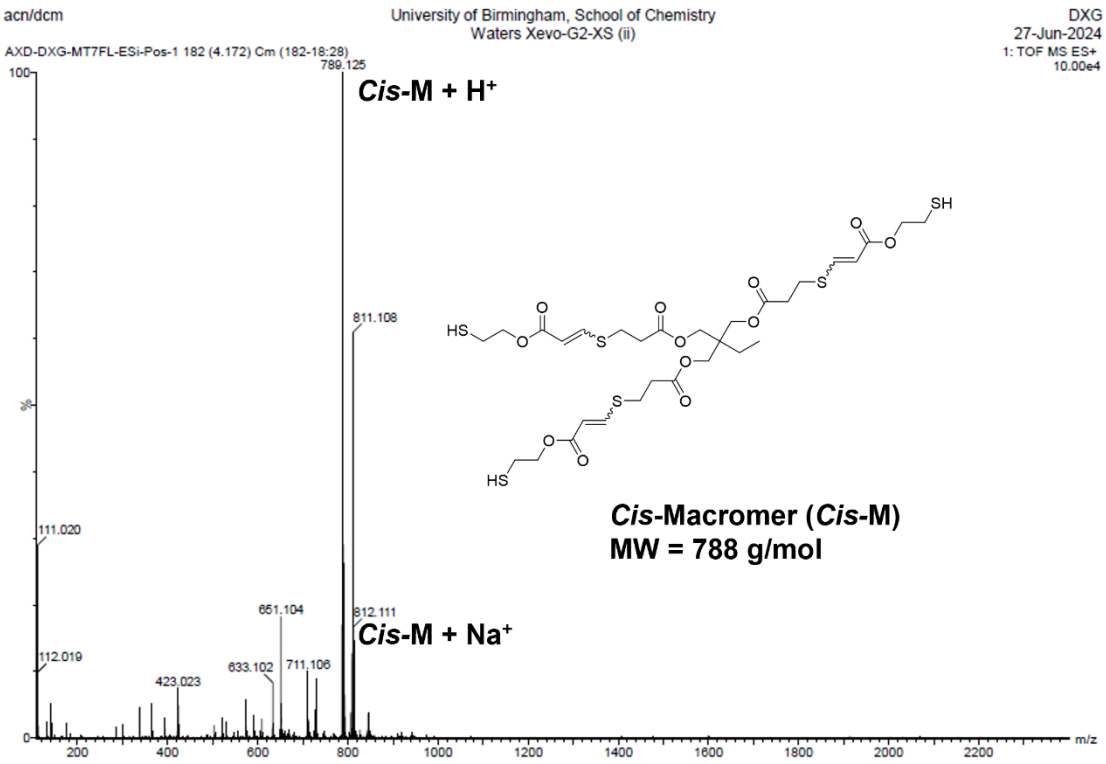


Figure S19. Mass spectrum (ES+) of degraded *cis*-NetC_2SS with plausible structure reported.

References

1. CWH Rajawasam, OJ Dodo, MASN Weerasinghe, IO Raji, SV Wanasinghe, D Konkolewicz and N De Alwis Watuthanthrige, *Polym. Chem.*, 2024, **15**, 219-247.
2. LRG Treloar, *Rep. Prog. Phys.*, 1973, **36**, 755-826.

Chapter 4 – Accessing diketopiperazines-based polymers through phenol-yne polymerisation

Manuscript and overview

Title: Accessing diketopiperazine-based polymers through phenol-yne polymerisation.

Authors: Daniele Giannantonio[a], Arianna Brandolese[a], Andrew P. Dove[a]

Affiliations: [a]School of Chemistry, University of Birmingham, Edgbaston, Birmingham, B15 2TT (UK)

Manuscript prepared

Co-authors contribution: Arianna Brandolese provided editing of the manuscript and guidance. Prof. Andrew P. Dove supervised in addition to providing guidance and funding acquisition.

Overview:

As great interest is placed into replacing commodity polymers with bio-sourced alternatives, the evaluation of different naturally sourced monomers is crucial to finding materials able to compete with the existing alternatives. This chapter aimed to leverage diketopiperazine, afforded from the cyclisation of amino acids, to build novel bio-based polymers displaying tuneable themomechanical properties depending on the co-monomer of choice.

Accessing diketopiperazines-based polymers through phenol-yne polymerisation

Daniele Giannantonio[a], Arianna Brandolese[a], Andrew P. Dove[a]

[a]School of Chemistry, University of Birmingham, Edgbaston, Birmingham, B15 2TT (UK).

Abstract: Amino acids have received considerable attention in the production of sustainable stereo-defined polymers, but their thermomechanical properties are usually modest and fail to compete with existing petroleum-based polymers. However, cyclizing amino acids to form diketopiperazine (DKP) moieties can potentially afford polymers with comparatively robust thermomechanical properties, but difficulties in their polymerisation has hindered investigation into these materials. By leveraging a greener organobase-catalysed phenol-yne polymerisation, the obtainment of tyrosine-DKP-based polymers of high weight-average molecular weight is demonstrated. Moreover, by variation of the co-monomer, a wide range of thermomechanical properties can be accessed, suggesting the versatility of the system.

Introduction

Current commodity polymeric materials possess many desirable characteristics such as low cost, versatility, chemical resistance, and high strength-to-weight, which makes them widely distributed in all aspects of modern society with an ever-increasing production rate.[1, 2] However, since the majority of plastics come from crude oil, their production relies on a finite resource and results in a high amount of greenhouse gases (GHGs) emitted into the atmosphere.[3] In order to decrease their environmental footprint, several efforts have been devoted to building more sustainable polymers leveraging on renewably sourced monomers.[4, 5] Among the different possibilities, amino acids represent an abundant and diversified sustainable feedstock that can endow polymers with particular chemical properties.[6, 7] Unfortunately, these materials often lack the thermomechanical properties to compete with common olefines, hampering their use as a plastic replacement.[8]

A strategy to modulate the thermomechanical properties of polymers is the introduction of cyclic structures in their backbone, because of the reduced degree of freedom associated with them.[9] By condensation of two amino acids, six-membered diketopiperazine (DKP) cyclodipeptides with stereocenters at the alpha-carbon of the carbonyl group can be obtained (Figure 1A). Given their advantageous characteristics such as accessibility and structural complexity, DKPs have received significant attention in drug discovery.[10] Moreover, in light of their extensive

hydrogen bonding, they have been widely investigated as gelators (Figure 1B).[11] These features make them a promising scaffold for material synthesis. [12, 13]

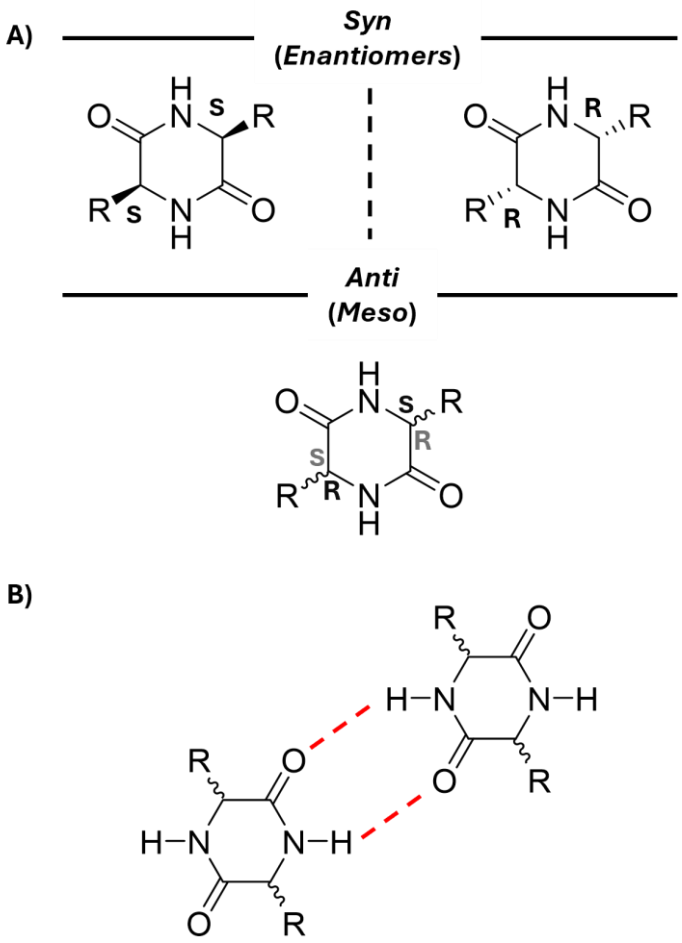


Figure 1. A) Stereoisomerism of DKP ring. B) Hydrogen bonding interaction between two DKP molecules.

The potential of including DKPs in polymers has been already recognised, and these materials have been proven to degrade into non-toxic component and to form supramolecular structures.[14, 15] However, their inclusion in polymers have been historically challenging because of difficulties associated with their treatment, mostly their lack of solubility. In fact, the preparation of polymers of high molar mass has rarely been reported, which limits investigation into their properties. Approaches deployed to synthesise these polymers include acyclic diene

metathesis (ADMET),[16, 17] polycondensation reactions to produce polyesters and polyamide,[14, 18-22] and polyadditions to produce polyurethanes.[23-25] Unfortunately, these methods require lengthy synthetic protocols that use toxic reagents and harsh conditions reactions, such as triphosgene and metal catalysis, or prolonged time under vacuum at high temperatures.

Inspired by recent reports of the Tang group on hydroxyl/phenol-yne "click" polymerisation,[26, 27] and the abundance of hydroxyl/phenol groups in natural products, it was decided to apply these concepts to the polymerisation of DKPs to produce polymeric materials of high M_w in a more sustainable and safe fashion. Nucleophilic addition to activated alkyne can be a particularly useful tool in polymer synthesis because of the controllable stereochemistry of the addition product (*E*/*Z* isomerism) and its influence over thermomechanical properties, alongside the possibility of using the resulting double bond as a handle for post-synthetic functionalisation.[28, 29]

Herein, the greener phenol-yne "click" polymerisation of cyclo(L-Tyr-L-Tyr) (TyrDKP) is reported as an efficient way to build high molecular weight DKP-based polymers (up to M_w = 89 kg/mol) under mild conditions.[30] By straightforward functionalisation of different biobased diols, polymers with a high share (> 80 % w/w) of renewably sourced content could be obtained. Most importantly, thermomechanical properties were found to be highly tuneable according to the co-monomer of choice, leading to a wide range of attainable glass transition

temperatures (−7.5 < T_gs < 114 °C), mechanical behaviours, and high thermal stability (up to 367 °C).

Results and discussion

Polymer synthesis and characterisation

The amino acid-derived monomer has been prepared in a one-step protocol *via* simple refluxing of L-Tyrosine in ethylene glycol under an inert atmosphere, affording the TyrDKP monomer in moderate yield (63%). The *syn*-DKP molecule was selected for this study because of the simple synthesis conditions and accessibility of the natural amino acid precursor. Suitable dialkynes for phenol-yne polymerisation were synthesised by Fisher esterification between propiolic acid and biobased diols such as 1,6-hexanediol, tetraethyleneglycol, and Pripol 2033™, to generate 1,6-hexanedipropiolate (HDP), tetraethyleneglycol dipropiolate (TEGDP) and Pripol™ dipropiolate (Prip-DP), respectively (Figure S1-S8). Given the poor solubility of TyrDKP in common organic non-polar solvents, dimethyl formamide (DMF) and dimethylsulfoxide (DMSO) were tested to conduct the polymerisation reaction. The latter was eventually selected considering its greater capacity to solubilise the monomer and diminished toxicity.[31] The polymerisation was performed by solubilising the monomers in the stated solvent (0.3 M) at 50 °C, followed by the addition of 1,4-diazabicyclo[2.2.2]octane (DABCO, 0.01 equivalents) pre-solubilised in DMSO as the catalyst (Figure 2A). Reactions were monitored using FT-IR spectroscopy to confirm the consumption of the terminal alkynes after three hours (Figure 2B). The polymers were recovered by precipitation

into a 1:1 *v:v* solution of acetone and hexane in good to excellent yields (75-99%) (Table 1). The structure of poly(TyrDKP-HDP) and poly(TyrDKP-TEGDP) was elucidated *via* ^{1}H NMR spectroscopy (Figure S12-S14), showing the predominant formation of *trans* linkages. This was determined by comparing the relative intensity of the signals of the *E* adduct (J = 12.1 Hz) with the intensity of the signals associated with the *Z* product (J = 6.9 Hz), estimating the *cis* content to be *ca*. 8%. The *cis*/*trans* ratio was found to be the same for poly(TyrDKP-HDP) and poly(TyrDKP-TEGDP), suggesting the selectivity of DABCO catalysed phenol-yne polymerisation towards the formation of *E* adducts (Figure 2C). Further product variability has been achieved through the preparation of poly(TyrDKP-PripDP) that turned out to be insoluble in the common solvents, hampering its full characterisation. In fact, the polymer was soluble only in boiling DMSO, even in the presence of trifluoroacetic acid (TFA) 20 % v/v. Notably, crosslinking events were excluded because of the lack of swelling even after prolonged exposure to solvents.

Notably, attempts to polymerise a L-serine-based diketopiperazine (Ser-DKP) only led to quantitative recovery of unreacted starting materials using both DABCO or 4-dimethylaminopyridine (DMAP) as the catalyst.[27] This reduced reactivity was attributed to the diminished acidity of hydroxyl proton when compared to a phenolic one, along with the fact that Ser-DKP hydroxyl group are folded above the ring because of their hydrogen bonding.[32]

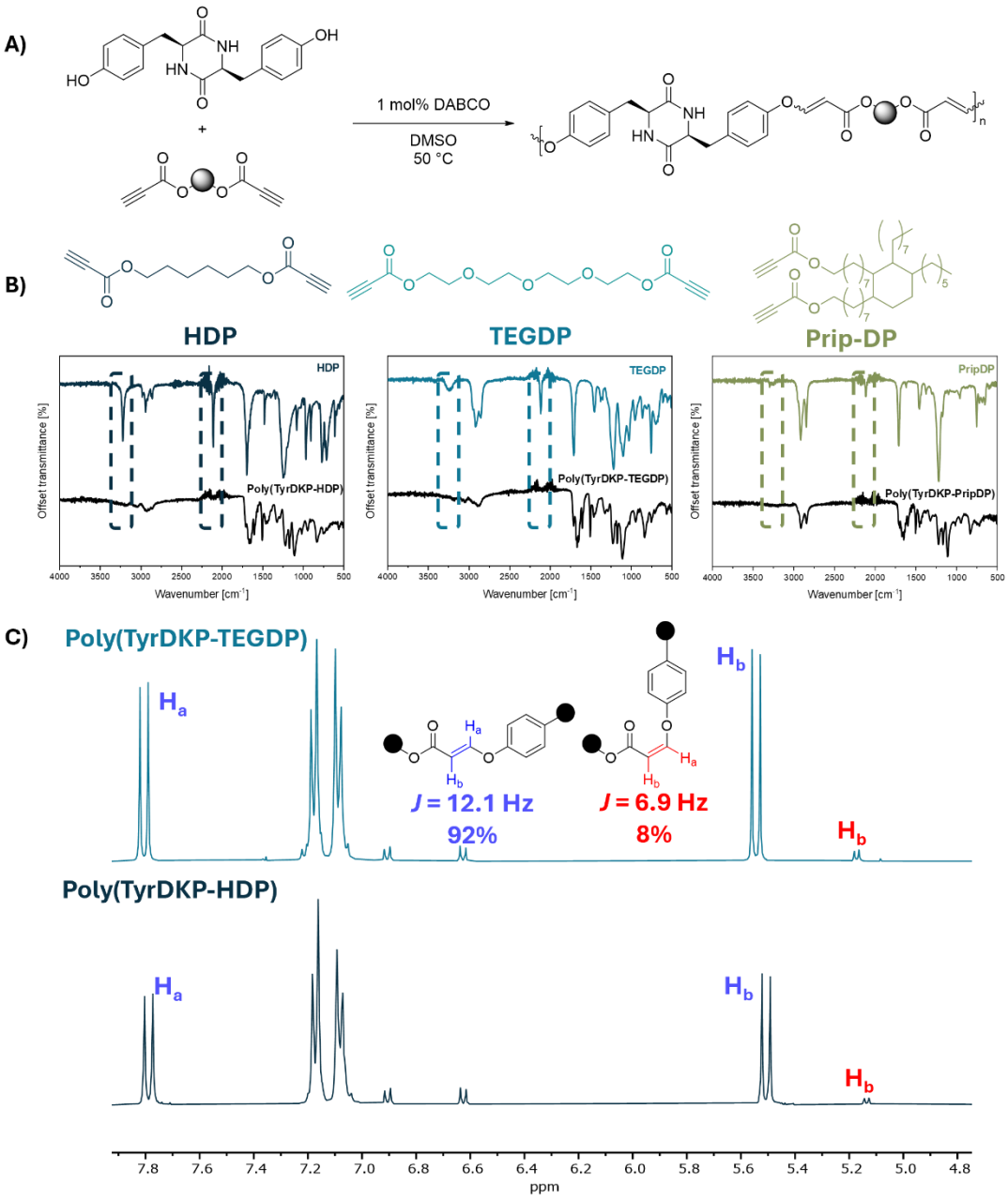


Figure 2. A) Nucleophilic phenol-yne polymerisation between TyrDKP and different dipropiolates comonomer used in this work. B) Structure of the different dipropiolates used in this work with corresponding FT-IR spectra showing the disappearance of the alkyne peaks after polymerisation. Signals highlighted by dashed boxes. C) Stacked ^{1}H NMR spectra (400 MHz, 295 K, d_6-DMSO) of TyrDKP polymers zoomed in between 4.8 and 7.9 ppm to highlight vinyl proton signal used to evaluate *E*/*Z* content in the polymers. The vinyl region of the polymer is displayed in the two possible conformations; the full repeating unit structure is omitted.

Table 1. Summary of yield, M_w, $Đ_M$, M_n, of TyrDKP-based polymers.

	Yield (%)	M_n[a] (kg × mol^{-1})	M_n[b] (kg × mol^{-1})	M_w[b] (kg × mol^{-1})	$Đ_M$[b]
Poly(TyrDKP-HDP)	99	12.707	16	52.8	3.3
Poly(TyrDKP-TEGDP)	75	17.828	20	86	4.3
Poly(TyrDKP-PripDP)	83	n.a.[c]	n.a.[c]	n.a.[c]	n.a.[c]

[a]Determined *via* ^{1}H NMR spectroscopy. [b]Determined *via* GPC (DMF, 5 mM NH_4BF_4, PMMA standard). [c]Values could not be determined as a result of the lack of solubility.

The presence TyrDKP end-groups in both poly(TyrDKP-HDP) and poly(TyrDKP-TEGDP) was suggested by ^{1}H NMR spectroscopy revealing signals relative to the TyrDKP aromatic rings at a slightly lower field when compared to the unreacted monomer ($\delta_{polymers}$ = 6.91 (*d*, *J* = 8.5 Hz), 6.63 (*d*, *J* = 8.5 Hz); δ_{TyrDKP} 6.90 (*d*, *J* = 8.6 Hz), 6.61 (*d*, *J* = 8.5 Hz)) (Figure 3A). Several rounds of precipitation did not cause the disappearance of the signals, confirming that they do not correspond to residual unreacted TyrDKP (Figure S16). Evaluation of molecular weight *via* end group analysis (Equation S1) revealed poly(TyrDKP-TEGDP) to possess a M_n of 17,828 kg × mol^{-1} while M_n of poly(TyrDKP-HDP) was slightly lower at 12,707 kg × mol^{-1}. To gain insight into the dispersity of the polymers, measurement by size exclusion chromatography (SEC) in DMF was performed (Figure 3B). This analysis revealed both polymers to possess a monomodal distribution with relatively narrow dispersity ($Đ_M$) values, especially for step-growth polymerisation (Table 1).[33]

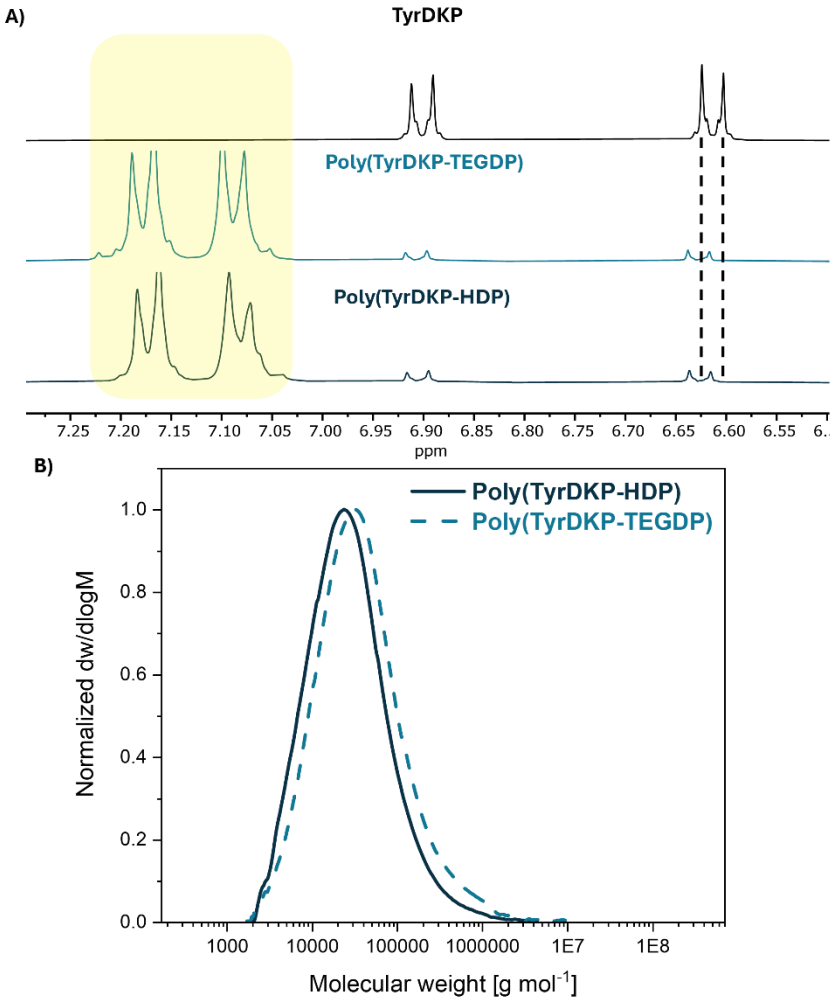


Figure 3. A) Stacked ^{1}H NMR (400 MHz, 300 K, d_6-DMSO) of the aromatic region of TyrDKP and TyrDKP polymers between displaying aromatic resonances of TyrDKP end group in the polymer used to calculate M_n *via* end group analysis. Dashed lines are used to highlight the shift when compared to TyrDKP aromatic peaks (top). Aromatic peaks relative to the repeating TyrDKP repeating units highlighted in yellow. B) GPC (DMF, 5 mM NH_4BF_4, comparison against PMMA standard) traces of TyrDKP polymers.

Thermal properties of Tyr-DKP polymers

The thermal stability of the polymers was evaluated *via* thermogravimetric analysis (TGA). All polymers showed excellent thermal stability with degradation temperature ($T_{d,5\%}$) associated with a 5% mass loss recorded at 356 °C for poly(TyrDKP-HDP) and poly(TyrDKP-TEGDP) and 367 °C for poly(TyrDKP-PripDP). The mass loss profile was also different: at 500 °C poly(TyrDKP-PripDP) displayed a far greater reduction in mass, with just under 10% of the initial mass preserved, while poly(TyrDKP-HDP) and poly(TyrDKP-TEGDP) retained the 37 and 32%, respectively (Figure 4A).

Differential scanning calorimetry (DSC) revealed an endothermic peak indicating melting transition (T_m) at 222 °C for poly(TyrDKP-HD) and 178 °C for poly(TyrDKP-TEG) in the first heating cycle but the following cycles did not display such transition, suggesting that these polymers are not recrystallising under the conditions screened but they are semicrystalline after synthesis (Figure S17-S18). Poly(TyrDKP-PripDP) displayed an endothermic peak at T_m = 182 °C in both the first and second heating cycles meaning that this polymer can crystallise from the melt (Figure 4B) (Figure S19). This different behaviour could be attributed to the larger gap between the glass transition temperature (T_g) and the T_m of poly(TyrDKP-PripDP) when compared to poly(TyrDKP-HDP) or poly(TyrDKP-TEGDP), meaning a greater window for chain mobility. T_g was found to decrease coherently with an increase in flexibility of the co-monomer, as it went from 114 °C to 78 °C when the shorter HDP was switched for the longer and more flexible TEGPD, while poly(TyrDKP-PripDP)

displayed the lowest value at -7.5 °C. Interestingly, the T_g of all the polymers was found to increase after subsequent heating cycles, which could be indicative of temperature-promoted crystallisation, as increased crystallinity increases the T_g (Figure S20-S22).[34]

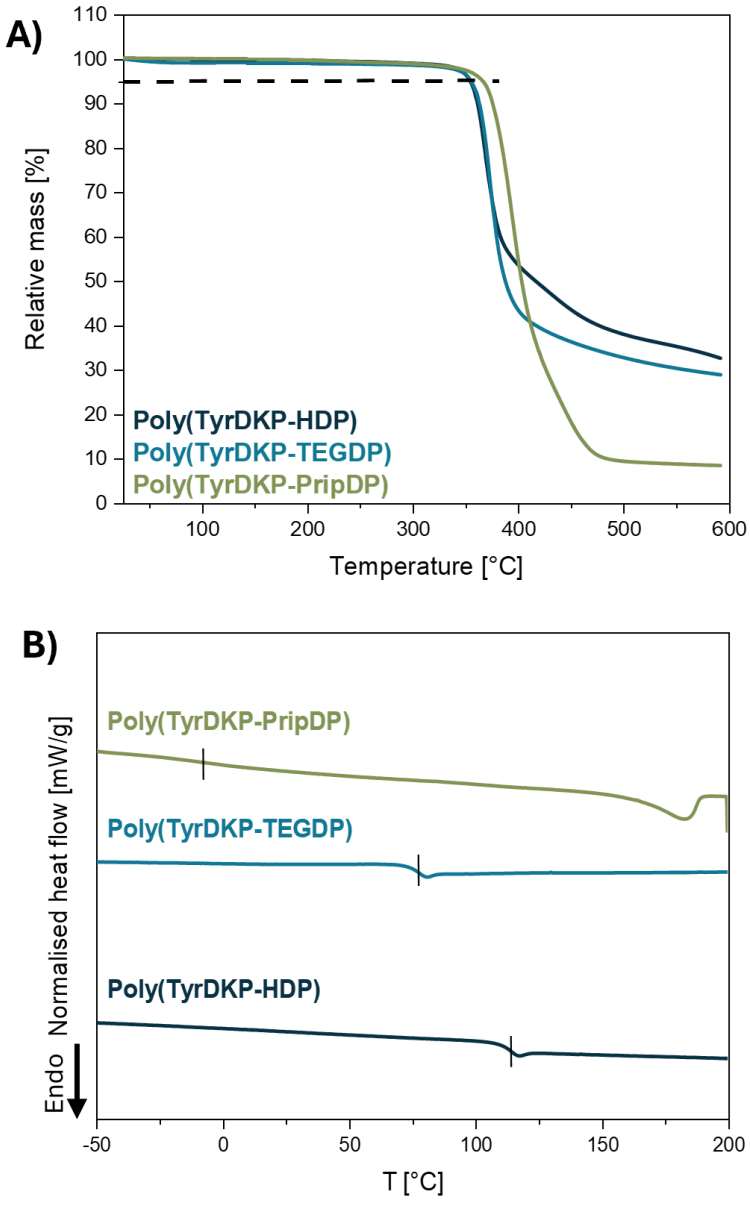


Figure 4. A) TGA thermograms of different TyrDKP-based polymers taken between 25 °C and 600 °C. 10 K/min, N_2 atmosphere. $T_{d,5\%}$ highlighted with a dashed line. B) Second heating cycle of DSC thermograms of different TyrDKP-based polymers between −50 °C and 200 °C. T_g highlighted with a vertical dash

Mechanical properties

Mechanical properties were assessed *via* uniaxial tensile testing of the polymers after heat compression moulding into dogbone specimens. Possibly in light of its higher T_g, poly(TyrDKP-HDP) was too brittle to be removed from the mould without fracturing. While both poly(TyrDKP-TEGDP) and poly(TyrDKP-PripDP) darkened significantly after the moulding process (Figure S23), FT-IR and ^{1}H NMR spectroscopic analyses did not reveal any difference compared to the virgin polymers (Figure 6B-C, S24), hence this change in appearance was attributed to the degradation of residual catalyst. However, slight broadening of the resonances in the ^{1}H NMR spectrum was observed, which could suggest certain degree of crosslinking happening. No significant difference in solubility was noticed. A significant difference (P<0.005) in Young's modulus (E) was observed between the polymers, with poly(TyrDKP-TEGDP) displaying the highest value, which probably reflects the fact that it was tested below T_g. No significant difference was found in terms of ultimate tensile strength, strain at break, or toughness (Table 2).

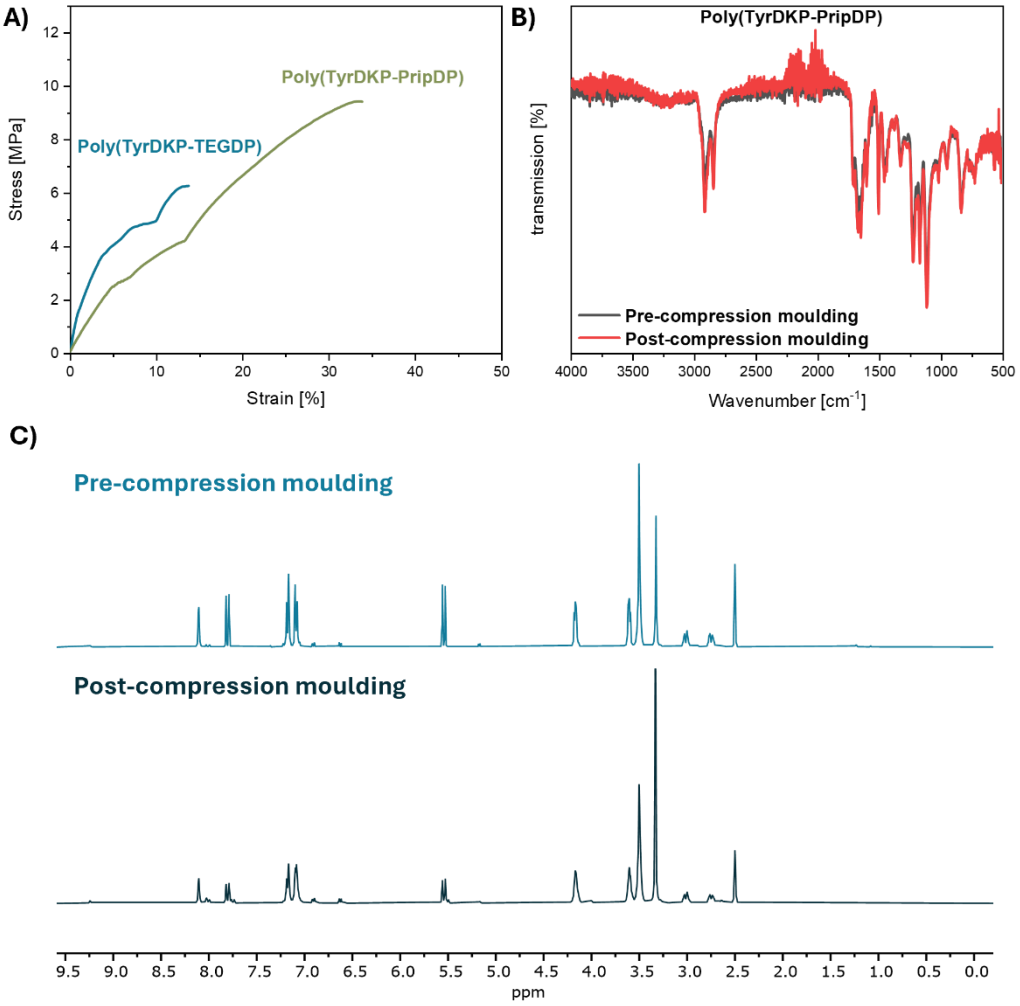


Figure 5. A) Exemplary stress *vs*. strain curves (10 mm/min, 22 °C) of different DKP-based polymers. B) FT-IR spectroscopy of Poly(TyrDKP-PripDP) before (black) and after (red) the moulding process. C) ^{1}H NMR spectra (400 MHz, 300 K, d_6-DMSO) of Poly(TyrDKP-TEGDP) before (top) and after (bottom) the moulding process.

Table 2. Summary of thermomechanical properties of poly(TyrDKP-HDP) poly(TyrDKP-TEGDP) and Poly(TyrDKP-PripDP).

Name	T_g[a] (°C)	T_m[b] (°C)	$T_{d,5\%}$[c] (°C)	E[d] [MPa]	σ[d] [MPa]	ε[d] [%]	U_T[d] [J·m^{-3}]
Poly(TyrDKP-HDP)	114	n.a.	356	n.a.	n.a.	n.a.	n.a.
Poly(TyrDKP-TEGDP)	78	n.a.	356	142±19.1	7±1.3	13.4±6.4	2.6±0.9
Poly(TyrDKP-PripDP)	−7.5	182	367	62.3±9.5	9.1±2.9	39.3±19.4	3.1±2.1

[a]Determined as the inflection point in the trace of the second heating cycle of the DSC. [b]Determined as the minimum of the endothermic peak detected in the trace of the second heating cycle of the DSC. [c]Determined as the temperature associated with a 5% mass loss in the TGA analysis. [d]Values calculated from an average of three samples. E = Young's Modulus, σ = stress at break, ε = strain at break, U_T = toughness.

Conclusion

In conclusion, this study demonstrates that phenol-yne polymersation can be used as a simple and effective method to produce TyrDKP-containing polymers, with a high mass content (>80%) derived from biobased units. When compared to previously reported methods, this approach offers a simpler and less energy-intensive method to synthesise these polymers allowing to reach high M_w polymers without the need for metal catalysis, laborious monomer functionalisation, or harsh conditions such as high temperature or vacuum. The obtained polymers revealed high $T_{d,5\%}$ (>350 °C) and tuneable T_g ranging from -7.5 °C to 117 °C, suggesting that intelligent monomer design can help to obtain TyrDKP-based materials with different thermal properties. Mechanical properties were investigated for the first time showing that it is possible to obtain free-standing materials with tuneable

Young's modulus. Current work is focused on optimising reaction conditions to modulate the *E*/*Z* content of the addition product of the phenol-yne reaction, rational evaluation of the influence of non-covalent interaction such as DKPs derived hydrogen bonding, and investigation into modulation of the physical properties *via cis*/*trans* isomerism of DKPs molecules. Moreover, given the vast chemical space afforded by amino acids, we suggest that other types of nucleophilic-yne polymerisation could be used to generate polymers. For example, cysteine and lysine based DKPs could be used to produce polymers *via* nucleophilic thiol-yne and amino-yne polymerisation, respectively.

References

1. AL Andrady and MA Neal, *Philos. Trans. R. Soc. B*, 2009, **364**, 1977-1984.
2. R Geyer, JR Jambeck and KL Law, *Sci. Adv.*, 2017, **3**, e1700782.
3. M Shen, W Huang, M Chen, B Song, G Zeng and Y Zhang, *J. Clean. Prod.*, 2020, **254**, 120138.
4. Y Zhu, C Romain and CK Williams, *Nature*, 2016, **540**, 354-362.
5. F Vidal, ER van der Marel, RWF Kerr, C McElroy, N Schroeder, C Mitchell, G Rosetto, TTD Chen, RM Bailey, C Hepburn, C Redgwell and CK Williams, *Nature*, 2024, **626**, 45-57.
6. W Khan, S Muthupandian, S Farah, N Kumar and AJ Domb, *Macromol. Biosci.*, 2011, **11**, 1625-1636.
7. K Bauri, M Nandi and P De, *Polym. Chem.*, 2018, **9**, 1257-1287.
8. K Numata, *Polym. J.*, 2015, **47**, 537-545.
9. CJ Stubbs and AP Dove, *Polym. Chem.*, 2020, **11**, 6251-6258.
10. AD Borthwick, *Chem. Rev.*, 2012, **112**, 3641-3716.
11. M Scarel and S Marchesan, *Molecules*, 2021, **26**, 3376.
12. RJ Wojtecki and A Nelson, *J. Polym. Sci., Part A: Polym. Chem.*, 2016, **54**, 457-472.
13. MB Avinash, D Raut, MK Mishra, U Ramamurty and T Govindaraju, *Sci. Rep.*, 2015, **5**, 16070.
14. X Huang, C-Y Shen, J-C Chen and Q Li, *J. Biomater. Sci. Polym. Ed.*, 2009, **20**, 935-955.
15. H Yin, K Takada, A Kumar, T Hirayama and T Kaneko, *RSC Advances*, 2021, **11**, 5938-5946.
16. FN Führer and H Schlaad, *Macromol. Chem. Phys.*, 2014, **215**, 2268-2273.
17. K Terada, EB Berda, KB Wagener, F Sanda and T Masuda, *Macromolecules*, 2008, **41**, 6041-6046.
18. Y Iwakura, S-I Izawa and F Hayano, *J. Polym. Sci., Part A:Polym. Chem.*, 1968, **6**, 1097-1108.
19. V Crescenzi, V Giancotti and F Quadrifoglio, *Macromol. Chem. Phys*, 1968, **120**, 220-224.
20. SH J. Akerlund, J. Pumphrey, D. C. Timm, J. I. Brand, *J. Appl. Polym. Sci.*, 2000, **78**.
21. K Terada, F Sanda and T Masuda, *J. Macromol. Sci. Chem.,A.*, 2007, **44**, 789-794.
22. H Xia, ZY Suo, GJ Qiang and CJ Chang, *J. Appl. Polym. Sci.*, 2008, **110**, 2168-2178.
23. V Crescenzi, A Ciana, V Giancotti, E Russo, L Salvestrini and L Ciceri, *Macromol. Chem. Phys*, 1971, **141**, 199-210.
24. K Sōsa, A Mori, M Sisido and Y Imanishi, *Biomaterials*, 1985, **6**, 312-324.
25. F Rafiemanzelat, A Fathollahi Zonouz and G Emtiazi, *Polym. Degrad. Stab.*, 2012, **97**, 72-80.
26. Y Shi, T Bai, W Bai, Z Wang, M Chen, B Yao, JZ Sun, A Qin, J Ling and BZ Tang, *Chem. Eur. J.*, 2017, **23**, 10725-10731.
27. H Si, K Wang, B Song, A Qin and BZ Tang, *Polym. Chem.*, 2020, **11**, 2568-2575.
28. JC Worch, AC Weems, J Yu, MC Arno, TR Wilks, RTR Huckstepp, RK O'Reilly, ML Becker and AP Dove, *Nat. Commun.*, 2020, **11**, 3250.

29. CA Bell, J Yu, IA Barker, VX Truong, Z Cao, AV Dobrinyin, ML Becker and AP Dove, *Angew. Chem. Int. Ed.*, 2016, **55**, 13076-13080.
30. JC Worch and AP Dove, *Acc. Chem. Res.*, 2022, **55**, 2355–2369.
31. L de Abreu Costa, M Henrique Fernandes Ottoni, MG Dos Santos, AB Meireles, V Gomes de Almeida, W de Fátima Pereira, B Alves de Avelar-Freitas and G Eustáquio Alvim Brito-Melo, *Molecules*, 2017, **22**.
32. G Gasparri Fava, M Ferrari Belicchi, R Marchelli and A Dossena, *Acta Crystallogr. B*, 1981, **37**, 625-629.
33. HR Kricheldorf, *Macromol. Rapid Commun.*, 2008, **29**, 1695-1704.
34. JF Mano, JL Gómez Ribelles, NM Alves and M Salmerón Sanchez, *Polymer*, 2005, **46**, 8258-8265.

Supplementary information

Accessing diketopiperazine-based polymers *via* phenol-yne polymerisation

Daniele Giannantonio[a], Arianna Brandolese[a], Andrew P. Dove[a]

[a]School of Chemistry, University of Birmingham, Edgbaston, Birmingham, B15 2TT (UK)

Experimental methods

Unless otherwise stated, all chemicals and solvents used were purchased from Sigma-Aldrich, VWR Chemicals, Apollo Scientific, or Fisher Scientific and used as received without further purifications. Pripol™2033 was supplied by Cargill. Propiolic acid was distilled before use.

NMR Spectroscopic Analysis. All NMR spectroscopy experiments were performed at 300 K on a Bruker DPX-400 NMR instrument equipped with a BBFO smart probe operating at 400 MHz for H (100.57 MHz for ^{13}C). ^{1}H NMR spectra are referenced to solvent residual proton (δ = 7.26 for $CDCl_3$, δ = 2.5 for d_6-DMSO) and ^{13}C NMR spectra are referenced to the solvent signal (δ = 77.16 for $CDCl_3$, δ = 39.52 for d_6-DMSO). The resonance multiplicities are described as s (singlet), d (doublet), t (triplet), q (quartet) or m (multiplet).

Mass Spectrometry: See Chapter 2 – Supporting information, experimental methods.

Fourier-transform Infrared Spectroscopy (FTIR): See Chapter 2 – Supporting information, experimental methods.

Size Exclusion Chromatography (SEC). SEC measurements were performed on an Agilent 1260 Infinity II Multi-Detector GPC/SEC System fitted with RI and ultraviolet (UV) detectors (λ = 309 nm) and PLGel 3 μm (50 × 7.5 mm) guard column and two PLGel 5 μm (300 × 7.5 mm) mixed-C columns with DMF containing 5 mM NH_4BF_4 as the eluent (flow rate 1 mL/min, 50 °C). A 12-point calibration curve (M_p = 550–2,210,000 g×mol^{-1}) based on poly(methyl methacrylate) standards

(PMMA, Easivial PM, Agilent) was applied for the determination of molecular weights.

Differential Scanning Calorimetry (DSC). The thermal characteristics of the polymers were determined using differential scanning calorimetry (STARe system DSC3, Mettler Toledo) from −80 to 270 °C at a heating rate of 10 °C·min^{-1} for three heating/cooling cycles unless otherwise specified. The glass transition temperature (T_g) was determined from the inflection point in the second heating cycle of DSC. Total enthalpy of melting (ΔH_m) was calculated from integration and normalization of all endothermic peaks present using the STARe software. The melting temperature was determined from the minimum value of the endothermic peak using the STARe software.

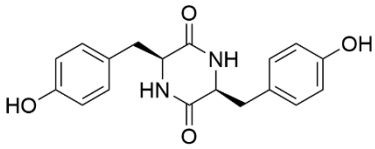
Thermogravimetric Analysis (TGA). See Chapter 2 – Supporting information, experimental methods.

Tensile testing. Samples were prepared into thin polymer films using 3 Specac Atlas™ Manual Hydraulic Press 15T fitted with Specac heated plates. The polymer was added into a dogbone shaped stainless steel mould and placed into pre-heated press at 220 °C. The sample was heated for 10 min (with no pressure) before degassing 5 × (500 kg pressure/release). Next, 3000 kg pressure was applied, and the sample was held at 220 °C for 5 min before cooling to ~ 180 °C (Poly(TyrDKP-TEGDP)) or ~ 45 °C (Poly(TyrDKP-PripDP)) under the same pressure. Uniaxial tensile testing was performed using a Testometric M350-5CT universal mechanical testing instrument fitted with a load cell of 10 kN. Each specimen was clamped into the

tensile holders and subjected to an elongation rate of 10 mm·min^{-1} until failure with an applied pretension of 0.1 N. All tensile tests were repeated 3 times (unless otherwise stated), and an average of the data was taken to find the ultimate tensile stress and strain. Data was analysed using winTest™ Analysis software (v.5.0.34) and OriginPro® software. Young modulus was calculated by taking the slope of the tensile curve at 1% strain. Toughness was calculated as the area under the curve up to break.

Synthetic procedures

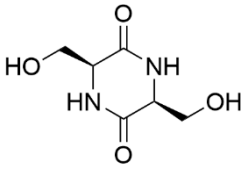
(3S,6S)-3,6-bis(4-hydroxybenzyl)piperazine-2,5-dione (TyrDKP): L-tyrosine



(10 g, 55 mmol) was refluxed in ethylene glycol (100 mL) for 24 h under inert atmosphere (N_2). Precipitation occurred upon cooling, the product was filtered and washed with hot acetic acid and recovered as an off-white solid (5.7 g, 63%). Spectroscopic data are in agreement with previously published results.[1]

^{1}H NMR (400 MHz, DMSO-d_6) δ 9.21 (s, 2H), 7.91 (d, J = 1.8 Hz, 2H), 6.90 (d, J = 8.5 Hz, 4H), 6.61 (d, J = 8.5 Hz, 4H), 3.32 – 3.28 (m, 2H), 2.89 (dd, J = 13.7 Hz, 3.6 Hz, 2H), 2.59 (dd, J = 13.8, 4.8 Hz, 2H) ppm. ^{13}C NMR (101 MHz, DMSO-d_6) δ 167.0, 156.1, 131.1, 125.8, 114.8, 54.82, 36.9 ppm.

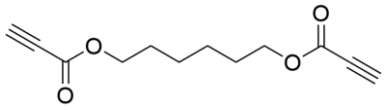
3,6-bis(hydroxymethyl)piperazine-2,5-dione (SerDKP): L-Serine methyl ester



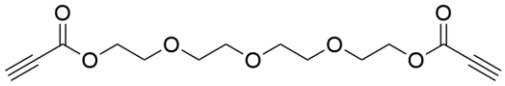
hydrochloride (10 g, 64 mmol) was solubilised in 150 mL of methanol and flushed through a column packed with 50 g of Amberlyst A21 free base, pretreated with 100 mL of $NaHCO_3$ (aq.) sat. solution, 100 mL of deionised water, and 100 mL of methanol. The solvent was removed at reduced pressure to obtain a dense colourless fluid that was left to dimerise in a vacuum oven at room temperature, to obtain a white solid. The solid was then triturated with a 1:1 solution of diethyl ether and methanol, the solid material was filtered and recrystallised from water to recover the pure product (54% yield). Spectroscopic data are in agreement with previously published results.[2]

^{1}H NMR (400 MHz, DMSO-d_6) δ 7.99 (*s*, 2 H), 5.00 (*t*, *J* = 5.4, 2 H), 3.76 (*dt*, *J* = 5.3, 2.8 Hz, 2H), 3.68 (*dt*, *J* = 10.9, 5.5 Hz, 2H), 3.57 (*ddd*, *J* = 10.6, 5.0, 3.2 Hz, 2H). ^{13}C NMR (101 MHz, DMSO-d_6) δ 165.9, 63.4, 57.2.

Hexane-1,6-diyl dipropiolate (HDP): See Chapter 2 Supplementary information. Synthetic procedures – Monomer M2.



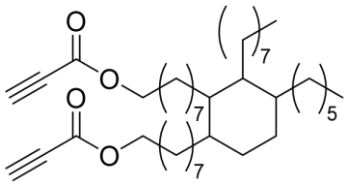
((oxybis(ethane-2,1-diyl))bis(oxy))bis(ethane-2,1-diyl) dipropiolate (TEGDP):



Tetraethylene glycol (5 g, 25.7 mmol), propiolic acid (4.5 g, 64.4 mmol) and *p*-toluenesulfonic acid monohydrate (2.45 g, 12.9 mmol) were stirred in toluene (100 mL) in a 250 mL round bottom flask equipped with a Dean-Stark apparatus. The temperature was raised until reflux occurred and the reaction was left running for 17 h. The reaction mixture was concentrated under reduced pressure and the residue was diluted with ethyl acetate (EtOAc) (50 mL), followed by washing with $NaOH_{aq.}$ 0.1 M (3 × 30 mL), prior to drying over anhydrous $MgSO_4$ that was subsequently filtered off. EtOAc was removed via a rotary evaporator to yield the product as a slightly yellow oil (6.2 g, 81% yield) and used without further purification. Spectroscopic data was in agreement with previously published results.[3]

^{1}H NMR (400 MHz, Chloroform-*d*) δ 4.42 – 4.24 (m, 4H), 3.81 – 3.72 (m, 4H), 3.66 (s, 8H), 2.90 (s, 2H).^{13}C NMR (101 MHz, Chloroform-*d*) δ 152.8, 75.2, 74.7, 70.9, 70.8, 68.7, 65.4. HRMS (TOF-MS-EI^{+}) (m/z): $[M]^{-}$ calculated for $C_{14}H_{18}O_{4,}$ 298.1058: found, 298.1055.

Pripol™2033 dipropiolate (PripDP): Pripol™2033 (1.1 g, 2 mmol), propiolic acid



(0.56 g, 8 mmol) and *p*-toluenesulfonic acid monohydrate (0.19 g, 1 mmol) were stirred in toluene (80 mL) in a 250 mL RBF equipped with a Dean-Stark apparatus. The temperature was raised until reflux occurred and the reaction was left running for 17 h. The solvent was removed *via* a rotary evaporator to obtain an orange fluid. The product was purified *via* column chromatography (Mobile phase = 10% EtOAc in hexane) and obtained as a colourless liquid (1.3 g, 99% yield).

^{1}H NMR (400 MHz, Chloroform-*d*) δ 4.19 (t, J = 6.7 Hz, 4H), 2.86 (s, 2H), 1.68 (t, J = 7.2 Hz, 5H), 1.37 – 1.19 (m, 52H), 0.98 – 0.78 (m, 9H). ^{13}C NMR (101 MHz, Chloroform-*d*) δ 152.9, 74.9, 74.5, 66.6, 37.5, 37.2, 33.8, 33.4, 32.9, 32.1, 30.3, 30.2, 29.9, 29.8, 29.7, 29.6, 29.5, 29.3, 28.5, 27.2, 26.8, 25.9, 23.3, 22.8, 19.9, 14.7, 14.3.

General procedure for phenol-yne polymerisation of TyrDKP

TyrDKP (1 equiv.) was weighed in a 20 mL scintillation vial. The desired dipropiolate ester (1 equiv.) was weighed out in a second vial and then quantitatively transferred to the vial containing TyrDKP using DMSO, to reach a final monomer concentration of 0.3 M. The mixture was left stirring at 50 °C until complete solubilisation of TyrDKP. 1 mol% of DABCO was added from a freshly prepared solution in DMSO. The reaction was left running for three hours before precipitation in a 1:1 v/v mixture of hexane:acetone (total volume = reaction volume × 10). The precipitated polymer was left decanting overnight before filtration. Residual solvent was removed by leaving the polymer in a vacuum oven at 100 °C.

Poly(TyrDKP-HD): Polymer was recovered as a slightly yellow hard solid (0.503 g, 99%). $M_{n,\,SEC}$ = 16 kg × mol^{-1} ($Đ_M$ = 3.3), $M_{n,\,NMR}$ = 12.707 kg × mol^{-1}.

^{1}H NMR (400 MHz, DMSO-d_6) %trans = 92% δ 8.11 (s, 2H), 7.79 (d, *J* = 12.0 Hz, *trans* 2H), 7.17 (d, *J* = 8.6 Hz, 4H), 7.08 (d, *J* = 8.7 Hz, 4H), 6.91 (d, *J* = 8.5 Hz, TyrDKP end group), 6.63 (d, *J* = 8.5 Hz, TyrDKP end group), 5.51 (d, *J* = 12.1 Hz, *trans* 2H), 5.14 (d, *J* = 6.9 Hz, *cis*), 4.05 (t, *J* = 6.6 Hz, 4H), 3.47 (t, *J* = 4.6 Hz, 4H), 3.01 (dd, *J* = 13.7, 3.9 Hz, 2H), 2.75 (dd, *J* = 13.7, 4.9 Hz, 2H), 1.58 (s, 4H), 1.32 (d, *J* = 6.3 Hz, 4H). ^{13}C NMR (101 MHz, DMSO-d_6) δ 167.3, 166.6, 159.5, 154.6, 133.3, 132.2, 117.9, 101.9, 64.0, 55.1, 37.5, 28.6, 25.5.

Poly(TyrDKP-TEG): Polymer was recovered as a slightly yellow hard solid (0.695 g, 75%). $M_{n,\,SEC}$ = 20 kg × mol^{-1} ($Đ_M$ = 4.3), $M_{n,\,NMR}$ = 17.828 kg × mol^{-1}.

^{1}H NMR (400 MHz, DMSO-d_6) %trans = 92 δ 8.11 (s, 2H), 7.81 (d, *J* = 12.1 Hz, *trans* 2H), 7.19 (d, *J* = 8.7 Hz, 4H), 7.10 (d, *J* = 8.7 Hz, 4H), 6.91 (d, *J* = 8.5 Hz, TyrDKP end group), 6.63 (d, *J* = 8.5 Hz, TyrDKP end group), 5.55 (d, *J* = 12.1 Hz, *trans* 2H), 5.18 (d, *J* = 6.9 Hz, *cis*), 4.21 – 4.14 (m, 4H), 3.67 – 3.58 (m, 4H), 3.50 (d, *J* = 6.5 Hz, 8H), 3.05 – 2.99 (m, 2H), 2.76 (dd, *J* = 13.4, 4.7 Hz, 2H). ^{13}C NMR (101 MHz, DMSO-d_6) δ 167.3, 166.6, 159.8, 154.6, 133.3, 132.2, 117.9, 101.8, 70.2, 68.8, 63.5, 55.1, 37.45.

Poly(TyrDKP-PripDP): Polymer was recovered as a white powder (0.250 mg, 83%).

Equation S1.

$$x_n = \frac{\text{Integral of the repeating unit}}{\text{n° proton repeating unit}} \times \frac{\text{n° proton of the end group}}{\text{Integral of the end group}}$$

$$M_n = x_n \times M_w^0$$

M_w^0 = molecular weight of the repeating unit

NMR spectroscopy of monomers and polymers

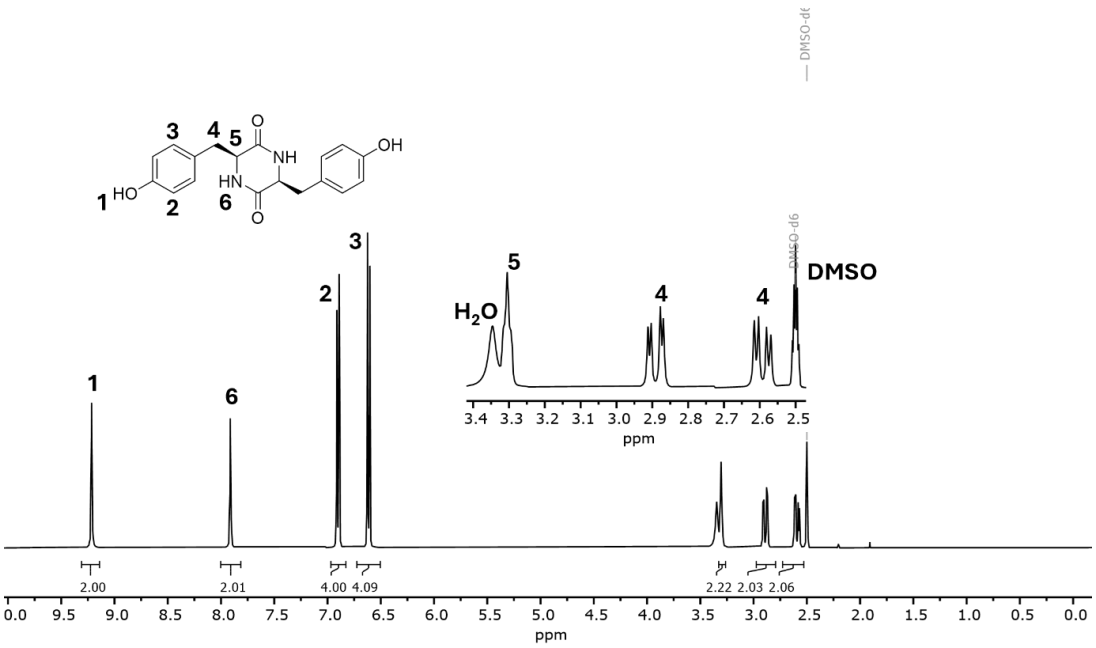


Figure S1. ^{1}H NMR spectrum (400 MHz, 300 K, d_6-DMSO) of TyrDKP.

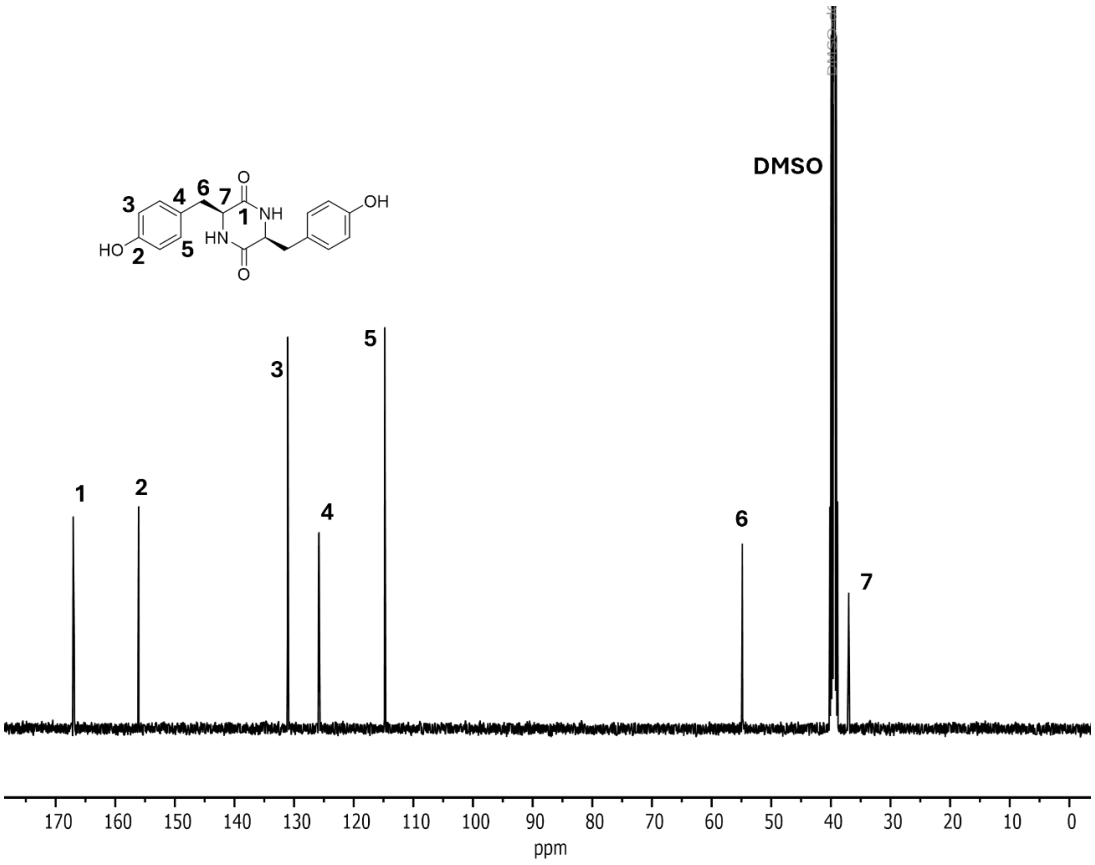


Figure S2. ^{13}C NMR spectrum (100.57 MHz, 300 K, d_6-DMSO,) of TyrDKP.

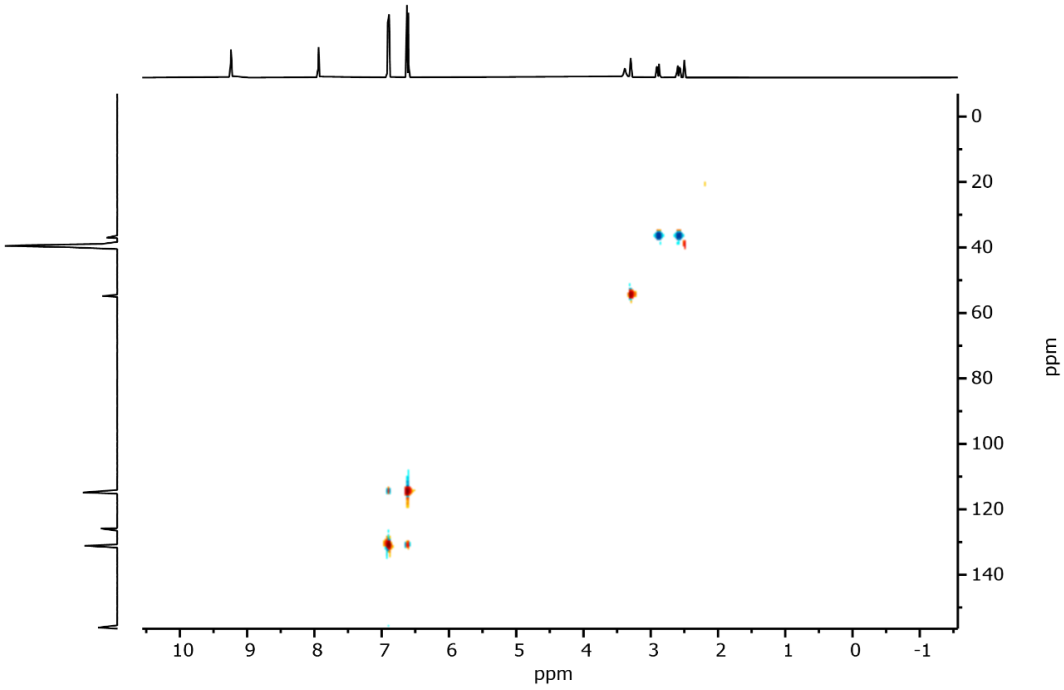


Figure S3. HSQC NMR spectrum (300 K, d_6-DMSO) of TyrDKP.

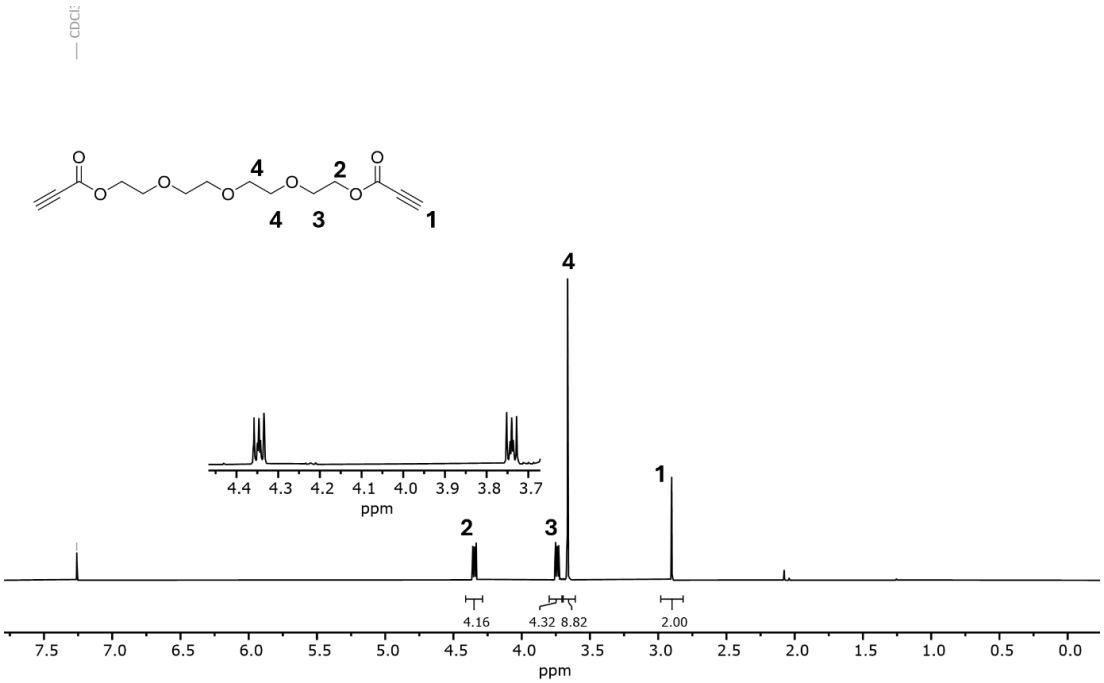


Figure S4. ^{1}H NMR spectrum (400 MHz, 300 K, $CDCl_3$) of tetraethylene glycol dipropiolate (TEGDP).

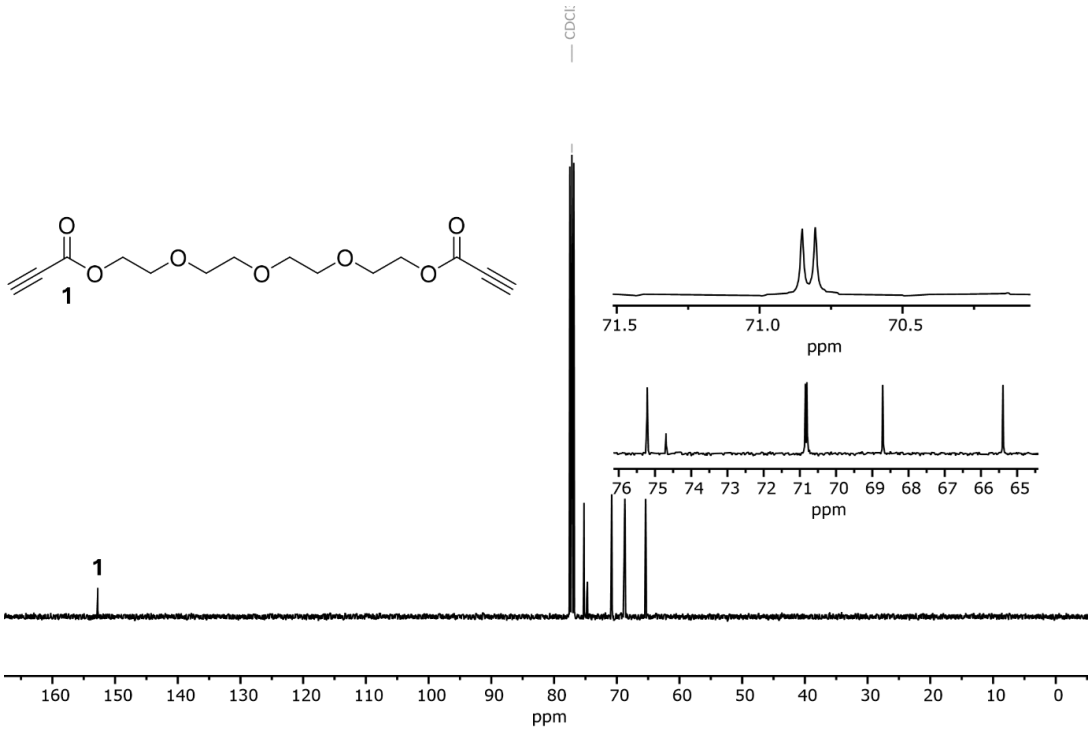


Figure S5. ^{13}C NMR spectrum (100.57 MHz, 300 K, $CDCl_3$) of tetraethyleneglycol dipropiolate (TEGDP).

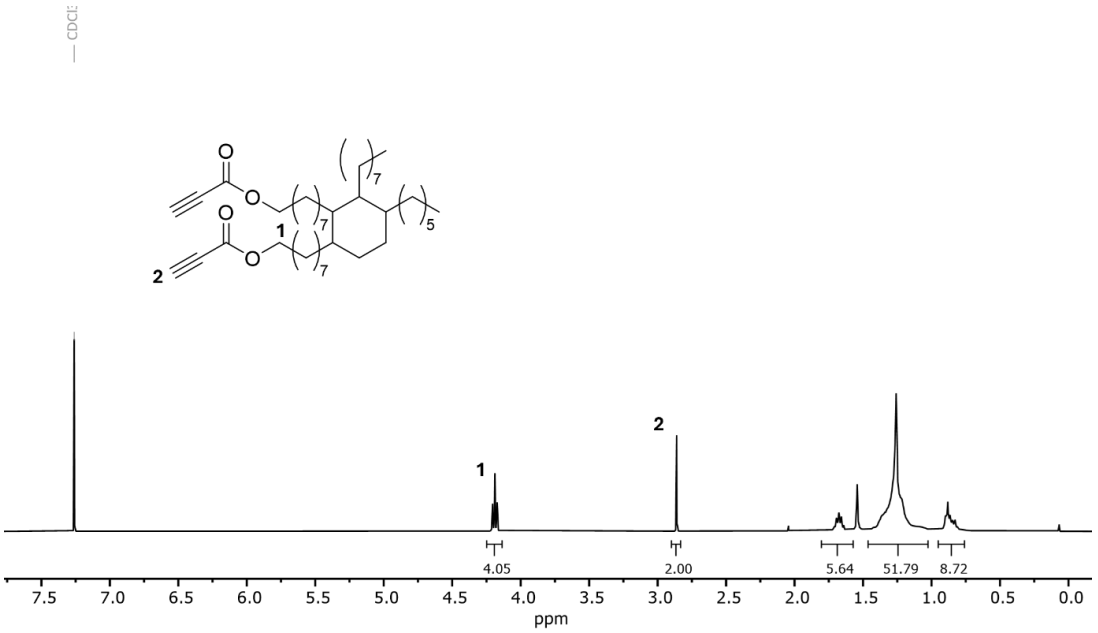


Figure S6. ^{1}H NMR spectrum (400 MHz, 300 K, $CDCl_3$) of Pripol™2033 dipropiolate (PripDP).

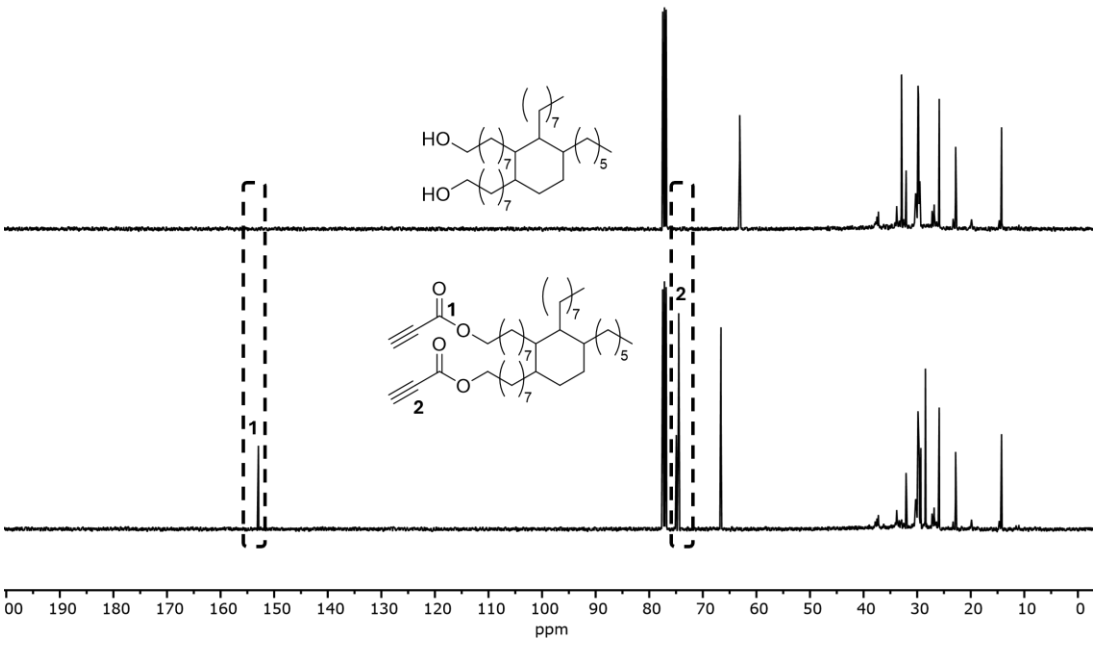


Figure S7. Stacked ^{13}C NMR spectra (100.57 MHz, 300 K, $CDCl_3$) of Pripol™2033 dipropiolate (PripDP) (bottom) compared with ^{13}C NMR of unfunctionalized Pripol™2033. Diagnostic peaks are highlighted with dashed boxes.

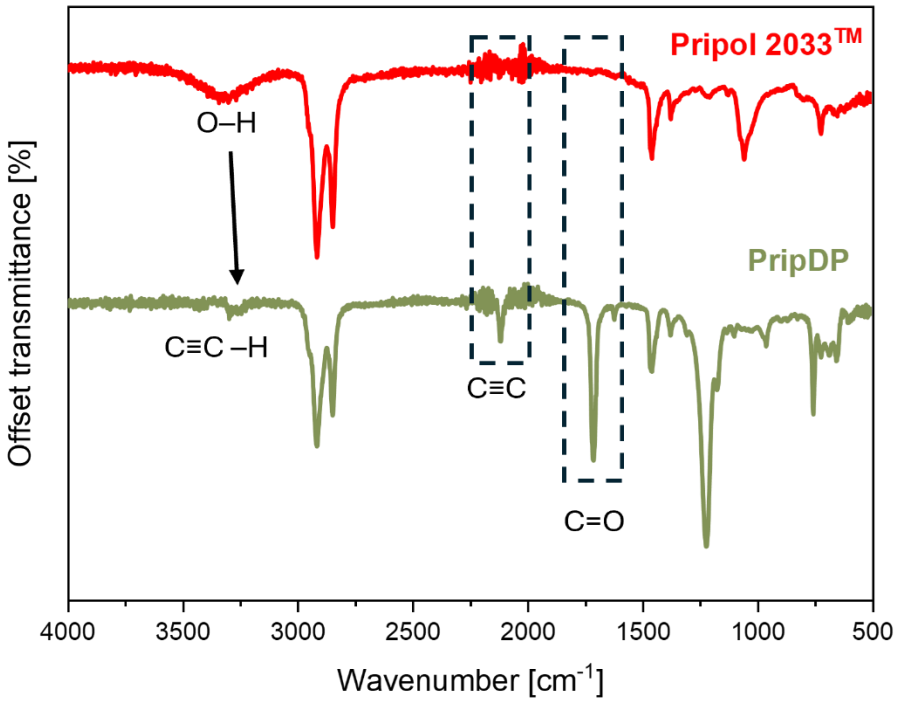


Figure S8. FTIR spectra of unfunctionalised Pripol 2033™ (top, red) and functionalised PripDP (bottom, green). Appearance of carbonyl (~1700 cm^{-1}) and alkyne (~2100 cm^{-1}, ~3300 cm^{-1}) stretching paired with the disappearance of broad -OH stretching further proof successful functionalisation.

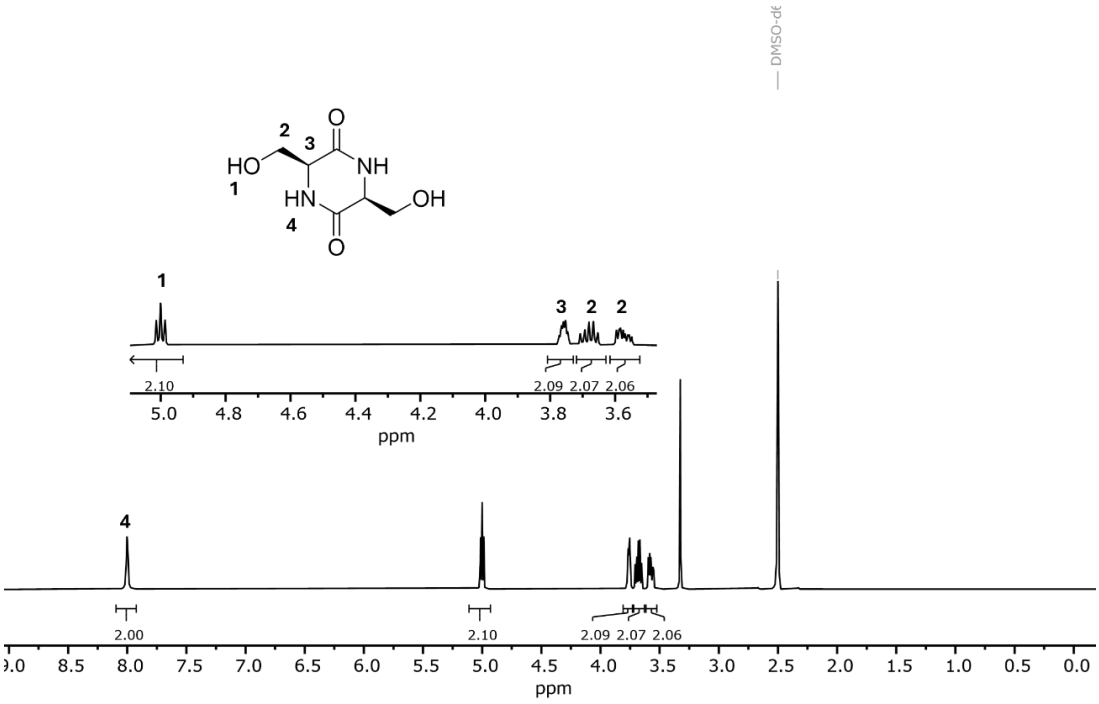


Figure S9. ^{1}H NMR spectrum (400 MHz, 300 K, d_6-DMSO) of SerDKP.

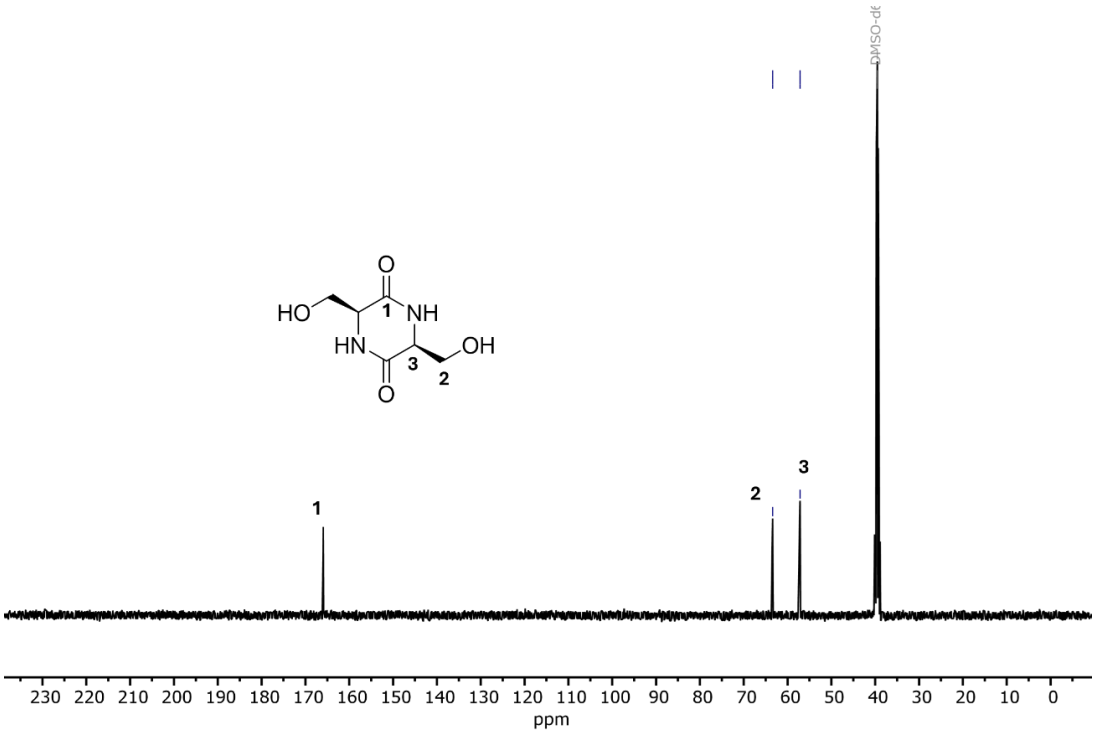


Figure S10. ^{13}C NMR spectrum (100.57 MHz, 300 K, d_6-DMSO,) of SerDKP.

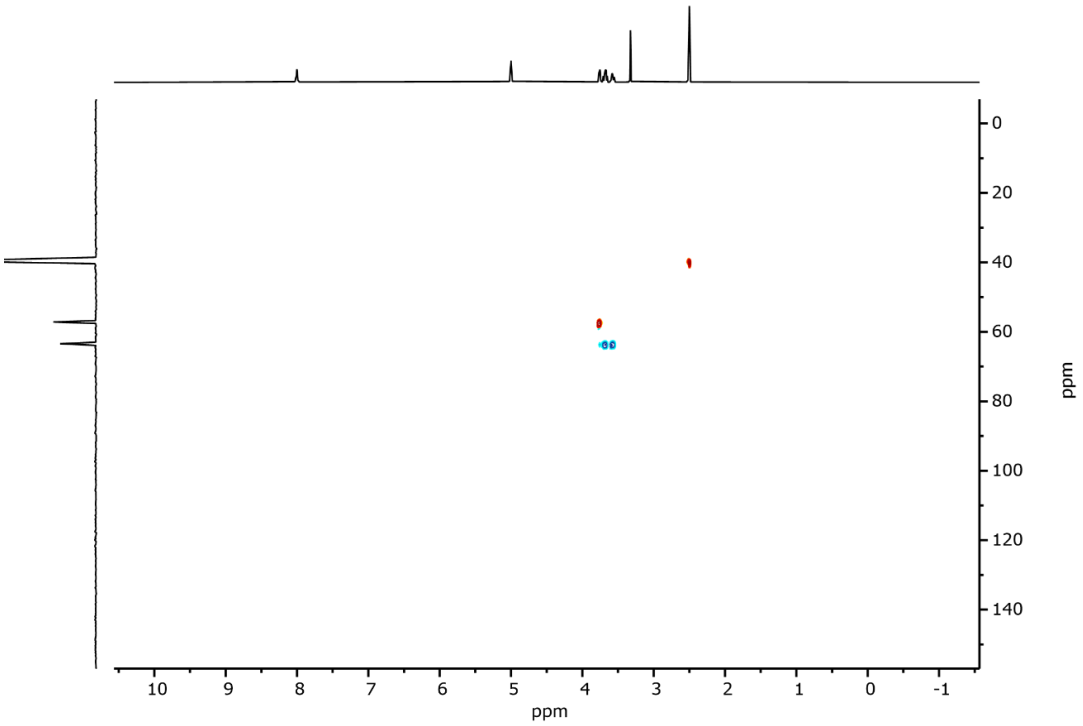


Figure S11. HSQC NMR spectrum (300 K, d_6-DMSO) of SerDKP.

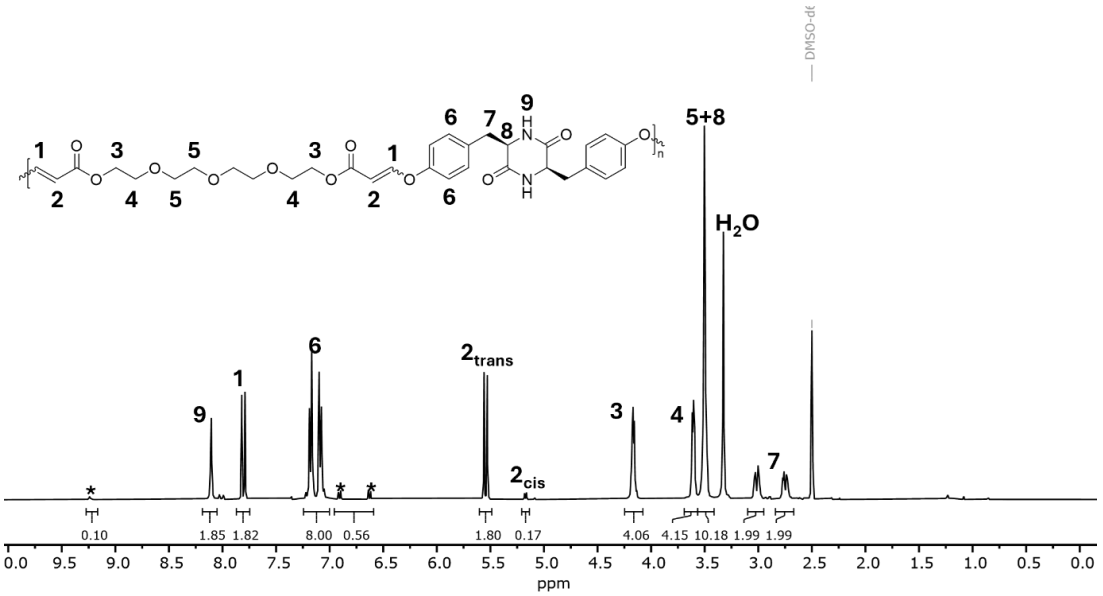


Figure S12. ^{1}H NMR spectrum (400 MHz, 300 K, d_6-DMSO) of poly(TyrDKP-TEGDP). TyrDKP end group signals marked (*) with integration values used for end group analysis reported.

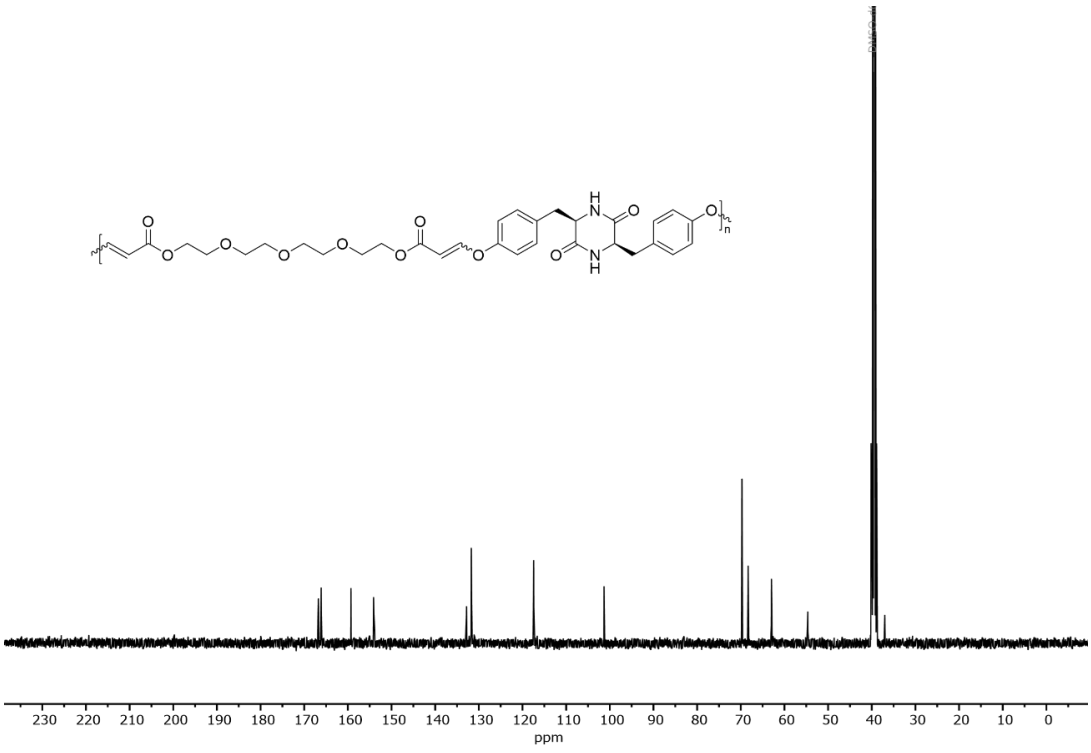


Figure S13. ^{13}C NMR spectrum (100.57 MHz, 300 K d_6-DMSO) of poly(TyrDKP-TEGDP).

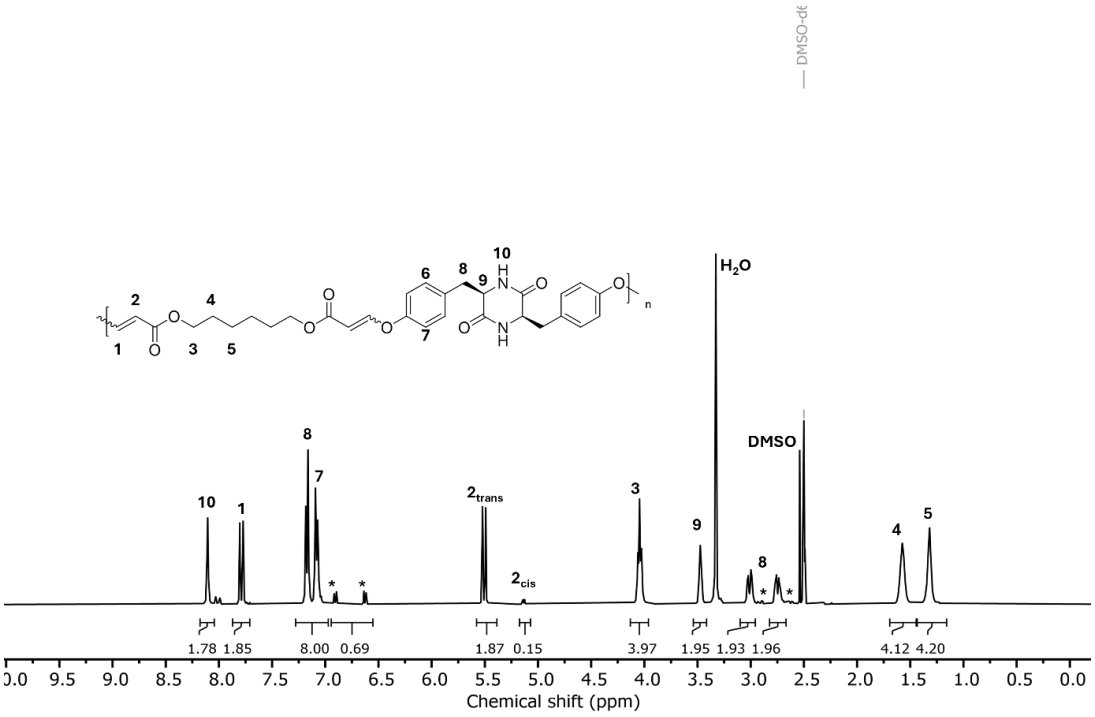


Figure S14. [1]H NMR spectrum (400 MHz, 300 K, d_6-DMSO) of poly(TyrDKP-HDP). TyrDKP end group signals marked (*) with integration values used for end group analysis reported.

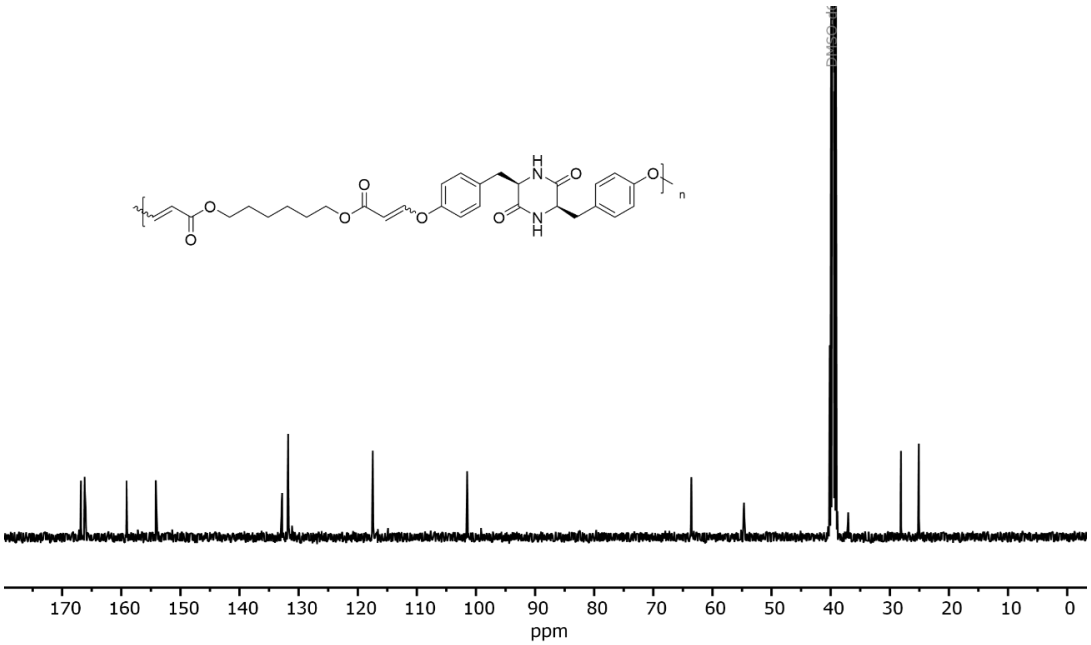


Figure S15. [13]C NMR spectrum (100.57 MHz, 300 K d_6-DMSO) of poly(TyrDKP-HDP).

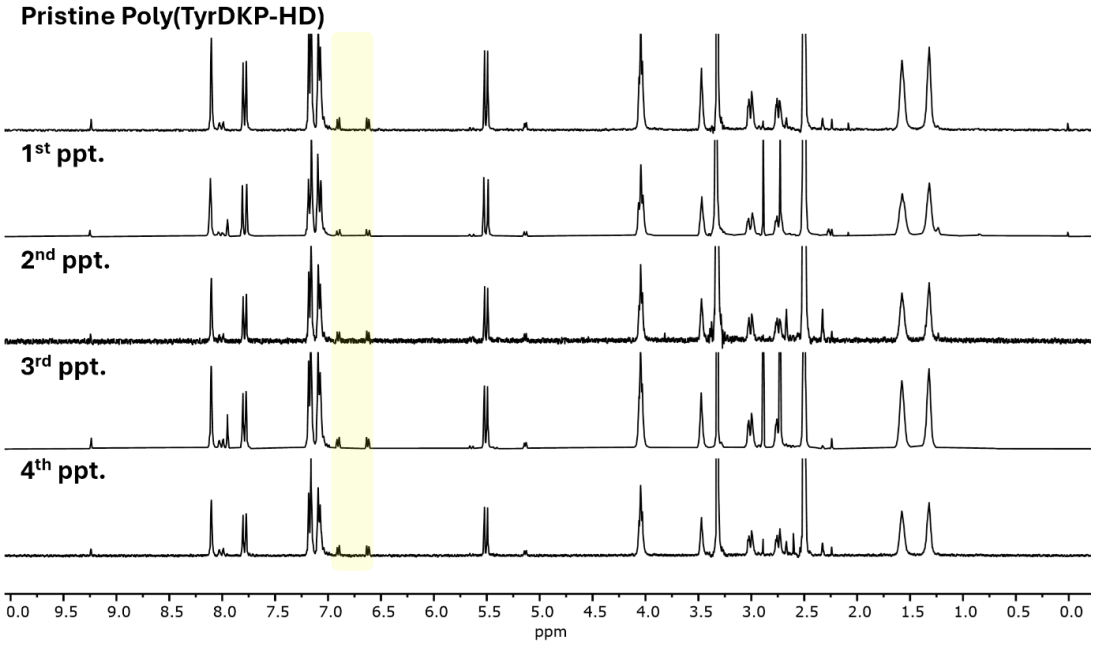


Figure S16. Stacked ^{1}H NMR spectra (400 MHz, 300 K, d_6-DMSO) of poly(TyrDKP-HD) after 4th rounds of reprecipitation. Presence of doublets between 6.5 ppm and 7.0 ppm belonging to end-group TyrDKP are highlighted.

Thermomechanical characterisation

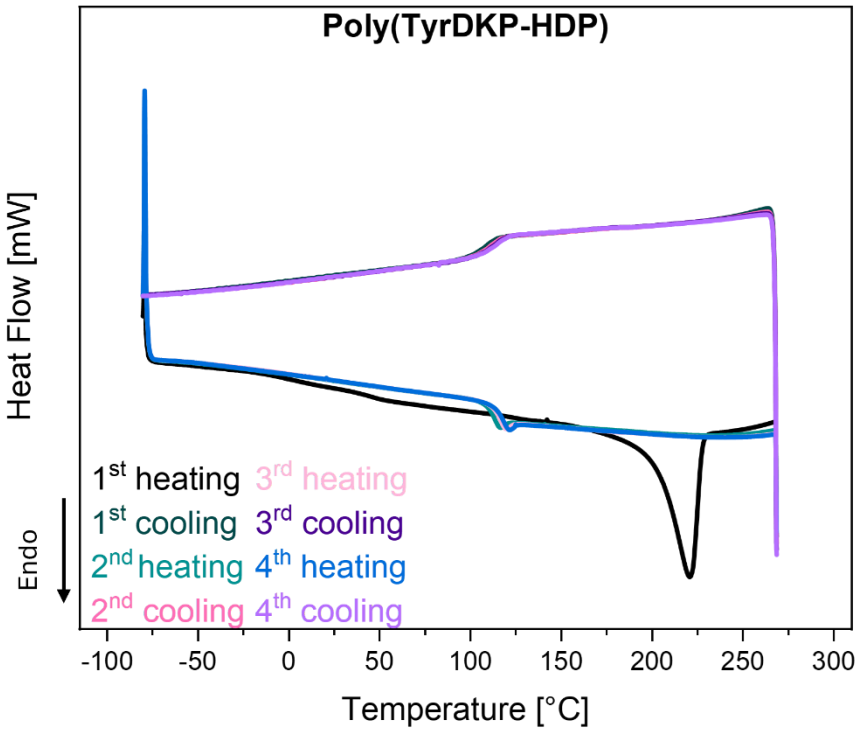


Figure S17. DSC (-80 °C – 270 °C, N_2 atmosphere) thermogram of Poly(TyrDKP-HDP). An increase in T_g after each heating cycle can be appreciated by the increased onset of the slope change associated with the increased heat capacity.

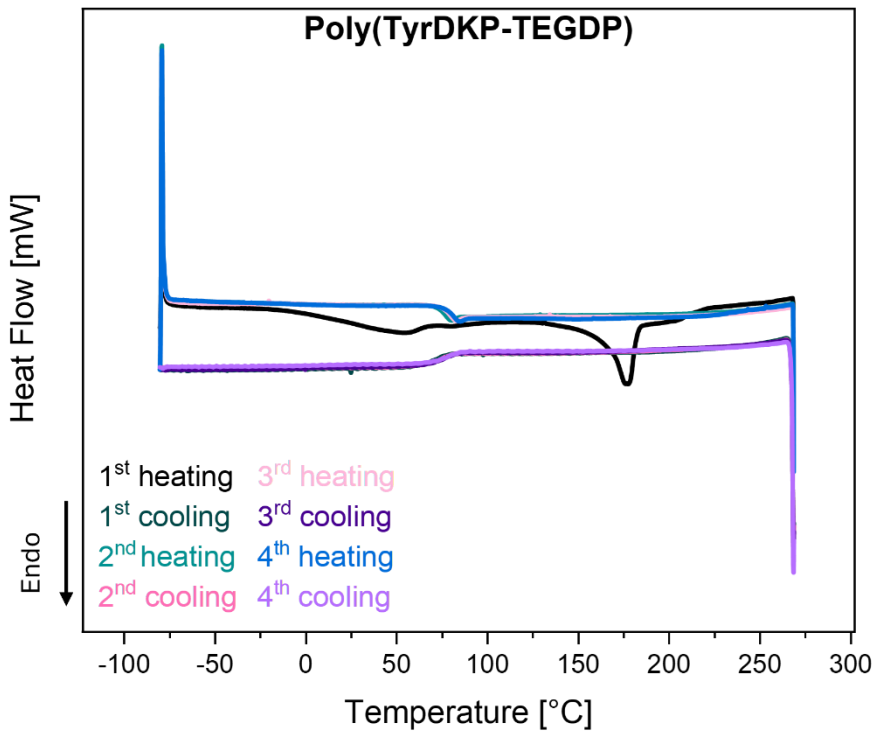


Figure S18. DSC (-80 °C – 270 °C, N_2 atmosphere) thermogram of Poly(TyrDKP-TEGDP). An increase in T_g after each heating cycle can be appreciated by the increased onset of the slope change associated with the increased heat capacity.

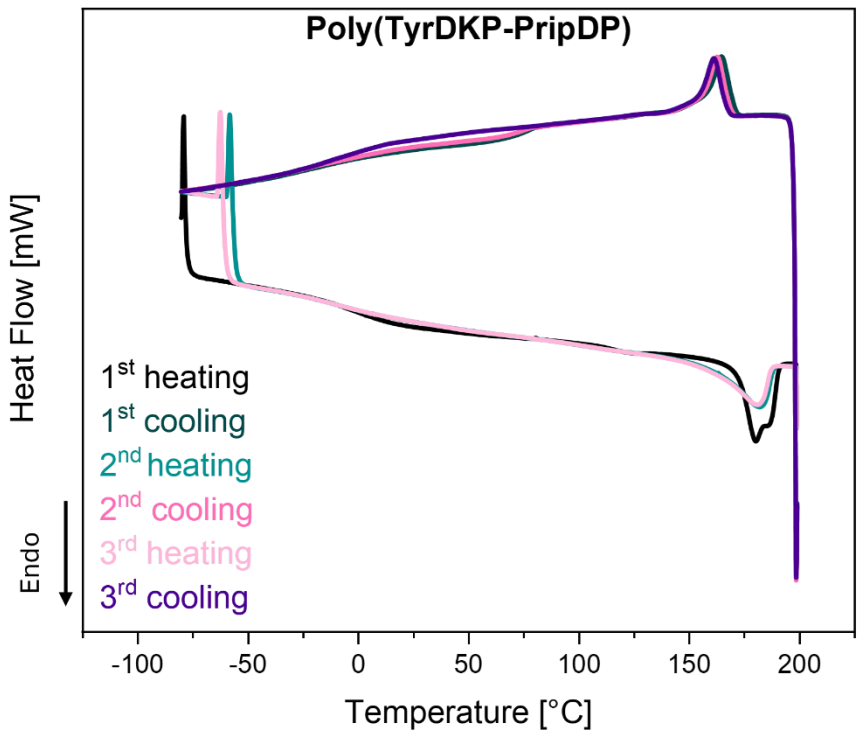


Figure S19. DSC (-80 °C – 200 °C, N_2 atmosphere) thermogram of Poly(TyrDKP-PripDP). An increase in T_g after each heating cycle can be appreciated by the increased onset of the slope change associated with the increased heat capacity.

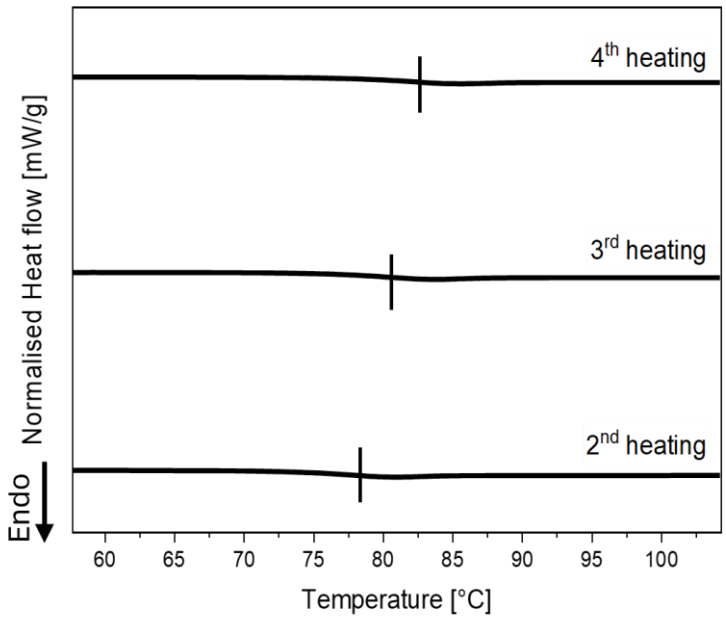


Figure S20. DSC thermograms of subsequent heating cycles of poly(TyrDKP-TEGDP). T_g marked with a vertical dash taken as the inflection point determined by the STARe software.

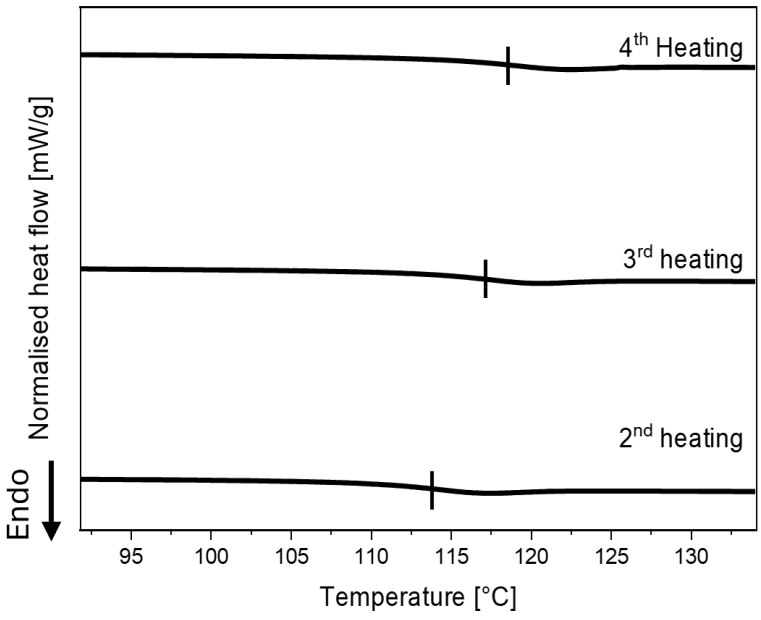


Figure S21. DSC thermograms of subsequent heating cycles of poly(TyrDKP-HDP). T_g marked with a vertical dash taken as the inflection point determined by the STARe software.

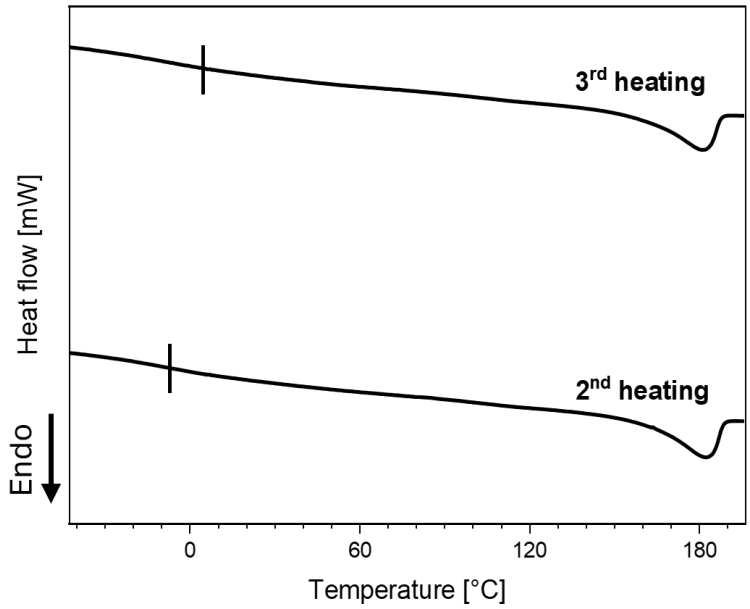


Figure S22. DSC thermograms of subsequent heating cycles of poly(TyrDKP-PripDP). T_g marked with a vertical dash taken as the inflection point determined by the STARe software.

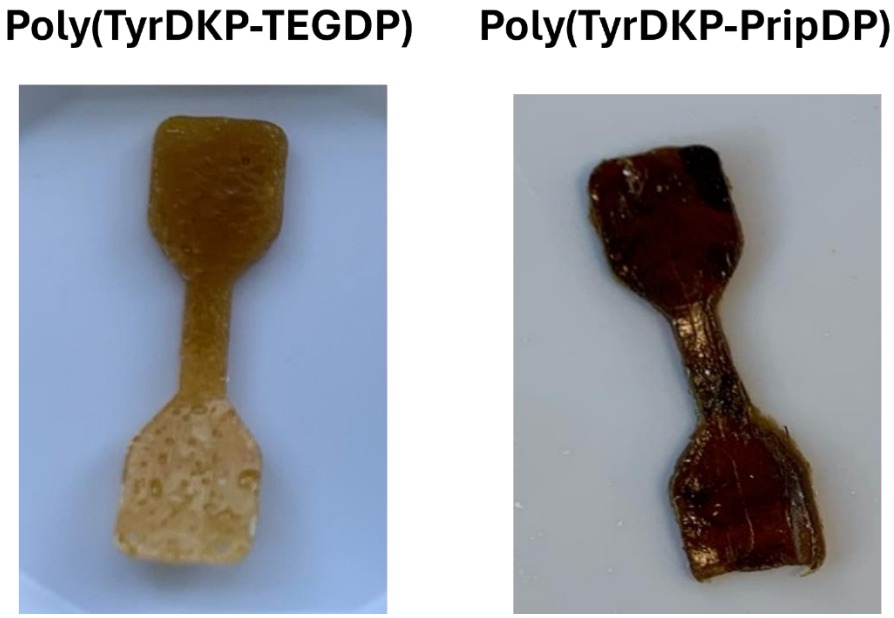


Figure S23. Exemplary dogbones of DKP-based polymers.

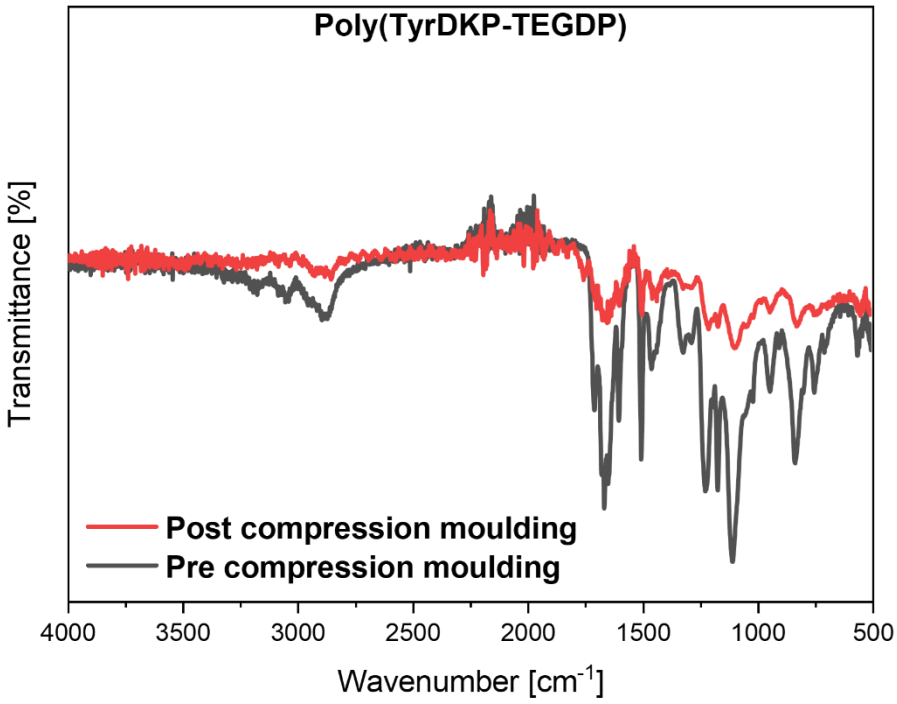


Figure S24. FTIR spectra of poly(TyrDKP-TEGDP) before (grey trace) and after (red trace) compression moulding.

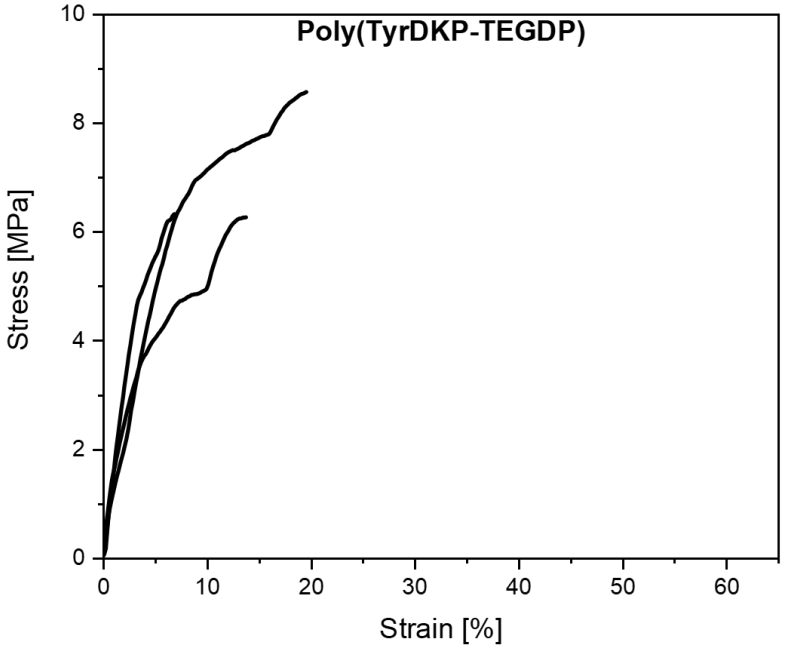


Figure S25. *Stress* vs. strain curves of poly(TyrDKP-TEGDP) samples tested at 10 mm/min, 22 °C.

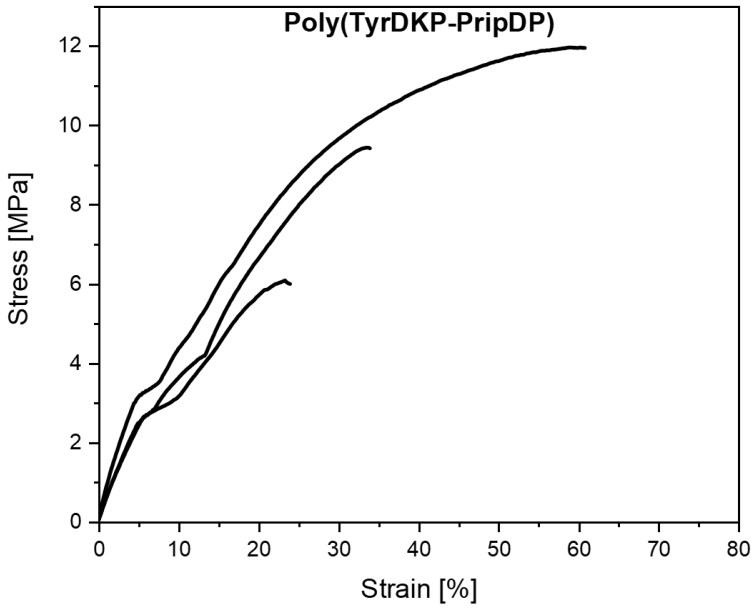


Figure S26. *Stress* vs. strain curves of poly(TyrDKP-TEGDP) samples tested at 10 mm/min, 22 °C.

References

1. J Liu, L Harken, Y Yang, X Xie and SM Li, *Angew. Chem. Int. Ed.*, 2022, **61**.
2. JLSaFM Menger, *J. Am. Chem. Soc.*, 2008, **130**.
3. IE Gorman, RL Willer, LK Kemp and RF Storey, *Polymer*, 2012, **53**, 2548-2558.

Chapter 5 – Enantiopure and racemic BINOL-based polymers by hydroxyl-yne polymerisation

Manuscript and overview

Title: Enantiopure and racemic BINOL-based polymers by hydroxyl-yne polymerisation

Authors: Daniele Giannantonio[a], Alexis Perrot[a,b], Arianna Brandolese[a], Andrew P. Dove[a]

Affiliations: [a]School of Chemistry, University of Birmingham, Edgbaston, Birmingham, B15 2TT (UK)

[b]LCMT, ENSICAEN, 6 bd Maréchal Juin, 14050 Caen, France.

Manuscript prepared

Co-authors contribution: Alexis G. Perrot provided synthetic, technical, and analytical guidance along with editing of the manuscript. Arianna Brandolese provided editing of the manuscript and guidance. Prof. Andrew P. Dove supervised in addition to providing guidance and funding acquisition.

Overview:

As the modulation of the properties of polymeric materials through stereochemical methods has been widely established in the context of point chirality and *cis*/*trans* isomerism, this chapter investigated whether atropisomers could be used to obtain polymers displaying different properties depending on the chirality of the monomer. The modular phenol-yne polymerisation reaction was used to reach such aim, as it allows complete control over the monomer insertion under mild conditions.

Enantiopure and racemic BINOL-based polymers by hydroxyl-yne polymerisation

Daniele Giannantonio[a], Alexis Perrot[a,b], Arianna Brandolese[a], Andrew P. Dove[a]

[a]School of Chemistry, University of Birmingham, Edgbaston, Birmingham, B15 2TT (UK)

[b]LCMT, ENSICAEN, 6 bd Maréchal Juin, 14050 Caen, France.

Abstract: A powerful method to control thermomechanical properties of polymers is through main-chain stereochemistry, i.e. controlling the precise spatial arrangement of the monomer's configuration in the backbone. While point chirality has been widely investigated, the use of different atropisomers to tune the bulk properties of polymeric materials has received significantly less attention. To investigate this phenomenon, the phenol-yne polymerisation of enantiopure and racemic 1,1'-bi-2-naphthol (BINOL) with activated dialkyne was explored to produce amorphous polyesters with high thermal resistance and glass transition temperature, which were not dependent on the configuration of the monomers.

Introduction

The specific configuration (*i.e.* chirality) of monomers has been exploited by chemists to modulate the thermomechanical properties of polymeric materials. The enantiopure poly-L-lactic acid (PLLA) and poly-D-lactic acid (PDLA) display considerably different properties when compared to their racemic counterpart, with the first two being highly crystalline and the latter amorphous.[1] Moreover, the formation of equimolar stereocomplexes of PLLA and PDLA was also shown to produce materials with a melting point roughly 50 °C higher.[2] These differences in tacticity, *i.e.* the spatial arrangement of chiral centres in macromolecules, result in variation of thermomechanical properties in other classes of polymers too. For example, isotatctic polypropylene (PP) is a semicrystalline polymer while atactic PP is amorphous.[3-5] Nonetheless, tacticity is not exclusively responsible for the ability of a polymer to form crystalline domains. Coates and co-workers reported a series of *cis*-poly(3-hydroxy-2-methylbutyrate)s (*cis*-PHMBs) displaying tacticity-independent crystallinity,[6] suggesting that further understanding regarding the influence of backbone chirality on polymer properties is needed.

Generally, the differences in thermomechanical properties observed by varying the stereochemistry of the monomeric units are thought to arise from the different conformations assumed by the polymer chains, leading to variation in the way chains can pack together to create ordered crystalline domains.[7] Harnessing control over the crystalline phase of a polymeric material is crucial in controlling its

thermomechanical properties, where a higher degree of crystallinity is generally associated with stiffer and harder materials.[8]

In addition to point chirality, another form of stereoisomerism is represented by axial chirality. This arises when two chemical groups display a non-planar arrangement over an axis of chirality, thus not being superimposable on their mirror image.[9] In many cases, this form of chirality is found in atropisomers, which are stereoisomers because of hindered rotation about a single bond, due to steric hindrance.[10] Introduction of these motifs into polymers main-chain has been generally exploited to produce conjugated helical polymers of different handedness, mostly in the context of optically active materials.[11] Classical molecules used are phenylacetylenes,[12] biphenyls,[13] and binaphthyls,[14, 15] in light of their accessibility. However, in contrast with point chirality, less attention has been devoted to understanding how this source of chirality can be used to modulate the bulk properties of polymeric materials.[16] An interesting study by Cao *et al*.[17] describes the access to axially chiral polyesters through the ring-opening polymerisation (ROP) of ring-strained biaryl-fused cyclic esters (Me-DBO) to produce chemically recyclable polyesters (P(Me-DBO)s). Interestingly, the authors found that these amorphous polymers could form semicrystalline stereocomplexes. However, no difference between the enantiopure polymers was observed but the authors did not investigate whether incorporating both monomers (*R* and *S*) would lead to different materials.

While ROP processes effectively control polymers' molecular weight and dispersity, they often lack modularity and requires strict monomer design that hinders access to diverse polymer structures in a simple manner, which is crucial when drawing precise structure-properties relationships. To overcome these limitations, the nucleophilic phenol-yne "click" polymerisation was selected considering its mild reaction conditions and modularity that allows the introduction of monomers possessing diverse chemical structures.[18, 19] 1,1′-Bi-2-naphthol (BINOL) was selected as a source of chirality because of its low cost, exceptional stability over isomerisation under a broad range of conditions, and phenolic groups that make it a perfect candidate to act as Michael donor.[20-23] The inclusion of BINOL in polymers has been mostly exploited to produce polymeric catalysts[24-27] or for sensing application[28, 29], but investigations into the thermomechanical properties of these polymers are lacking, especially with varying BINOL isomers. Only recently Kelber *et al*. introduced enantiomerically pure and racemic BINOL in 3D printed networks and observed that variation of the dihedral angle was possible upon stretching.[30] However, differences in properties were not observed, possibly in light of the low level of introduction (0.2 % in weight).

Herein, we present a study into the thermomechanical properties of polyesters containing main chain enantiopure and racemic BINOL. Polymers are synthesised in step-growth fashion using mild phenol-yne addition with multiple dipropiolates monomers and the effect of stereochemistry in the chain is also investigated.

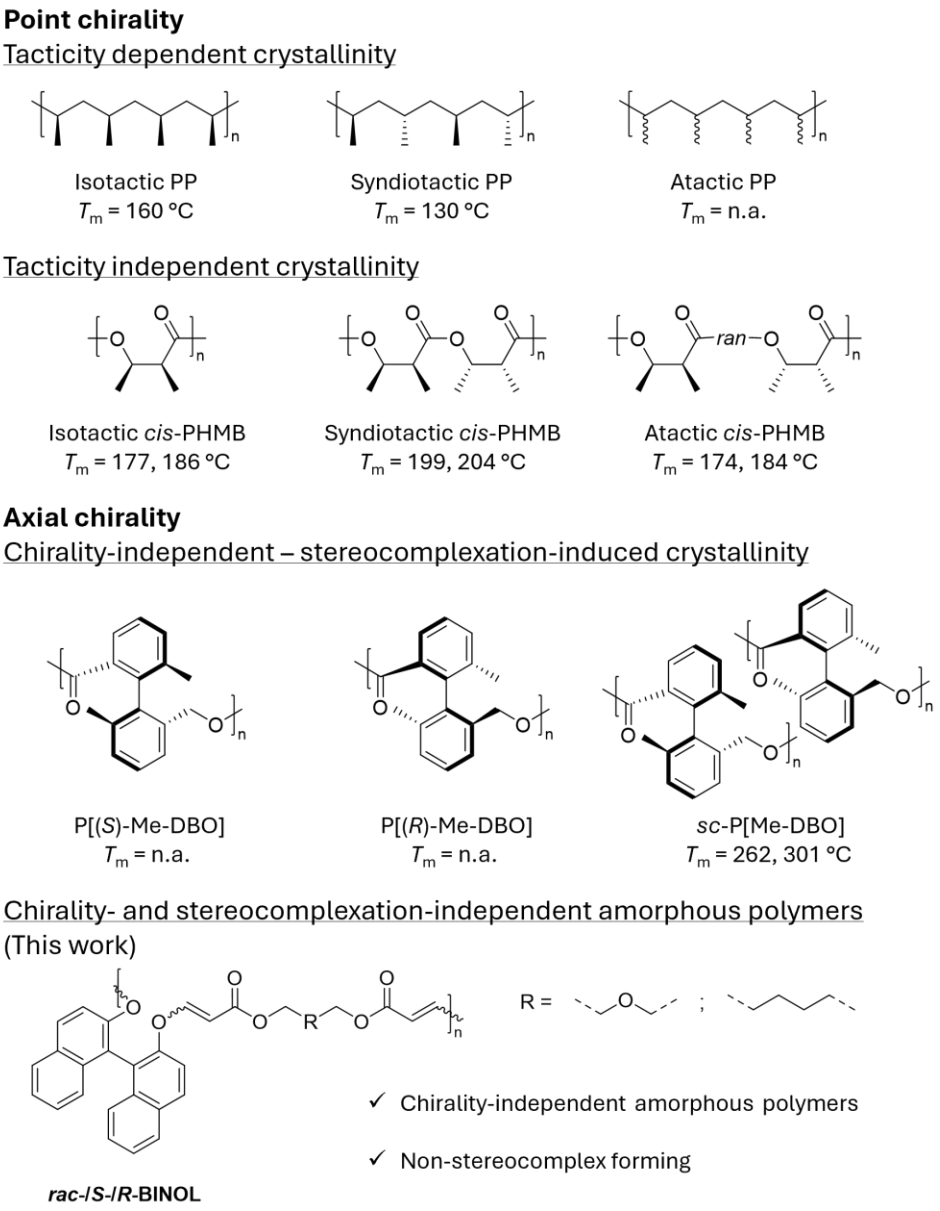
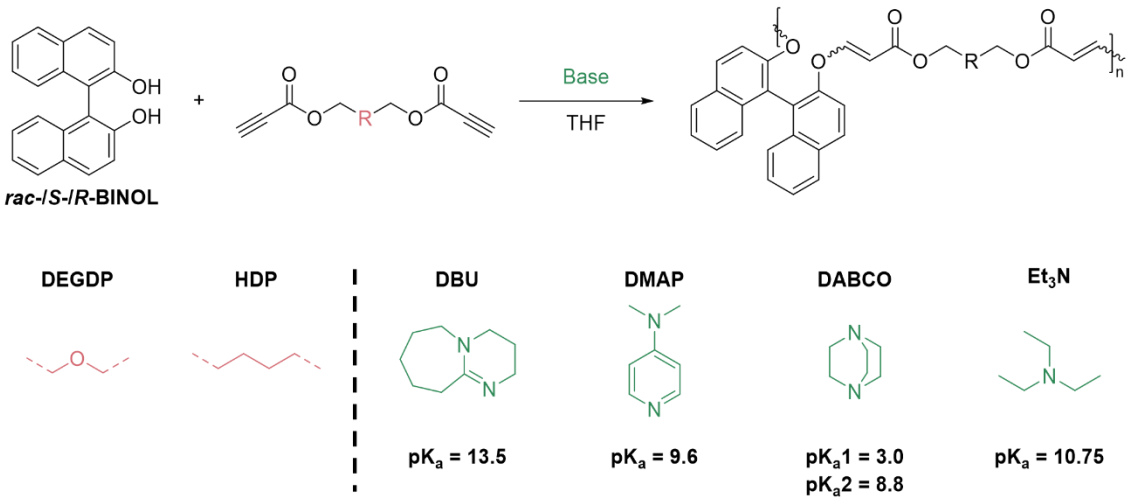


Figure 1. Examples of polymers with stereochemical-rich backbone displaying tacticity-dependent crystallinity,[3-5] tacticity-independent crystallinity,[6] chirality-independent but stereocomplexation-induced crystallinity,[17] and chirality- and stereocomplexation-independent crystallinity (this work).

Results and discussion

Optimisation of organobase-catalysed phenol-yne polymerisation of BINOL

To fully understand how BINOL stereochemical features affect polymer properties, both enantiopure and racemic BINOL monomers were employed and initial efforts were addressed to selecting a suitable catalyst for the polymerisation reaction. In addition to 1,4-diazabicyclo[2.2.2]octane (DABCO, pK_a = 3.0; 8.8) and 4-dimethylaminopyridine (DMAP, pK_a = 9.6) reported by Tang and co-workers,[18, 19] the use of a stronger base such as 1,8-diazabicyclo[5.4.0]undec-7-ene (DBU, pK_a = 13.5) was also investigated for the phenol-yne polymerisation of *rac*-BINOL with hexanedipropiolate (HDP) (Scheme 1). Reactions were performed at room temperature (*ca.* 25 °C) at a monomer concentration of 0.1 M with catalyst loading of 1 mol%, and the outcome was evaluated *via* size exclusion chromatography (SEC) following precipitation in hexane after 1 h of reaction.



Scheme 1. Organobase catalysed phenol-yne polymerisation between BINOL and different dipropiolates with the bases screened for the polymerisation. pK_a values in water reported.

Dramatic differences were observed when different catalysts were employed. In fact, the DABCO-catalysed reaction was the only one showing the formation of polymeric species, as highlighted by the SEC trace (Figure S1), indicating that nucleophilic character of the catalyst is required. Nonetheless, the obtained weight-average molecular weight (M_W) was low (M_W = 8500 g/mol) and the dispersity ($Đ_W$) modest ($Đ_W$ = 4.8), hence DABCO was selected for further optimisation.

Intrigued by the lack of polymerisation witnessed when using DBU or DMAP, it was hypothesised that using bases stronger than DABCO may lead to formation of salts that prevent BINOL from reacting further. To test this hypothesis, *rac*-BINOL was exposed to two equivalents of DABCO and triethylamine (Et_3N, pK_a = 10.75) in THF, and salt formation was evaluated by ^{1}H NMR spectroscopy. Et_3N was selected considering its non-nucleophilic behaviour and being a stronger base than DABCO. Downfield shifting of Et_3N proton resonances (triplet from 0.9 to 1.12 ppm and quadruplet from 2.41 to 3.15 ppm) evidenced formation of BINOL-Et_3N salt, while the singlet resonance associated with DABCO protons signal did not shift. Disappearance of the phenolic proton resonance was observed in both cases (Figure S2-S3). Notably, other peaks appeared in the ^{1}H NMR spectrum of the Et_3N-BINOL combinations, which may be attributed to the happening of side reactions that could also help explain the lack of polymerisation. To corroborate these results, equimolar amounts of dialkyne compared to BINOL were added to the previously prepared solutions and polymerisation was evaluated *via* GPC analysis, showing formation of polymer only in the DABCO catalysed reaction, even after 20 hours of reaction time (Figure 2A). The broad and bimodal GPC trace was

associated with an inferior degree of control of the polymerisation due to the high catalyst loading (2 equiv.) and relative acidy of the terminal alkyne protons, which could cause side reactions such as homocoupling.[31, 32] For instance, Adimurthy *et al.* reported self-coupling of 1-octyne with a 71% yield when in the presence of 1 equivalent of DABCO in acetonitrile.[33] Notably, ^{1}H NMR spectroscopic analysis of the reaction mixture revealed consumption of the alkyne only for the DABCO-catalysed reaction, as the singlet associated with the terminal alkyne was still visible in the Et_3N-catalysed system (Figure 2B). This is consistent with the findings reported by Santos *et al.*[34] In fact, in this study probing the dynamic nature of the phenol-yne addition, it is described that no exchange reaction between *p*-methoxyphenol and a vinyl ether compound obtained by reacting methylpropiolate with cresol was observed in a week at 90 °C, using Et_3N as catalyst.

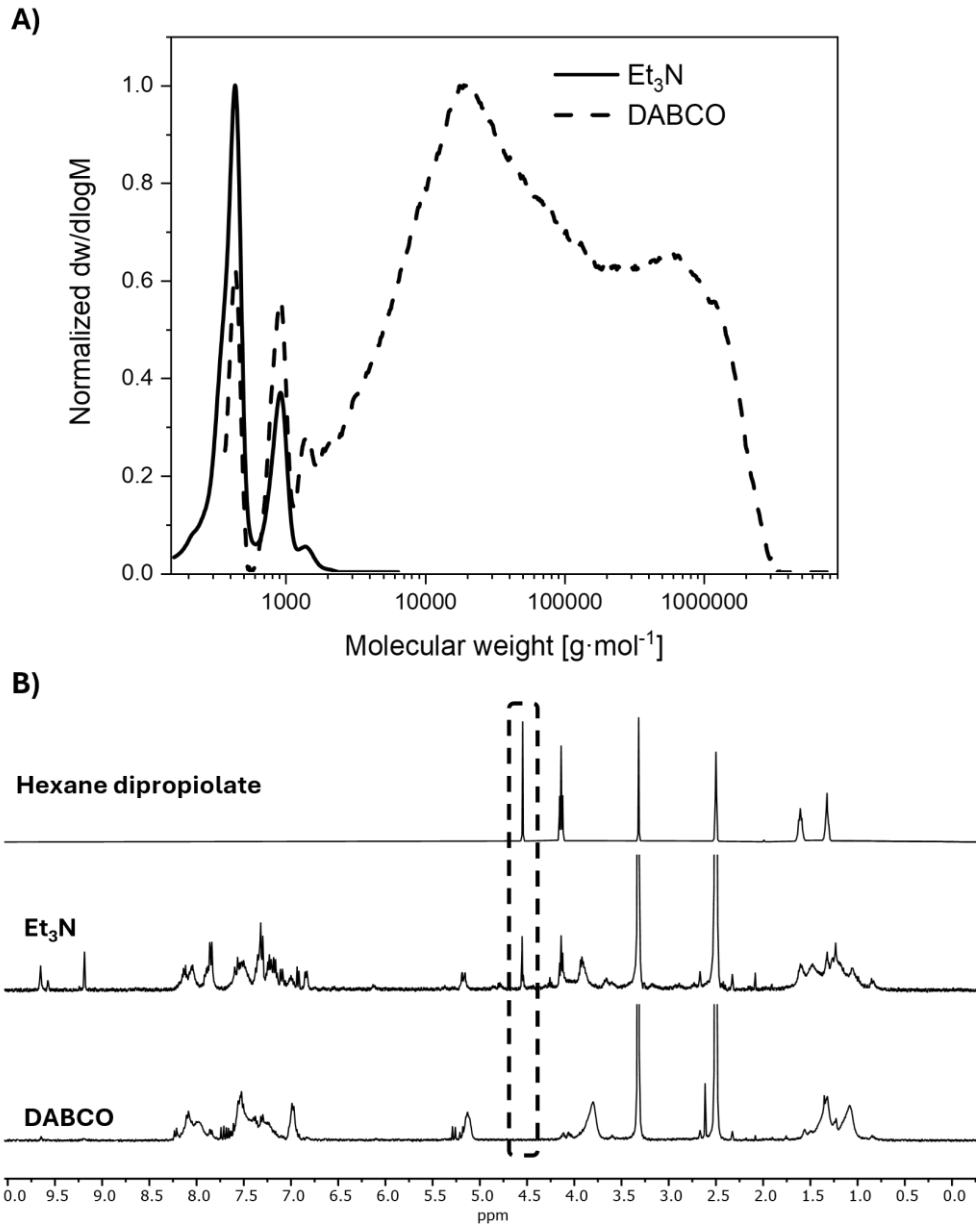


Figure 2. A) GPC ($CHCl_3$ + 0.5% v/v Et_3N, against polystyrene standards) of DABCO- (dashed line) and Et_3N-(full line) catalysed polymerisation between BINOL and HDP. B) ^1H NMR (d_6–DMSO, 400 MHz, 22 °C) spectra of 1,6-hexane dipropiolate (top), Et_3N-catalysed polymerisation (middle) and DABCO-catalysed polymerisation (bottom). Alkyne proton signal (highlighted) absent for the DABCO-catalysed polymerisation only.

To further understand the behaviour of the DABCO-catalysed phenol-yne polymerisation, a kinetic analysis was performed keeping a monomer concentration of 0.1 M at 25 °C. GPC analysis showed a sharp increase in M_W in the

first 45 minutes, followed by a plateau (Figure 3A), suggesting the reaction to reach completion after a short time.

Given the high dispersity and multimodal distribution of the GPC curves (Figure 3B), the effect of the concentration of the reaction mixture was investigated performing a series of polymerisation increasing the concentration of the monomers, from 0.05 to 0.5 M. Interestingly, the intensity of the low-molecular-weight region of the GPC trace decreased when increasing the concentration, accompanied by an overall increase in the final molecular weight of the polymer (Figure 3C). This behaviour could be explained by the formation of cyclic polymers, as this is a common phenomenon in step-growth polymerisation that is favoured by high dilution.[35] Moreover, the conformation of BINOL and the proximity of its reactive phenolic groups may facilitate intramolecular reactions. Investigation of these polymers *via* matrix-assisted laser desorption/ionization time-of-flight mass spectrometry (MALDI-ToF MS) may be used to confirm the cyclic nature of these polymers.[36, 37] Further increase of the concentration reaction to 1 M yielded a significant improvement of the polymerisation outcome, but further improvement could not be observed when the concentration was increased to 1.5 M, hence 1 M was selected as the optimal concentration as not all of the BINOL was solubilising at 1.5 M (Figure S8).

The effect of temperature on the reaction outcome was investigated by conducting reactions at 0, 25, and 50 °C at a monomer concentration of 0.1 M. Differently from what has been previously reported, it was found that temperature

influences greatly the attainable molecular weight, with higher values being reached at lower temperatures (Figure 3D). This result was thought to arise from higher chances of transesterification and/or reversibility of the phenol-yne addition with an increase in temperature.[34]

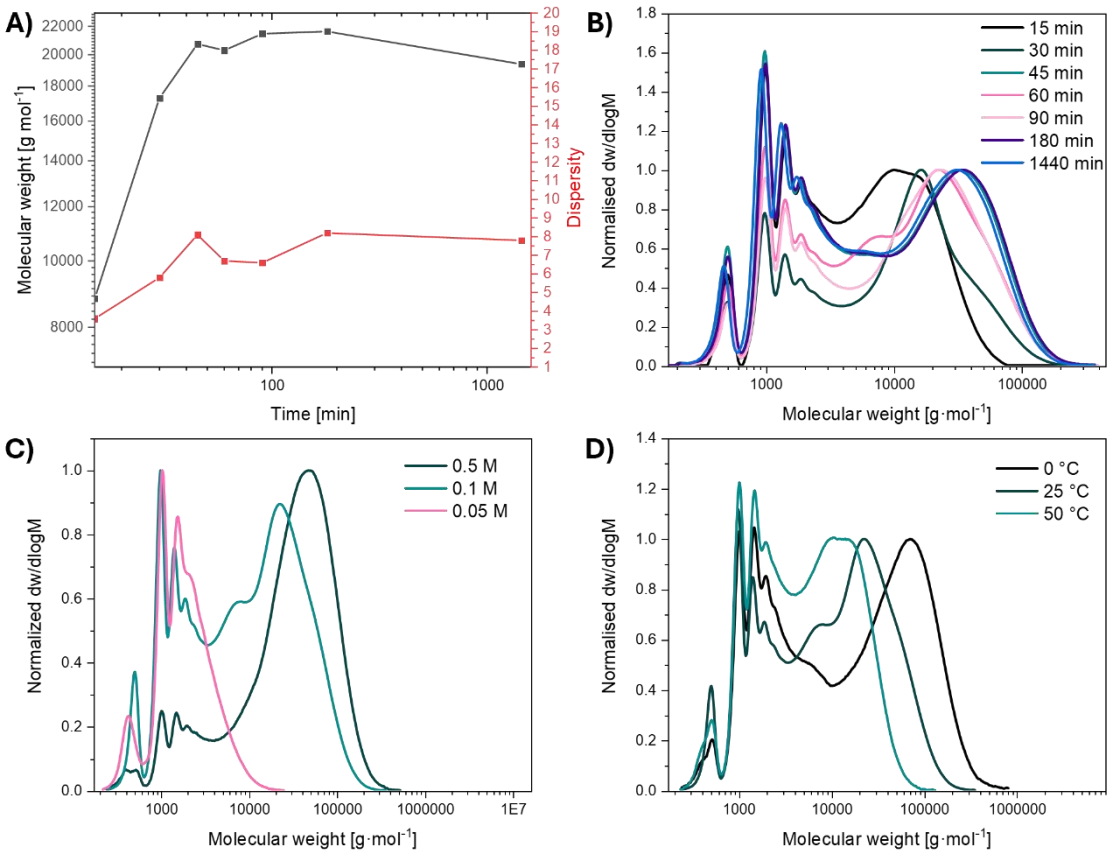


Figure 3. A) M_W and dispersity data against reaction time of reaction conducted at a concentration of 0.1 M at 25 °C and B) Full GPCs ($CHCl_3$ + 0.5% v/v Et_3N, against polystyrene standards) of phenol-yne polymerisation of BINOL at 25 °C with monomer concentration of 0.1 M taken at different time. C) The influence of monomer concentration on DABCO-catalysed phenol-yne polymerisation at a temperature of 25 °C evaluated by GPC ($CHCl_3$ + 0.5% v/v Et_3N, against polystyrene standards). D) The influence of temperature on the phenol yne reaction performed at a monomer concentration of 0.1 M evaluated by GPC ($CHCl_3$ + 0.5% v/v Et_3N, against polystyrene standards).

Finally, to test the scope of this polymerisation, a reaction was performed with a hindered diynone possessing a terminal methyl group at a monomer concentration of 0.5 M at 25 °C (Figure 4A). Interestingly, GPC analysis indicated

the formation of exclusively low molecular-weight species, even after longer reaction time (up to 67 h) or higher catalyst loading up to 1 equivalent (Figure 4B). This result suggests that the acceptor group must be accessible as steric hindrance can inhibit the polymerisation even in the presence of a more activated alkyne, as the ester group of a propiolate would have a diminished electron-withdrawing effect when compared to a carbonyl group.[38] This lack of polymerisation is also supported by the diminished acidity and nucleophilic character of phenols when compared to thiols, as the thiol-yne addition to hindered alkynes is a highly efficient reaction.[38, 39]

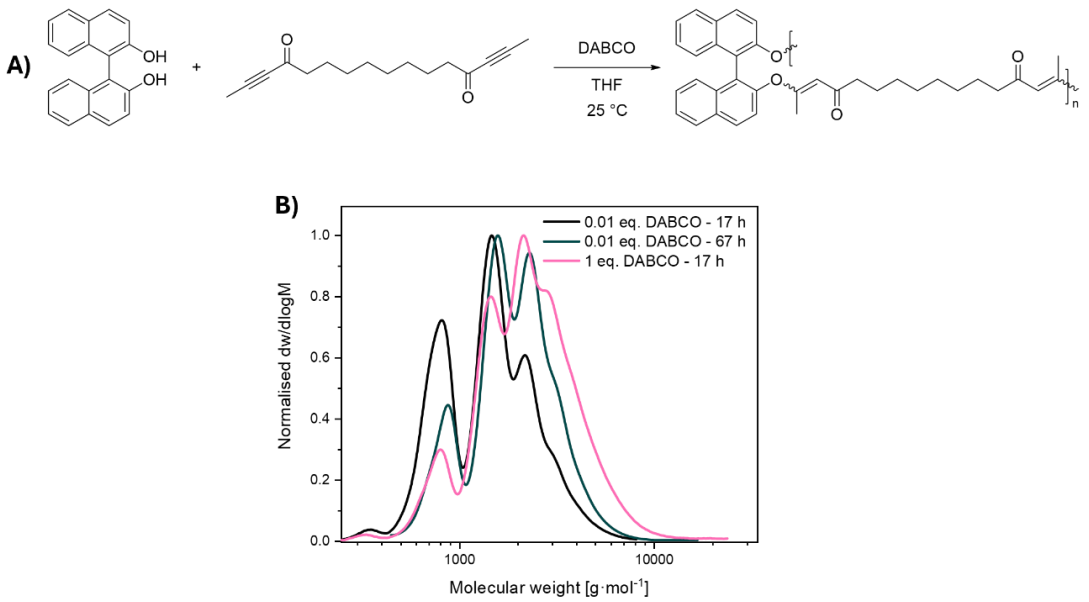


Figure 4. A) Phenol-yne polymerisation between DABCO and activated diynone. B) GPC ($CHCl_3$ + 0.5% v/v Et_3N, against polystyrene standards) of resulting products at different catalyst loading and reaction time.

Polymers synthesis and characterisation

With the optimised reaction conditions in hand, the phenol-yne polymerisation of racemic and enantiopure BINOL and different dipropiolates was performed at a concentration of 1 M at a temperature of 0 °C obtaining polymers of high molecular

weight in excellent yield (99%) (Table 1, Figure S5-S6). Diethyleneglycol dipropiolate (DEGDP) and HDP were selected considering the different tendencies to crystallisation observed in Chapter 2. While HDP was found to crystallise easily giving origin to semicrystalline polymers, DEGDP did not display the same behaviour originating amorphous polymers. It was hypothesised that using these two monomers could serve as controlled conditions to evaluate the influence of the bulky BINOL structure on the crystallinity of the polymers. Polymer structures were elucidated *via* ^{1}H NMR spectroscopy. The presence of *E* and *Z* isomers was quantified using the ratio between the intensity of the relevant vinyl proton signal in the ^{1}H NMR spectrum, as the doublet associated with a *Z* conformation displays a lower coupling constant (J = 7.0 Hz) than the doublet associated with an *E* conformation (J = 12.3 Hz). In agreement with previous report,[18] the phenol-yne addition seems to favour the formation of bonds in the *trans* conformation, but the *cis* isomer was detected as well to be around 9% for polymers synthesised using HDP as a comonomer and 12% for polymers synthesised using DEGDP (Figure 5). Previously performed DFT calculation performed using bis(aroylacetylene)s monomers showed that the formation of predominantly *trans*-linkages is favored because of a greater Gibbs free energy gain (ΔG = − 2.04 kcal × mol^{-1}), after a proton rearrangement following the formation of *Z* intermediates.[18]

Table 1. M_W, $Đ_W$, and yield of polymers obtained reacting racemic or enantiopure BINOL with different dialkynes.

Name	M_W [kg×mol^{-1}][a]	$Đ_W$[a]	Yield[b]
Poly(DEG-*rac*-BINOL)	126	14.8	>99%
Poly(DEG-(*S*)-BINOL)	62	10	>99%
Poly(DEG-(*R*)-BINOL)	46	7.8	>99%
Poly(HD-*rac*-BINOL)	75	6.2	>99%
Poly(HD-(*S*)-BINOL)	34	3	>99%
Poly(HD-(*R*)-BINOL)	31	3	>99%

[a]determined *via* GPC ($CHCl_3$, 0.5% Et_3N), comparison with polystyrene standard. [b]isolated yield after drying.

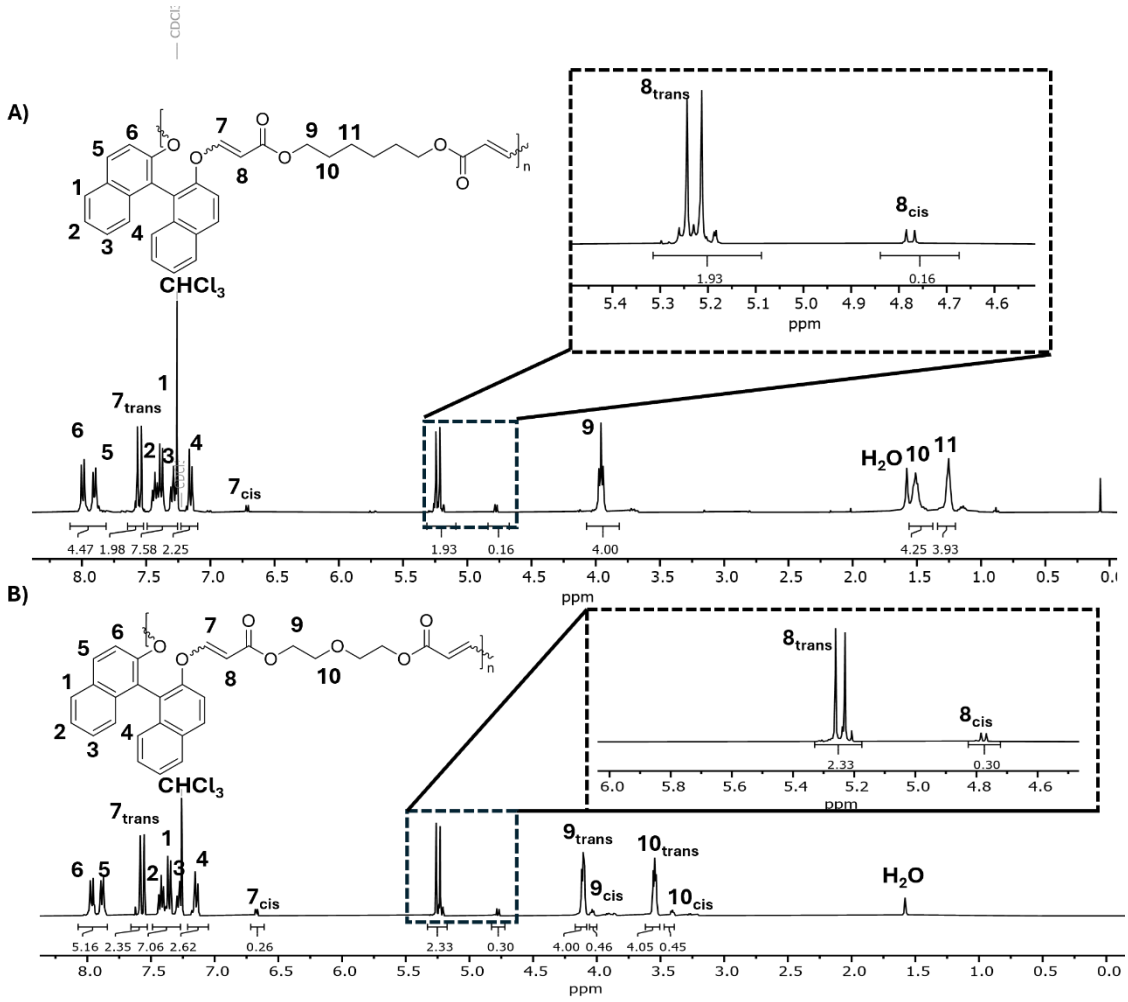


Figure 5. ^{1}H NMR ($CDCl_3$, 400 MHz, 22 °C) spectra of A) Poly(HD-*rac*-BINOL) and B) Poly(DEG-*rac*-BINOL). Vinyl signal used to evaluate *E*/*Z* ratio highlighted.

Thermomechanical characterisation of polymers and stereocomplexation

Thermal properties of polymers synthesised *via* phenol-yne polymerisation were characterised by thermogravimetric analysis (TGA) and differential scanning calorimetry (DSC). All these polymers were found to be highly thermally stable, with decomposition temperatures ($T_{d,5\%}$) (recorded as temperature associated with a 5% mass loss) above 360 °C (Figure 6A-6B). For instance, polyethylene terephthalate (PET), a commonly used polyester displaying phenyl groups in the backbone, displayed $T_{d,5\%}$ = 400 °C.[40] DSC scans revealed glass transition temperatures (T_g)

between 84 and 89 °C regarding the polymers obtained from the hexanedipropiolate co-monomer, while it was found to be roughly 10 °C higher in polymers synthesised using diethylene glycol dipropiolate (Figure 6C-6D). A similar behaviour*, i.e.* increase in T_g, is observed for polyethylene and poly(ethylene oxide) and can be rationalised by increased electrostatic interactions between polymer chains in the presence of a more electronegative and polarisable oxygen atom.[41, 42] Moreover, DSC did not reveal any endothermic peak indicating a melting transition, suggesting these polymers are amorphous. Wide angle X-ray scattering (WAXS) was used to confirm the DSC results, as the absence of sharp peaks further indicates the lack of a crystalline phase in the polymers (Figure 6E-F).

Table 2. Summary of thermal properties of polymers synthesised in this work.

Name	T_g[a] [°C]	$T_{d,5\%}$[b] [°C]
Poly(DEG-*rac*-BINOL)	88.9	375
Poly(DEG-(*S*)-BINOL)	85.5	375
Poly(DEG-(*R*)-BINOL)	84.3	375
Poly(HD-*rac*-BINOL)	95.8	378
Poly(HD-(*S*)-BINOL)	96.9	378
Poly(HD-(*R*)-BINOL)	97.9	366

[a]Determined as the inflection point of the second heating cycle of the DSC analysis. [b]Determined as the temperature associated with a 5% mass loss.

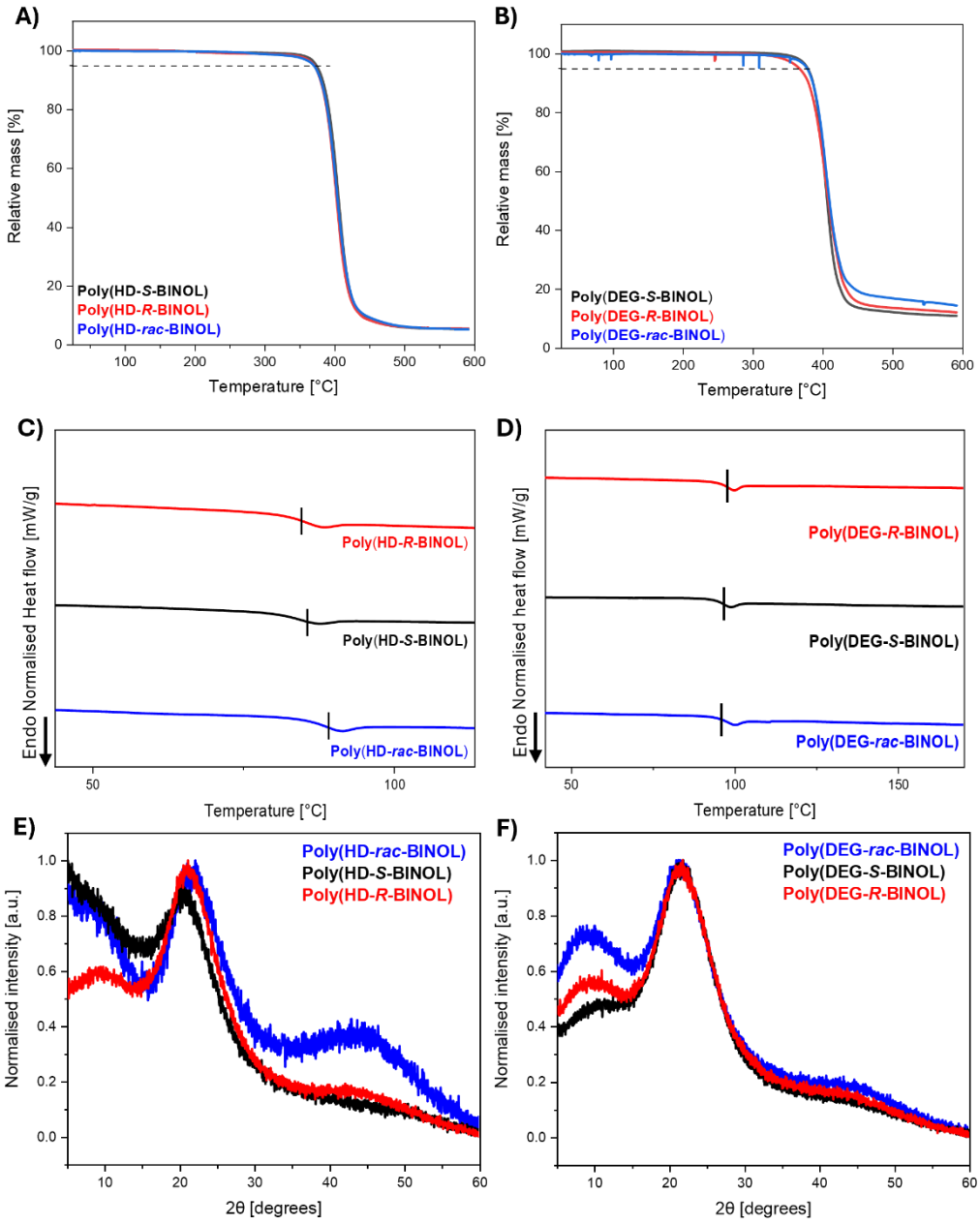


Figure 6. (A-B) TGA thermograms (25 – 600 °C, 10 °C/min, N_2) (a dashed line is used to highlight 5% degradation), (C-D) Second heating cycle of DSC thermograms (−80 – 300 °C, N_2) with vertical dash to highlight the T_g, and (E-F) WAXS profiles of polymers obtained reacting racemic or enantiopure BINOL with different dialkynes

Uniaxial tensile testing was selected to investigate the mechanical properties of these materials; hence attempts were made to cast the polymers into dogbones shaped objects. Unfortunately, heat-compression moulding proved unsuitable

considering the brittleness displayed by these materials, likely in light of their high T_g and low level of entanglement. Solvent casting was used as alternative way to produce polymeric films. To do so, 0.500 g of each polymer were solubilised in dichloromethane (CH_2Cl_2) and then left to dry in a Teflon beaker to obtain free-standing films. Finally, the residual solvent was removed by drying it in a vacuum oven until constant weight. Again, attempts to cut dogbones out of the dried film failed because of their brittleness. Notably, only poly(HD-*rac*-BINOL) displayed enough toughness to withstand the cut without shattering (Figure 7A-C), which is probably due to the higher M_W leading to greater entanglement.[43] Eventually, dogbones could be cut out of the solvent cast films of the DEG-BINOL polymers before the final drying, which were then dried prior performing uniaxial tensile testing (Figure 7D-F). High variability among the samples was observed: the measured values displayed wide uncertainty, and no significant difference was found among these samples (Figure 7G, Table 3). This variability could be attributed to the brittleness of the materials and the formation of bubbles following the drying process, which can be a source of error in the measurement. Further investigation into the processing of these polymers is needed before drawing any significant conclusions, but axial chirality does not seem to produce any influence on thermomechanical behaviour in these polymers.

Table 3. Summary of mechanical properties of poly(DEG-BINOL) of differentiated BINOL isomerism.

Name	E^a [MPa]	σ^b [MPa]	ε^c [MPa]	Toughness (U_T) [J·m^{-3}]
Poly(DEG-*rac*-BINOL)	134.6 ± 122.5	18.5 ± 12.3	19.3 ± 13.9	3.5 ± 4.3
Poly(DEG-*S*-BINOL)	208.9 ± 77.9	6.8 ± 5	6.3 ± 3.6	0.5 ±0.6
Poly(DEG-*R*-BINOL)	172.2 ± 77.1	20.1 ± 14.1	12.9 ± 7.6	2.3 ± 2.6

[a]Young's modulus. [b]Stress at break. [c]Strain at break. Standard deviation taken as uncertainty.

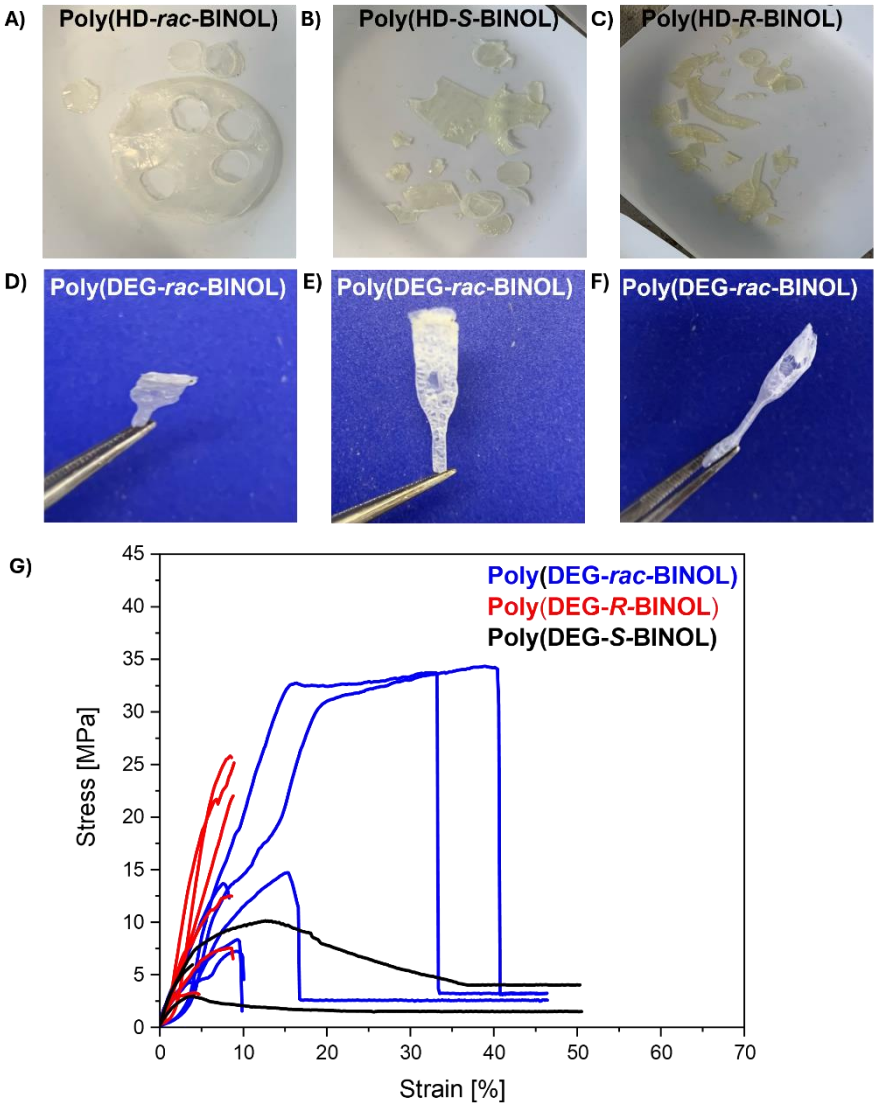


Figure 7. A-C) Solvent-cast films of poly(HD-BINOL)s showing that poly(HD-*rac*-BINOL) was the only film not shattering after cutting disks. D-F) Dog bones of Poly(DEG-*rac*-BINOL) showing the shrinkage and formation of bubbles after solvent removal. G) uniaxial tensile testing (10 mm/min, 22 °C) of different poly(HD-BINOL)s.

As Cao *et al.*[17] reported stereocomplexation between two amorphous polymers displaying axial chirality, we sought to investigate whether this phenomenon was occurring. Attempts to form stereocomplexes between poly(HD-*S*-BINOL) and poly(HD-R-BINOL) were performed by adapting a protocol devised by Coates and Lu and co-workers regarding the stereocomplexation of polyesters.[44] Equivalent amounts of poly(HD-*R*-BINOL) and poly(HD-*S*-BINOL) were solubilised in CH_2Cl_2,

followed by coprecipitation in hexane, and evaluation of their formation *via* TGA and DSC. Unfortunately, as the recovered material did not display any melting temperature and only a slight increase in T_g (+1.2 °C when compared to Poly(HD-*S*-BINOL), +2 °C when compared to Poly(HD-*R*-BINOL), it is concluded that stereocomplexation is not happening between these polymers (Figure 8A-B). This could be a result of the much more flexible conformation of these polymers when compared to the polyesters reported by Cao *et al*.

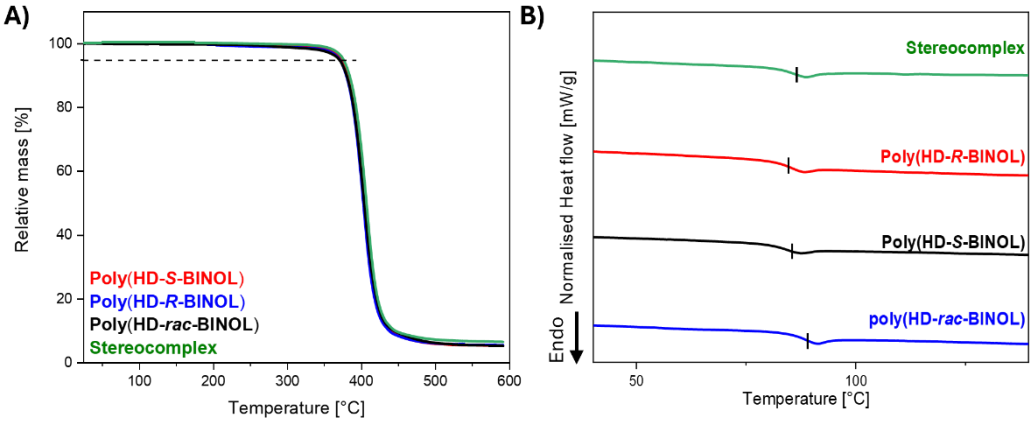


Figure 8. TGA thermograms (25 – 600 °C, 10 °C/min, N_2) (A) and DSC thermograms (−80 – 300 °C, N_2) (B) of polymers obtained reacting racemic or enantiopure BINOL with hexanedipropiolate and the solid obtained from the stereocomplexation attempt. A dashed line is used in the TGA thermograms to highlight 5% degradation. The second heating cycle of the DSC is displayed, with vertical dash to highlight the T_g.

Conclusions

The phenol-yne polymerisation of BINOL with different dipropiolate comonomers was established and optimised with respect to the influence of temperature and concentration. Investigation into the effects of incorporating BINOL molecules of opposite chirality, or a racemic mixture thereof, in the polymer backbone revealed that axial chirality does not seem to influence the

thermomechanical properties, differently from what is observed for other examples of stereoisomerism. The reason for this may be that the stereochemical information is lost in the flexible co-monomer, or that BINOL is too bulky and does not allow for crystallisation of the polymer chains to take place. In order to test these hypotheses, BINOL could be substituted with [1,1'-binaphthalene]-2,2'-diamine (BINAM) because the presence of hydrogen bonds donor and acceptor groups may help to stabilise the conformation of the polymer thanks to long-range intrachain interactions. Another option would be to increase the length of the dipropiolate monomer spacer, for example through polymerisation of 1,12-dodecanedipropiolate, to balance the bulkiness of BINOL and allow the polymeric chains to align in an ordered manner.

References

1. N Othman, C Xu, P Mehrkhodavandi and SG Hatzikiriakos, *Polymer*, 2012, **53**, 2443-2452.
2. Y Ikada, K Jamshidi, H Tsuji and SH Hyon, *Macromolecules*, 1987, **20**, 904-906.
3. G Natta, P Pino, P Corradini, F Danusso, E Mantica, G Mazzanti and G Moraglio, *J. Am. Chem. Soc.*, 1955, **77**, 1708-1710.
4. J Karger-Kocsis, *Polypropylene: an AZ reference*, Springer Science & Business Media, 2012.
5. N Ahmad, R Di Girolamo, F Auriemma, C De Rosa and N Grizzuti, *Macromolecules*, 2013, **46**, 7940-7946.
6. Z Zhou, AM LaPointe and GW Coates, *J. Am. Chem. Soc.*, 2023, **145**, 25983-25988.
7. JC Worch, H Prydderch, S Jimaja, P Bexis, ML Becker and AP Dove, *Nat. Rev. Chem.*, 2019, **3**, 514-535.
8. N Dusunceli and OU Colak, *Int. J. Plast.*, 2008, **24**, 1224-1242.
9. IUoPaAC (IUPAC), *axial chirality*, 3.0.1 edn., 2019.
10. SR LaPlante, LD Fader, KR Fandrick, DR Fandrick, O Hucke, R Kemper, SP Miller and PJ Edwards, *J. Med. Chem.*, 2011, **54**, 7005-7022.
11. S-P Wan, H-Y Lu, M Li and C-F Chen, *J. Photochem. Photobiol. C: Photochem. Rev.*, 2022, **50**, 100500.
12. Z Zhao, S Wang, X Ye, J Zhang and X Wan, *ACS Macro Lett.*, 2017, **6**, 205-209.
13. D-W Zhang, M Li and C-F Chen, *Angew. Chem. Int. Ed.*, 2022, **61**, e202213130.
14. K Kokado, Y Tokoro and Y Chujo, *Macromolecules*, 2009, **42**, 9238-9242.
15. J Chen, Q Nan, L Guo and Y Zhou, *J. Appl. Polym. Sci.*, 2010, **115**, 2190-2196.
16. A Shockravi, A Javadi and E Abouzari-Lotf, *RSC Adv.*, 2013, **3**, 6717-6746.
17. Q Cao, Y-M Tu, H-Z Fan, S-Y Shan, Z Cai and J-B Zhu, *Angew. Chem. Int. Ed.*, 2024, **63**, e202400196.
18. Y Shi, T Bai, W Bai, Z Wang, M Chen, B Yao, JZ Sun, A Qin, J Ling and BZ Tang, *Chem. Eur. J.*, 2017, **23**, 10725-10731.
19. H Si, K Wang, B Song, A Qin and BZ Tang, *Polym. Chem.*, 2020, **11**, 2568-2575.
20. JM Brunel, *Chem. Rev.*, 2005, **105**, 4233-4233.
21. EP Kyba, GW Gokel, F De Jong, K Koga, LR Sousa, MG Siegel, L Kaplan, GDY Sogah and DJ Cram, *J. Org. Chem.*, 1977, **42**, 4173-4184.
22. L Meca, D Řeha and Z Havlas, *J. Org. Chem.*, 2003, **68**, 5677-5680.

23. M Noji, M Nakajima and K Koga, *Tetrahedron Lett.*, 1994, **35**, 7983-7984.
24. H-B Yu, Q-S Hu and L Pu, *J. Am. Chem. Soc.*, 2000, **122**, 6500-6501.
25. D Jayaprakash, Y Kobayashi, S Watanabe, T Arai and H Sasai, *Tetrahedron: Asymmetry*, 2003, **14**, 1587-1592.
26. P Yan and H Jing, *Adv. Synth. Catal.*, 2009, **351**, 1325-1332.
27. A-L Zhang, Z-d Yu, L-W Yang and N-F Yang, *Tetrahedron: Asymmetry*, 2015, **26**, 173-179.
28. G Wei, Y Jiang, F Li, Y Quan, Y Cheng and C Zhu, *Polym. Chem.*, 2014, **5**, 5218-5222.
29. A Valverde-González, MC Borrallo-Aniceto, M Pintado-Sierra, F Sánchez, A Arnanz, M Boronat and M Iglesias, *ACS Appl. Mater. Interfaces*, 2022, **14**, 53936-53946.
30. JB Kelber, A Bensalah-Ledoux, S Zahouani, B Baguenard, P Schaaf, A Chaumont, S Guy and L Jierry, *Angew. Chem. Int. Ed.*, 2020, **59**, 23283-23290.
31. HA Stefani, AS Guarezemini and R Cella, *Tetrahedron*, 2010, **66**, 7871-7918.
32. B He, J Huang, X Liu, J Zhang, JWY Lam and BZ Tang, *Prog. Polym. Sci.*, 2022, **126**, 101503.
33. S Adimurthy, CC Malakar and U Beifuss, *J. Org. Chem.*, 2009, **74**, 5648-5651.
34. T Santos, Y Pérez-Pérez, DS Rivero, R Diana-Rivero, F García-Tellado, D Tejedor and R Carrillo, *Org. Lett.*, 2022.
35. HR Kricheldorf, *Macromol. Rapid Commun.*, 2008, **29**, 1695-1704.
36. H Räder and W Schrepp, *Acta Polym.*, 1998, **49**, 272-293.
37. FM Haque, CrM Schexnayder, JM Matxain, F Barroso-Bujans and SM Grayson, *Macromolecules*, 2019, **52**, 6369-6381.
38. N Van Herck, D Maes, K Unal, M Guerre, JM Winne and FE Du Prez, *Angew. Chem. Int. Ed.*, 2020, **59**, 3609-3617.
39. JC Worch, CJ Stubbs, MJ Price and AP Dove, *Chem. Rev.*, 2021, **121**, 6744-6776.
40. S Ray and RP Cooney, *Chapter 9 - Thermal Degradation of Polymer and Polymer Composites*, William Andrew Publishing, 2018.
41. DE Kirkpatrick and B Wunderlich, *Makromol.*, 1985, **186**, 2595-2607.
42. M Polaskova, P Peer, R Cermak and P Ponizil, *Polymers*, 2019, **11**, 1384.
43. J-M Chenal, L Chazeau, L Guy, Y Bomal and C Gauthier, *Polymer*, 2007, **48**, 1042-1046.
44. Z-Q Wan, JM Longo, L-X Liang, H-Y Chen, G-J Hou, S Yang, W-P Zhang, GW Coates and X-B Lu, *J. Am. Chem. Soc.*, 2019, **141**, 14780-14787.
45. WLF Armarego, *Purification of Laboratory Chemicals*, Elsevier, 2017.

Supporting information

Enantiopure and racemic BINOL-based polymers by hydroxyl-yne polymerisation

Daniele Giannantonio[a], Alexis Perrot[a,b], Arianna Brandolese[a], Andrew P. Dove[a]

[a]School of Chemistry, University of Birmingham, Edgbaston, Birmingham, B15 2TT (UK)

[b]LCMT, ENSICAEN, 6 bd Maréchal Juin, 14050 Caen, France.

Experimental methods

All compounds, unless otherwise indicated were purchased from commercial sources and used as received. Unlesss otherwise stated. (±)-1,1'-Bi-(2-naphthol) was recrystallised from toluene. (+)-1,1'-Bi-(2-naphthol) and (-)-1,1'bi-(2-naphthol) were recrystallised from aqueous ethanol.[45]

NMR Spectroscopic Analysis: See Chapter 2- Experimental methods

Mass Spectrometry: See Chapter 2- Experimental methods

Size Exclusion Chromatography (SEC): See Chapter 2- Experimental methods

Differential Scanning Calorimetry (DSC). The thermal characteristics of the polymers were determined using differential scanning calorimetry (STARe system DSC3, Mettler Toledo) from −80 to 120 °C at a heating rate of 10 °C·min^{-1} for three heating/cooling cycles unless otherwise specified. The glass transition temperature (T_g) was determined from the inflection point in the second heating cycle of DSC. Total enthalpy of melting (ΔH_m) was calculated from integration and normalization of all endothermic peaks present using the STARe software. The melting temperature was determined from the minimum value of the endothermic peak using the STARe software.

Wide angle X-ray scattering (WASX): Wide Angle X-ray Scattering (WAXS) was performed on a Panalytical Empyrean utilising Cu radiation (Kα1 and Kα2 radiation (l = 1.5406 Å and 1.5444 Å respectively)) and equipped with a Pixel Medipix 3D detector. Powdered samples were prepared onto low background Si-wafer sample

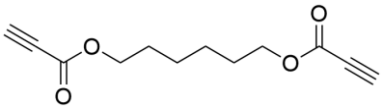
holders and standard "powder" 2θ–θ diffraction scans were carried out in the angular range from 4° to 70° 2θ at room temperature.

Thermogravimetric Analysis (TGA). See Chapter 2- Experimental methods

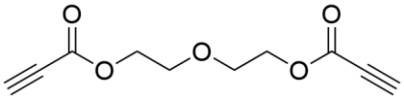
Tensile testing. Samples were prepared into thin polymer films by solubilising 500 mg of polymer into 2.5 mL of dichloromethane (DCM). The solution was uptaken with a syringe and filtered in a teflon beacher through a PTFE filter (0.22 μm × 25 mm) into a Teflon beacher. Solvent was left evaporating and dumbbell shaped samples were cut using custom ASTM Die D-638 Type 5, before drying in a vacuum oven until drynessUniaxial tensile testing was performed using a Testometric M350-5CT universal mechanical testing instrument fitted with a load cell of 10 kN. Each specimen was clamped into the tensile holders and subjected to an elongation rate of 10 mm·min^{-1} until failure with an applied pretension of 0.1 N. All tensile tests were repeated 3 times (unless otherwise stated), and an average of the data was taken to find the ultimate tensile stress and strain. Data was analyzed using winTest™ Analysis software (v.5.0.34) and OriginPro® software. Young modulus was calculated by taking the slope of the tensile curve at 1% strain. Toughness was calculated as the area under the curve up to break.

Synthetic procedures

Hexane dipropiolate (HD): See Chapter 2 Synthetic procedures regarding monomer M2 for synthesis and spectroscopic data.



Diethylene glycol dipropiolate (DEG): See Chapter 2 Synthetic procedures regarding monomer M3 for synthesis and spectroscopic data.



General procedure for polymer synthesis

BINOL (*rac,S, or R)* (1 equivalent) was weighed in a 20 mL scintillation vial. Comonomer (HD or DEG, 1 equivalent) was weighed in different vial and quantitatively transferred to the vial containing BINOL using the appropriate volume of THF to reach the desired final monomer concentration (0.05 to 1.5 M according to the experiment). The solution was cooled down in an ice bath for 10 minutes, before addition of DABCO (1% mol) presolubilised in THF. The reaction was left proceed for the desired period. A noticeable increase in viscosity was generally observed after 1 hour. The solution was diluted with chloroform ($CHCl_3$) ($V = V_{THF} \times 4$), and the solution poured through a cotton filter into hexane ($V = V_{THF} \times 10$) to precipitate the polymer. The polymer was decanted and recovered *via* filtration, then dried in a room-temperature vacuum oven.

Poly(DEG-*rac*-BINOL): Recovered as a white fibrous solid (0.5100 g, 99%). GPC analysis ($CHCl_3$, 0.5% Et_3N, PS standard) M_W = 126 kg × mol^{-1}, $Đ_M$ = 14.8

^{1}H NMR (400 MHz, Chloroform-*d*) %trans = 88; ^{1}H NMR (400 MHz, Chloroform-*d*) *δ* 7.97 (d, *J* = 8.9 Hz, 2H), 7.88 (d, *J* = 8.2 Hz, 2H), 7.57 (d, *J* = 12.3 Hz, 2H *trans*), 7.42 (ddd, *J* = 8.1, 6.8, 1.2 Hz, 2H), 7.36 (d, *J* = 8.9 Hz, 2H), 7.29 (dt, *J* = 8.6, 1.6 Hz, 2H), 7.18 – 7.02 (m, 2H), 6.67 (d, *J* = 7.0 Hz, *cis*), 5.25 (d, *J* = 12.3 Hz, 2H *trans*), 4.78 (d, *J* = 7.0 Hz, *cis*), 4.19 – 4.01 (m, 4H *trans*), 4.04 (t, *J* = 4.9 Hz, *cis*), 3.55 (t, *J* = 4.9 Hz, 4H *trans*), 3.41 (t, *J* = 4.9 Hz, *cis*). ^{13}C NMR (101 MHz, Chloroform-*d*) *δ* 166.9, 159.9, 151.1, 133.6, 131.4, 130.9, 128.4, 127.5, 125.8, 121.5, 118.6, 101.7, 69.2, 63.1.

Poly(DEG-*R*-BINOL): Recovered as a white fibrous solid (0.4900 g, 99%). GPC analysis ($CHCl_3$, 0.5% Et_3N, PS standard) M_W = 46 kg × mol^{-1}, $Đ_M$ = 7.8

^{1}H NMR (400 MHz, Chloroform-*d*) %trans = 88; *δ* 7.88 (d, *J* = 9.0 Hz, 2H), 7.80 (d, *J* = 8.1 Hz, 2H), 7.49 (d, *J* = 12.3 Hz, 2H *trans*), 7.34 (ddd, *J* = 8.2, 6.8, 1.2 Hz, 2H), 7.28 (d, *J* = 8.9 Hz, 2H), 7.24 – 7.19 (m, 2H), 7.13 – 6.98 (m, 2H), 6.59 (d, *J* = 6.9 Hz, *cis*), 5.17 (d, *J* = 12.3 Hz, 2H *trans*), 4.70 (d, *J* = 7.0 Hz, *cis*), 4.03 (t, *J* = 4.9 Hz, 4H *trans*), 3.96 (t, *J* = 4.9 Hz, *cis*), 3.60 – 3.38 (m, 4H *trans*), 3.33 (t, *J* = 4.9 Hz, *cis*). ^{13}C NMR (101 MHz, Chloroform-*d*) *δ* 166.9, 159.9, 151.1, 133.6, 131.4, 130.9, 128.4, 127.5, 125.8, 121.5, 118., 101.6, 69.2, 63.1.

Poly(DEG-*S*-BINOL): Recovered as a white fibrous solid (0.5100 g, 99%). GPC analysis ($CHCl_3$, 0.5% Et_3N, PS standard) M_W = 62 kg × mol^{-1}, $Đ_M$ = 10

^{1}H NMR (400 MHz, Chloroform-*d*) %trans = 88; *δ* 8.04 – 7.93 (m, 2H), 7.92 – 7.75 (m, 2H), 7.57 (d, *J* = 12.2 Hz, 2H *trans*), 7.42 (ddd, *J* = 8.2, 6.8, 1.2 Hz, 2H), 7.36 (d, *J* = 8.9 Hz, 2H), 7.31 – 7.27 (m, 2H), 7.18 – 7.05 (m, 2H), 6.67 (d, *J* = 7.0 Hz, *cis*), 5.25 (d, *J* = 12.3 Hz, 2H *trans*), 4.78 (d, *J* = 7.0 Hz, *cis*), 4.18 – 4.05 (m, 4H *trans*), 4.04 (t, *J*

= 4.9 Hz, *cis*), 3.61 – 3.50 (m, 4H *trans*), 3.41 (t, *J* = 4.9 Hz, *cis*). ^{13}C NMR (101 MHz, Chloroform-*d*) δ 166.9, 159.9, 151.1, 133.6, 131.3, 130.3, 128.4, 127.4, 125.8, 121.5, 118.6, 101.7, 69.1, 63.1.

Poly(HD-*rac*-BINOL): Recovered as a off-white crystalline solid (0.5491 g, 99%). GPC analysis ($CHCl_3$, 0.5% Et_3N, PS standard) M_W = 75 kg × mol^{-1}, $Đ_M$ = 6.2

^{1}H NMR (400 MHz, Chloroform-*d*) %trans = 92; δ 8.00 (d, *J* = 8.9 Hz, 2H), 7.91 (d, *J* = 8.3 Hz, 2H), 7.56 (d, *J* = 12.3 Hz, 2H *trans*), 7.44 (ddd, J = 8.1, 6.8, 1.2 Hz, 2H), 7.39 (d, *J* = 9.0 Hz, 2H), 7.29 (ddd, *J* = 8.3, 6.8, 1.3 Hz, 2H), 7.16 (dd, *J* = 8.5, 1.2 Hz, 2H), 6.72 (d, *J* = 7.0 Hz, *cis*), 5.24 (d, *J* = 12.2 Hz, 2H *trans*), 4.79 (d, *J* = 7.1 Hz, *cis*), 3.97 (t, *J* = 6.7 Hz, 4H), 1.51 (d, *J* = 6.2 Hz, 4H), 1.26 (t, *J* = 3.8 Hz, 4H). ^{13}C NMR (101 MHz, Chloroform-*d*) δ 167.1, 159.5, 151.2, 133.6, 131.3, 130.9, 128.4, 127.4, 125.8, 125.8, 121.5, 118.6, 102.1, 64.0, 28.6, 25.7.

Poly(HD-*R*-BINOL): Recovered as a slightly yellow crystalline solid (0.5600 g, 99%). GPC analysis ($CHCl_3$, 0.5% Et_3N, PS standard) M_W = 31 kg × mol^{-1}, $Đ_M$ = 3

^{1}H NMR (400 MHz, Chloroform-*d*) %trans = 92; δ 8.00 (dd, *J* = 8.9, 3.3 Hz, 2H), 7.90 (t, *J* = 6.1 Hz, 2H), 7.56 (d, *J* = 12.3 Hz, 2H *trans*), 7.44 (ddd, *J* = 8.2, 6.8, 1.2 Hz, 2H), 7.39 (d, *J* = 9.0 Hz, 2H), 7.29 (ddd, *J* = 8.3, 6.8, 1.3 Hz, 2H), 7.16 (dd, *J* = 8.6, 1.2 Hz, 2H), 6.72 (d, *J* = 7.0 Hz, *cis*), 5.24 (d, *J* = 12.3 Hz, 2H *trans*), 4.79 (d, *J* = 7.0 Hz, *cis*), 3.97 (t, *J* = 6.6 Hz, 4H), 1.54 – 1.48 (m, 4H), 1.28 – 1.24 (m, 4H). ^{13}C NMR (101 MHz, Chloroform-*d*) δ 167.1, 159.6, 151.2, 133.6, 131.3, 130.9, 128.4, 127.4, 125.8, 125.8, 121.5, 118.6, 102.1, 64.0, 28.6, 25.7.

Poly(HD-*S*-BINOL): Recovered as a slightly yellow crystalline solid (0.544 g, 99%). GPC analysis ($CHCl_3$, 0.5% Et_3N, PS standard) M_W = 34 kg × mol^{-1}, $Đ_M$ = 3

^{1}H NMR (400 MHz, Chloroform-*d*) %trans = 92; δ 8.01 (d, *J* = 8.9 Hz, 2H), 7.92 (d, *J* = 8.3 Hz, 2H), 7.57 (d, *J* = 12.4 Hz, 2H *trans*), 7.44 (ddd, *J* = 8.2, 6.8, 1.2 Hz, 2H), 7.40 (d, *J* = 8.9 Hz, 2H), 7.30 (ddd, *J* = 8.2, 6.8, 1.3 Hz, 2H), 7.21 – 7.14 (m, 2H), 6.73 (d, *J* = 7.0 Hz, *cis*), 5.25 (d, *J* = 12.2 Hz, 2H *trans*), 4.80 (d, *J* = 7.0 Hz, *cis*), 3.98 (t, *J* = 6.5 Hz, *trans*), 3.82 – 3.51 (m, 4H), 1.84 – 1.43 (m, 4H), 1.27 (t, *J* = 3.8 Hz, 4H). ^{13}C NMR (101 MHz, Chloroform-*d*) δ 166.9, 159.5, 151.1, 133.5, 131.2, 130.8, 128.3, 127.3, 125.7, 125.7, 121.4, 118.5, 101.9, 63., 28.5, 25.6.

NMR spectroscopy and Size exclusion chromatography (SEC) data

.

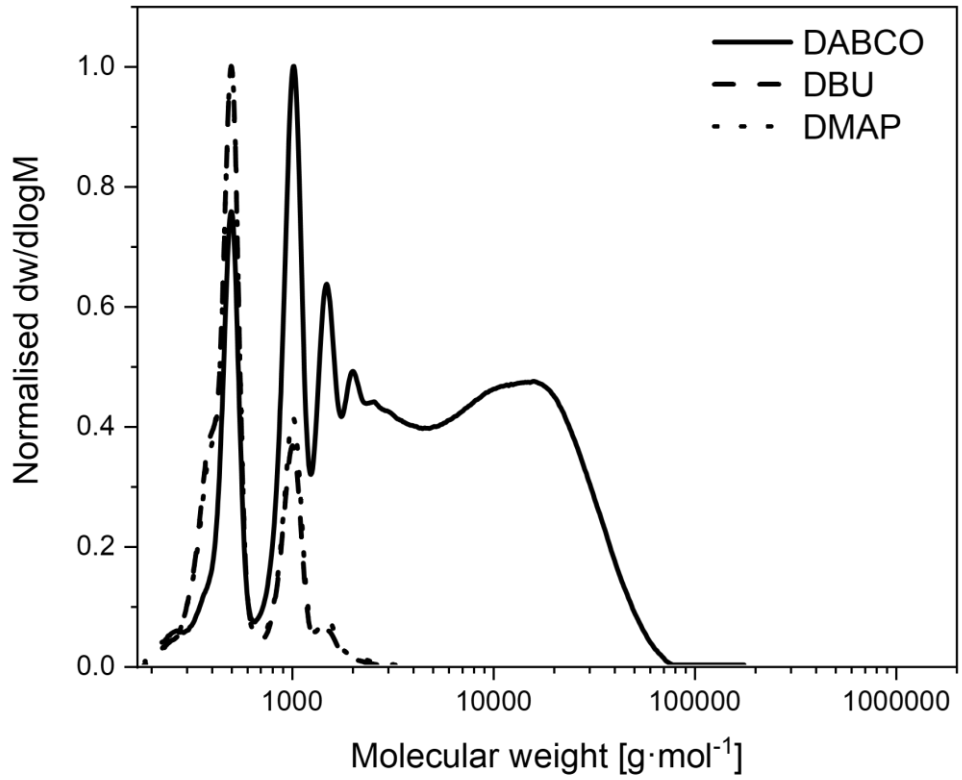


Figure S1. SEC of polymerisation reactions catalysed by DABCO (full line), DBU (dashed line), DMAP (dash and dot) after 1 hour.

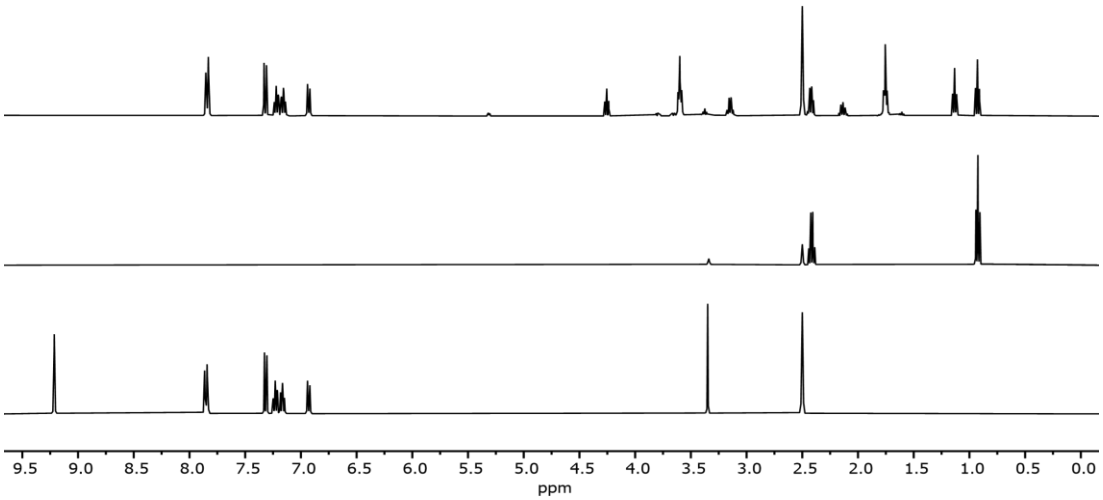


Figure S2. ^{1}H NMR spectrum (d_6 – DMSO, 400 MHz, 300 K) spectra of BINOL (bottom), Et_3N (middle) and combination of the two (top). Shifting of Et_3N peaks suggesting salt formation is highlighted. Solvent peaks marked. Not all Et_3N participated in the formation of the salt.

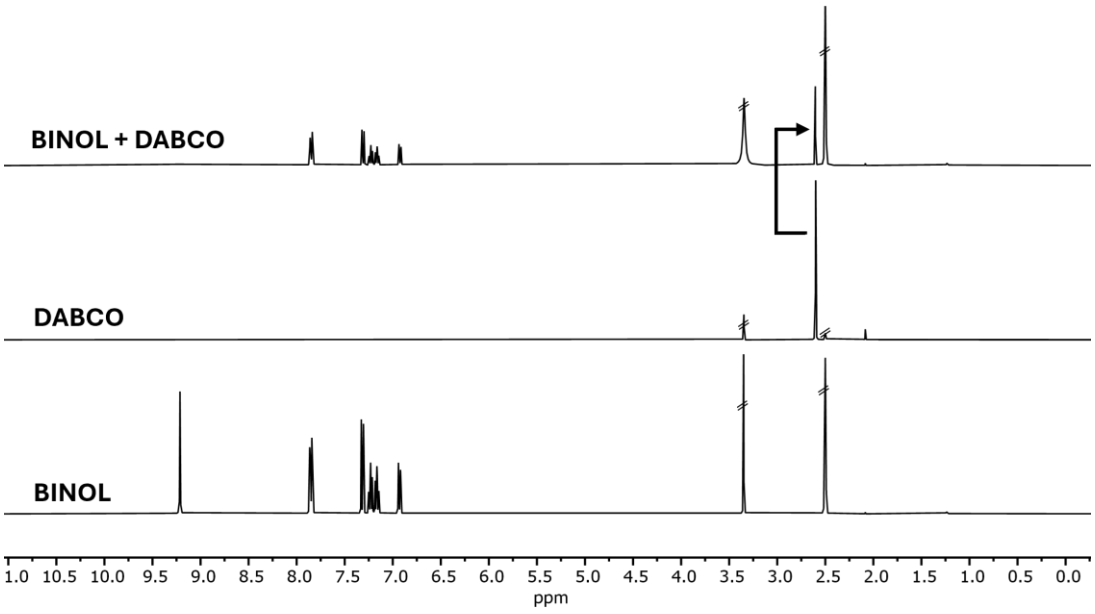


Figure S3. ^{1}H NMR spectrum (d_6 – DMSO, 400 MHz, 300 K) spectra of BINOL (bottom), DABCO (middle) and combination of the two (top). DABCO singlet did not shift suggesting that a salt is not being formed.

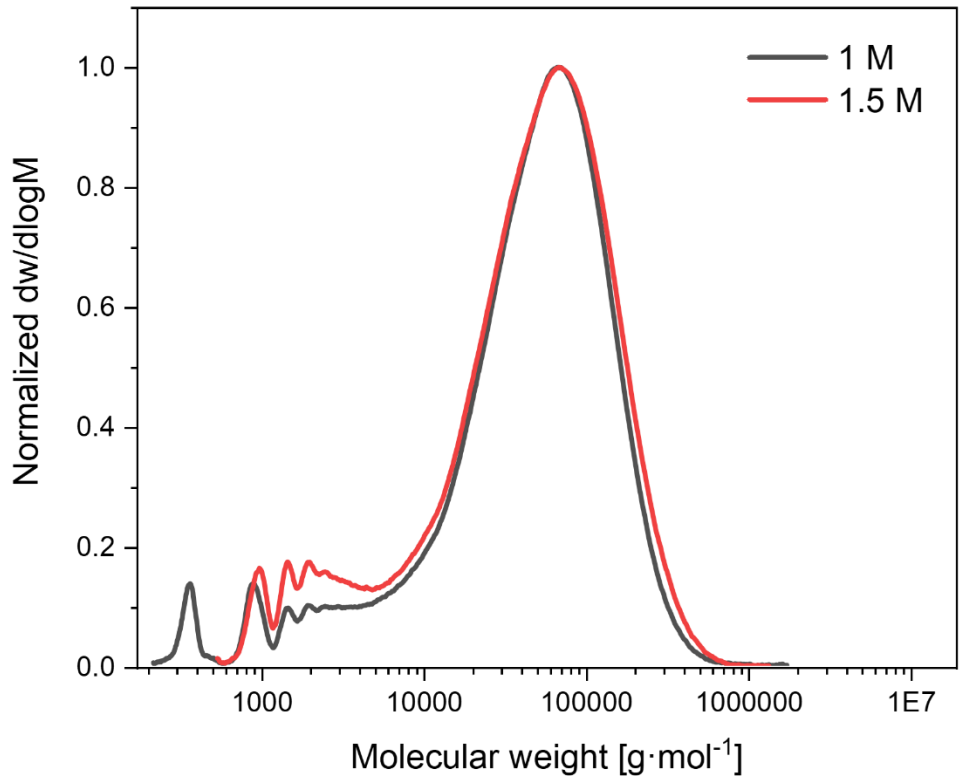


Figure S4. SEC ($CHCl_3$ + 0.5% v/v Et_3N, against polystyrene standards) of polymers resulting from the nucleophilic phenol-yne polymerisation of rac-BINOL and hexanedipropiolate at different monomer concentrations.

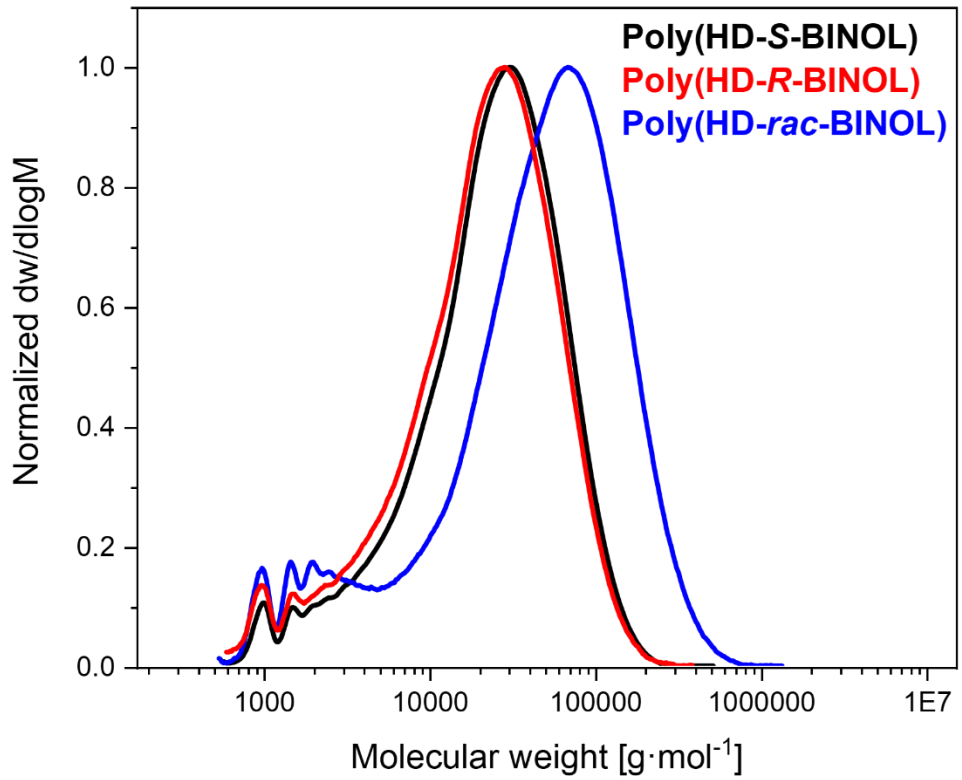


Figure S5. SEC ($CHCl_3$ + 0.5% v/v Et_3N, against polystyrene standards) of polymers resulting from the nucleophilic phenol-yne polymerisation of enantiopures or racemic BINOL and hexane dipropiolate (HD) under the optimised conditions.

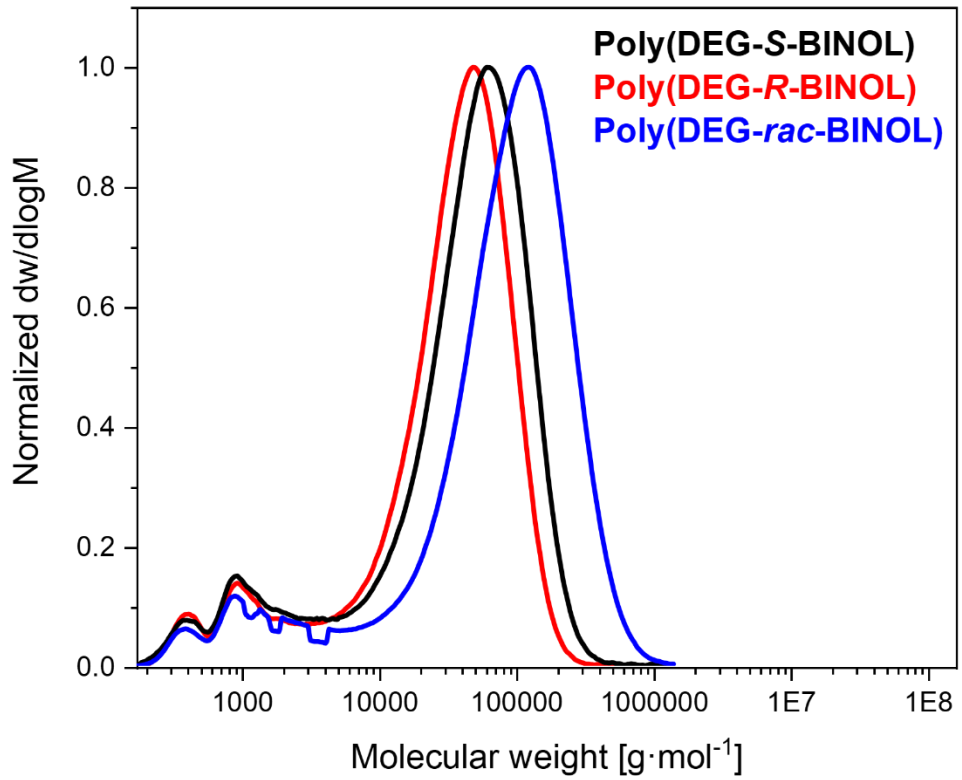


Figure S6. SEC ($CHCl_3$ + 0.5% v/v Et_3N, against polystyrene standards) of polymers resulting from the nucleophilic phenol-yne polymerisation of enantiopures or racemic BINOL and diethylene glycol dipropiolate (DEG) under the optimised conditions.

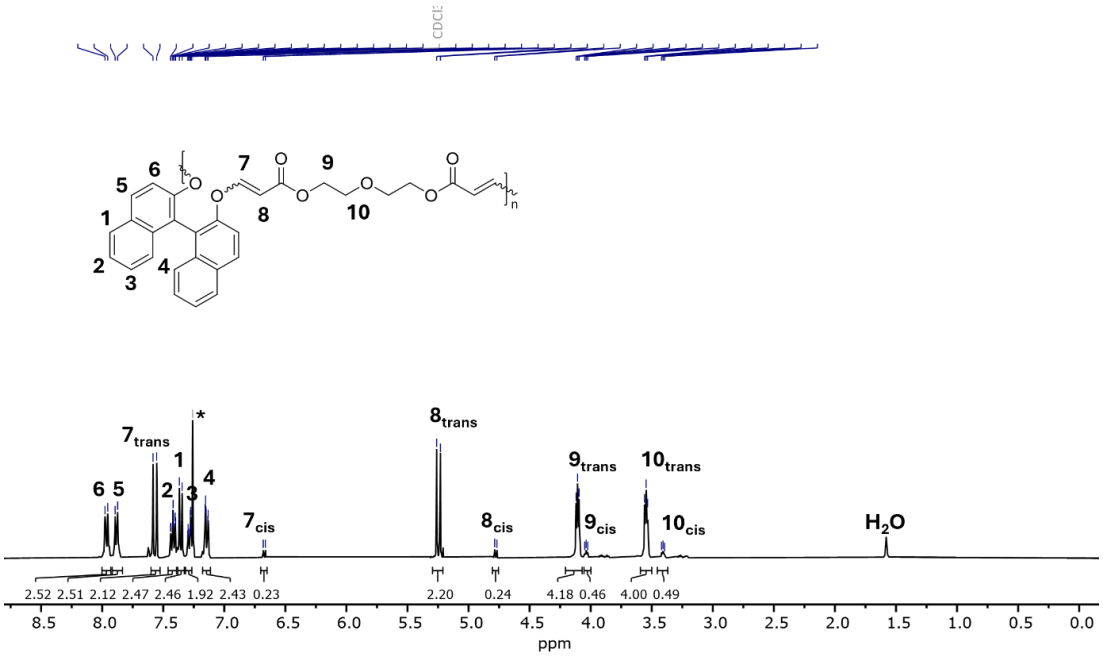


Figure S7. ^{1}H NMR spectrum ($CDCl_3$, 400 MHz, 300 K) spectra of Poly(DEG-rac-BINOL). Solvent peak marked *.

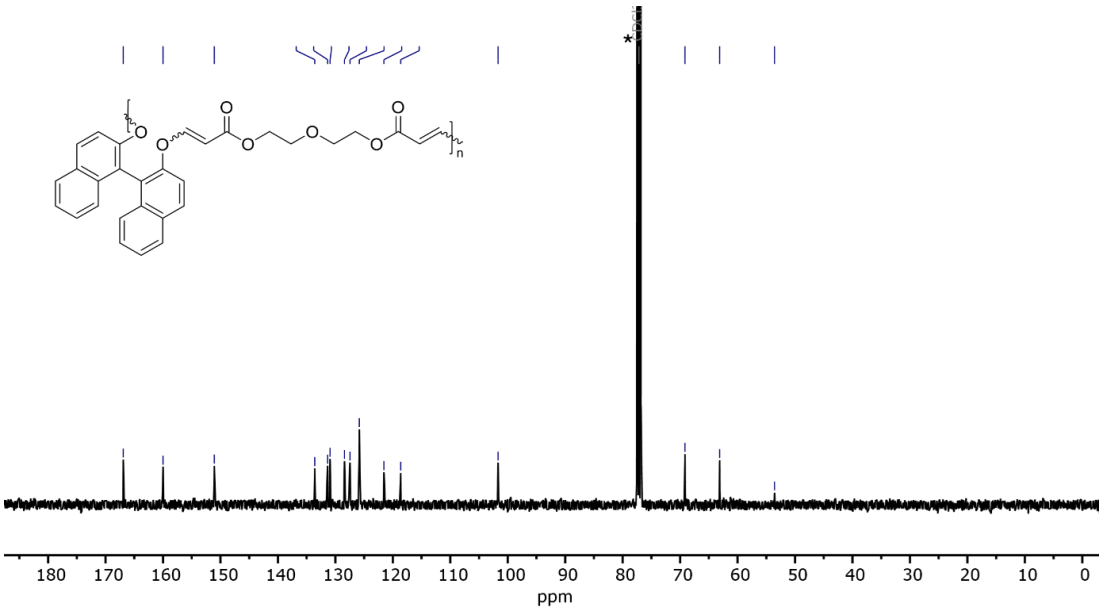


Figure S8. ^{13}C NMR spectrum ($CDCl_3$, 101 MHz, 300 K) spectra of Poly(DEG-rac-BINOL). Solvent peak marked *.

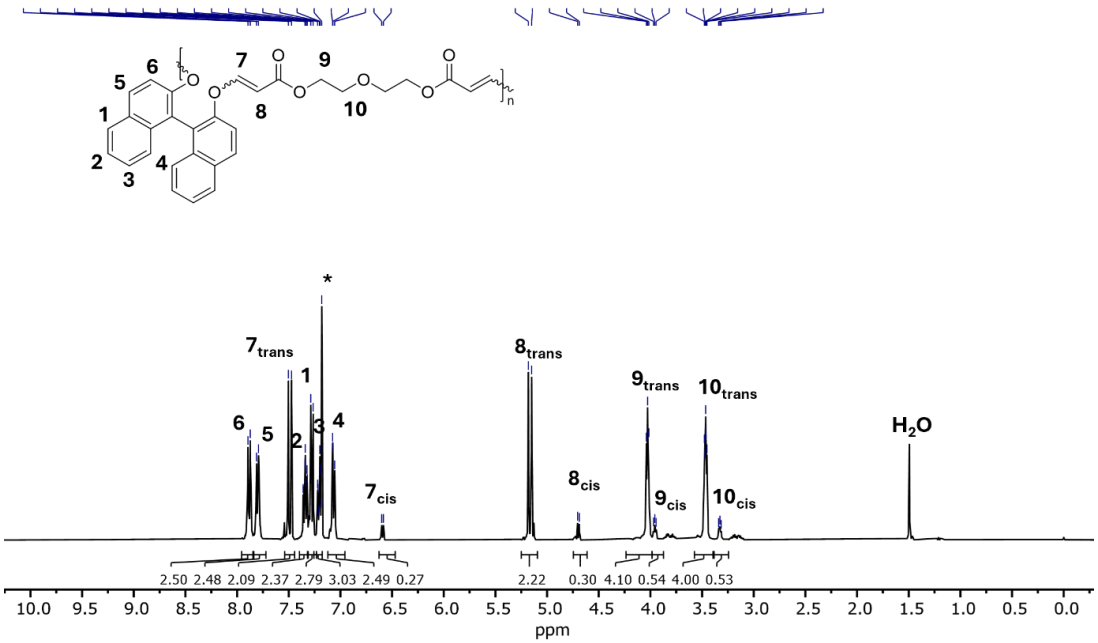


Figure S9. ^{1}H NMR spectrum ($CDCl_3$, 400 MHz, 300 K) spectra of Poly(DEG-R-BINOL). Solvent peak marked *.

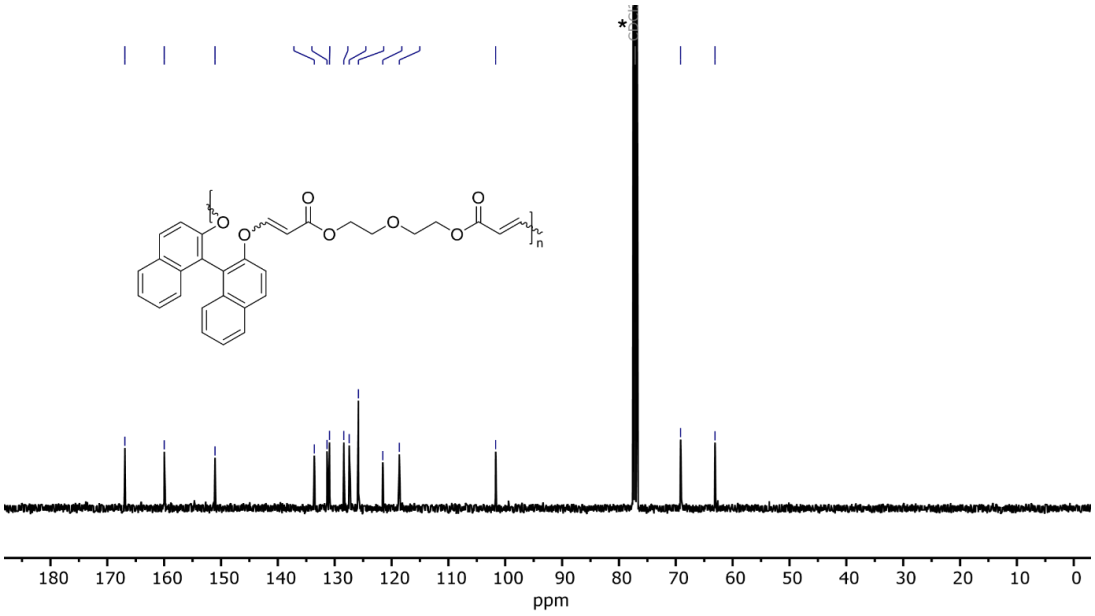


Figure S10. ^{13}C NMR spectrum ($CDCl_3$, 101 MHz, 300 K) spectra of Poly(DEG-R-BINOL). Solvent peak marked *.

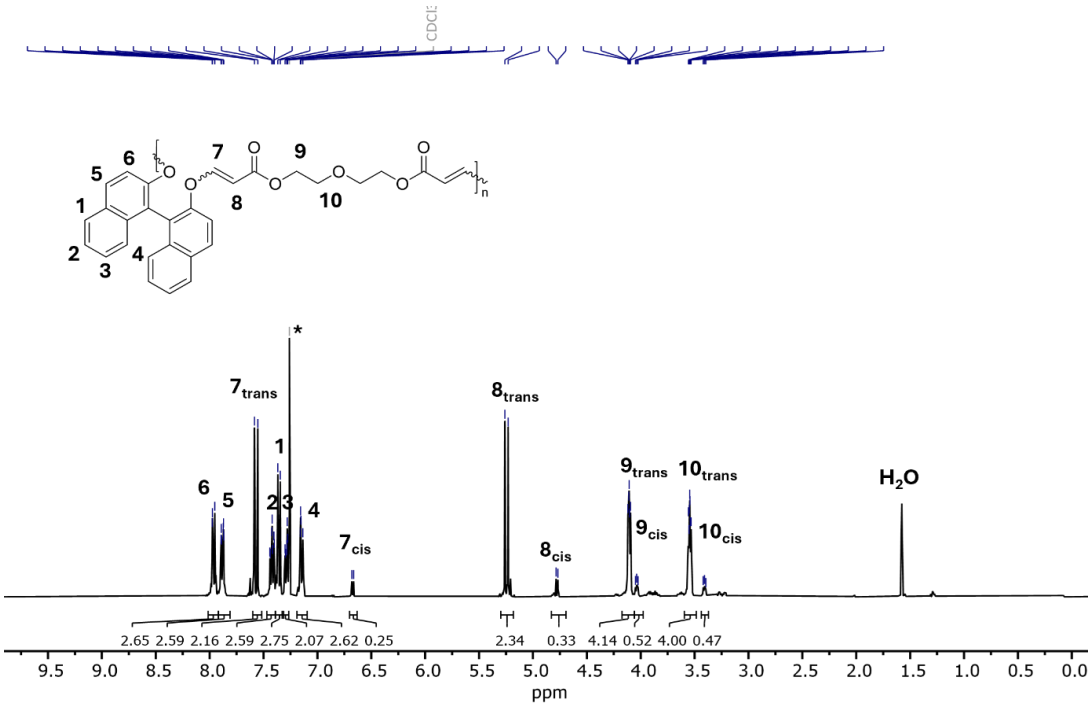


Figure S11. ^{1}H NMR spectrum ($CDCl_3$, 400 MHz, 300 K) spectra of Poly(DEG-S-BINOL). Solvent peak marked *.

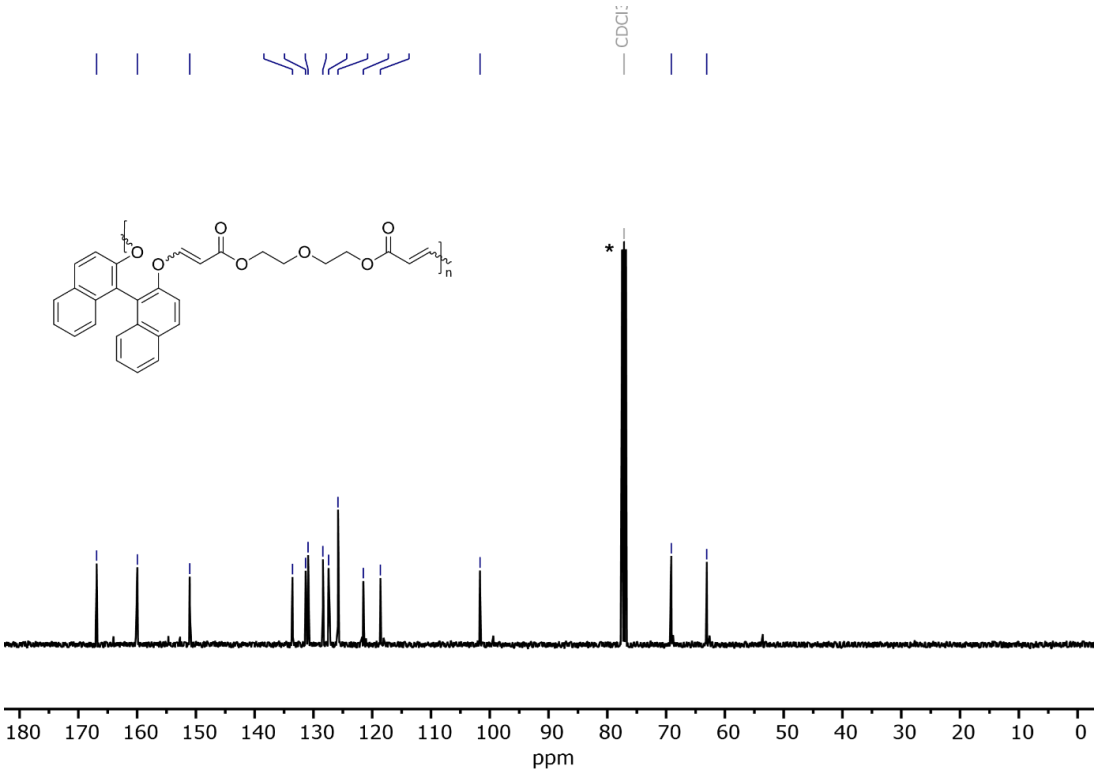


Figure S12. ^{13}C NMR spectrum ($CDCl_3$, 101 MHz, 300 K) spectra of Poly(DEG-S-BINOL). Solvent peak marked *.

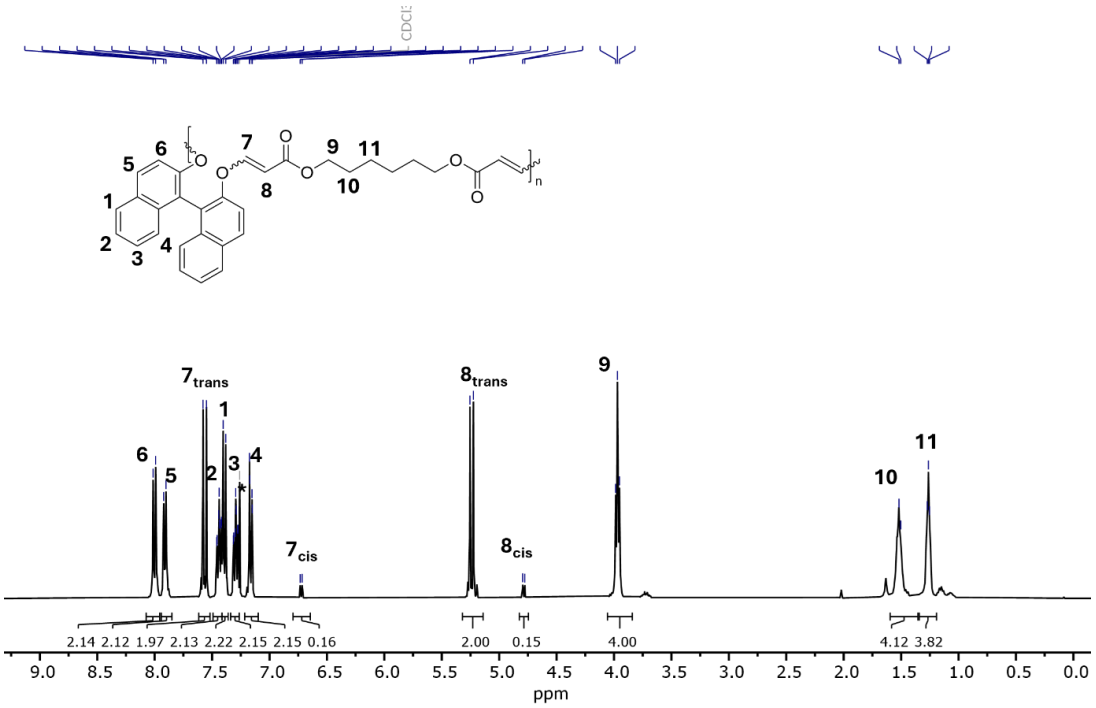


Figure S13. ^{1}H NMR spectrum ($CDCl_3$, 400 MHz, 300 K) spectra of Poly(HD-rac-BINOL). Solvent peak marked *.

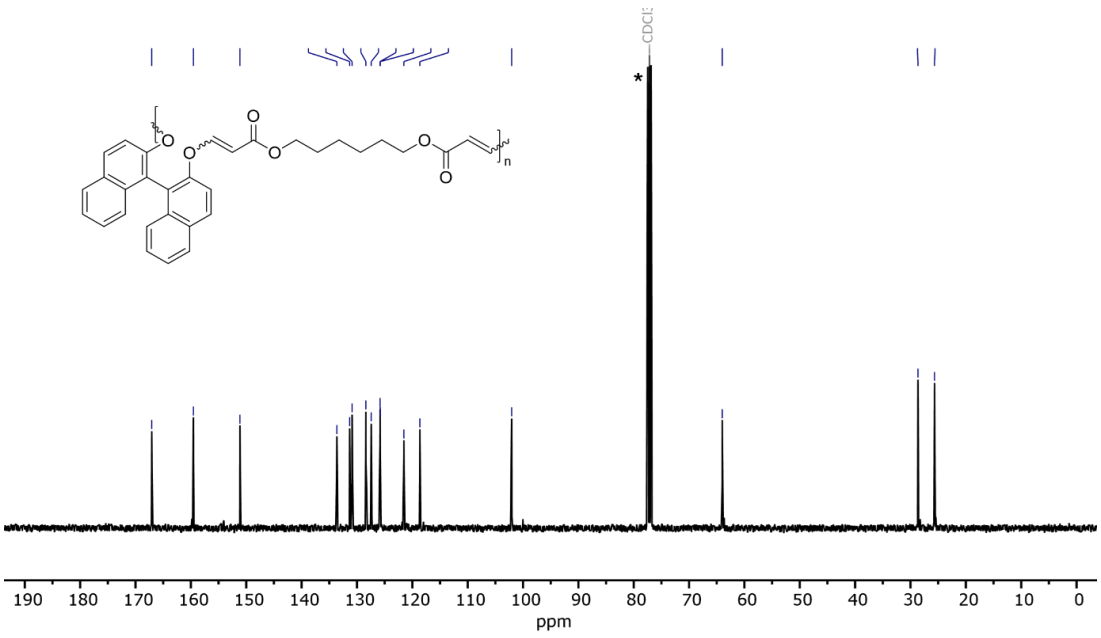


Figure S14. ^{13}C NMR spectrum ($CDCl_3$, 101 MHz, 300 K) spectra of Poly(HD-rac-BINOL). Solvent peak marked *.

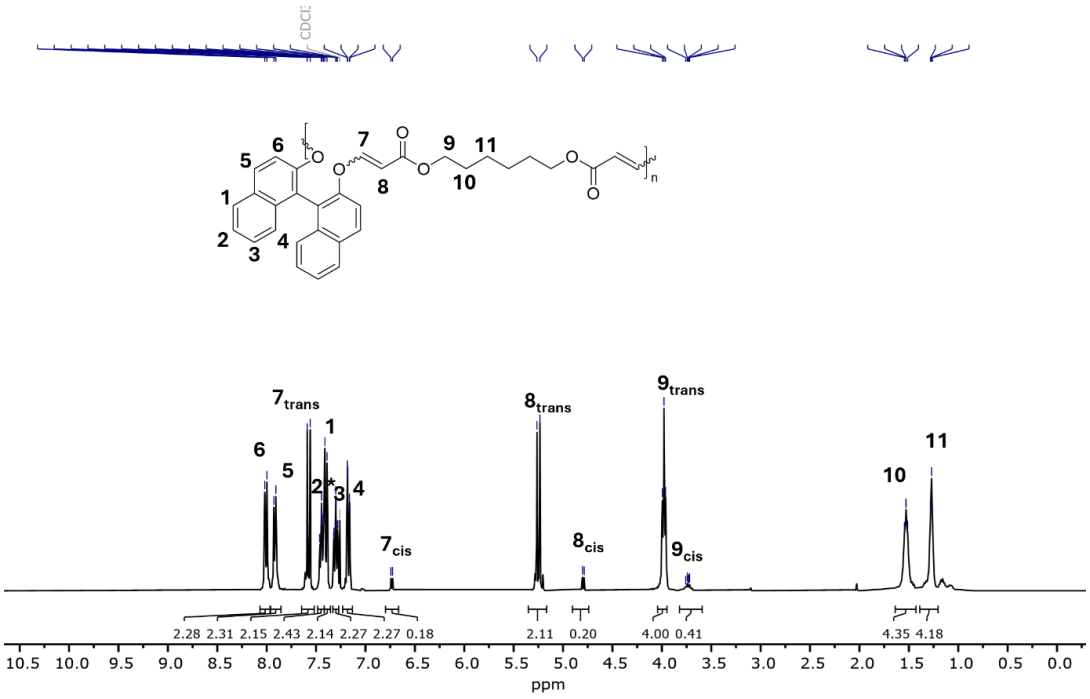


Figure S15. ^{1}H NMR spectrum ($CDCl_3$, 400 MHz, 300 K) spectra of Poly(HD-S-BINOL). Solvent peak marked *.

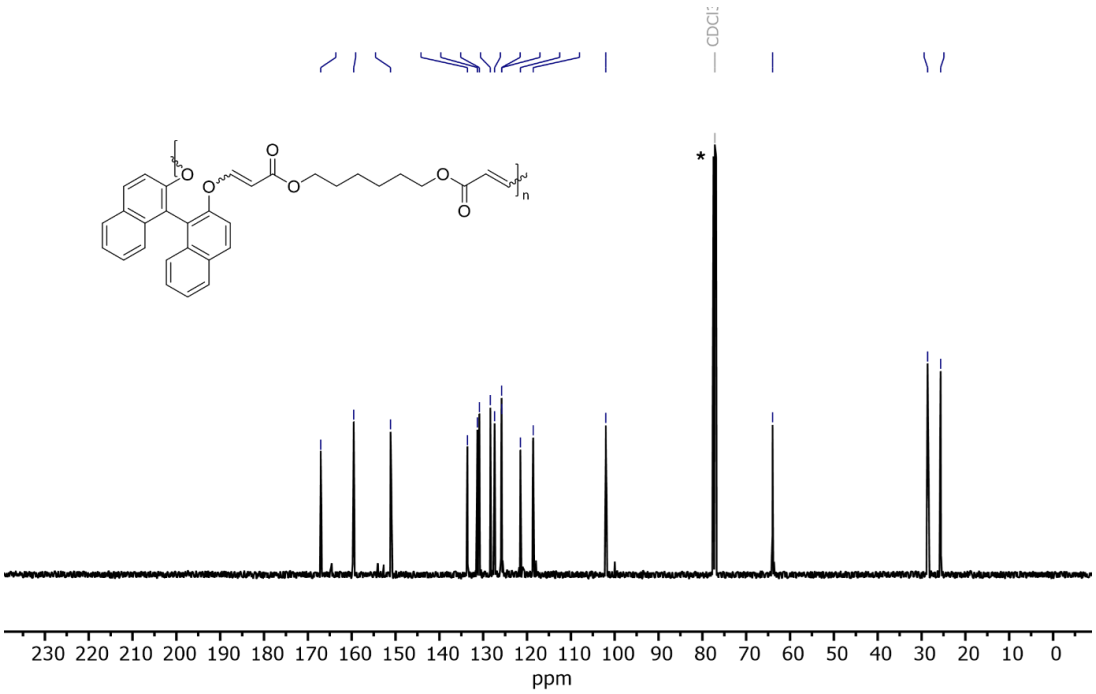


Figure S16. ^{13}C NMR spectrum ($CDCl_3$, 101 MHz, 300 K) spectra of Poly(HD-S-BINOL). Solvent peak marked *.

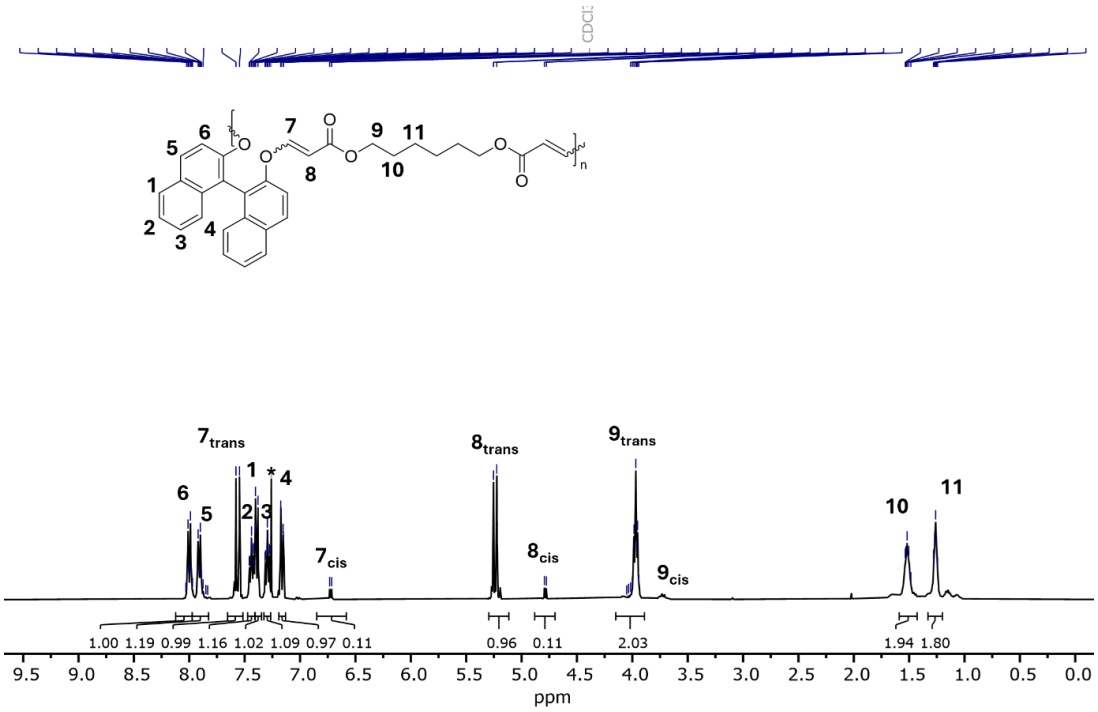


Figure S17. ^{1}H NMR spectrum ($CDCl_3$, 400 MHz, 300 K) spectra of Poly(HD-R-BINOL). Solvent peak marked *.

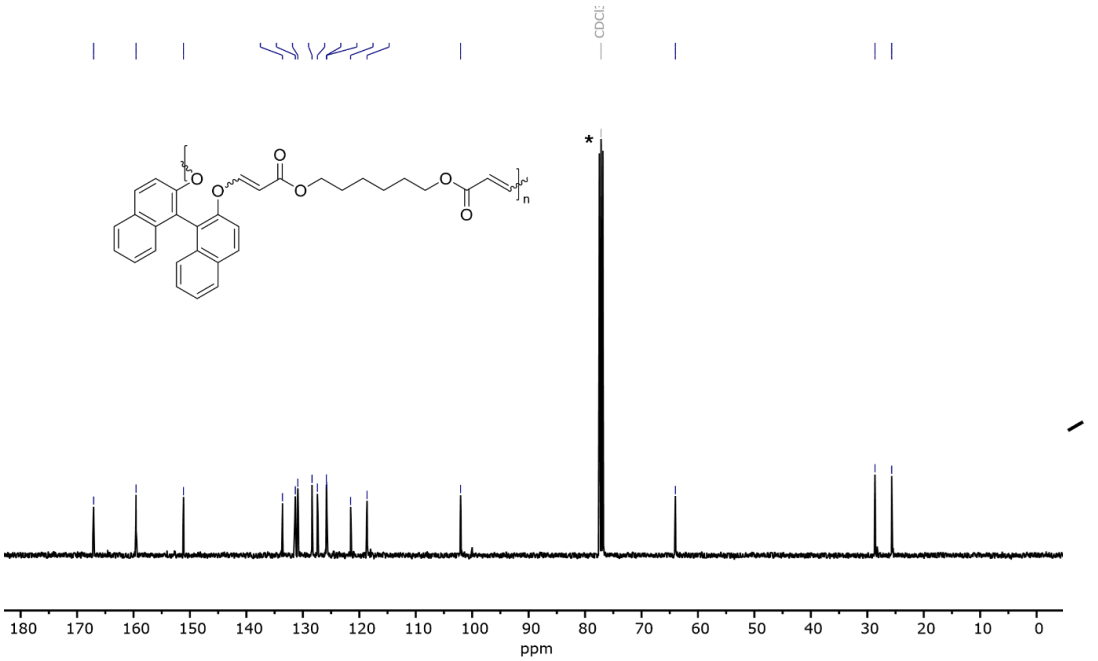


Figure S18. ^{13}C NMR spectrum ($CDCl_3$, 101 MHz, 300 K) spectra of Poly(HD-R-BINOL). Solvent peak marked *.

Thermomechanical characterisation

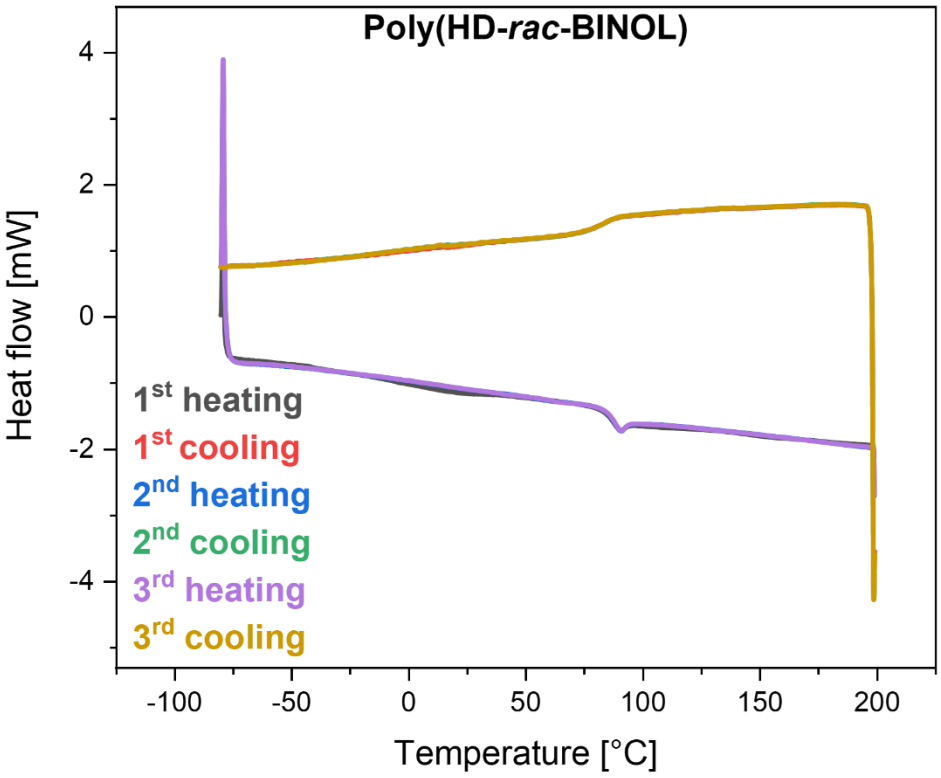


Figure S19. DSC thermogram (−80 – 200 °C, 10 °C/min, N_2) of Poly(HD-*rac*-BINOL).

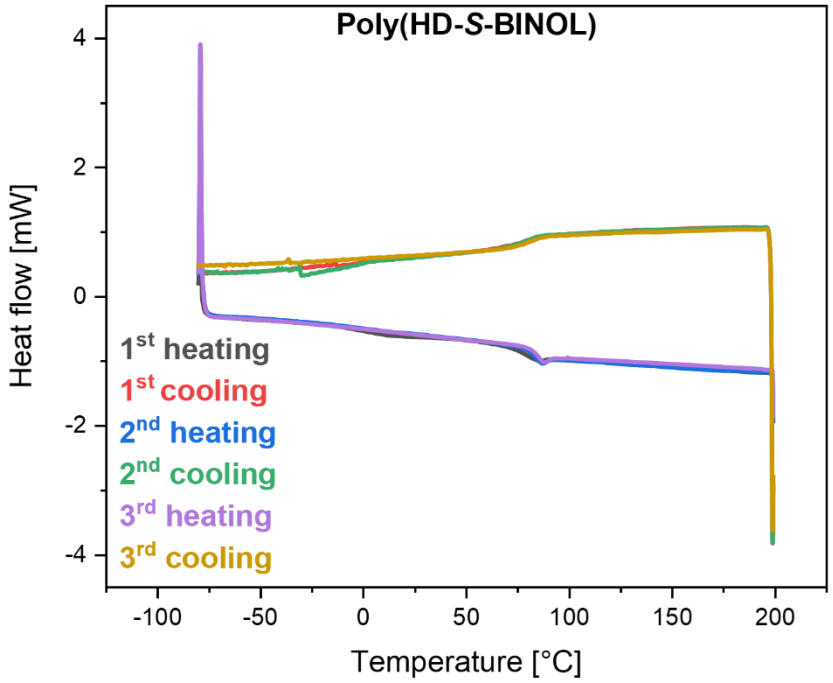


Figure S20. DSC thermogram (−80 – 200 °C, 10 °C/min, N_2) of Poly(HD-*S*-BINOL).

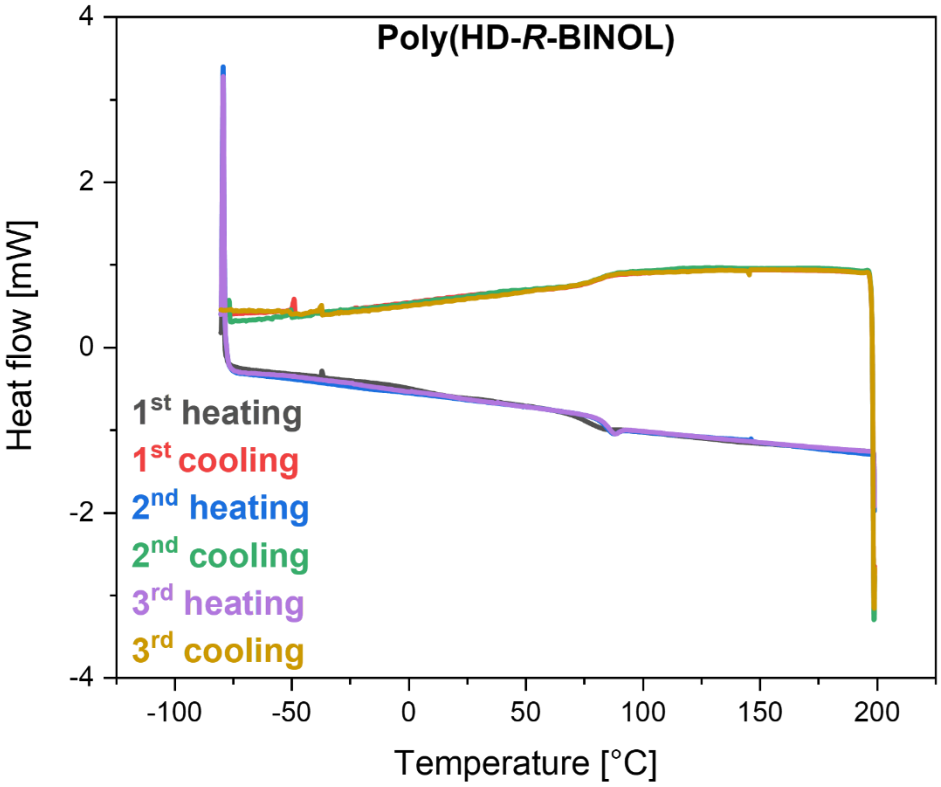


Figure S21. DSC thermogra (−80 – 200 °C, 10 °C/min, N_2) of Poly(HD-*R*-BINOL).

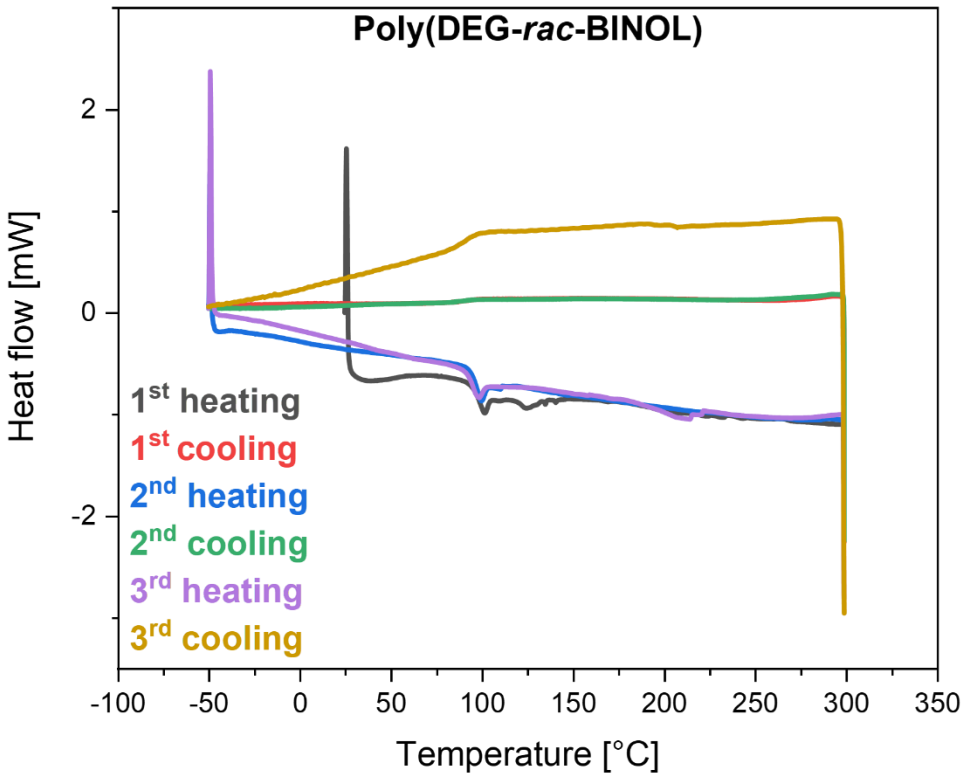


Figure S22. DSC thermogram (−80 – 300 °C, 10 °C/min, N_2) of Poly(DEG-*rac*-BINOL).

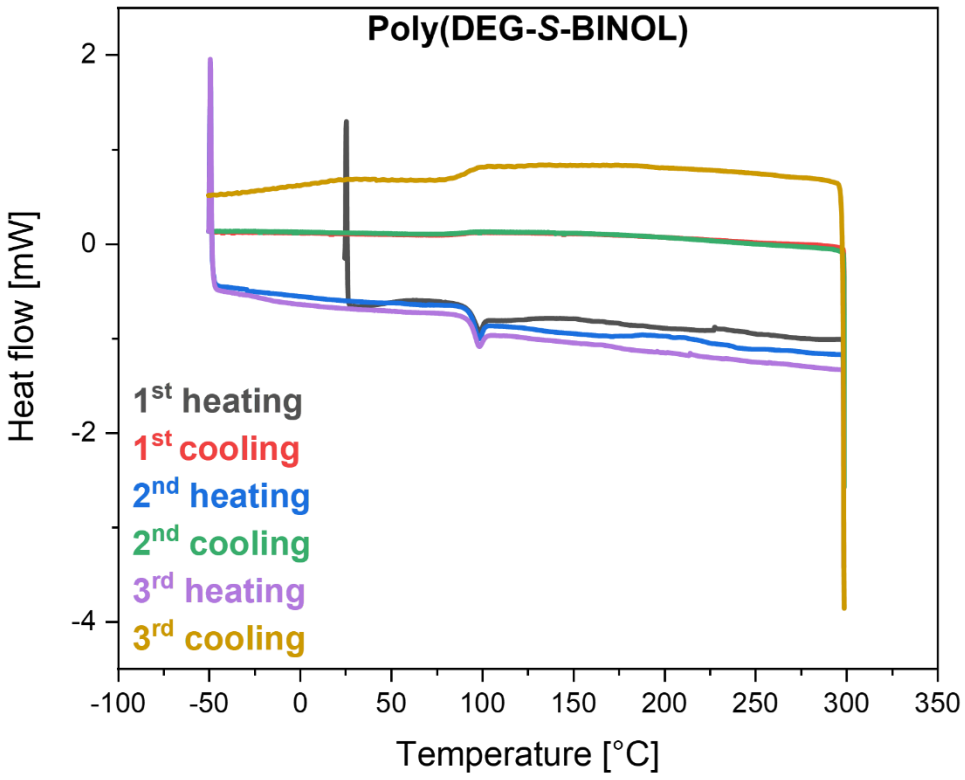


Figure S23. DSC thermogram (−80 – 300 °C, 10 °C/min, N_2) of Poly(DEG-*S*-BINOL).

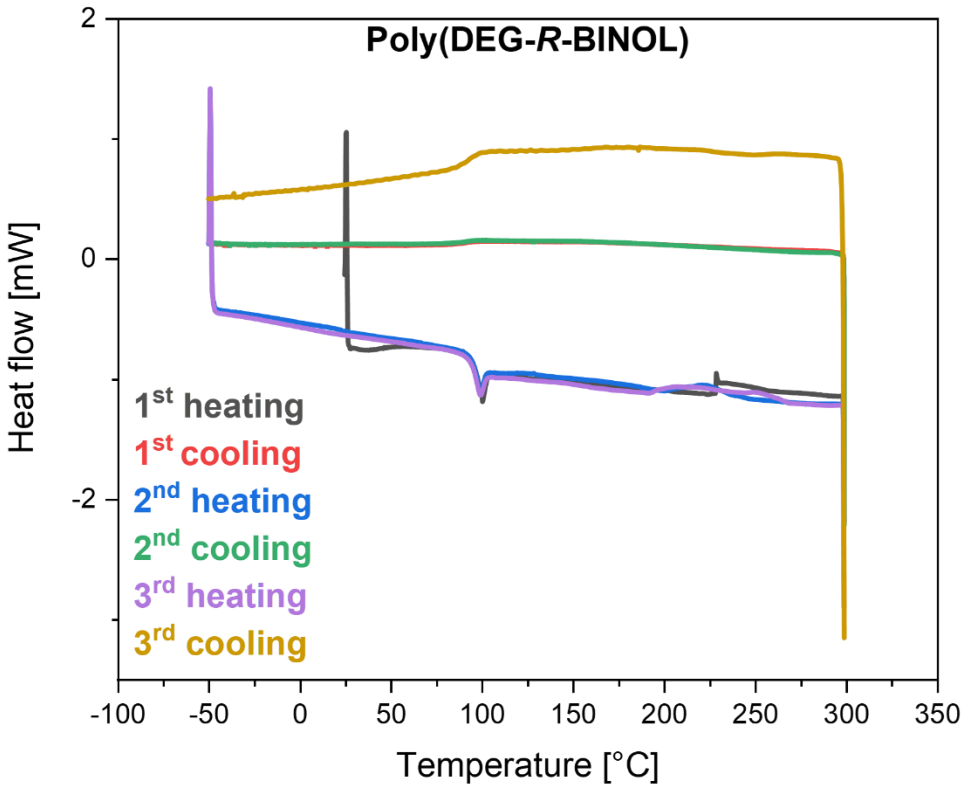


Figure S24. DSC thermogram (−80 – 300 °C, 10 °C/min, N_2) of Poly(DEG-*R*-BINOL).

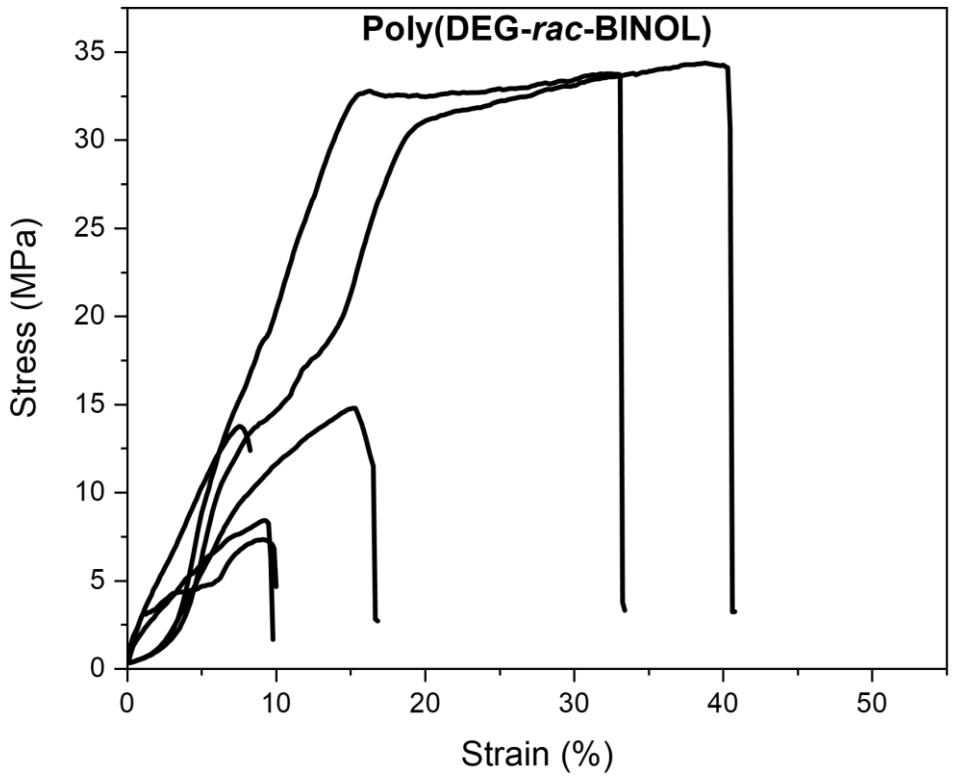


Figure S25. Stress vs. strain curves (22 °C, 10 mm/min) of Poly(DEG-*rac*-BINOL).

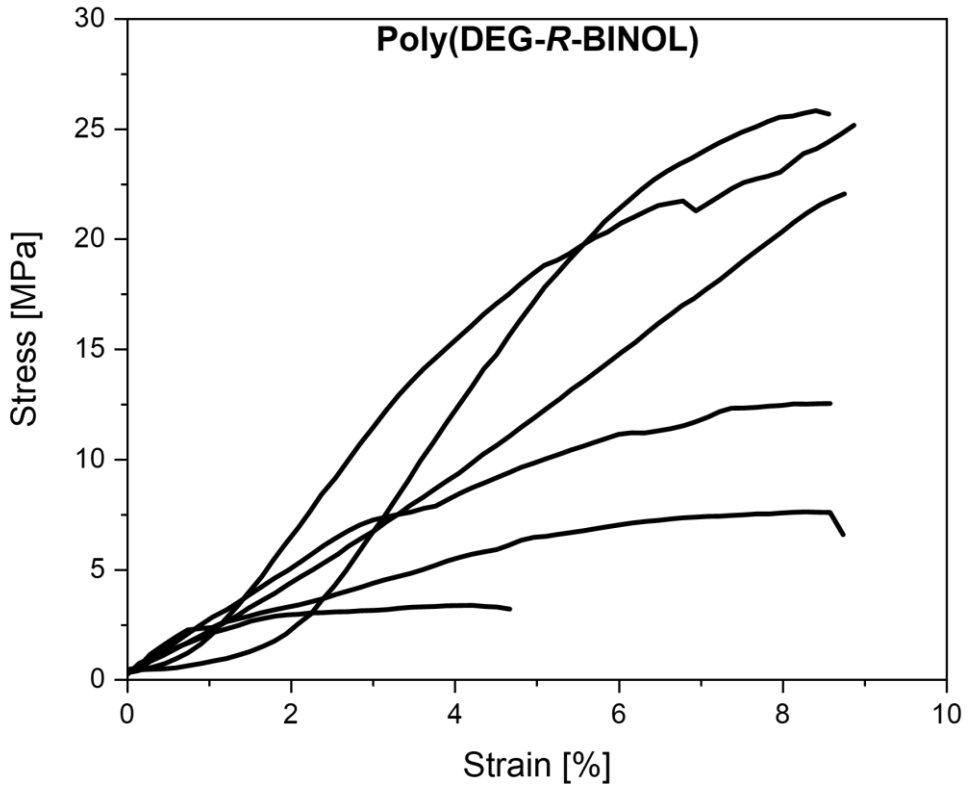


Figure S26. Stress vs. strain curves (22 °C, 10 mm/min) of Poly(DEG-*R*-BINOL).

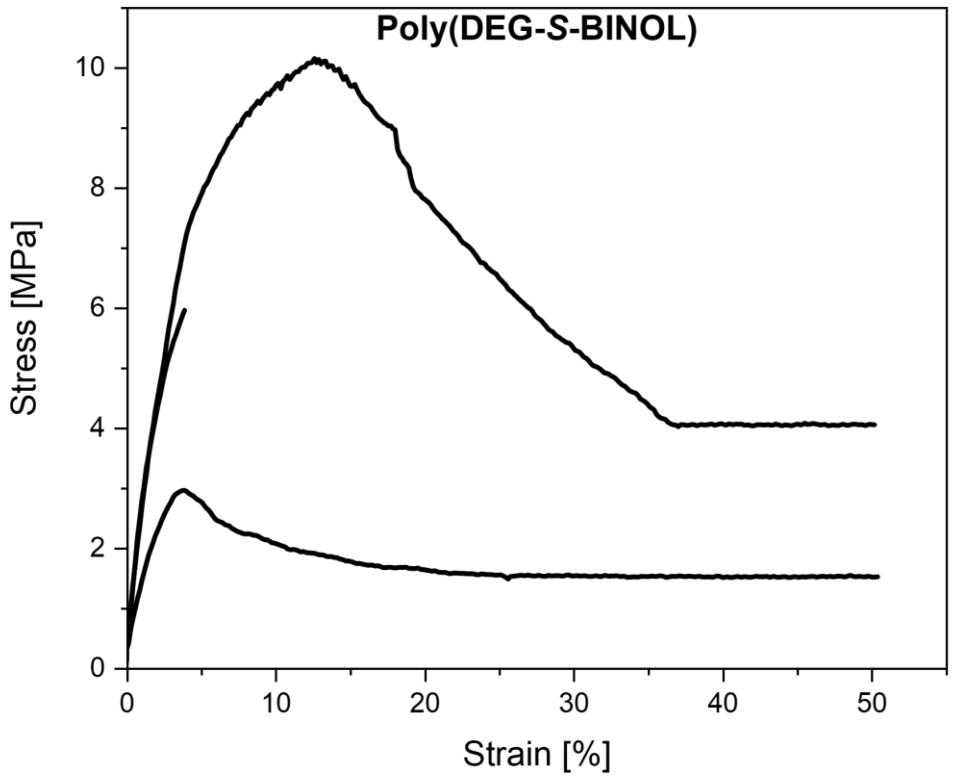


Figure S27. Stress vs. strain curves (22 °C, 10 mm/min) of Poly(DEG-*S*-BINOL).

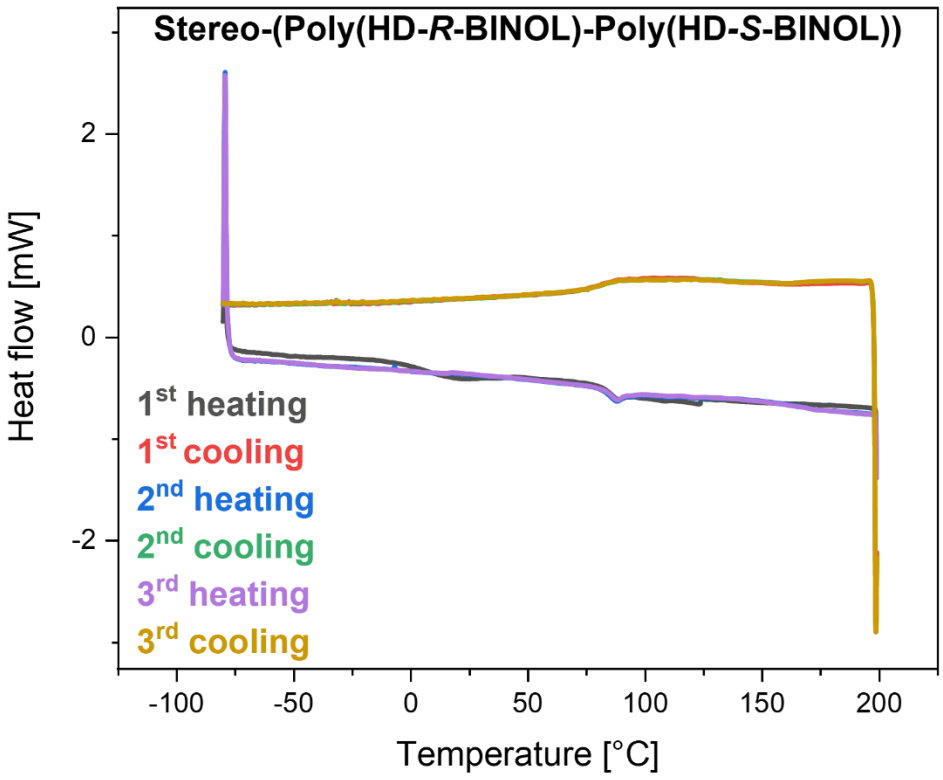


Figure S28. DSC thermogram (−80 – 200 °C, 10 °C/min, N_2) of Stereo-(Poly(HD-R-BINOL)-Poly(HD-S-BINOL)).

Chapter 6 – Conclusions and outlook

This thesis aimed to investigate the nucleophilic Michael addition reaction to activated alkynes to synthesise functional polymeric materials. While traditional step-growth polycondensation reactions are usually performed at high temperatures, often paired with reduced pressure to ensure the removal of the side products and maximise the reaction yield, leveraging “click” protocols could offer significant advantages. Generally, the conditions required by polycondensation reactions mean high energy consumption. Moreover, the high temperature could lead to degradation of the starting materials and incompatibility with volatile monomers, which translates into stoichiometric imbalance, resulting in low molecular weight polymers. Moreover, certain functional groups such as alkene or dynamic bonds may not be compatible with the high temperature used, thus limiting the range of functionalities of the final polymers. When reactions proceed under milder conditions, less energy is required, and greater substrate compatibility is achieved.

Through chapters 2, 4, and 5, it was demonstrated that different polyesters could be obtained at low temperatures (≤ 50 °C), thus showing the nucleophilic Michael addition to activated alkynes to be less energy-consuming when compared to traditional polycondensation. Moreover, by using an addition-type reaction, atom economy is maximised as no side products are developed. Of these chapters, chapter 4 provides a significant example of the versatility of these reactions. In fact, previously difficult-to-polymerise DKPs could be easily incorporated into different polymers by reaction with diverse biobased activated dipropiolates, thus offering

insight into a novel generation of biobased materials with highly tuneable thermomechanical properties.

Another advantage granted by this polymerisation method is the exceptional modularity. In chapter 2 it was demonstrated that the same protocol can be used to incorporate monomers with different structures (aromatic, aliphatic, comprising heteroatoms) hence offering a simple way to finely tune materials properties and impart functionalities. This, paired with control over the monomer feeding ratio, allowed for orthogonal control over the crystallinity of the polymers meaning that a wide range of properties (from semicrystalline thermoplastic to amorphous elastomeric) could be accessed by using only three different monomers. This variability was further increased thanks to the controllable *cis*/*trans* isomerism resulting from the addition reaction. In fact, by changing parameters such as catalyst strength or solvent polarity, the conformation of the resulting alkene can be predicted, translating into a controllable crystalline phase of the final polymer. This means that polymers having the same composition but differing exclusively in backbone *cis*/*trans* ratio can display considerably different properties.

These concepts were expanded in chapter 3 where they were applied to crosslinked polymers. This work shows that nucleophilic thiol-yne reaction is compatible with the synthesis of crosslinked materials with tuneable properties. When the nucleophilic thiol-yne reaction is used instead of the radical alternative, greater selectivity is obtained, and the residual double bond can be used to tune the properties of the materials, where increased *cis* content seems to impart greater

elasticity and improve the toughness. Moreover, the compatibility of this chemistry with aliphatic disulfide bonds was demonstrated (chapters 2 and 3) thus allowing the synthesis of degradable and reprocessable materials by monomer design.

While the impact of *cis*/*trans* isomerism was demonstrated in chapter 2 and 3, chapter 5 shows that the modularity of this class of reactions can be leveraged to precisely evaluate the influence of another kind of stereoisomerism, namely atropisomerism, on the properties of polymeric materials. While no actual difference could be exerted with the monomers used in this work, it still provides valuable insights into the design of polymers exploiting this kind of chirality, that could be tested in the future.

To conclude, given the growing need to develop more sustainable materials, the use of reactions proceeding under milder conditions allowing the inclusion of different functional groups constitutes a significant advantage, and the nucleophilic Michael addition to activated alkynes represents a valuable tool in this regard. The exceptional modularity paired with the controllable *cis*/*trans* isomerism allows for precise control over the property of the material, thus offering the ability to synthesise materials able to meet different needs from a limited pool of monomers, which is particularly relevant given the difficulties associated with the treatment of a highly heterogeneous waste stream. Moreover, as efforts to include bio-derived monomers are growing, the development of reactions able to produce materials from widely abundant functional groups such as alcohols, amines, and thiols may be particularly useful on this matter.